Slovak Society for Geometry and Graphics

28th Symposium on Computer Geometry SCG'2019

Proceedings of the SLOVAK-CZECH CONFERENCE ON GEOMETRY AND GRAPHICS 2019

Trenčianske Teplice

September 9–12, 2019

39th Conference on Geometry and Graphics

Czech Society for Geometry and Graphics

of the Union of Czech Mathematicians and Physicists

Vydavatelský servis
Republikánská 28, Plzeň

Proceedings of the Slovak-Czech Conference on Geometry and Graphics 2019
First edition

ISBN 978-80-86843-65-0 (online)
ISBN 978-80-86843-66-7 (CD-ROM)

Slovak-Czech Conference on Geometry and Graphics 2019

Organized by:
Slovak Society for Geometry and Graphics

Organizing Committee:

Daniela **Velichová** – STU v Bratislave
Daniela **Richtáriková** – STU v Bratislave
Dagmar **Szarková** – SSGG, Bratislava

Scientific Committee:

Roman **Hašek** – Jihočeská univerzita v Českých Budějovicích (CZ)
Michaela **Holešová** – Žilinská univerzita v Žiline (SK)
Pavel **Chalmovianský** – Univerzita Komenského v Bratislave (SK)
Ema **Jurkin** – Sveučilište u Zagrebu (HR)
Mária **Kmeťová** – Univerzita Konštantína Filozofa v Nitre (SK)
Miroslav **Lávička** – Západočeská univerzita v Plzni (CZ)
Emil **Molnár** – Budapesti Muszaki és Gazdaságtudományi Egyetem (HU)
Pavel **Pech** – Jihočeská univerzita v Českých Budějovicích (CZ)
Monika **Sroka-Bizoń** – Politechnika Śląska, Gliwice (PL)
Zbyněk **Šír** – Univerzita Karlova, Praha (CZ)
Daniela **Velichová** – Slovenská technická univerzita v Bratislave (SK)
Gunter **Weiss** – Technische Universität Wien (AT)

Table of Contents

Forewords

The *Slovak–Czech Conference on Geometry and Graphics* was held on September 9–12, 2019 in famous Slovak spa Trenčianske Teplice, as the fifth joint event of the 28$^{\text{th}}$ SYMPOSIUM ON COMPUTER GEOMETRY SCG´2019 of the Slovak Society for Geometry and Graphics and the 39$^{\text{th}}$ CONFERENCE ON GEOMETRY AND GRAPHICS of the Czech Society for Geometry and Graphics.

About 55 conference participants from 6 countries – Slovakia, Czech Republic, Austria, Slovenia, Poland and Hungary enjoyed rich programme from a variety of geometry areas. Three invited plenary lectures were presented. ANDREJ FERKO from Comenius University in Bratislava (Slovakia) gave lecture *On specializing triangulations*, in which he summarized results of the common work with Ivana Kolingerová from Czech Republic on applications of multiple single-criteria triangulations, and demonstrated how to solve any multi-criteria problem by genetic optimization. Invited lecture *Computing projective equivalences of algebraic varieties* presented by JAN VRŠEK from University of West Bohemia in Plzeň (Czech Republic) was devoted to the investigation of the computation of projective equivalences of rational curves and rational ruled surfaces, the detection of affine transformations between planar curves, and computation of similarities between two implicitly given algebraic surfaces. ZLATAN MAGAJNA from Ljubljana University in Slovenia presented lecture entitled *Automated observation of dynamic geometric constructions in school geometry* about some basic principles of automatic proving in geometry, in which he raised several important questions and dilemmas on concepts related to proving and ways of working out and presenting proofs, and introduced software OK Geometry for automated observation of dynamic constructions.

Submitted 28 contributed talks from applied and pure geometry, graphics and education of geometry are published in this proceedings. GeoGebra Workshop was important part of the conference attended by about 10 practising teachers from primary and secondary schools, who could benefit from interesting presentations of experienced users of this dynamic mathematical software in school mathematics.

Conference was organized by the Slovak Society for Geometry and Graphics at the Institute of Mathematics and Physics, Mechanical Engineering Faculty of the Slovak University of Technology in Bratislava, Slovakia. Social programme included the Grand tour of the monumental Trenčín castle, short tourist walks in the White Carpathians Haluzice gorge, and conference dinner with musical piano accompaniment.

We would like to invite you to attend the next joint event of the 29th Symposium on Computer Geometry SCG´2020 and the 40th Conference on Geometry and Graphics that will be held again together by representatives of both societies for geometry and graphics as *Czech–Slovak Conference on Geometry and Graphics* in September 2020 in Czech Republic, in order to keep the good tradition of our common meetings deeply rooted in the history.

Bratislava & Plzeň, November 3, 2019

Daniela Velichová
chair of SSGG

Miroslav Lávička
chair of ČSGG

PLENARY TALKS

On projective equivalence between rational algebraic curves

Michal Bizzarri [a,1], **Miroslav Lávička** [b,a,2] **and Jan Vršek** [b,a,3]

[a] *NTIS – New Technologies for the Information Society, Faculty of Applied Sciences, University of West Bohemia, Univerzitní 8, 301 00 Plzeň, Czech Republic*

[b] *Department of Mathematics, Faculty of Applied Sciences, University of West Bohemia, Univerzitní 8, 301 00 Plzeň, Czech Republic*

[1]*bizzarri@ntis.zcu.cz,* [2]*lavicka@kma.zcu.cz,* [3]*vrsekjan@kma.zcu.cz*

Abstract. In this paper, we will briefly discuss the method for the computation of projective equivalences between rational curves. This is based on the usage of the so called osculating form. It turns out that there are only finitely many non-equivalent curves with the same osculating form. We conjecture the formula for the number of such curves. In addition, we conclude the paper with a brief discussion about spatial quartic curves.

Keywords: Algebraic curve, projective equivalence, osculating form, rational quartic curve

1 Equivalences of rational curves

Let $\mathbb{P}^n$ be the complex projective space of dimension n and write $\mathrm{Aut}(\mathbb{P}^n)$ for the group of all projective transformations. If X, Y are subsets of $\mathbb{P}^n$ then the set of all transformations mapping X to Y will be denoted by $\mathrm{Aut}(\mathbb{P}^n)_{X,Y}$ or simply $\mathrm{Aut}(\mathbb{P}^n)_X$ whenever $Y = X$. In this paper we will discuss projective equivalences between two rational curves. Recall that a rational curve $C \subset \mathbb{P}^n$ is an algebraic curve possessing a birational morphism $\xi : \mathbb{P}^1 \to C$, the so called parametrization. The curve is said to be non-degenerated if it is not contained in a hyperplane. In what follows we will consider non-degenerated curves only.

Locally each curve has a formal parametrization

$$\left(u^{\ell_1+1} + \cdots, u^{\ell_2+2} + \cdots, \ldots, u^{\ell_n+n} + \cdots\right), \tag{1}$$

where $0 \leq \ell_1 \leq \ell_2 \leq \ldots$. The point $(0, \ldots, 0)$ is a called stationary point if some $\ell_i > 0$. (Examples of stationary points are cusps, flexes and stall points.) We will apply two following two observations relevant to our problem: Curve of degree $d > n$ in $\mathbb{P}^n$ has only finitely many stationary points. Stationary points are preserved under projective transformations. One can easily see that two curves of degree n in $\mathbb{P}^n$ are always projectively equivalent, and thus we can consider curves of degree greater then the dimension of the ambient space. Then the problem of finding mappings between two curves is reduced to finding transformations between finite sets of points on these curves – stationary points. Instead of approaching the problem directly we will focus on its translation into the parameter domain.

Lemma 1.1 *Let $[s:t]$ be coordinates on $\mathbb{P}^1$ and let $\xi : \mathbb{P}^1 \to C$ be a birational parametrization of the curve C. Then the pre-image of stationary points in $\mathbb{P}^1$ is given by vanishing of the so called osculating form*

$$\Delta_\xi(s,t) = \det\left[\frac{\partial^n \xi(s,t)}{\partial s^n}, \frac{\partial^n \xi(s,t)}{\partial s^{n-1}\partial t}, \cdots, \frac{\partial^n \xi(s,t)}{\partial t^n}\right]. \tag{2}$$

Let $C, D \subset \mathbb{P}^n$ be two curves, ξ, ζ their parametrizations and Δ_ξ, Δ_ζ the corresponding osculating forms. Assume that there exists a projective transformation $\phi : C \to D$. Then the map

$$\psi = \zeta^{-1} \circ \phi \circ \xi : \mathbb{P}^1 \to \mathbb{P}^1. \tag{3}$$

is an isomorphism and thus it must be a projective transformation. Thus $\phi \in \mathrm{Aut}(\mathbb{P}^n)_{C,D}$ induces the $\psi \in \mathrm{Aut}(\mathbb{P}^1)$. In addition ψ maps zeroes of Δ_ξ to zeroes of Δ_ζ. The group $\mathrm{Aut}(\mathbb{P}^1)$ acts on the set of forms in two variables via $(\psi, f) \mapsto f \circ \psi$. Thus after denoting

$$\mathrm{Aut}(\mathbb{P}^1)_{\Delta_\xi,\Delta_\zeta} := \{\psi \in \mathrm{Aut}(\mathbb{P}^1) \mid \exists \lambda \in \mathbb{C}^* : \Delta_\zeta \circ \psi = \lambda \Delta_\xi\}, \tag{4}$$

we have the inclusion $\mathrm{Aut}(\mathbb{P}^n)_{C,D} \hookrightarrow \mathrm{Aut}(\mathbb{P}^1)_{\Delta_\xi,\Delta_\zeta}$. The idea behind the computation of equivalences between two curves is that the latter set is relatively easy to compute and it is a matter of linear algebra to find its pre-image in $\mathrm{Aut}(\mathbb{P}^n)_{C,D}$. The technical details can be found e.g. in [1].

Recall that the birational parametrization of curve is unique only up to an element of $\mathrm{Aut}(\mathbb{P}_1)$. It follows that the osculating form (which is a polynomial of degree $(n-d)(n+1)$, where d is the degree of the curve and n the dimension of the ambient space) associated to the curve is again well-defined only modulo an automorphism of $\mathbb{P}^1$. Therefore we have the following map

$$\left\{\begin{array}{c} C \subset \mathbb{P}^n \\ \text{rational curve of degree } d \\ \text{modulo projective equivalence} \end{array}\right\} \longrightarrow \left\{\begin{array}{c} \text{form in two variables} \\ \text{of degree } (n-d)(n+1) \\ \text{modulo equivalence of forms} \end{array}\right\}$$

Although it is not a bijection, the above map is finite. In other words there exists only finitely many projectively non-equivalent curves with the same osculating form. Their number is predicted by the following conjecture.

Conjecture 1.2 *Let $d > n$ be natural numbers and let be given a generic form in two variables of degree $(n+1)(d-n)$ then there exists exactly*

$$((n+1)(d-n))! \prod_{i=0}^{n} \frac{i!}{(d-n+i)!} \tag{5}$$

projectively non equivalent rational curves of degree d in $\mathbb{P}^n$, whose osculating forms are equivalent to the given form.

The partial solution of this conjecture is known for $d = n + 1$. In this case the curve is unique and forms of degree $n + 1$ classify rational curves of degree $n + 1$ in $\mathbb{P}^n$ up to the projective equivalence. This is a generalization of Telling theorem, see [2].

In particular projective symmetries $\mathrm{Aut}(\mathbb{P}^n)_C$ of rational curve of degree $n + 1$ correspond to the projective symmetries of $n + 1$ points in $\mathbb{P}^1$ – the roots of osculating form. From this point of view, the most interesting case are quartic curves in $\mathbb{P}^3$. Recall from classical projective geometry that two ordered quadruples of points in $'p^1$ are projectively equivalent if and only if their cross-ratios equal. Since there exists 24 permutations on four points and only 6 different values of cross-ratio associated to these permutations, we conclude that a generic spatial rational quartic, possesses 4 projective symmetries (More precisely $\mathrm{Aut}(\mathbb{P}^1) \cong \mathbb{Z}_2 \times \mathbb{Z}_2$). Let us specify what we mean by generic more precisely.

If λ is the cross-ratio of a given quadruple, then all the possible values of the cross-ratios corresponding to permutations of points are

$$\lambda, \frac{1}{\lambda}, \frac{1}{1-\lambda}, 1-\lambda, \frac{\lambda}{\lambda-1}, \frac{\lambda-1}{\lambda}. \tag{6}$$

There are few exceptions:

$\lambda = -1$ In this case there are only 4 values of cross-ratio and the group of symmetries is dihedral group D_4. The corresponding quartic is not smooth, but it has one node. In fact the harmonic cross-ratio implies the existence of the node and thus two nodal quartics in $\mathbb{P}^3$ are always projectively equivalent.

$\lambda = \mathrm{e}^{\frac{\mathrm{i}\pi}{3}}$ The group of symmetries of this quartic is isomorphic to group of euclidean symmetries of the tetrahedron. The quartic is smooth wit coplanar stationary points. It can be shown that there exists the unique quadric containing smooth rational quartic in $\mathbb{P}^3$. The intersection of the plane containing the stationary points and the quadric is a conic section with a following extraordinary property. Projecting the quartic from any of point of the conic section (except of their four intersection points) produces a planar quartic with three cusps and no node. Remark that projecting a general quartic we can obtain at most two cusps.

The last situation to mention is the osculating form with multiple roots. Now it makes no sense to speak about the cross-ratio. Depending on multiplicities we can briefly summarize the possibilities:

- s^4 degenerates to a cubic,
- s^3t singular with a cusp,
- $s^2(s^2 - t^2)$ one inflection point,
- s^2t^2 two inflection points.

Acknowledgments

The authors were supported by the project LO1506 of the Czech Ministry of Education, Youth and Sports.

References

[1] M. Bizzarri, M. Lávička, J. Vršek: *Computing projective equivalences of special algebraic varieties,* Journal of Computational and Applied Mathematics Volume 367, 2020

[2] H. Telling: The Rational Quartic Curve in Space of Three and Four Dimensions: Being an Introduction to Rational Curves, Cambridge tracts in mathematics and mathematical physics, Cambridge University Press, 1936

On Specializing Triangulations

Andrej FERKO [1], Ivana KOLINGEROVÁ [2]

[1] Comenius University, Mlynská dolina, 842 45 Bratislava, Slovak Republic
[2] West Bohemian University, Univerzitní 8, 306 14 Pilsen, Czech Republic
ferko@fmph.uniba.sk, kolinger@kiv.zcu.cz

Abstract. Triangulation of the given point set in the plane is frequently solved for diverse applications [Aurenhammer et al. 2013, Chalmoviansky et al. 2001]. Many criteria have been developed to provide specialized meshes, namely weight and angular criteria. We study how to compute a triangulation which satisfies more than one criterion or which contains parts according to several various criteria. We discuss selected results and applications of multiple single-criteria triangulations and we demonstrate how to solve any multi-criteria problem by genetic optimization.

The triangulations and their duals, resulting from natural algorithms, can be observed at microscale (e.g. fulleren C60), in Chladni patterns visualising sound waves propagation, and even on the sky in star constellations. The majority of their edges can be characterised as subgraphs of Delaunay triangulation [Delaunay 1934]. Given n points in the Euclidean plane, the Delaunay edges satisfy the empty circle criterion when the circumcircle of three of them does not contain another input point. This way we characterise a Delaunay triangle. The prominent subgraph od Delauanay triangulation was discovered by a Czech mathematician Boruvka more than 90 years ago. Today, it is named the Euclidean minimum spanning tree and it consists of n-1 edges. It is a subgraph of both Dealunay and greedy triangulation, but its edges do not belong to the most prominent minimum-weight triagulation. However, six edges from all 719 ones cannot be characterized easily like 713 Delaunay or 594 Boruvka edges [Ferko et al., 2016]. The single-criterion triangulation, like Delaunay or greedy, can be generalized to multi-criteria problem [Kolingerová-Ferko, 2001].

While single-criteria triangulator can directly employ the criterion to compute edges, the multi-criteria problem formulation requires more flexible stochastic procedure. We opted for genetic optimization, based on Lawson's edge flip procedure. We claim, that this approach is applicable to wide multi-criteria requirements, e.g. those systematized by [Veltcamp, 1992]. The stochastic procedures proved their feasibility in solving selected problems in 2D and even in 3D data-dependent triangulations, where even each edge may have another criterion given by application data.

Our recent research, focusing on kinetic triangulations [Kolingerová et al., 2016], proved the superiority of locally minimal triangulation over the Delaunay one in terms of computational time complexity.

Keywords: Computer graphics, Computational geometry, Minimum weight triangulation, Delaunay triangulation, Genetic optimization

References

[1] AURENHAMMER, F., KLEIN, R., Der-Tsai LEE. 2013. *Voronoi diagrams and Delaunay Triangulations.* Singapore: World Scientific.

[2] CHALMOVIANSKÝ, P. et al. 2001. *Zložitosť geometrických algoritmov.* Bratislava: FMFI UK.

[3] DELAUNAY, B. 1934. Sur la sphere vide. *Bulletin of Academy of Sciences of the USSR*, pp.793-800, 1934.

[4] FERKO, A., MORAVČÍK, J., KOLINGEROVÁ, I. 2016. Souhvězdí jako podgrafy triangulací (Star Constellations as Subgraphs of Triangulations, in Czech). *Pokroky matematiky, fyziky a atronomie*, 2016, roč. 61, č. 1, pp. 14-20. ISSN: 0032-2423.

[5] KOLINGEROVÁ, I., FERKO, A. 2001. Multicriteria-optimized triangulations. *The Visual Computer* 17 (6), 380-395.

[6] KOLINGEROVÁ, I. et al. 2018. Neighbourhood graphs and locally minimal triangulations. *Transactions on Computational Science* 31. Berlin, Heidelberg : Springer, 2018. pp. 115-127 ((Lecture Notes in Computer Science, ISSN 0302-9743 ; 10990)).

[7] VELTKAMP, R.C. 1992. The γ-neighborhood graph. *Comput. Geom.* **1**(4), 227–246 (1992).

Tools for automated hypothesising and proving in geometry classroom

Zlatan Magajna

Faculty of Education, University of Ljubljana,
Kardeljeva pl. 16, 1000 Ljubljana, Slovenia
zlatan.magajna@pef.uni-lj.si

Abstract. We present the basic elements of automated observation as is implemented in software OK Geometry, a program for observing dynamic constructions. We also describe a geometry course for prospective mathematics teachers, in which students obtained hypotheses using automated observation and proved them with software a for automated proving.

Key words: dynamic geometry systems, automated observation, software for automated proving

1 Introduction

Proving facts is, from the perspective of a mathematician, the essence of mathematics. However, in classroom students and teachers are mostly focused on understanding concepts, on executing procedures, on solving problems that do not require a formal proof, and not on argumentative discourses. Yet, proofs and proving are important in school mathematics. Hanna lists several functions of proofs in school mathematics, among them are verification and explanation [2]. In school setting an explanatory proof is more relevant than a mere verification: it is usually more important to understand why something is true that knowing that something is true. Understanding proofs requires, besides the basic understanding of geometric concepts and various procedures, the understanding of deductive argumentation, the concept of proof, and of some proving strategies. Geometry was traditionally considered an appropriate polygon for learning formal deductive proving. The reason perhaps lays in the dual nature of geometric objects: the formal nature, based on properties deduced from the underlying system of axioms and theorems, and the properties that can be visualised from representations of geometric objects and properties. After Descartes, a third way, based on algebraic representations (e.g. Cartesian plane, complex numbers), of considering geometry was introduced. In general, proofs based on algebraic approach, have great verification and small explanatory power.

Argumentation in (school) geometry is related to various processes: (1) objects and properties are often represented graphically by a drawing; (2) properties to be proved or properties to be used in proofs are observed in a drawing; (3) properties need to be related to definitions and known facts; and, finally, (4) facts and observations have to be organised into a deductive structure. Today's technology provides a considerable help on this path.

Dynamic geometry systems (DGS) allow the representation of geometric objects and properties as dynamic constructions, on which simple and precise measurements and numerical checking of properties can be performed. In recent years also algebra based automated proving methods of geometric facts were implemented in educational software on personal computers, e.g. Java Geometry Expert (JGEX) [1],[5]. Finally, let us mention OK Geometry, an example of a less known software for observation and generating hypothesis related to dynamic geometric constructions.

Tools and technology are thus becoming part of sociocultural context of school geometry. The relation between an activity (e.g. school mathematics) and the tools used in a community of practice (mathematics teachers and students) is complex and difficult to tackle, for it requires a sociocultural analysis that takes into account activity structure, social component and participants' knowledge [4], as well as other factors, ranging from motives of the activity to historical elements. It is almost impossible to predict the 'trajectories of usage' in school setting of potentially relevant tools. Thus, little can be said about the future role of programs for automated observation or automated proving in school setting.

2 From automated observation to automated proving

The section begins with a presentation of OK Geometry, a program for automated observation of dynamic geometry constructions, which is followed by a short account of a course for prospective mathematics teachers, based on the usage of a programs: Geogebra, OK Geometry, and Java Geometry Expert (JGEX).

2.1 OK Geometry

OK Geometry is a computer program designed for observing geometric properties of dynamic constructions and, consequently, for generating hypotheses related to a dynamic construction[1]. The observed constructions can made in OK Geometry itself or can be imported from a variety of available DGS programs. The basic idea of automated observation is quite simple [3]. In a given dynamic construction OK Geometry randomly moves all free points in the constructions and produces several static instances of the dynamic construction. The static constructions are numerically checked for a wide range of geometric properties. A property is considered to be observed if it is numerically confirmed in each instance of the generated static constructions. Clearly, this produces hypotheses and not proofs. In order to produce usable

[1] OK Geometry is freeware program. The basic module is in Czech, Slovenian and English. It is available at http://z-maga.si/index?action=article&id=40 .

and relevant hypotheses from observations OK Geometry uses some additional mechanisms. We present three of them.

1. Consider the example in Fig. 1: In a right triangle ABC let D be the midpoint of BC, and let E be the base of altitude from C in the triangle ABD (Fig. 1, left). A dynamic drawing, made in GeoGebra or some other DGS, of this simple construction is imported to OK Geometry. The number of properties observed by OK Geometry depends on the desired level of expertise. The advanced level, for example, gives rise 62 observed properties. In general, among the found properties there are many properties that one would not think of or expect them, some may result in relevant hypotheses, some properties may turn out to be important steps in proving some fact, and there are also several trivial properties.

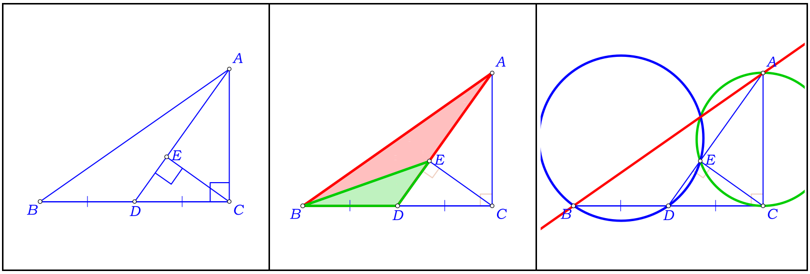

Fig. 1: Observation of a dynamic construction

OK Geometry, for example, observes in the configuration a pair of similar triangles ABD and BED (Fig. 1, middle). Fig. 1 (right) shows another property detected by OK Geometry: the circumcircles of triangles BDE and AEC intersect on the hypotenuse AB. This property perhaps appears artificial, but it can be profitably used in proving the similarity of triangles ABD and BED. This example illustrates that OK Geometry when detecting properties considers besides the objects that are part of the construction also all lines, all circles, and all conics determined by the points in the construction.

2. Often we want to find properties of configurations that we are not able to construct. But how to numerically observe instances of dynamic construction if one does not know how do the construction? To override this OK Geometry allows implicit and optimisation ‘constructions’, which are not proper geometric construction but rather solutions found by some numerical method. A solution obtained in this way can be observed and the found properties may indicate how to make a proper geometric construction. We illustrate this with the following task: Given is a triangle ABC and a point D in it. Consider three circles inside the triangle, each passing through D and touching a different pair

of sides (Fig. 2, left). The problem is: where to position D so that the three circles are congruent (Fig. 2, right)?

For some students the construction of the three circles for a given point D (Fig. 2, left) may present an obstacle that prevents them from analysing the task. To overcome such situations OK Geometry contains several non-basic construction commands, e.g. the construction of a circle passing through a point and touching two lines or a circle touching three given circles. Once the three circles are constructed we proceed to the next step. We ask OK Geometry to move the point D so that an additional condition (i.e. the congruence of the three circles) is met (Fig. 2, right). Actually, the program produces several copies of configuration with a precision that allows numeric observation.

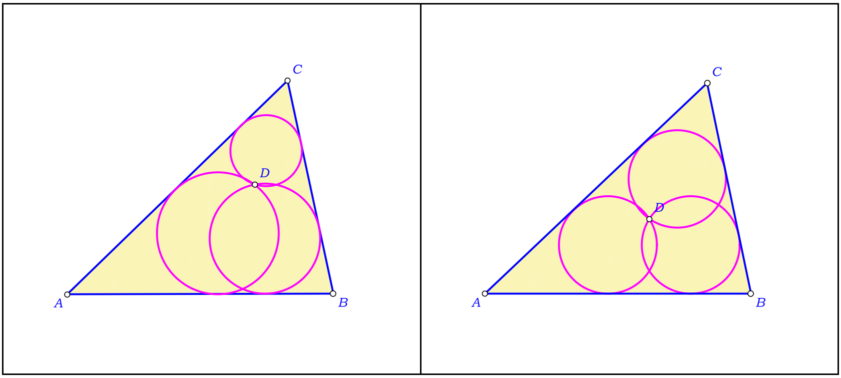

Fig. 2: An example of implicit construction

3. If the considered problem or construction is related to the geometry of a triangle, OK Geometry relates the observations to a large database of triangle objects. The database consists of several thousands of triangle centres, characteristic lines, circles, triangles and conics and many transformations of these objects. It may turn out, for example, that an investigated point is a known triangle centre or that it lays on some lines through known centres or that an investigated line is tangent to the nine point circle of the orthic triangle of the studied triangle. To continue the example in Fig. 2, we investigate how is the point D in the solution (Fig. 2, right) related to the reference triangle ABC. Fig. 3 (left) is an edited list of properties of the point D with regard to the database objects of the triangle ABC.

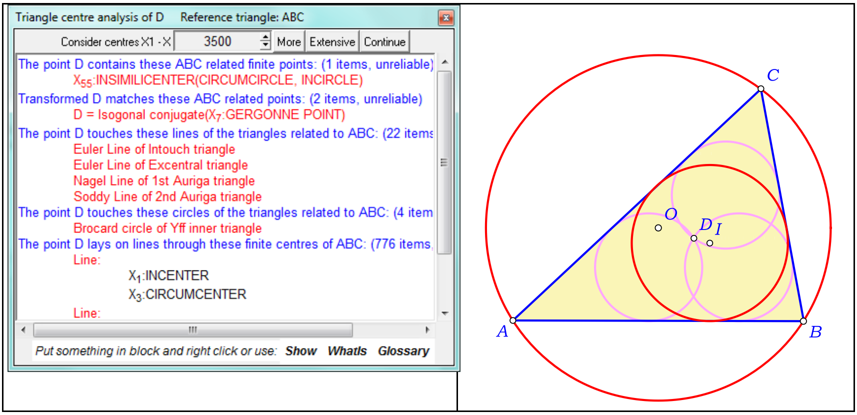

Fig. 3: Relating a solution to the database of triangle objects

The observation states that the point D is the insimilicentre of the incircle and excircle. In other words: we got the hypothesis that the point D lays between the incentre I and the circumcentre O of the triangle ABC, so that D divides the segment OI in the same ratio as is the ratio of radiuses of circumscribed and inscribed circle of the triangle ABC.

2.2 An experience

In order to gain some experience in using programs for automated proving and observational geometry software we introduced them in the seminar on triangle geometry. The participants were 33 prospective two-subjects teachers of the Pedagogy faculty in Ljubljana, Slovenia. They had previously attended a course in abstract geometry and they had some previous training in using Geogebra. At the beginning the students attended a short workshop (4 hours) in which they were shown the basics of algebraic methods of proving geometric statements, the basics of automated observation with OK Geometry, and the basics of Java Geometry Expert (JGEX). As part of the seminar each student had to prepare a seminar report on a topic of triangle geometry and give a short presentation (15 min) of his work. The usage of various software was inferred from a document analysis of the students' reports.

Most, but not all, of the students' reports were structured in similar way and contained three elements: 1. A presentation of a new concept (e.g. the contact triangle of a triangle) and its properties. This part had to contain some rigorous proofs written in a two column fashion. 2. An exploration of the properties related to the considered concept. Using OK Geometry the students studied some configuration related to the presented concept (e.g. how is the contact triangle related to the tangent triangle). In the report they wrote observations they considered relevant. 3. Documentation (usually just screenshots) related to the automated proof, whether successful or not, in Java Geometry Expert (JGEX) of a selected property among the observed ones.

The students preferred to use Geogebra for working out constructions and the related figures in the report. In fact, for drawing/construction purposes Geogebra was used by 94% of students, OK Geometry by 38%, and JGEX by 22% of students. For the exploration of properties OK Geometry was used by 78% of students, GeoGebra by 30%, and JGEX by 22% of students. Finally, 66% of students included in their report their experience in proving facts with JGEX. Students had no problems in using the software tools, at least at the basic level. They were used to make constructions in GeoGebra and preferred to import them to OK Geometry. Some students found JGEX very attractive not only for proving but as well for making constructions.

3 Conclusion

OK Geometry is a software for observing dynamic geometry constructions. It can analyse constructions made by various dynamic geometry systems and it gives rise to plausible hypotheses. Some of them may be difficult to prove, so programs for automated proving can be profitably used. Only time will show if such programs will find their place in school mathematics.

We reported of an example of a course for prospective mathematics teacher, in which such programs played an essential role. Though proofs, obtained with programs for automated proving, have little or no explanatory power, the students appreciated they could produce proofs for facts discovered by themselves using an observational software. The usage of programs for automated proving made clear to students that observing is important, but what counts in mathematics is a proof.

References

[1] S. Chou, X. Gao, J. Zhang: *A deductive database approach to automated geometry theorem proving and discovering*, J. Automated Reasoning, Vol. 25, 2000, pp 219–246.

[2] G. Hanna: *Proof, Explanation and Exploration: an Overview*, Educational Studies in Mathematics, Vol. 44, 2000, pp. 5-23.

[3] Z. Magajna: *Automated observation of dynamic constructions*, International Journal for Technology in Mathematics Education Vol. 24, No. 3, 2017, pp. 115-120.

[4] G. Saxe: *Culture and Cognitive Development: Studies in Mathematical Understanding*, Psychology Press, 1991.

[5] Y. Zheng, C. Shang-Ching: *Visually Dynamic Presentation of Proofs in Plane Geometry - Part 1*, Journal of Automated Reasoning Vol. 45 No. 3, 2010, pp. 213-241.

CONTRIBUTED TALKS

Kinetic Curves in Cartographic Projections

Andrea Ábrahámová, Margita Vajsáblová

Department of Mathematics and Descriptive Geometry, Faculty of Civil Engineering
Slovak Technical University in Bratislava
Radlinského 11, 810 05 Bratislava, Slovak Republic
andrea.abrahamova@stuba.sk, margita.vajsablova@stuba.sk

Abstract. The creation of map projections is highly variable in using various geometric objects. In this paper we will introduce the use of cycloids, epicycloids and evolvents in cartographic projections. Jervis's cycloidal projection, which was published in 1895, originally uses cycloids as an image of parallels. August's epicycloidal projection (1873) refines Lagrange's circular projection (1779), while preserves the conformity of map projection. The outline meridians in August's projection are displayed in an epicycloid, called nephroid and the other meridians and parallels are displayed into the evolvents of epicycloids of the same type. The description of the constructability of the images of the points of the reference sphere in the Jervis's and August's projection and their geometric properties was also supplemented by a distortion analysis. The aim of comparing the scale distortion was to show the advantages and disadvantages of using cycloids and epicycloids in mentioned cartographic projections. Jervis's cycloidal projection was compared with using circles in conical projection equidistant on the meridians. The use of epicycloids and evolvents in August's projection we compared with an alternative to using circles in the Lagrange's projection.

Key words: epicycloid, cycloid, evolvent, cartographic projections, distortion

1 Introduction

The use of geometric objects in map projections is highly variable. In this paper we will introduce the use of kinetic curves, specifically cycloids, epicycloids and evolvents, in cartographic projections. Jervis's cycloidal projection, which was published in 1895, originally uses cycloids as an image of parallels. August's epicycloidal projection (1873) refines Lagrange's circular projection (1779), while preserves the conformity of map projection. The outline meridians in August's projection are displayed in the two-cusped epicycloid and the other meridians and parallels are displayed into the evolvents of epicycloids of the same type.

Cycloid is defined as a trace of a point fixed on the circle, which rolls along a straight line, epicycloid is defined similarly, but the circle (epicycle) rolls along a fixed circle. Evolvent (Involute) is the trace of a point fixed on a line and this line rolls around the given curve. We showed the use of evolvents of cycloid and epicycloid in the cartographic projection. It holds, that evolvent of the cycloid is the cycloid and evolvent of the epicycloid is the epicycloid.

2 Jervis's cycloidal and conical equidistant projection

In the middle of 19th century was devised and employed a new cartographic projection by a British Colonial Officer, Thomas Best Jervis (1796 – 1857). He was an officer of the Bombay Engineers and director of the Topographical and Statistical Depot of the British War Department. His projection was apparently first published posthumously on July 22, 1895 in Turin by his son. Today this projection is called Jervis´s cycloidal projection. [3]

It was also published a historical map, so-called "New cycloidal projection". This map of Middle East (Fig. 1) has the least distortion of any projection until then known for the range of longitude from 25° to 65° East from Greenwich and the range of latitude from 30° to 46°. The standard (central) meridian is 45°. The shape of the geographic network is as follow: parallels are projected as cycloids and meridians are projected as straight lines.

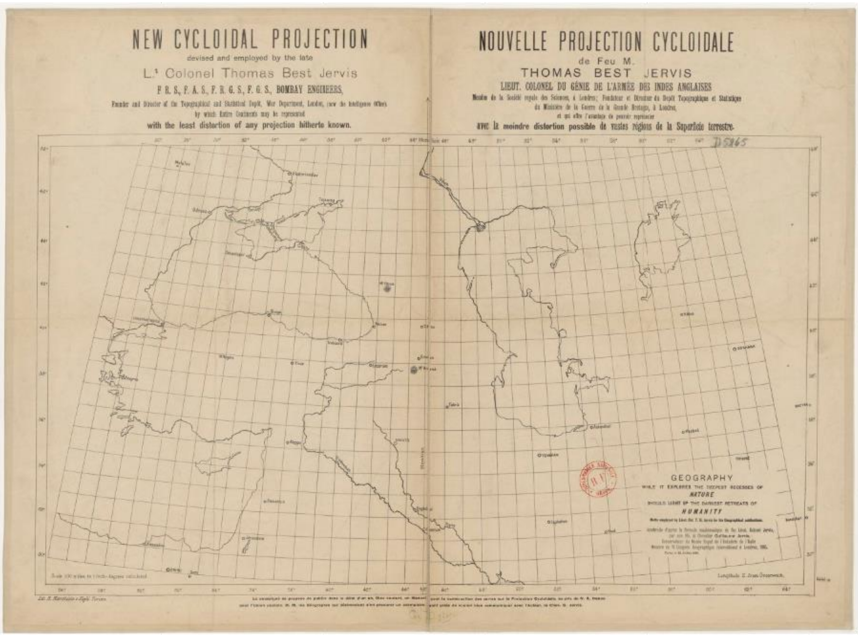

Fig. 1: New cycloidal projection of Middle East [7]

The use of cycloids in Jervis's projection we compared with similar cartographic projection, conical equidistant, where images of parallels are circles. Meridians on the both projections are straight lines, in Jervis's projection the lengths on the standard meridian are preserved and in conical equidistant projection the lengths on all of the meridians are preserved.

2.1 Geometric characteristic and construction of Jervis's cycloidal projection

Jervis long studied a method for the most faithful possible projection of the sphere on a plane surface, and he defined his cycloidal projection, in which the scale distortion of the area displayed by him is minimized. [4] In this type of projection the parallels are projected as cycloids and the meridians are straight lines. The lengths on the central meridian are preserved. The Fig. 2 shows this projection using the map equations, which can be written in the form:

$$x = r(V + \sin V), \qquad y = -r(1 + \cos V), \tag{1}$$

where, r is the diameter of the rolling circle:

$$r = \frac{R}{2}\left(\frac{\pi}{2} - U\right). \tag{2}$$

R is radius of reference sphere, U and V are geographic coordinates of the point.

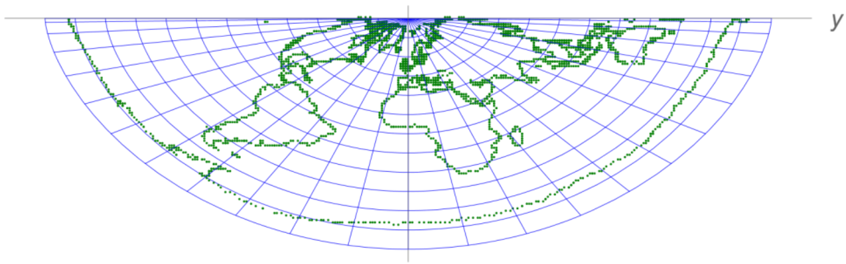

Fig. 2: World and geographic network in Jervis's projection

Jervis's cycloidal projection is relatively easy able to construct. The geometric construction of the geographic network is shown in the Fig. 3. The first step of the graphic representation of this type of projection is drawing of a vertical abscissae AB, which is the preserved central meridian with length $AB = \pi R$, divided into the parts represented the points of parallels labelled B, B', B'', etc. Then we draw the horizontal line CD, passing through the pole A. Through one of the points B, B', B'' (point corresponding to the constructed parallel) we construct the circle k with radius r, according to the formula (2). The diameter of the circle is represented by the distance of the constructed parallel from the Pole A. Parallels, which are the curves of latitude, are given by one of the points B, B', and B'' in the rolling of a circle k along the line CD. Meridians are determined by the corresponding arc of the revolving circle, their images are the straight lines.

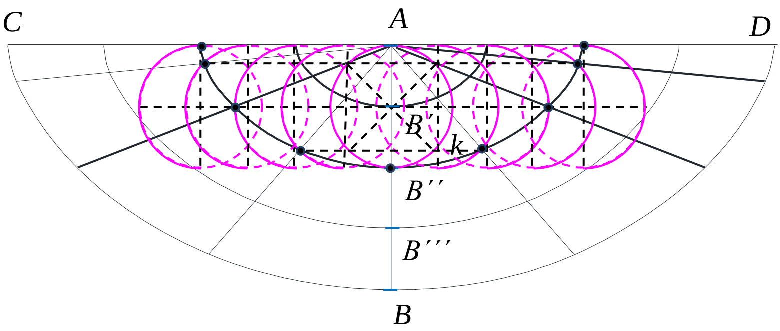

Fig. 3: Geometric construction of Jervis's projection

2.2 Conical equidistant cartographic projection

Conical equidistant projection is cartographic projection of the reference sphere on the conical surfaces unfolded to the plane, where lengths on the meridians are preserved. Meridians are projected as the straight lines and parallels are projected as the concentric circles (Fig. 4). For comparison with Jervis's projection we analysed the conical projection with map equations [2]:

$$x = R\left(\frac{\pi}{2} - U\right)\cos\frac{V}{2},$$
$$y = R\left(\frac{\pi}{2} - U\right)\sin\frac{V}{2}, \qquad (3)$$

where R is radius of reference sphere, U and V are geographic coordinates of the point.

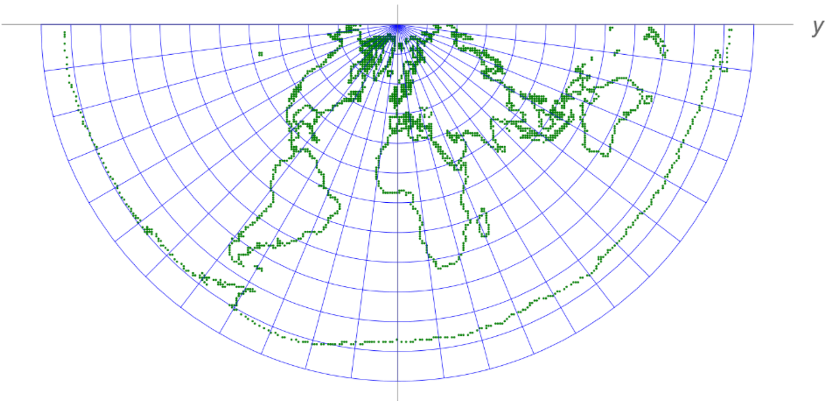

Fig. 4: World and geographic network in conical equidistant projection

2.3 Comparison of Jervis's cycloidal with conical equidistant projection

After the calculating the values of scale distortion in Jervis's cycloidal cartographic projection, we are compared this values with the scale distortion of conical equidistant projection. The comparison for the area of the historical map in Jervis's projection is in the Table 1. As we can see, the scale distortion of parallels in Jervis's projection is from -114 m/km to -550 m/km for the territory of the Middle East. The scale distortion of meridians in Jervis's projection is constant for each meridian, for the territory Middle East is from 45 m/km to 243 m/km. In the case of conical equidistant projection, meridians are preserved, but range of the scale distortion of the parallels is from -546 m/km to -733 m/km. It's follows that the use of cycloids in Jervis's projection has proved to be more effective than the use of circles in conical equidistant projection.

Scale distortion of parallels [m/km]			
		V	
		25°	**65°**
U	**30°**	-114	-235
	46°	-479	-550
Scale distortion of meridians [m/km]		45	243

Table 1: Scale distortion of parallels and meridians of Jervis´s projection

3 Conformal projections by Lagrange and August

Map equations of Lagrange's circular projection are derived from the stereographic azimuthal conformal projection and map equations of August's epicycloidal is derived from the Lagrange's projection. Construction image of the point in August's projection is realized by its image in stereographic projection. Lagrange and August formulated their cartographic projections with the condition of conformity. The use of epicycloids and evolvents in August's projection we compared with an alternative to using circles in the Lagrange's projection by distortion analysis.

3.1 Lagrange's circular projection

This projection mentioned in the title is usually called the Lagrange's projection, however, after mathematician and astronomer Joseph Louis Lagrange (1736 in Turin – 1813 in Paris), who generalized Lambert's concept in 1779. Johann Heinrich Lambert, a Swiss polymath, was born in 1728 into a Huguenot family in the city Alsace, which is now in France. In 1772, Lambert published seven new map projections under the title *Notes and Comments on the Composition of*

Terrestrial and Celestial Maps. One of cartographic projections published by Lambert is now known as Lagrange's projection. [1]

The Lagrange's projection is sometimes classified as a polyconic. Outlines meridians are projected as the two arcs of circles. Parallels and other meridians are projected as arcs of circles (orthogonal in the intersection points). The geometric properties of Lagrange's projection are in the Fig. 5. This projection is also named the circular.

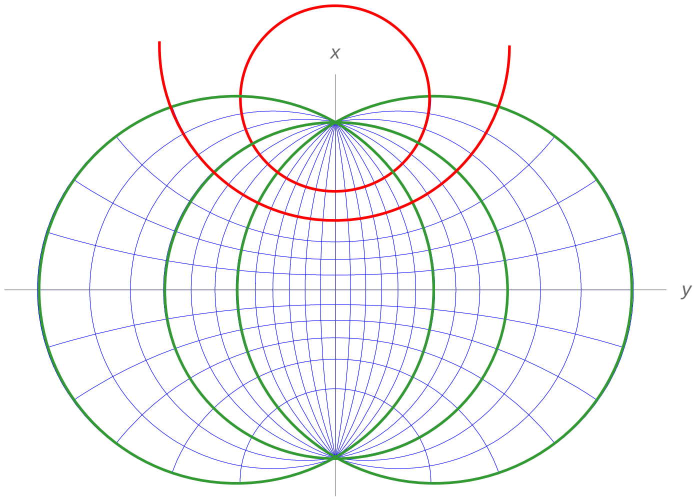

Fig. 5: Geometric properties of Lagrange's conformal projection

This type of projection belongs to a large group of orthogonal circular conformal projections. The map equations have the next form [1]:

$$x = \frac{R \sinh \dfrac{\ln \operatorname{tg}\left(\dfrac{U}{2}+\dfrac{\pi}{4}\right)}{n}}{\cosh \dfrac{\ln \operatorname{tg}\left(\dfrac{U}{2}+\dfrac{\pi}{4}\right)}{n} + \cos \dfrac{V}{n}}, \quad y = \frac{R \sin \dfrac{V}{n}}{\cosh \dfrac{\ln \operatorname{tg}\left(\dfrac{U}{2}+\dfrac{\pi}{4}\right)}{n} + \cos \dfrac{V}{n}}, \tag{4}$$

where R is radius of reference sphere, n is constant that defines variant of the Lagrange's projection. For stereographic azimuthal projection it holds: $n = 1$. In the case of $n = 2$ the entire Earth will appear in a circle with radius $4R$ (Fig. 6). However, this depiction does not give a good concept of the Earth, especially in the Polar Regions. If we want to preserve the correct ratio of the length of the Prime Meridian and the length of the Equator, we must choose a constant $n = 3/2$ (Fig. 7).

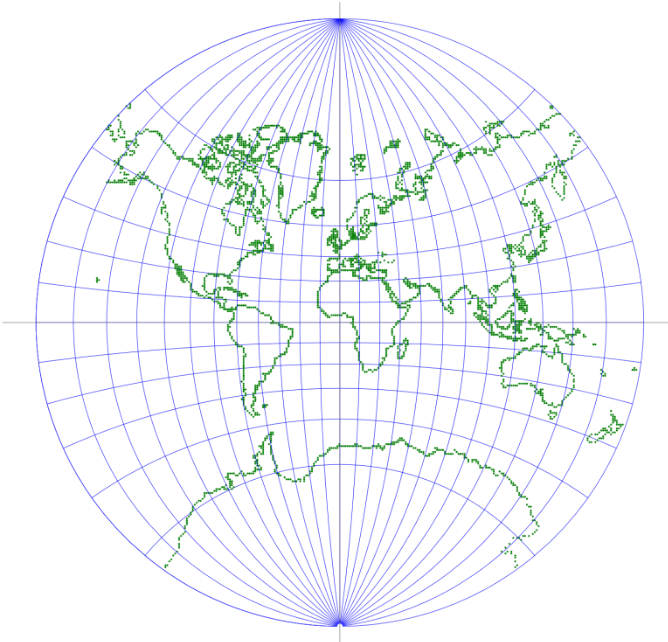

Fig. 6: Lagrange's conformal projection with n =2.

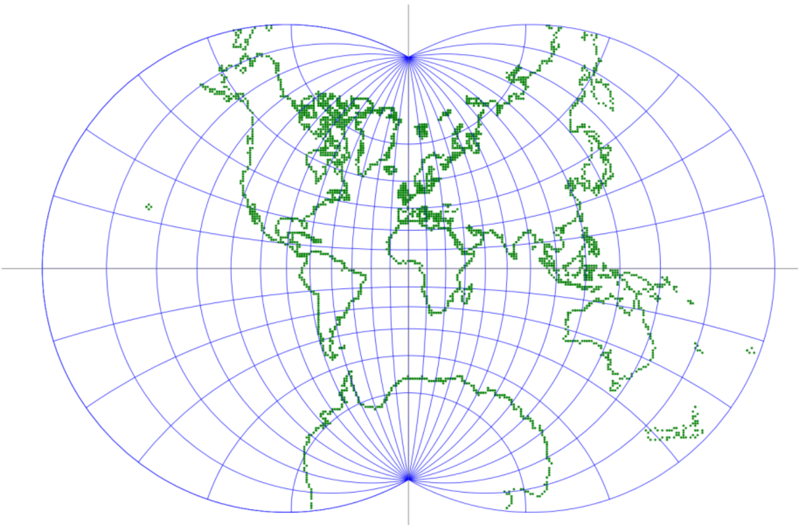

Fig. 7: Lagrange's conformal projection with n = 3/2.

3.2 August's epicycloidal projection

The author of mentioned map projection is Friedrich W. O. August, who was a German professor of mathematics as well as his father. He published in geometry and conformal mappings since his position at the Royal Bavarian Artillery and Engineering School. In the book *Research on the imaginaries in Geometry* he published an essay *„A conformal mapping of the Earth in epicycloidal projection"* in 1874 in Berlin. Here was also published the map *„Degree net of the whole earth in the epicycloidal projection designed by Dr. F. August"* (Fig. 8). Publisher of this map is Dietrich Reimer and the drawing is by Richard Kiepert. The main idea that he followed to the discovery of this type of projection, comes from his friend, Dr. G. Bellermann in Berlin, who has for some time been concerned with the idea of creating a conformal image of a sphere inside an epicycloid. [6] One of main advantages is that the shape of the curve maintained a particularly advantageous limit. August's projection belongs to non-classified cartographic projections and it is conformal.

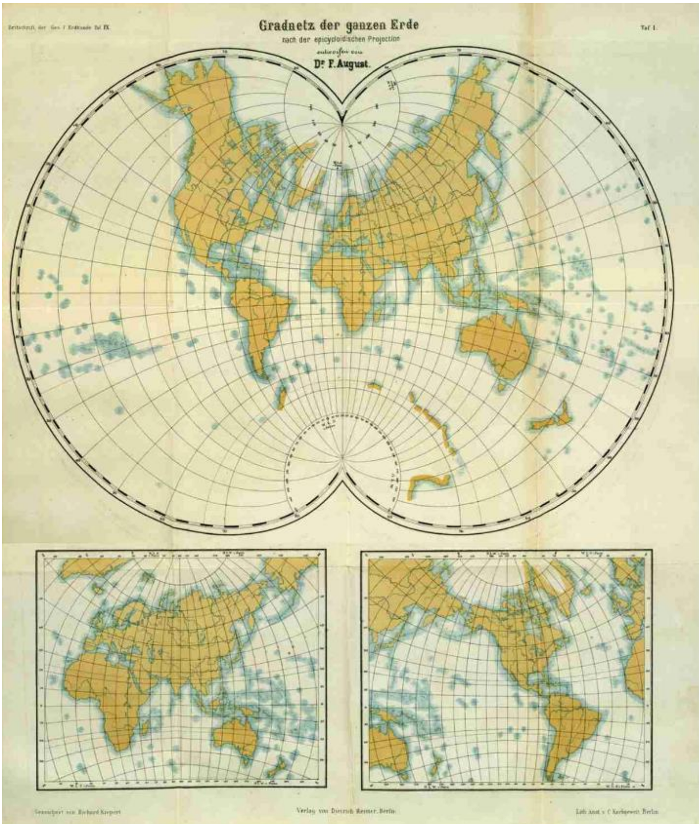

Fig. 8: Historical map in August's epicycloidal projection [6]

August's epicycloidal projection is a conformal, in which the geographic network is projected in epicycloid and evolvents. Outline meridians are projected as the two-cusped epicycloid called nephroid, its shape resembles the kidney. Parallels and other meridians are projected as the evolvents of the same type of epicycloids. Meridians have two real cuspidal points and parallels are without real cuspidal points. Analytically, the contour meridian image can be expressed from equations of epicycloid (nephroid):

$$x = \frac{3}{2} r \cos U - \frac{1}{2} r \cos 3U,$$
$$y = \frac{3}{2} r \sin U - \frac{1}{2} r \sin 3U, \text{ kde } r = \frac{\pi}{2} R. \tag{5}$$

where $U \in \langle -90°, 90° \rangle°$ is spherical latitude, R is radius of reference sphere. The map equations of August's epicycloidal projection are derived from Lagrange's projection, and then it holds:

$$X = \frac{\pi R}{4} y\left(3 + 3x^2 - y^2\right),$$
$$Y = \frac{\pi R}{4} x\left(3 + x^2 - 3y^2\right), \tag{6}$$

where R is radius of reference sphere, x and y are coordinates of the point in Lagrange's projection with map equations (4) with n = 2. The geographic network in August's projection is in the Fig. 9.

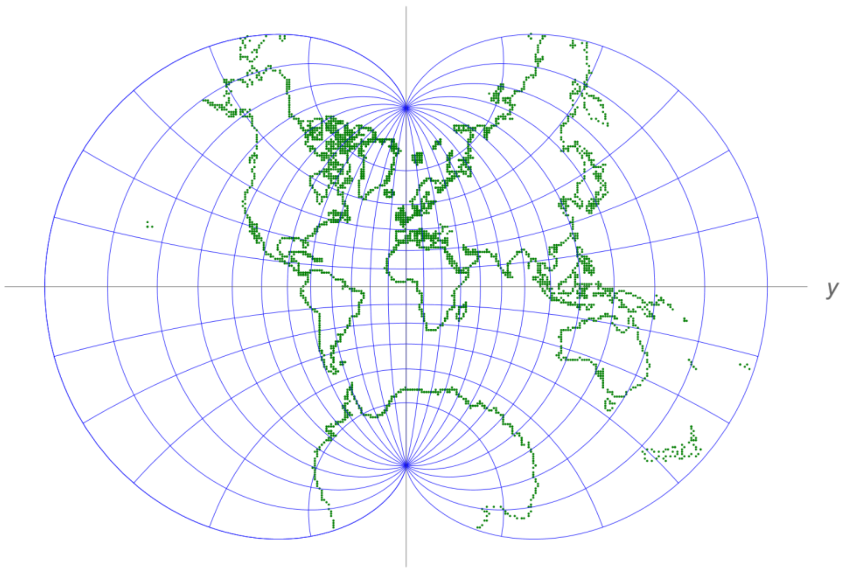

Fig. 9: Image of the geographic network in August's conformal epicycloid projection [5]

August's projection is relatively easy able to construct from stereographic conformal azimuthal projection in transversal position [4]. Point *P*, with spherical latitude *U* and spherical longitude *V*, we construct from stereographic conformal azimuthal projection of the point *Q*, its spherical longitude is *V*/2 and spherical latitude is *U**, where it holds:

$$\sin U^* = \operatorname{tg}\frac{U}{2}. \tag{7}$$

The process of constructing image of the point *P* is (Fig. 10):

1. Circle *k* with center *O* and radius *R* – stereographic projection of the meridian lied in plane parallel with plane of projection (P_N and P_S are North and South Pole, *AB* is horizontal diameter).
2. The point *C* on the circle *k* that the angle P_NOC are geographic longitude *V*.
3. The intersection of the chord P_NC with the diameter *AB* is the point *D*.
4. Circle *k′* with the center *D* passing through the poles P_N and P_S are stereographic projection of the meridian with spherical longitude *V*/2.
5. The point *E* on the circle *k*, while the angle $\measuredangle AOE$ are equal to the spherical latitude *U*.
6. The intersection of lines *AE* and P_NP_S is *F*, from which we construct the tangents *t* and *t′* to the circle *k*, where *T* and *T′* are the tangent points.
7. The circle *k′′* with the center *F* passing through the points *T* and *T′* is stereographic projection of the parallel with latitude *U** defined by (7).
8. Stereographic projection of the point *Q* (with spherical coordinates *U** and *V*/2) is *Q′* - the intersection of the circles *k′* (meridian) and *k′′* (parallel).
9. The point *K* on the line *OQ′* so that it holds: $|OK| = 3|OQ'|$.
10. In the point *K* we construct the line *p* so that its angle with line *OQ′* is 2α, where: $\alpha = \measuredangle P_NOQ'$.
11. The point *L* on the line P_NP_S: $|OL| = |OQ'|$.
12. The point *M* on the *AB*: $ML \perp BL$.
13. The point *N* on the P_NP_S: $MN \parallel BL$.
14. We construct the point *P′* on the line *p*: $|KP'| = |ON|$.

The point *P′* is image of the given point *P* in August's epicycloidal projection.

August's projection shows the characteristics of one of the approaches to mapping in 19th century. August's cartographic projection is just one of many conformal cartographic projections of that time, which is based on exact mathematical foundations, but it is not possible to determine type of used projection surface, and therefore we are talking about unclassified projection. Nevertheless, the authors of unclassified representations use geometric elements very widely on maps.

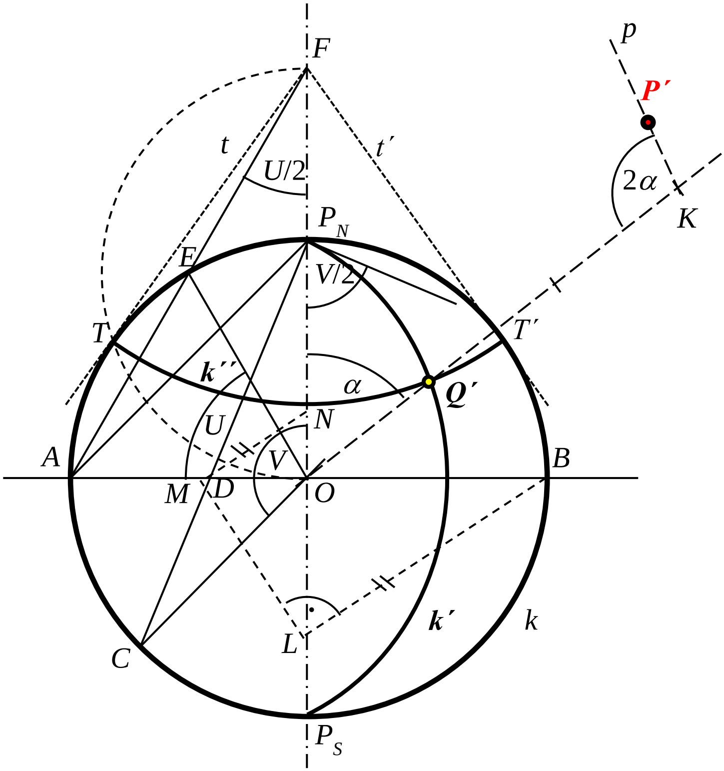

Fig. 10: The construction of a point in August's conformal epicycloidal projection [5]

3.3 Comparison of scale distortions in August's and in Lagrange's projection

The both of projections are conformal, therefore the angles are preserved and the scale distortions are independent to the azimuth.

In the Lagrange's projection, where image of the parallels and meridians are circles, after the calculation we expected values of scale distortion listed in the Table 2. The interval of scale distortion is from -685 m/km to 7309 m/km.

In the August's projection, where the parallels and meridians are epicycloids or evolvents of epicycloids, after the calculation we expected values of scale distortion listed in the Table 3. The interval of scale direction is from 0 m/km to 7000 m/km. It's follows that the use of epicycloids in August's projection has proved to be more effective.

	0°	10°	20°	30°	40°	50°	60°	70°	80°	90°
0°	-685	-684	-681	-676	-669	-660	-648	-633	-615	-593
10°	-680	-679	-676	-671	-664	-655	-643	-627	-609	-586
20°	-665	-664	-661	-656	-648	-638	-625	-610	-590	-567
30°	-637	-635	-632	-626	-618	-607	-594	-576	-555	-530
40°	-589	-588	-584	-578	-568	-556	-540	-521	-497	-468
50°	-510	-509	-504	-497	-486	-471	-452	-429	-401	-366
60°	-370	-369	-363	-353	-339	-320	-296	-266	-230	-185
70°	-80	-77	-68	-54	-33	-6	29	73	126	191
80°	813	818	835	863	904	958	1027	1113	1218	1346
90°	7049	7050	7053	7059	7066	7076	7087	7100	7115	7132
	100°	**110°**	**120°**	**130°**	**140°**	**150°**	**160°**	**170°**	**180°**	
0°	-566	-533	-494	-446	-387	-313	-221	-103	50	
10°	-559	-526	-486	-437	-377	-303	-209	-89	66	
20°	-538	-503	-461	-410	-347	-269	-171	-45	117	
30°	-499	-461	-416	-360	-292	-207	-100	36	212	
40°	-433	-391	-339	-276	-199	-103	17	171	371	
50°	-325	-274	-213	-138	-46	69	212	395	633	
60°	-132	-67	12	109	227	374	558	794	1100	
70°	270	365	480	621	794	1008	1278	1622	2070	
80°	1500	1688	1915	2192	2533	2956	3487	4165	5046	
90°	7149	7168	7187	7207	7228	7249	7269	7289	7309	

Table 2: Scale distortion of Lagrange's projection [m/km]

	0°	10°	20°	30°	40°	50°	60°	70°	80°	90°
0°	0	4	15	35	63	101	149	203	282	373
10°	11	16	30	42	75	116	162	222	298	388
20°	47	52	64	83	113	152	202	263	341	434
30°	112	116	129	151	186	221	274	339	419	517
40°	214	218	232	256	288	331	387	458	543	638
50°	371	377	390	416	453	501	564	638	730	844
60°	616	622	639	668	708	762	829	914	1019	1143
70°	1029	1035	1055	1089	1136	1197	1275	1374	1491	1632
80°	1859	1866	1890	1937	1985	2057	2149	2268	2395	2556
90°	7000									

	100°	110°	120°	130°	140°	150°	160°	170°	180°	
0°	482	615	778	976	1221	1524	1904	2386	3000	
10°	498	633	796	995	1243	1548	1929	2412	3030	
20°	547	687	822	1057	1302	1619	2008	2498	3124	
30°	635	778	952	1166	1426	1746	2146	2648	3287	
40°	772	924	1108	1333	1606	1941	2355	2875	3530	
50°	979	1143	1340	1579	1870	2225	2660	3169	3870	
60°	1294	1474	1689	1948	2259	2635	3091	3649	4333	
70°	1801	2000	2238	2518	2850	3246	3720	4284	4961	
80°	2741	2961	3212	3506	3845	4238	4691	5213	5816	
90°	7000									

Table 3: Scale distortion of August's projection [m/km]

4 Conclusions

In this paper we showed the variability and significance of using kinetic curves in cartographic projections and interconnection between cartographic projections. The aim of comparing the scale distortion was to show the advantages and disadvantages of using cycloids and epicycloids in mentioned cartographic projections. We compared using the cycloids in Jervis's projection with using circles in conical projection equidistant on the meridians. The use of epicycloids and evolvents in August's projection we compared with an alternative to using circles in the Lagrange's projection. The analysis of cartographic projections showed, that the use of cycloids and epicycloids in Jervis's and August's projection have proved to be more effective. Benefit of using the kinetic curve in cartographic projection is also from esthetic point of view.

Acknowledgements

The paper was supported by grant from Grant Agency VEGA no. 1/0682/16.

References

[1] AUGUST, F.: Concerning a Conformal Map of the Earth on the Epicycloidal Projection. *Zeitschrift der Gesellschaft für Erdkunde zu Berlin*. 1874, Volume 9, p. 1-22. ISSN 1614-2055 [in German]

[2] HOJOVEC, V et al.: *Cartography*. Praha: Institute of Geodesy and Cartography, 1987. pp. 434-435. ISBN 29-621-87. [in Czech]

[3] SYNDER, J. P.: *Flattening the Earth: Two Thousand Years of Map Projections*, University of Chicago Press, 1993, ISBN 978-0226767475, pp. 144 – 145

[4] SCHMID, E.: *World Maps on the August Epicycloidal Conformal Projection*: Technical Report NOS 63, Rockville: NOAA, 1974. 22 p.

[5] VAJSÁBLOVÁ, M.: Geometric and mathematic analyse of the map Bohemiae Rosa, Blaeu´s historical maps of 17th century and August´s projection. *G - Slovak journal on geometry and graphics*, 16. pp. 19-38. [in Slovak]

[6] http://www.digizeitschriften.de/dms/img/?PID=GDZPPN002854368 [Cited: July 21, 2019]

[7] https://gallica.bnf.fr/ark:/12148/btv1b8444245p/f1.item.zoom [Cited: June 13, 2019]

Studijní materiály v GeoGebře pro výuku pravoúhlé axonometrie

Study materials in GeoGebra for teaching orthogonal axonometry

Daniela Bímová, Petra Pirklová

Dept. of mathematics and didactics of mathematics,
Fac. of Science, Humanities and Education, Technical University of Liberec
Univerzitní náměstí 1410/1, 460 01 Liberec 1, Czech Republic
daniela.bimova@tul.cz, petra.pirklova@tul.cz

Abstract. Orthogonal axonometry is a kind of a parallel projection that is illustrative for displaying relatively small 3D objects. On the contrary, the principles of constructions in the orthogonal axonometry are more complicated in comparison with e. g. the Monge projection. There are some texts concerning the basic principles and properties of the orthogonal axonometry. These texts contain mostly the static black and white figures that are not enough helpful for the students which spatial imagination is not developed on sufficient level. Consequently, the study text, containing the basic principles, properties of the orthogonal axonometry, the coloured illustrative figures, and the corresponding figures in the version for anaglyphic glasses, was written. The coloured figures as well as the figures in the version for anaglyphic glasses were generated from the dynamic applets created in GeoGebra. Using the dynamic applets together with the study text seems to be very helpful for the students during their study.

Keywords: orthogonal axonometry, GeoGebra, GeoGebra book, dynamic applets, coloured illustrative figures, figures in the version for anaglyphic glasses

Klíčová slova: pravoúhlá axonometrie, GeoGebra, GeoGebra kniha, dynamické applety, barevné ilustrativní obrázky, obrázky ve verzi pro anaglyfické brýle

1 Úvod

Speciální případ rovnoběžného promítání – pravoúhlá axonometrie – je vyučován pro studenty dvou různých fakult Technické univerzity v Liberci, a to pro studenty Fakulty přírodovědně-humanitní a pedagogické (FP) v předmětu Geometrie 2 a pro studenty Fakulty umění a architektury (FUA) v předmětu Deskriptivní geometrie 1.

Existují knihy, např. [1] nebo [2], ve kterých jsou sepsány a vysvětleny základní principy a vlastnosti pravoúhlé axonometrie, zobrazování bodů, přímek, rovin, rovinných útvarů a základních těles, polohové úlohy v pravoúhlé axonometrii. Výklad i řešené příklady jsou v obou knihách doplněny o černobílé statické obrázky. Obzvláště v knize [1] se nacházejí především obrázky s finálními podobami konstrukcí, v případě složitějších konstrukcí jsou mnohdy téměř nepřehledné a některé dílčí konstrukce jsou v nich dokonce vynechány. Pro méně znalého čtenáře bývá vyhledávání jednotlivých kroků konstrukcí na základě uvedeného slovního komentáře problematické.

Z našich dosavadních zkušeností je zřejmé, že studenti s nižší úrovní prostorové představivosti mívají problémy jak s vyhledáváním jednotlivých kroků v černobílém obrázku výsledné konstrukce, tak i s vytvořením si představ prostorových situací při pohledu na dvojrozměrný obrázek zobrazený v pravoúhlé axonometrii. Za tímto účelem jsme pro studenty FP a FUA sepsaly studijní text vysvětlující základní principy a vlastnosti pravoúhlé axonometrie, popisující zobrazování bodů, přímek, rovin, rovinných útvarů a základních těles v pravoúhlé axonometrii a komentující řešení polohových úloh v pravoúhlé axonometrii. Studijní text jsme doplnily o barevné ilustrativní obrázky prostorových situací, dále o jim odpovídající konstrukce v pravoúhlé axonometrii. Přitom barevné ilustrativní obrázky prostorových situací vznikly z dynamických appletů vytvořených pro jednotlivé úlohy ve 3D okně programu GeoGebra. Současně byly také v programu GeoGebra pro většinu obrázků prostorových situací vygenerovány dynamické applety ve verzi pro anaglyfické brýle. Statické obrázky konstrukcí v pravoúhlé axonometrii vložené do studijního textu jsou výsledkem nastavení 3D okna v kolmém pohledu do axonometrické průmětny. Pro toto nastavení je užito předdefinovaného tlačítka.

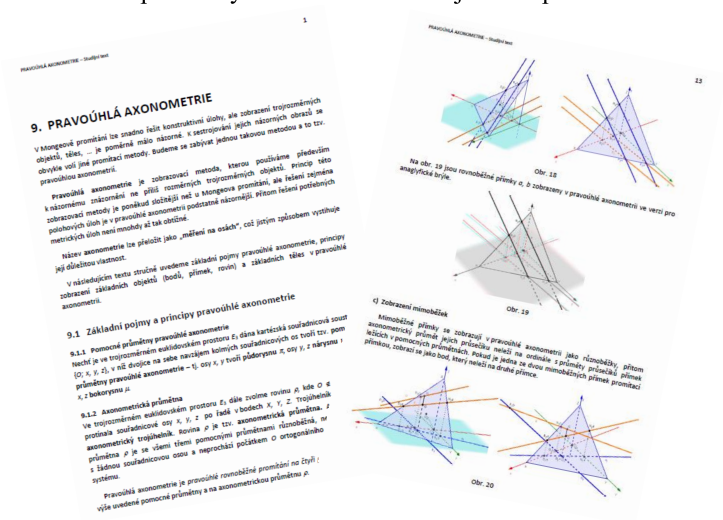

Obr. 1: Ukázka studijního textu

Z appletů v jejich původní dynamické podobě jsme vytvořily tzv. GeoGebra knihu s názvem „Pravoúhlá axonometrie“. A právě vytvořená GeoGebra kniha „Pravoúhlá axonometrie“ se jeví pro studenty vhodným pomocníkem při studiu tohoto promítání.

2 GeoGebra kniha „Pravoúhlá axonometrie“

GeoGebra kniha „Pravoúhlá axonometrie“ je oproti běžným tištěným knihám interaktivní knihou. Obsahuje devět kapitol, přičemž první kapitola je nazvána „Studijní text“. Jak sám název napovídá, v této kapitole je vložen sepsaný studijní text ve formátu pdf. Dále následuje osm kapitol obsahujících dynamické applety. Přitom se kapitoly vždy po dvou téměř shodují ve svých názvech, rozdíl je pouze ve slově anaglyf, a tedy také ve formátu vložených appletů. Kapitoly GeoGebra knihy odpovídají kapitolám uvedeným ve studijním textu a mají po řadě názvy „Základní pojmy a principy pravoúhlé axonometrie“, „Polohové úlohy“, „Zobrazení rovinných geometrických útvarů v pravoúhlé axonometrii“ a „Prostorové úlohy“.

2.1 Dvě verze GeoGebra knihy „Pravoúhlá axonometrie“

GeoGebra kniha „Pravoúhlá axonometrie“ byla vytvořena ve dvou verzích – ve verzi pro studenty, viz [3], a ve verzi pro učitele, viz [4]. Obě verze knih jsou obsahově totožné, tzn. jsou sestaveny z ekvivalentních kapitol, do kterých jsou vloženy analogické applety. Na obr. 2 viz titulní stranu GeoGebra knih.

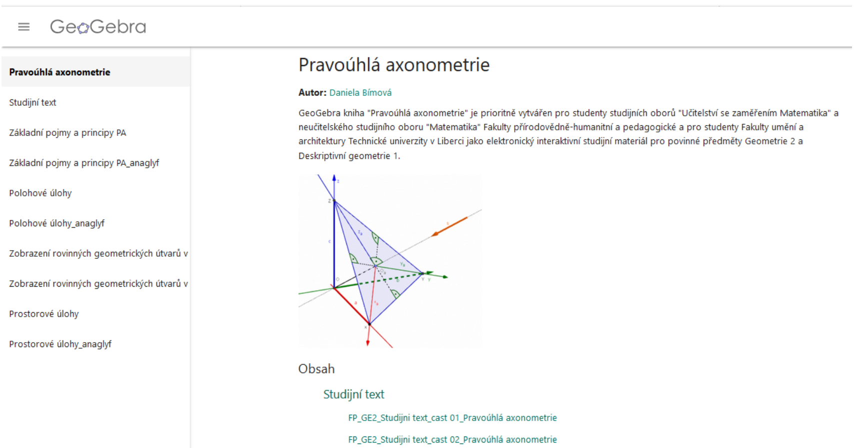

Obr. 2: Ukázka titulní strany GeoGebra knih

Obě verze GeoGebra knih se od sebe odlišují pouze applety u řešených příkladů. V GeoGebra knize ve verzi pro studenty jsou v případě řešených příkladů vloženy pouze texty zadání příkladů a jsou také zobrazena příslušná grafická zadání. Vzhledem ke skutečnosti, že je v současné době možné vkládat na webové stránky a v návaznosti tedy i do GeoGebra knih dynamické applety včetně zobrazení menu, panelu nástrojů, vstupního pole a formátovacího panelu programu GeoGebra, lze nechat studenty řešit příklady s užitím těchto zobrazených nástrojů přímo v předpřipravených appletech.

Na obr. 3 je zobrazen náhled dynamického appletu obsahujícího zadání příkladu sestrojení rovinného řezu hranolu v pravoúhlé axonometrii, který je vložen v kapitole „Prostorové úlohy“ v uvedené GeoGebra knize ve verzi pro studenty.

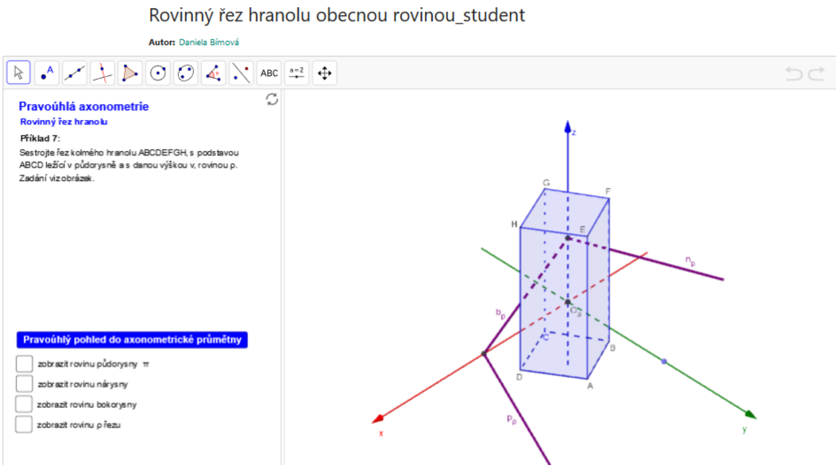

Obr. 3: Náhled dynamického appletu zadání příkladu vloženého v GeoGebra knize ve verzi pro studenty

V GeoGebra knize „Pravoúhlá axonometrie“ ve verzi pro učitele je v dynamických appletech příkladů kromě 2D nákresny obsahující texty zadání příkladů a 3D okna s grafickými zadáními, ale i řešeními příkladů zobrazena ještě druhá 2D nákresna, ve které je popsáno řešení příkladu. Řešení příkladu není po otevření appletu zobrazeno okamžitě. Je provázáno s posuvníkem pojmenovaným „krok“ a vloženým ve druhé 2D nákresně. Řešení je zpravidla popsáno krátkým slovním komentářem doplněným o symbolické zápisy konstrukcí. Řešení příkladu se nezobrazí celé najednou, ale objevuje se po jednotlivých krocích v závislosti na pohybování posuvníkem „krok“. V příslušných krocích se ve druhé 2D nákresně zobrazí buď slovní komentář, anebo odpovídající symbolický zápis konstrukce. Ve 3D okně programu se současně vykreslí právě konstruovaný objekt, resp. objekty.

Na obr. 4 je znázorněn náhled dynamického appletu obsahujícího část řešení příkladu sestrojení rovinného řezu hranolu v pravoúhlé axonometrii, vloženého do kapitoly „Prostorové úlohy“ v GeoGebra knize „Pravoúhlá axonometrie“ ve verzi pro učitele.

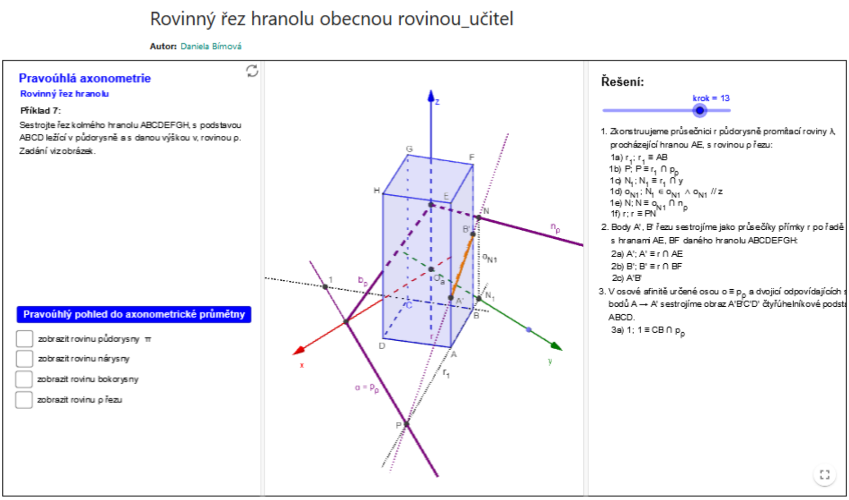

Obr. 4: Náhled dynamického appletu řešení příkladu vloženého v GeoGebra knize ve verzi pro učitele

2.2 Dynamické applety ve verzi pro anaglyfické brýle

Všechny čtyři výše vložené obrázky představují barevné ilustrativní obrázky prostorových situací. Byly vytvořeny ve 3D okně programu GeoGebra pomocí nástrojů pro 3D konstrukce. Aktivováním vložených tlačítek, jejichž funkce jsou předdefinovány příslušnými příkazy v záložce skriptování, je možné velmi snadno a rychle nechat program zobrazit prostorovou situaci v přednastavených úhlech pohledu, tj. v pravoúhlém pohledu do axonometrické průmětny a v rovnoběžném pohledu, který vhodně zobrazuje danou prostorovou situaci.

Pokud by si studenti při užití barevných dynamických ilustrativních obrázků ve 3D okně programu GeoGebra stále ještě nedokázali vytvořit představy daných prostorových situací a jim odpovídajících konstrukcí v pravoúhlé axonometrii, mohou ještě využít dalších verzí dynamických appletů, a to verzí pro tzv. anaglyfické brýle. Tyto verze byly vytvořeny pro většinu vyhotovených dynamických appletů. Všechny funkce a kroky v nich užité jsou shodné jako u appletů s barevnými dynamickými ilustrativními obrázky.

Na obr. 5 je znázorněn náhled dynamického appletu, odpovídajícího dynamickému appletu z obr. 4, ve verzi pro anaglyfické brýle.

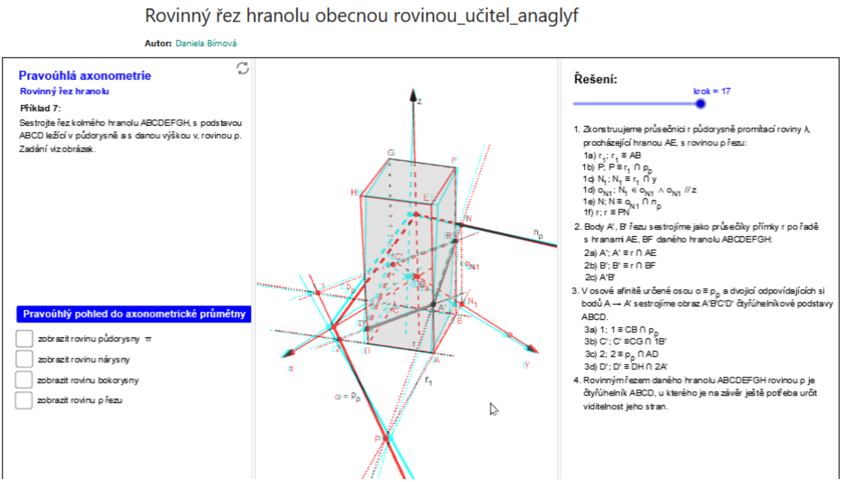

Obr. 5: Náhled dynamického appletu ve verzi pro anaglyfické brýle

3 Závěr

GeoGebra knihu s názvem „Pravoúhlá axonometrie“ jsme začaly s výhodou užívat při výuce kapitoly pravoúhlá axonometrie na FP a FUA. Studenti práci s GeoGebra knihou hodnotí velmi kladně. Do výuky si sami přinášejí elektronická zařízení (tablety, notebooky, …), během výkladu si místo nahlížení na statické obrázky ve studijním textu zobrazují příslušné prostorové situace v dynamických appletech GeoGebra knihy, což jim dle jejich slov pomáhá s vytvářením si představ prostorových situací, ale také s pochopením některých principů základních konstrukcí.

Poděkování

Tento článek vznikl za podpory Institucionálního plánu TUL pro rok 2019.

Literatura

[1] A. Urban: *Deskriptivní geometrie.* SNTL, Praha 1965.

[2] E. Pomykalová: *Deskriptivní geometrie pro střední školy*. Prometheus, Praha 2010. ISBN 978-80-7196-400-1

[3] https://www.geogebra.org/m/tf7gwvnp

[4] https://www.geogebra.org/m/xkd953yx

[5] D. Bímová, P. Pirklová: *Basic Principles of Orthogonal Axonometry with the Use of GeoGebra*. In Proceedings of the 17th Conference on Applied Mathematics - Aplimat 2018. Slovak University of Technology in Bratislava, SPEKTRUM STU. Bratislava 2018, pp. 86-96. ISBN 978-80-227-4765-3

Note on approximate symmetries of perturbed planar curves

Michal Bizzarri [a,1], **Miroslav Lávička** [b,a,2] **and Jan Vršek** [b,a,3]

[a] *NTIS – New Technologies for the Information Society, Faculty of Applied Sciences, University of West Bohemia, Univerzitní 8, 301 00 Plzeň, Czech Republic*

[b] *Department of Mathematics, Faculty of Applied Sciences, University of West Bohemia, Univerzitní 8, 301 00 Plzeň, Czech Republic*

[1]*bizzarri@ntis.zcu.cz,* [2]*lavicka@kma.zcu.cz,* [3]*vrsekjan@kma.zcu.cz*

Abstract. In this paper, we formulate a certain modification of the method for an approximate reconstruction of an inexact planar curve which is assumed to be a perturbation of some unknown planar symmetric curve. The input curve is given by a perturbed polynomial and the approach follows results from the recent paper [8]. The computation is presented on one particular example.

Keywords: Planar algebraic curves, symmetry detection, harmonic polynomials, Laplace operator, approximation

1 Introduction and motivation

This paper is devoted to the symmetries of planar curves. Being symmetric is a very useful feature which many real shapes possess and symmetries in the natural world has significantly inspired people when producing tools, buildings, artwork etc. One can find many papers devoted to the detection and computation of symmetries and some equivalences of curves, see e.g. [10, 9, 12, 11], or recent series of papers [1, 2, 3, 4, 5]. The problem of deterministically computing the symmetries of a given planar algebraic curve was recently studied in [6].

As already stated, many real world shapes exhibit a symmetry. However, in most cases this symmetry is not perfect but only approximate – which may happen, for instance, when some input error (or some error caused by numerical computations) occurs. And, of course, in this situations all subsequent exact algorithms and scenarios formulated for algebraic curves with symmetries fail.

Recently, see [8], we designed an algorithm for an approximate reconstruction of an inexact planar curve which is assumed to be a perturbation of some unknown planar curve. The initial step of the reconstruction algorithm is to find a suitable approximate centre of symmetry and a particular regular m-gon to whose group of symmetries the group of symmetries of the curve is isomorphic. In this paper, we modify the part devoted to finding the approximate centre of symmetry and present an alternative approach that more closely matches the original exact algorithm based on computing with Laplace operator.

2 Preliminaries

First we recall selected elementary notions, basic properties and suitable methods whose knowledge is further assumed.

2.1 Symmetric algebraic curves in plane

A *planar algebraic curve* $\mathcal{C}$ is a subset of $\mathbb{E}^2_{\mathbb{R}}$ defined as the the zeroset of a polynomial $f(x, y)$. We will assume that f has real coefficients, is irreducible over $\mathbb{C}$ and $\dim_{\mathbb{R}} \mathcal{C} = 1$. Any *isometry* $\phi \in \mathbf{Iso}_2$ of $\mathbb{E}^2_{\mathbb{R}}$ possesses the form $\mathbf{x} \mapsto A\mathbf{x} + \mathbf{b}$, where $A \in \mathbf{O}(\mathbb{R}, 2)$ and $\mathbf{b} \in \mathbb{R}^2$. For $\det(A) = 1$, or $= -1$ we speak about *direct*, or *indirect* isometries, respectively.

We write $\mathbf{Sym}(\mathcal{C})$ for the group of symmetries of the curve $\mathcal{C}$, i.e.,

$$\mathbf{Sym}(\mathcal{C}) := \{\phi \in \mathbf{Iso}_2;\ \phi(\mathcal{C}) = \mathcal{C}\}. \tag{1}$$

It is well known that $\mathbf{Sym}(\mathcal{C})$ is finite unless $\mathcal{C}$ is a union of parallel lines or a union of concentric circles. Moreover, if $\mathbf{Sym}(\mathcal{C})$ is finite then it is isomorphic to a subgroup of the group of symmetries of some regular m-gon, $m \leq \deg(\mathcal{C})$. In what follows we are interested solely in curves with a finite group of symmetries. The elements of a finite symmetry group are rotations (all of them with the same center) and reflections (axes of all of them passing through the same point).

We recall the following statement, which can be efficiently used to verify whether $\phi \in \mathbf{Sym}(\mathcal{C})$, see [7] for more details:

Proposition 2.1 *An isometry $\phi \in \mathbf{Sym}(\mathcal{C})$ if and only if $f(A\mathbf{x} + \mathbf{b}) = \lambda f(\mathbf{x})$, where $\lambda = 1$ or $\lambda = -1$.*

Then analogously to $\mathbf{Sym}(\mathcal{C})$ we can write that $\phi \in \mathbf{Sym}(f)$, as well.

2.2 Symmetries of planar curves via harmonic polynomials

We start with recalling the exact approach which has been formulated recently. For the sake of brevity we will mention only basic steps and a generic scenario; the reader who is more interested in this topic is kindly referred to [7], where all proofs and further explanations can be found.

In general, it is not easy to find symmetries ϕ belonging to $\mathbf{Sym}(\mathcal{C})$ directly and one has to apply a suitable computational approach – for instance to find some new polynomial $h(x, y)$ such that $\mathbf{Sym}(h)$ is finite, easy to determine (i.e., easier then $\mathbf{Sym}(f)$) and $\mathbf{Sym}(\mathcal{C}) = \mathbf{Sym}(f) \subset \mathbf{Sym}(h)$. In [7], a successive application of the Laplace operator yielding the sequence

$$f \longmapsto \triangle f \longmapsto \triangle^2 f \longmapsto \cdots \longmapsto \triangle^\ell f = h, \tag{2}$$

and followed by the associated chain of groups of symmetries

$$\mathbf{Sym}(f) \subset \mathbf{Sym}(\triangle f) \subset \mathbf{Sym}(\triangle^2 f) \subset \cdots \subset \mathbf{Sym}(\triangle^\ell f) = \mathbf{Sym}(h), \tag{3}$$

was efficiently used for finding such a polynomial h. Application of this technique is justified by the fact that the *Laplace operator* as a linear mapping

$\triangle : \mathbb{R}[x, y] \to \mathbb{R}[x, y]$ defined by

$$\triangle f = \frac{\partial^2 f}{\partial x^2} + \frac{\partial^2 f}{\partial y^2} \tag{4}$$

commutes with isometries, i.e., it holds

$$(\triangle f) \circ \phi = \triangle (f \circ \phi). \tag{5}$$

A polynomial h satisfying $\triangle h = 0$ is called *harmonic*. By repeatedly computing the Laplacian, cf. (2), in general we come down to either harmonic polynomials, or conic sections, or lines. All situations are discussed in the original paper, here we recall only the most interesting part, i.e., when one arrives at a harmonic polynomial h. We recall that if h is harmonic and $\deg(h) > 1$ then $\mathbf{Sym}(h)$ is finite.

Next, we identify $\mathbb{C}$ with $\mathbb{R}^2$ via $z = x + \mathrm{i}y \leftrightarrow (x, y)$. For a polynomial $h(x, y)$ we consider a complex function

$$g(x, y) = \partial_x h - \mathrm{i}\partial_y h, \tag{6}$$

where $\partial_x h, \partial_y h$ represent the partial derivatives of h with respect to x, y. The standard substitution

$$x = \frac{1}{2}(z + \overline{z}) \qquad \text{and} \qquad y = -\frac{\mathrm{i}}{2}(z - \overline{z}) \tag{7}$$

allows to write $g(x, y)$ as a complex function $g(z, \overline{z})$ in the complex variable z. Moreover, as h is harmonic then $g(x, y)$ satisfies the Cauchy-Riemann conditions and thus $g(x, y)$ is holomorphic and $g(z, \overline{z})$ does not depend on $\overline{z}$, i.e.,

$$g(z, \overline{z}) = g(z) = \sum_{j=0}^{\delta} b_j z^j. \tag{8}$$

The roots of $g(z)$ yield the singular points of the vector field $(\partial_x h, -\partial_y h)$. As any $\phi \in \mathbf{Sym}(h)$ maps real singular points of the considered vector field onto real singular points of this field, we finally obtain

$$\mathbf{Sym}(h) \subset \mathbf{Sym}(\Sigma), \tag{9}$$

where $\Sigma = \{\zeta_1, \ldots, \zeta_\delta\} \subset \mathbb{C}$ is the set of all roots of $g(z)$ (counted with multiplicity). Symmetries of $h(x, y)$ are then derived from Σ, resp. $g(z)$. For instance, a possible center of any rotational symmetry of $h(x, y)$ is encoded in the barycenter of Σ, i.e.,

$$\mathbf{p} = \frac{1}{\delta} \sum_{i=1}^{\delta} \zeta_i. \tag{10}$$

In addition, using Vieta's formulas on $g(z)$, one can see that the computation of the roots is not necessary and we obtain

$$\mathbf{p} = -\frac{b_{\delta-1}}{\delta b_\delta}. \tag{11}$$

Potential candidates for the rotation angle are of the type $\frac{2\pi}{m}$, where $m \leq \delta+1 = \deg(h)$.

Similarly, a method how to determine the potential axes of symmetry of $h(x, y)$ from the coefficients of $g(z)$ is also presented in [7].

3 Formulation of the problem and modified algorithm

In paper [7] exact symmetries of algebraic curves in plane were studied. Recently, this problem has been extended in [8] also to approximate symmetries. In latter case, the input to the algorithm is a planar curve $\mathcal{C}$ which is a perturbation of some unknown symmetric planar curve $\mathcal{C}_0$. This perturbed curve is described by a polynomial $f(x, y)$ of degree d, i.e.,

$$\mathcal{C} : f(x,y) = \sum_{\substack{i,j \geq 0 \\ i+j \leq d}}^{d} a_{i,j} x^i y^j = 0, \quad a_{ij} \in \mathbb{R}. \tag{12}$$

The perturbed curve $\mathcal{C}$ possesses no symmetries. Nonetheless, the original curve $\mathcal{C}_0$ was by assumption symmetric and thus using the exact approach, recalled in the previous section, one could arrive at a distinguished point $\mathbf{p}$ (a center of any possible rotation, or a point through which the axes of reflection are passing). The following strategy for approximate reconstruction of $\mathcal{C}_0$ was suggested in [8] (for more details see the original reference):

(a) Determine a point $\widetilde{\mathbf{p}}$ (the approximate center) and an integer m (the number of vertices of a regular polygon) from the known perturbed curve $\mathcal{C}$;

(b) Construct a new curve $\widetilde{\mathcal{C}}$ having the symmetry of an m-gon with the center at $\widetilde{\mathbf{p}}$ and being as close as possible to the given perturbed curve $\mathcal{C}$.

(c) Determine all the symmetries of the computed exact symmetric curve $\widetilde{\mathcal{C}}$ to obtain the approximate symmetries of the perturbed curve $\mathcal{C}$.

In this paper we focus on the crucial part of the algorithm and formulate an alternative approach for determining a suitable approximate center of symmetry $\widetilde{\mathbf{p}}$ of the resulting curve $\widetilde{\mathcal{C}}$, i.e., we will deal with step (a) only. Computing m is not part of this modified approach – one has to consider all m between 0 and $d-1$ and consequently choose the best approximation. The remaining parts of the original algorithm remain the same. Unlike in [8], we formulate the approach based on applying a sequence of Laplacians, see (2) – which was the method used originally in paper on exact symmetries, cf. [7]. From this reason we assume that the original symmetric curve $\mathcal{C}_0$ was transformable by the chain of Laplacians to a harmonic curve satisfying (2). As another new contribution, we solve the problem using complex variables.

First we substitute (7) into $f(x,y)$ and write the polynomial in the following matrix form

$$f(z,\bar{z}) = (1, z, z^2, \dots, z^d)\,\mathbf{M}\begin{pmatrix} 1 \\ \bar{z} \\ \bar{z}^2 \\ \vdots \\ \bar{z}^d \end{pmatrix}, \tag{13}$$

where $\mathbf{M}$ is a Hermitian matrix with a zero submatrix $\mathbf{0}_{(d-\ell)\times(d-\ell)}$, i.e.,

$$\mathbf{M} = \begin{pmatrix}
m_{0,0} & \overline{m}_{1,0} & \dots & \overline{m}_{\ell,0} & \overline{m}_{\ell+1,0} & \dots & \overline{m}_{k,0} & \overline{m}_{k+1,0} & \dots & \overline{m}_{d-1,0} & \overline{m}_{d,0} \\
m_{1,0} & m_{1,1} & \dots & \overline{m}_{\ell,1} & \overline{m}_{\ell+1,1} & \dots & \overline{m}_{k,1} & \overline{m}_{k+1,1} & \dots & \overline{m}_{d-1,1} & 0 \\
\vdots & \vdots & \ddots & \vdots & \vdots & & \vdots & \vdots & & \vdots & \vdots \\
m_{\ell,0} & m_{\ell,1} & \dots & m_{\ell,\ell} & \overline{m}_{\ell+1,\ell} & \dots & \overline{m}_{k,\ell} & 0 & \dots & 0 & 0 \\
m_{\ell+1,0} & m_{\ell+1,1} & \dots & m_{\ell+1,\ell} & 0 & \dots & 0 & 0 & \dots & 0 & 0 \\
m_{\ell+2,0} & m_{\ell+2,1} & \dots & m_{\ell+2,\ell} & 0 & \dots & 0 & 0 & \dots & 0 & 0 \\
\vdots & \vdots & \ddots & \vdots & \vdots & \ddots & \vdots & \vdots & \ddots & \vdots & \vdots \\
m_{k,0} & m_{k,1} & \dots & m_{k,\ell} & 0 & \dots & 0 & 0 & \dots & 0 & 0 \\
m_{k+1,0} & m_{k+1,1} & \dots & 0 & 0 & \dots & 0 & 0 & \dots & 0 & 0 \\
\vdots & \vdots & \ddots & \vdots & \vdots & \ddots & \vdots & \vdots & \ddots & \vdots & \vdots \\
m_{d-1,0} & m_{d-1,1} & \dots & 0 & 0 & \dots & 0 & 0 & \dots & 0 & 0 \\
m_{d,0} & 0 & \dots & 0 & 0 & \dots & 0 & 0 & \dots & 0 & 0
\end{pmatrix}.$$

It is well known that the Laplacian operator works in complex variables as

$$\triangle f(z,\bar{z}) = 4\frac{\partial}{\partial z}\frac{\partial f}{\partial \bar{z}}, \tag{14}$$

and therefore we obtain

$$\triangle f(z,\bar{z}) = (1, z, z^2, \dots, z^{d-2})\,\mathbf{M}_1\begin{pmatrix} 1 \\ \bar{z} \\ \bar{z}^2 \\ \vdots \\ \bar{z}^{d-2} \end{pmatrix}, \tag{15}$$

where $\mathbf{M}_1$ is of the form

$$\mathbf{M}_1 = 4\begin{pmatrix}
m_{1,1} & \dots & \ell\,\overline{m}_{\ell,1} & (\ell+1)\,\overline{m}_{\ell+1,1} & \dots & k\,\overline{m}_{k,1} & (k+1)\,\overline{m}_{k+1,1} & \dots & (d-1)\,\overline{m}_{d-1,1} \\
\vdots & \ddots & \vdots & \vdots & & \vdots & \vdots & & \vdots \\
\ell\, m_{\ell,1} & \dots & \ell^2\, m_{\ell,\ell} & \ell(\ell+1)\,\overline{m}_{\ell+1,\ell} & \dots & \ell k\,\overline{m}_{k,\ell} & 0 & \dots & 0 \\
(\ell+1)\, m_{\ell+1,0} & \dots & (\ell+1)\ell\, m_{\ell+1,\ell} & 0 & \dots & 0 & 0 & \dots & 0 \\
\vdots & \ddots & \vdots & \vdots & \ddots & \vdots & \vdots & \ddots & \vdots \\
k\, m_{k,0} & \dots & k\ell\, m_{k,\ell} & 0 & \dots & 0 & 0 & \dots & 0 \\
(k+1)\, m_{k+1,0} & \dots & 0 & 0 & \dots & 0 & 0 & \dots & 0 \\
\vdots & \ddots & \vdots & \vdots & \ddots & \vdots & \vdots & \ddots & \vdots \\
(d-1)\, m_{d-1,0} & \dots & 0 & 0 & \dots & 0 & 0 & \dots & 0
\end{pmatrix}.$$

Hence, the chain of Laplacians (2) can be replaced by the chain of matrices

$$\mathbf{M} \longmapsto \mathbf{M}_1 \longmapsto \mathbf{M}_2 \longmapsto \cdots \longmapsto \mathbf{M}_\ell, \tag{16}$$

where the matrix $\mathbf{M}_\ell$ of a harmonic polynomial of degree $k-\ell$ has the form

$$\mathbf{M}_\ell = 4^\ell \ell^2 \begin{pmatrix} \binom{\ell}{\ell} m_{\ell,\ell} & \binom{\ell+1}{\ell} \overline{m}_{\ell+1,\ell} & \dots & \binom{k}{\ell} \overline{m}_{k,\ell} & 0 & \dots & 0 \\ \binom{\ell+1}{\ell} m_{\ell+1,\ell} & 0 & \dots & 0 & 0 & \dots & 0 \\ \vdots & \vdots & \ddots & \vdots & \vdots & \ddots & \vdots \\ \binom{k}{\ell} m_{k,\ell} & 0 & \dots & 0 & 0 & \dots & 0 \\ 0 & 0 & \dots & 0 & 0 & \dots & 0 \\ \vdots & \vdots & \ddots & \vdots & \vdots & \ddots & \vdots \\ 0 & 0 & \dots & 0 & 0 & \dots & 0 \end{pmatrix}.$$

Let us recall that it was assumed that the sequence is ending with a harmonic polynomial. Then it is evident that the harmonic polynomial $h = \triangle^\ell f$ in the chain (including the values of k, ℓ) can be easily identified from the position of the block of zeros in the original matrix $\mathbf{M}$. Moreover, we will see that the center can be decoded from the matrix $\mathbf{M}$, as well.

Following the previous approach we write polynomial (8) associated to the harmonic polynomial h given by the matrix $\mathbf{M}_\ell$. It holds

$$\frac{\partial h}{\partial z} = \frac{1}{2}\left(\partial_x h - \mathrm{i}\partial_y h\right), \tag{17}$$

and thus we obtain

$$g(z) = 2\frac{\partial h}{\partial z} = 2 \cdot 4^\ell \ell^2 \sum_{i=0}^{k-\ell-1} (i+1)\binom{i+\ell+1}{\ell} m_{i+\ell+1,\ell} z^i. \tag{18}$$

Finally using expression (11) we arrive at the center of symmetry of the curve $\mathcal{C}$

$$\mathbf{p} = \frac{-1}{k-\ell-1} \cdot \frac{(k-\ell-1)\binom{k-1}{\ell} m_{k-1,\ell}}{(k-\ell)\binom{k}{\ell} m_{k,\ell}} = -\frac{m_{k-1,\ell}}{k\, m_{k,\ell}}. \tag{19}$$

Next we consider a perturbation of the original symmetric curve. This influences also the matrix $\mathbf{M}$ which contains a block of “almost zeros”, now. Our goal is to identify this almost-zero-submatrix and set it as zero matrix. This yields a new curve $\widehat{\mathcal{C}}$ described by the equation

$$\widehat{\mathcal{C}} : (1, z, z^2, \dots, z^d) \begin{pmatrix} m_{0,0} & \dots & \overline{m}_{\ell,0} & \dots \\ \vdots & \ddots & \vdots & \ddots \\ m_{\ell,0} & \dots & m_{\ell,\ell} & \dots \\ \vdots & \ddots & \vdots & 0 \end{pmatrix} \begin{pmatrix} 1 \\ \overline{z} \\ \overline{z}^2 \\ \vdots \\ \overline{z}^d \end{pmatrix} = 0. \tag{20}$$

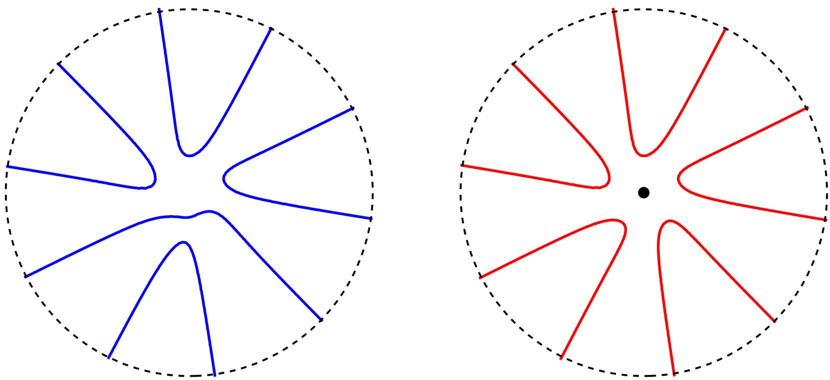

Fig. 1: Left: A perturbation of an symmetric curve. Right: The closest symmetric curve with the guessed center of symmetry from Example 3.2.

Then we continue as in the exact case, determine the point (19) and set it as the approximate center $\widetilde{\mathbf{p}}$.

Moreover, the previous result implies that the perturbation of the center is not worsen by applying the sequence of Laplacians and it respects the order of perturbation of the coefficients of the original curve. For this purpose, we recall some details dealing with the error propagation during computing with inexact quantities. Consider $A = a + \alpha$, $B = b + \beta$, where $\alpha \ll a$, $\beta \ll b$ and $|\alpha| \leq \epsilon$, $|\beta| \leq \epsilon$. Then it holds

$$\left| \frac{A}{B} - \frac{a}{b} \right| \lesssim \frac{(a+b)\epsilon}{b^2} \tag{21}$$

and we can formulate.

Lemma 3.1 *For the error ϵ_1 of the centre of the symmetric curve whose coefficients are given with maximal error ϵ it holds*

$$\epsilon_1 \lesssim \frac{(m_{k_1,\ell} + m_{k,l})\epsilon}{k^2 m_{k,\ell}^2}. \tag{22}$$

The next step of the reconstruction algorithm is to find a suitable symmetric curve $\widetilde{\mathcal{C}}$ sufficiently "close" to the given perturbed curve $\mathcal{C}$ when the center $\widetilde{\mathbf{p}}$ of $\widetilde{\mathcal{C}}$ is prescribed. From this part, we may follow the approach designed in [8]. In particular, we construct a basis of all curves of degree d with the rotational symmetry of m-gon and with the center of rotation $\widetilde{\mathbf{p}}$, and compute the orthogonal projection of the perturbed cubic to the space spanned by the spanned basis, see for more details [8].

Example 3.2 Consider a curve $\mathcal{C}$ given by a polynomial with floating coefficients (which is a perturbation of an unknown symmetric curve), see Fig. 1, left.

$$\begin{aligned} f = {} & 1.9x^7 + 10.x^6y + 10.x^6 - 17.9x^5y^2 - 35.9x^5y - 20.1x^5 - 10.1x^4y^3 - 30.1x^4y^2 \\ & - 20.x^4y + 0.1x^4 - 9.9x^3y^4 - 39.9x^3y^3 - 40.1x^3y^2 + 0.1x^3y + 10.x^3 - 18.1x^2y^5y^3 \\ & - 90.1x^2y^4 - 199.9x^2 - 239.9x^2y^2 - 149.9x^2y - 40.x^2 + 10.1xy^6 + 60.1xy^5 + 140.1xy^4 \\ & + 159.9xy^3 + 90.xy^2 + 20.xy + 0.1x + 1.9y^7 + 14.y^6 + 44.1y^5 + 80.y^4 + 89.9y^3 + 60.1y^2 + 19.9y \end{aligned}$$

First, we transform f into the complex representation, cf. (7), and use the matrix form (13) – for the sake of compactness we display the coefficients of the matrices with three decimal places only.

$$\mathbf{M} = \begin{pmatrix} 0 & 0.05+9.95\mathrm{i} & -25.025+5.\mathrm{i} & -10.-29.975\mathrm{i} & 20.-9.988\mathrm{i} & 5.003+7\mathrm{i} & -1.+1.002\mathrm{i} & -0.002+0.001\mathrm{i} \\ 0.05-9.95\mathrm{i} & 10.05 & 15.+14.975\mathrm{i} & -19.975+20\mathrm{i} & -15.022-15.012\mathrm{i} & 6.006-6\mathrm{i} & 0.995+0.998\mathrm{i} & 0 \\ -25.025-5.\mathrm{i} & 15.-14.975\mathrm{i} & 0.05 & -0.031+0.038\mathrm{i} & 0.+0.02\mathrm{i} & -0.027+0.013\mathrm{i} & 0 & 0 \\ -10.+29.975\mathrm{i} & -19.975-20\mathrm{i} & -0.031-0.038\mathrm{i} & -0.012 & -0.017-0.034\mathrm{i} & 0 & 0 & 0 \\ 20.+9.988\mathrm{i} & -15.022+15.012\mathrm{i} & 0.-0.02\mathrm{i} & -0.017+0.034\mathrm{i} & 0 & 0 & 0 & 0 \\ 5.003-7.\mathrm{i} & 6.006+6.\mathrm{i} & -0.027-0.013\mathrm{i} & 0 & 0 & 0 & 0 & 0 \\ -1.-1.002\mathrm{i} & 0.995-0.998\mathrm{i} & 0 & 0 & 0 & 0 & 0 & 0 \\ -0.002-0.001\mathrm{i} & 0 & 0 & 0 & 0 & 0 & 0 & 0 \end{pmatrix}.$$

Next, we find the maximal almost-zero-submatrix in $\mathbf{M}$ and create a new one with this submatrix being exactly-zero.

$$\begin{pmatrix} 0 & 0.05+9.95\mathrm{i} & -25.025+5\mathrm{i} & -10.-29.975\mathrm{i} & 20.-9.988\mathrm{i} & 5.003+7\mathrm{i} & -1.+1.002\mathrm{i} & -0.002+0.001\mathrm{i} \\ 0.05-9.95\mathrm{i} & 10.05 & 15.+14.975\mathrm{i} & -19.975+20\mathrm{i} & -15.022-15.012\mathrm{i} & 6.006-6\mathrm{i} & 0.995+0.998\mathrm{i} & 0 \\ -25.025-5\mathrm{i} & 15.-14.975\mathrm{i} & 0 & 0 & 0 & 0 & 0 & 0 \\ -10.+29.975\mathrm{i} & -19.975-20\mathrm{i} & 0 & 0 & 0 & 0 & 0 & 0 \\ 20.+9.988\mathrm{i} & -15.022+15.012\mathrm{i} & 0 & 0 & 0 & 0 & 0 & 0 \\ 5.003-7\mathrm{i} & 6.006+6\mathrm{i} & 0 & 0 & 0 & 0 & 0 & 0 \\ -1.-1.002\mathrm{i} & 0.995-0.998\mathrm{i} & 0 & 0 & 0 & 0 & 0 & 0 \\ -0.002-0.001\mathrm{i} & 0 & 0 & 0 & 0 & 0 & 0 & 0 \end{pmatrix}.$$

Hence we have $\ell = 1$ and $k = 6$ and using (19) we obtain an approximate center of symmetry

$$\mathbf{p} \doteq (-0.00069, -1.00405). \tag{23}$$

Then projecting subsequently $\mathcal{C}$ to all curves with the symmetry of m-gon with the center $\mathbf{p}$, where $m \in \{2, \ldots, 6\}$, we obtain the best solution for $m = 5$, see Fig. 1, right.

4 Conclusion

In this paper, we formulated a possible modification of the recently designed algorithm for an approximate reconstruction of a planar curve which is assumed to be a perturbation of some unknown symmetric planar curve. We focused mainly on the initial step of the original algorithm which lies in determining a suitable approximate centre of symmetry and a particular regular m-gon to whose group of symmetries the group of symmetries of the curve is isomorphic. The method suitably uses, as the algorithm for the exact case, the sequence of Laplacians. The functionality of the designed scenario was presented on one example.

Acknowledgments

The authors were supported by the project LO1506 of the Czech Ministry of Education, Youth and Sports.

References

[1] J. G. ALCÁZAR, *Efficient detection of symmetries of polynomially parametrized curves*, Journal of Computational and Applied Mathematics, 255 (2014), pp. 715 – 724.

[2] J. G. ALCÁZAR, C. HERMOSO, AND G. MUNTINGH, *Detecting similarity of rational plane curves*, Journal of Computational and Applied Mathematics, 269 (2014), pp. 1 – 13.

[3] ——, *Detecting symmetries of rational plane and space curves*, Computer Aided Geometric Design, 31 (2014), pp. 199 – 209.

[4] ——, *Symmetry detection of rational space curves from their curvature and torsion*, Computer Aided Geometric Design, 33 (2015), pp. 51 – 65.

[5] ——, *Similarity detection of rational space curves*, Journal of Symbolic Computation, 85 (2018), pp. 4 – 24. 41th International Symposium on Symbolic and Algebraic Computation (ISSAC'16).

[6] J. G. ALCÁZAR, M. LÁVIČKA, AND J. VRŠEK, *Symmetries and similarities of planar algebraic curves using harmonic polynomials*, ArXiv e-prints, (2018).

[7] ——, *Symmetries and similarities of planar algebraic curves using harmonic polynomials*, Journal of Computational and Applied Mathematics, 357 (2019), pp. 302–318.

[8] M. BIZZARRI, M. LÁVIČKA, AND J. VRŠEK, *Approximate symmetries of planar algebraic curves with inexact input*, Computer Aided Geometric Design (to appear), (2019).

[9] P. Brass and C. Knauer, *Testing congruence and symmetry for general 3-dimensional objects*, Computational Geometry, 27 (2004), pp. 3 – 11. Computational Geometry - EWCG'02.

[10] Z. Huang and F. S. Cohen, *Affine-invariant b-spline moments for curve matching*, in 1994 Proceedings of IEEE Conference on Computer Vision and Pattern Recognition, Jun 1994, pp. 490–495.

[11] P. Lebmeir, *Feature detection for real plane algebraic curves*, PhD thesis, Technische Universität München, 2009.

[12] P. Lebmeir and J. Richter-Gebert, *Rotations, translations and symmetry detection for complexified curves*, Computer Aided Geometric Design, 25 (2008), pp. 707 – 719. Classical Techniques for Applied Geometry.

[13] L. Robbiano and J. Abbott, eds., *Approximate Commutative Algebra*, Texts & Monographs in Symbolic Computation, Springer-Verlag Wien, 2010.

Focal curve and its properties

Jiří Blažek, Pavel Pech

Faculty of Education, University of South Bohemia
České Budějovice, Czech Republic
blazej02@pf.jcu.cz, pech@pf.jcu.cz

Abstract. In a plane a complete quadrilateral $ABCDEF$ is given. Consider a set of conics tangent to the lines of the quadrilateral. Locus of conics foci is denoted as a focal curve. This article deals with some properties of this curve.

Keywords: Complete quadrilateral, focal curve, conics.

1 Introduction

In a plane a complete quadrilateral $ABCDEF$ is given. Consider a set of conics tangent to the lines of the quadrilateral. Locus of conics foci represents a focal curve. This article deals with some properties of this curve. First mentions about a focal curve (FC) turned up in articles of H. Schröter [5] (1872), H. Durège [3] (1872), and again H. Schröter [6] (1873). The approach of these articles to the curve is projective, approach in this article is more elementary, see also [1], [2].

2 Properties of the focal curve

Let $ABCD$ be a quadrilateral and let there exist intersections of the lines $(AB, CD) = F$ and $(BC, DA) = E$. A necessary and sufficient condition for a point F_1 to be a focus of a conic tangent to the quadrilateral $ABCD$ is, that the feet K, L, M, N of perpendiculars dropped from the point F_1 to the lines AB, BC, CD and DA lie on a circle or a line (the case of a parabola). It is obvious that intersections A, B, C, D, E, F of the side lines of $ABCD$ lie on the focal curve (FC), Fig. 1. It can be shown, that if

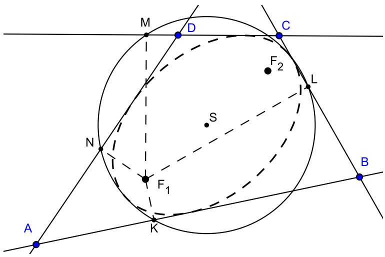

Fig. 1: Points F_1, F_2 and A, B, C, D, E, F lie on the focal curve

the feet K, L, M, N of perpendiculars dropped from the point F_1 lie on a circle with centre S, the same holds for a point F_2, the image of reflection of the point F_1 in the point S. Hence the points F_1, F_2 belong to the same conic. The condition of concyclicity of the points K, L, M, N states the following theorem.

Theorem 1: Feet of perpendiculars dropped from the point F_1 to the sides of the quadrilateral lie on a circle if and only if the opposite sides of the quadrilateral (for example AD and BC) subtend the same oriented angle from the point F_1 (for example $\angle DF_1A + \angle BF_1C = 0 \equiv \bmod 180°$).

Proof: Considerations are based on Fig. 2. There are several cyclic quadrilaterals and hence:

$$\angle NMF_1 = \angle NDF_1 = \alpha$$

$$\angle NAF_1 = \angle NKF_1 = \gamma$$

$$\angle LCF_1 = \angle LMF_1 = \beta$$

$$\angle LBF_1 = \angle LKF_1 = \delta.$$

Further:

$$\angle DF_1A = 180° - \alpha - \gamma$$

$$\angle CF_1B = 180° - \beta - \delta.$$

Since the quadrilateral $KLMN$ is cyclic, we can write:

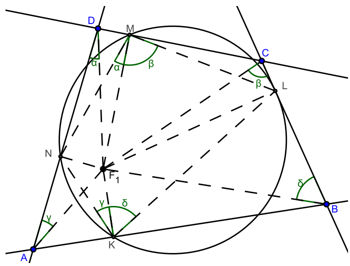

Fig. 2: AD and BC subtend the same oriented angle from the point F_1

$$\alpha + \beta + \gamma + \delta = 180° = 0 \equiv \bmod 180°.$$

Now, let us consider the sum

$$= \angle DF_1A + \angle BF_1C = 180° - \alpha - \gamma + 180 - \beta - \delta =$$

$$360° - (\alpha + \beta + \gamma + \delta) = 180° = 0 \equiv \bmod 180°.$$

Although the considerations were based on a particular figure, the theorem can be easily generalized for an arbitrary point F_1, Fig. 2.

Corollary 1: In complex coordinates $A = a_1 + ia_2$, $B = b_1 + ib_2$, $C = c_1 + ic_2$, $D = d_1 + id_2$, $X = x + iy$ it is possible to express the condition for a point X to be a focus of a conic

$$\angle DXA + \angle BXC = 0 \equiv \text{mod } 180^\circ$$

by the equation

$$\mathrm{Im}\{\overline{(A - X)} \cdot (B - X) \cdot \overline{(C - X)} \cdot (D - X)\} = 0. \tag{1}$$

This is the equation of the *focal curve.*

Corollary 2: The equation (1) is the third degree polynomial equation.

Theorem 2: Let us choose two arbitrary conics tangent to the quadrilateral $ABCD$. Denote P_1, P_2 the foci of the first conic and F_1, F_2 the foci of the second one. Then the focal curve of the quadrilateral $P_1F_1P_2F_2$ is identical with focal curve of the quadrilateral $ABCD$. Further, all pairs of foci of conics tangent to the quadrilateral $ABCD$ are identical with pairs of foci of conics tangent to the quadrilateral $P_1F_1P_2F_2$.

Proof: Consider foci F_1, F_2 of a conic tangent to the quadrilateral $ABCD$. Due to the Second Poncelet theorem, the following equality holds

$$\angle DAF_1 + \angle BAF_2 = 0 \equiv \text{mod } 180^\circ.$$

Then, the Theorem 1 implies that the point A is a focus of a conic tangent to the quadrilateral F_1BF_2D.

This fact is generalized in the following Lemma.

Lemma: If the points F_1, F_2 are foci of a conic tangent to a quadrilateral $ABCD$, then the points A, C are foci of a conic tangent to the quadrilateral F_1BF_2D. We express it by symbolic notation

$$(F_1F_2) \in FC(ABCD) \Leftrightarrow (AC) \in FC(F_1BF_2D),$$

where FC means a focal curve.

Returning back to the proof of the Theorem 2, it is sufficient to show that the theorem holds for an arbitrary quadrilateral F_1BF_2D. Since

$$FC(ABCD) = FC(F_1BF_2D) = FC(F_1P_1F_2P_2)$$

the general theorem follows from the transitivity. The focal curve $FC(ABCD)$ determined by the quadrilateral $ABCD$ is passing through all six vertices of the complete quadrilateral $ABCDEF$. By the assumption it is passing through the foci F_1, F_2. Let us denote by P_1,

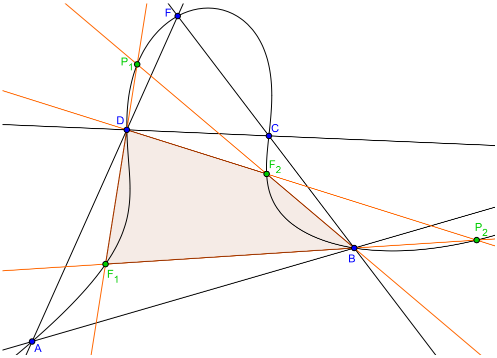

Fig. 3: $FC(ABCD)$ coincides with $FC(F_1BF_2D)$

P_2 the two remaining vertices of the complete quadrilateral F_1BF_2D. We will prove that these vertices are foci of a conic, like F_1, F_2, which is tangent to the quadrilateral $ABCD$. By the Lemma it holds

$$(F_1F_2) \in FC(ABCD) \;\Rightarrow\; (AC) \in FC(F_1BF_2D). \tag{2}$$

However it is possible to express the quadrilateral F_1BF_2D as P_1BP_2D and apply the Lemma again

$$(AC) \in FC(P_1BP_2D) \;\Rightarrow\; (P_1P_2) \in FC(ABCD).$$

Hence, on the curve $FC(ABCD)$ there lie the following 10 points $A, B, C, D, E, F, P_1, P_2, F_1, F_2$.
Now let us turn our attention to the curve $FC(F_1BF_2D)$. By (2) it follows that the points A, C are foci of a conic tangent to the quadrilateral F_1BF_2D. This is completely analogical to the preceding situation. We can directly conclude that on the curve $FC(F_1BF_2D)$ there lie 10 points $A, B, C, D, E, F, P_1, P_2, F_1, F_2$.
The curves $FC(ABCD)$ and $FC(F_1BF_2D)$ have 10 points in common and since a cubic curve is uniquely determined by 9 points then the curves are identical.
We have proved that if a point L_1 is a focus in a case of the quadrilateral $ABCD$, then it is a focus in the case of the quadrilateral F_1BF_2D as well. Now, our aim is to prove that the pairs (L_1, L_2) of foci of a conic are identical in both cases.
Let one focus L_1 and the quadrilaterals $ABCD$ and F_1BF_2D be given. Denote by L_2 or L_2' the second focus of the conic tangent to the quadrilateral $ABCD$ or F_1BF_2D. It follows from the Second Poncelet Theorem

(see [4], Theorem 2.2.4, p.42) that the angle bisector of L_1BL_2 is identical with the angle bisector of ABC, which is identical with angle bisector of F_1BF_2 and which is identical with angle bisector of L_1BL_2'. Hence, the points B, L_2', L_2 are collinear. If we apply the same consideration on the point D, we arrive at the conclusion that the points D, L_2', L_2 are collinear. Thus $L_2' = L_2$ and the proof of the theorem is completed.

Theorem 3: Let us select an arbitrary point P_1 on FC and an arbitrary pair of foci F_1, F_2. Then the angle bisector of the angle F_1PF_2 is common for all pairs F_1, F_2 on FC.

Proof: Consider a quadrilateral AP_1CP_2. Then, according to Theorem 2, the points F_1, F_2 are foci of a conic tangent to AP_1CP_2. From the Poncelet theorem the angle bisector of $\angle F_1P_1F_2$ is identical with the angle bisector of $\angle AP_1C$, which does not depend on a particular choice of F_1F_2, Fig. 4.

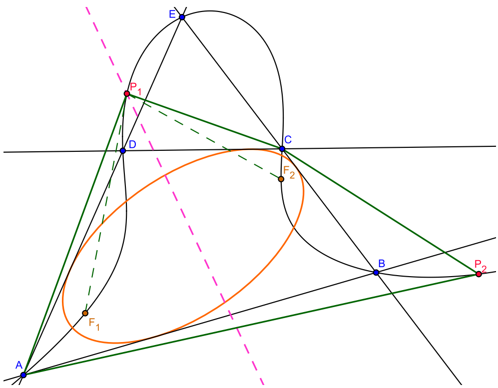

Fig. 4: Angle bisector of F_1PF_2 is common to all pairs F_1, F_2 on FC.

Theorem 4: Let F_1, F_2 and P_1, P_2 be two arbitrary pairs of foci. Then the tangent to their FC at P_1 is symmetric to the line P_1P_2 with respect to the angle bisector of $\angle F_1P_1F_2$.

Proof: According to the Theorem 3 the angle bisector of $\angle F_1P_1F_2$ is independent on the particular choice of F_1, F_2. Consider the limit case $F_2 \to P_2$. Then the angle bisector of $P_1F_1P_2$ is identical with the angle bisector of "angle" $P_1P_1P_2$, where the "line" P_1P_1, is the tangent at P_1 Fig. 5.

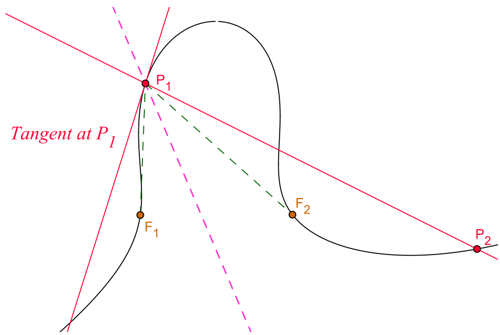

Fig. 5: Construction of a tangent at the point P_1

Theorem 5: The centres of conics tangent to a quadrilateral lie on a line (so called Newton-Gauss line).

Proof: A parabola which is tangent to a quadrilateral $ABCD$ has one focus P_I at infinity. On the basis of the concept of limit, let us consider the angle bisector of "angle" $F_1P_IF_2$. The angle bisector is

- parallel to the parabolas axis,
- passing through the centre of the segment F_1F_2,
- common for all pairs foci of the focal curve (Theorem 3).

From this the Theorem 5 follows.

References

[1] J. Blažek, P. Pech: *Locus Computation in Dynamic Geometry Environment.* Mathematics in Computer Science 13(1-2), 2018, 31-40.

[2] J. Blažek, P. Pech: *On one locus in the plane.* Advances in Intelligent Systems and Computing 809, 2019, 184-196.

[3] H. Durège: *Über die Curve 3-ter Ordnung, welche den geometrischen Ort der Brennpunkte einer Kegelschnittschaar bildet.* Mathematische Annalen, Bd. 5 (1872), 83 - 94.

[4] G. Glaeser, H. Stachel, B. Odehnal: *The Universe of Conics.* Springer, Berlin, Heidelberg, 2016.

[5] H. Schröter: *Über eine besondere Curve 3-ter Ordnung und eine einfache Erzeugungsart der allgemeinen Curve 3-ter Ordnung.* Mathematische Annalen, Bd. 5 (1872), 50 - 82.

[6] H. Schröter: *Über Curven dritter Ordnung.* Mathematische Annalen, Bd. 6 (1873), 85 - 111.

Topografické plochy v GeoGebra

Topographic surfaces in GeoGebra

Jana Bulantová, Alžběta Lachová

Fakulta stavební, Vysoké učení technické v Brně
Veveří 331/95, Brno, Česká Republika
bulantova.j@fce.vutbr.cz

Abstract. The paper presents new material for students created in GeoGebra. These GeoGebra Applets deal with Topographic surfaces.

Keywords: GeoGebra, Topography

Klíčová slova: GeoGebra, Topografické plochy

1 Úvod

V tomto příspěvku chceme seznámit s novými výukovými materiály pro předmět Konstruktivní geometrie na FAST VUT v Brně. Jedná se o sbírku řešených příkladů na téma Topografické plochy, vytvořených v programu GeoGebra. Příklady je možno najít zde: https://math.fce.vutbr.cz/studium.php

2 Topografické plochy – úvod do problému

Ve stavební praxi se setkáváme s problémem, jak propojit stavební objekt s terénem. Jako zjednodušený obraz zemského povrchu (terénu) využíváme topografické plochy – terén je znázorněn vrstevnicemi. Vrstevnice jsou obecné křivky. V případě, že terén si lze zjednodušeně představit jako rovinu, jsou vrstevnice přímky. Základna stavebního objektu je útvar, který leží ve vodorovné nebo šikmé rovině. Rovinu základny pak pomocí výkopových či násypových rovin předem daného spádu spojujeme s topografickou plochou a sestrojujeme průsečnice výkopových a násypových rovin s topografickou plochou.

2.1 Typy příkladů, které jsme řešili

Všechny vyřešené příklady jsou shrnuty do knihy v GeoGebra. Stručný přehled příkladů, které jsme řešili:

1. vodorovná + šikmá cesta, vrstevnice křivky
2. kruhové hřiště, vrstevnice přímky
3. vodorovná cesta + parkoviště, vrstevnice přímky
4. vodorovná plošina, vrstevnice křivky
5. kruhové hřiště + šikmá cesta, vrstevnice křivky

6. plošina + vodorovná cesta, vrstevnice křivky
7. plošina + klesající cesta, vrstevnice křivky
8. plošina + vodorovná cesta +šikmá cesta, vrstevnice přímky
9. křižovatka, vrstevnice křivky

Obr. 1: Kniha v GeoGebra

2.2 Krokování konstrukce

Příklady jsme řešili v programu GeoGebra. Velkou výhodou GeoGebry je možnost rozdělit výslednou konstrukci do několika kroků a jednotlivé dílčí konstrukce zobrazovat postupně pomocí nástroje posuvník. Pro studenty je takto vyřešený příklad přehlednější a snadněji pochopitelný. Pro lepší orientaci v dílčích konstrukcích jsme také využili dynamické barvy – konstrukce, která se v daném kroku objevuje, je provedena červenou barvou (jak ukazuje obrázek na následující straně) a)

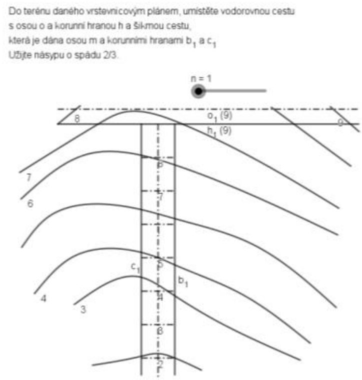

b)

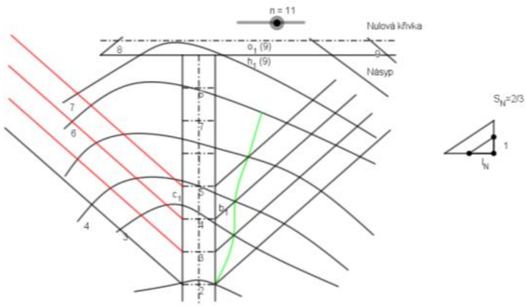

c)

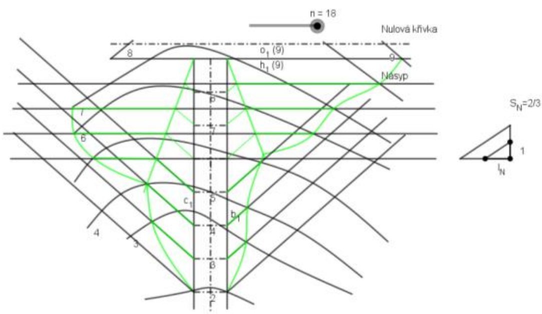

Obr. 2: Vodorovná a klesající cesta

a) zadání b) jeden z kroků konstrukce c) výsledek

2.3 Další možnosti GeoGebry

Kromě krokované konstrukce je možné v GeoGebře sestrojit prostorový obrázek, který lze otáčet. Pochopení daného problému je tak ještě názornější a jednodušší. Toho bychom chtěli využít při tvorbě dalších materiálů.

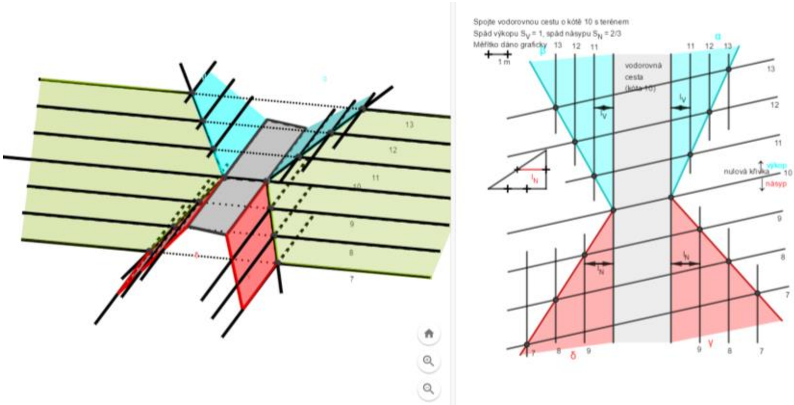

Obr. 3: Vodorovná cesta (řešení a prostorový obrázek v GeoGebra)

3 Závěr

Příspěvek ukazuje možnosti využití programu GeoGebra pro tvorbu výukových materiálů, které používáme při výuce Konstruktivní geometrie na FAST VUT v Brně. Tyto materiály jsou dostupné na stránkách našeho ústavu a mohou je tedy využít i studenti nebo vyučující na jiných školách.

Literatura

[1] URL: http://www.geogebra.com

Řešení historických geometrických úloh pomocí počítače – Trisektorie J. R. Vaňause

Solving of historical geometric problems using computer – Trisectrix by J. R. Vaňaus

Roman Hašek

Jihočeská univerzita v Českých Budějovicích, Pedagogická fakulta
Jeronýmova 10, 371 15 České Budějovice, Česká republika
hasek@pf.jcu.cz

Abstrakt. The paper is based on the contribution to the GeoGebra workshop, part of the Slovak-Czech conference on geometry and graphics. Its aim is to introduce the use of GeoGebra, the free dynamic software for teaching and learning mathematics, to bring a historical mathematical topic into the classroom in a beneficial way. We will particularly deal with a method of the use of an oblique strophoid to trisect an angle, discovered in the second half of the 19th century by the Czech grammar school mathematics teacher Josef Rudolf Vaňaus.

Keywords: Trisection, strophoid, GeoGebra, locus of points.

Klíčová slova: Trisekce, strofoida, GeoGebra, množina bodů.

1 Úvod

Příspěvek je inspirován dvěma příspěvky Josefa Rudolfa Vaňause, profesora na gymnáziu v Jičíně, mimo jiné jednoho ze zakladatelů *Jednoty českých matematiků a fyziků*, které publikoval v *Časopise pro pěstování mathematiky a fysiky*; článkem o využití šikmé strofoidy k trisekci úhlu [6] a zadáním geometrické úlohy pro čtenáře tohoto časopisu [7]. Obsahy příspěvků jsou představeny s využitím volně dostupného programu pro studium a výuku matematiky GeoGebra (www.geogebra.org), s ohledem na možné použití ve výuce matematiky.

Josef Rudolf Vaňaus, narozený 2. května 1839 v Komárově u Soběslavi, patřil mezi čtyři studenty Karlo-Ferdinandovy univerzity v Praze, kteří ustavením *Spolku pro volné přednášky z mathematiky a fysiky* v roce 1862 položili základy dnešní *Jednoty českých matematiků a fyziků.* Většinu své kariéry působil jako profesor matematiky na gymnáziu v Jičíně. Zemřel 16. ledna 1910 v Praze. Svými články nebo zadáními úloh pro čtenáře přispíval do *Časopisu pro pěstování mathematiky a fysiky* [1], který *Jednota* vydávala v letech 1872 až 1950.

Cílem článku je představit, jak může být současná interpretace historického tématu za použití vhodného software, konkrétně programu GeoGebra, použita ve výuce matematiky. Jeho dalším, neméně významným, cílem je připomenutí osobnosti Josefa Rudolfa Vaňause, výrazné postavy historie české matematiky, od jehož narození letos uplynulo 180 let.

2 Úloha 36

V roce 1902 byla v sekci úloh k samostatnému řešení 3. čísla *Časopisu pro pěstování mathematiky a fysiky* uvedena pod číslem 36 následující úloha zadaná J. R. Vaňausem: „Poloměrem AB opsány jsou z bodů A, B kruhové oblouky protínající se v bodě C. Ustanoviti jest v oblouku AC bod M a v oblouku BC bod N tak, aby MN bylo rovnoběžno k AB, a úhel MAN aby rovnal se danému ostrému úhlu“, [7], viz Obr. 1.

V pátém čísle téhož ročníku časopisu byli uveřejněni tři úspěšní řešitelé; Bohuslav Hostinský, Karel Rychlík a Bohuslav Závada, studenti středních škol ve věku mezi 12 a 17 lety, viz [8]. Sluší se poznamenat, že se jednalo o tři budoucí výrazné osobnosti našeho národa. Všichni došli k závěru, že cesta k řešení úlohy vede přes trisekci úhlu. Všichni také věděli, že tato úloha není eukleidovsky sestrojitelná. Hostinský se Závadou tím svá řešení skončili, Rychlík ještě rozpracoval provedení trisekce pomocí hyperboly. K poznatku o nutnosti uplatnění trisekce se každý ze studentů dopracoval jedním ze dvou postupů lišících se od sebe pouze označením pro řešení rozhodujících úhlů, viz Obr. 1. V postupu na Obr. 1 vlevo vede k cíli se-

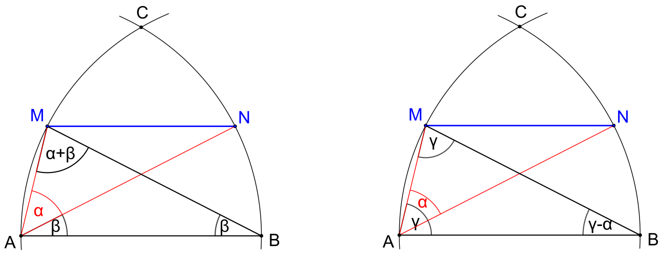

Obr. 1: Úloha 36; dva přístupy k jejímu řešení

strojení úhlu $\beta = \angle BAN$. Z obrázku zřejmým způsobem vyplývá, že pro jeho velikost platí $\beta = 60^\circ - \frac{2}{3}\alpha$. V případě zachyceném na obrázku vpravo jde o úhel $\gamma = \angle BAM$, pro který platí $\gamma = 60^\circ + \frac{1}{3}\alpha$. Po představení úspěšných řešení je na str. 474 časopisu uvedena následující redakční poznámka: „Úloha jest stupně třetího; rozdělení úhlu na 3 stejné díly nelze – jak známo – vykonati přesnou geometrickou konstrukcí užívající pouze přímek a kružnic. K účelu tomu vymyšleny byly též rozmanité křivky vyšších stupňů; o jedné z nich pojednává prof. Dr. Josef Vaňaus v článku Trisektorie (tohoto Časopisu ročník X. str. 153). Viz též Lošťák, Příspěvek ku trisekci úhlu (Časopis, ročník XIV., str. 38)“, [8]. Vaňaus v uvedeném článku navrhuje k trisekci úhlu využít algebraickou křivku třetího stupně, nyní známou jako šikmá strofoida [5]. Jedná se o zcela originální postup, který ani dnes, téměř 140 let po publikování Vaňausova článku, nepatří mezi obecně známé metody, viz např. [4]. Lošťák použil křivku, která byla afinní s Descartovým listem, křivkou, jejíž využití k trisekci úhlu bylo v té době již známo. Touto rovněž pozoruhodnou metodou se zde ale zabývat nebudeme. Za zmínku však určitě stojí skutečnost, že J. Lošťák byl též již od roku 1862 činný ve *Spolku pro volné přednášky z mathematiky a fysiky*.

Než se začneme věnovat Vaňausově metodě trisekce, pojďme se podívat, jak může být postup řešení úlohy 36 ovlivněn použitím dynamického geo-

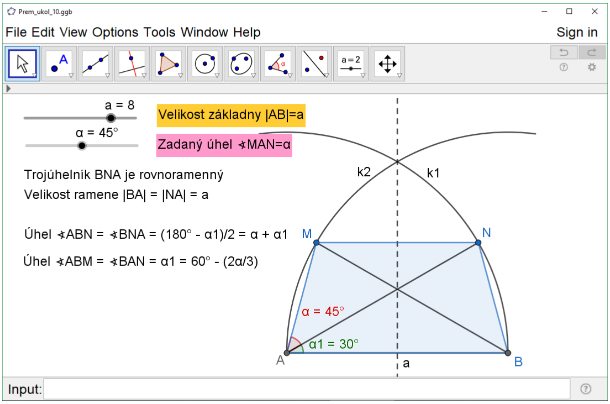

Obr. 2: Dynamický náčrtek řešení Úlohy 36

metrického software, v našem případě GeoGebry. Na Obr. 2 vidíme náhled materiálu, kterým doprovodila své řešení jedna studentka Pedagogické fakulty JU. Úlohu vyřešila analogicky s výše uvedenými postupy dobových úspěšných řešitelů, GeoGebru pak využila k vytvoření dynamické ilustrace svého řešení.

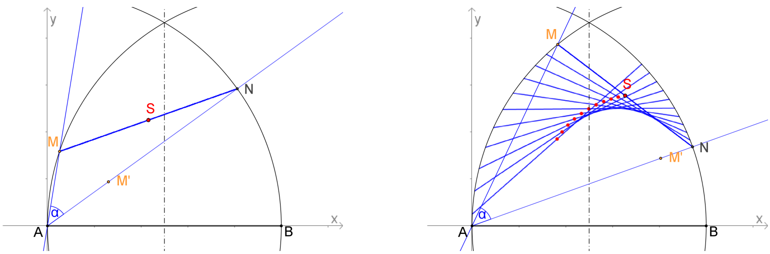

Obr. 3: Dynamické geometrické řešení Úlohy 36

Obr. 3 pak přináší ilustrace ryze dynamického přístupu k řešení úlohy, který těží z možností dynamického geometrického software. Zde je cílem nalezení společného bodu množiny středů S příček MN, které jsou z bodu A vidět pod úhlem α, a osy úsečky AB. Tato „dynamická“ interpretace úlohy 36 okamžitě indukuje otázku na podobu množiny středů uvedené příčky. Jak vypadá křivka, jejíž částí tato množina je? Jakou má rovnici?

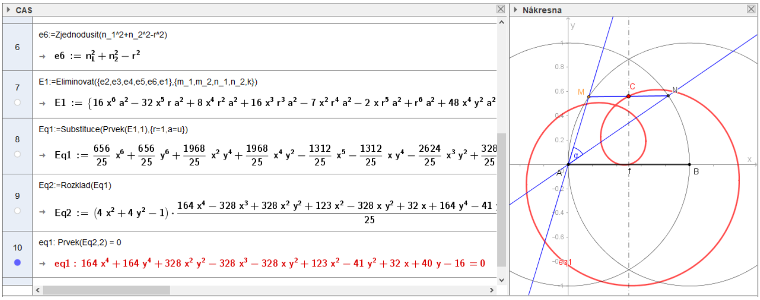

Obr. 4: Množina středů příčky MN užitím nástrojů symbolické algebry a dynamické geometrie programu GeoGebra

Na tyto otázky lze snadno odpovědět při využití kombinace nástrojů GeoGebry pro dynamickou geometrii a symbolickou algebru, z nichž oceníme především funkce `Eliminovat` a `Rozklad` pro řešení a úpravy příslušné soustavy polynomických rovnic. Jak vidíme na Obr. 4, vyšetřovanou křivkou je tzv. Pascalova závitnice, též zvaná limacon [3].

3 Trisektorie J. R. Vaňause

J. R. Vaňaus se ve svém článku [6] věnoval zevrubnému zkoumání algebraických křivek 3. stupně, které jsou dány rovnicí ve tvaru $Ax^3 + By^3 + Cxy^2 + Dyx^2 + Ex^2 + Fy^2 + Gxy = 0$. Všímá si zvláštní jednoduchosti tvarů této křivky, které dostává pro určité vztahy koeficientů A, B, C, D, E, F, G za podmínky, že $A = C, B = 1$ a $E = -F$. Dostává se tím ke křivce, kterou dnes nazýváme šikmá strofoida. Vaňaus ovšem ve svém článku tento pojem nepoužívá. Protože odhalí možnost využití křivky pro trisekci úhlu, nazývá jí *trisektorie* a definuje ji následujícím způsobem jako množinu bodů dané vlastnosti, viz Obr. 5: *Opišme libovolným poloměrem r kružnici a veďme průměr OA. První bod průměru O budiž počátkem souřadnic pravoúhlých a OA osou úseček. Bodem A veďme v libovolném úhlu α k ose X nakloněnou sečnu. Paprsky z bodu O k sečně vedené protínají kružnici. Jeden z nich budiž OB, jenž protíná kružnici v bodu D. Přenesme pokaždé úsek paprsku mezi kružnicí a sečnou na druhou stranu příslušného paprsku, tedy učiňme $DM = DB$. Bod M jest bodem trisektorie, anať souvislost všech takto utvořených geometrických míst podává tuto křivku.*

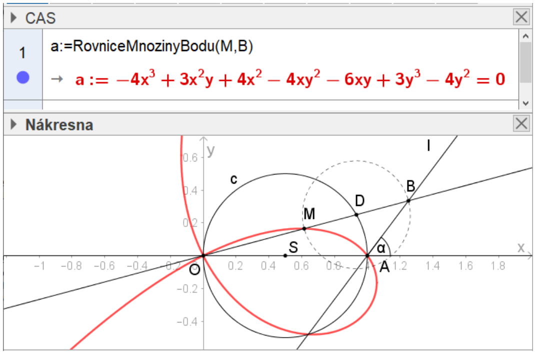

Obr. 5: Šikmá strofoida – Vaňausova trisektorie a výpočet její rovnice v GeoGebře zadáním příkazu `RovniceMnozinyBodu(M,B)`

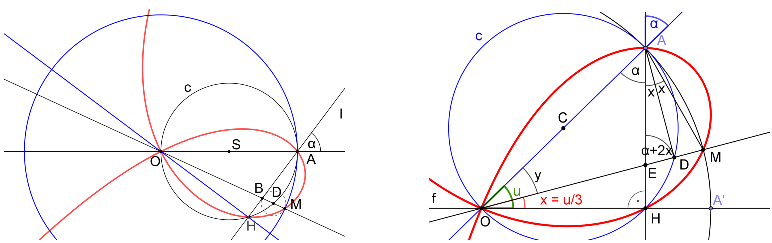

Obr. 6: Trisekce úhlu strofoidou

Rovnice Vaňausovy trisektorie (tj. šikmé strofoidy) je $a(y^2(2r+x) - x^2(2r-x)) = y(y^2+x^2-4rx)$, kde $a = \tan\alpha$. Výpočet rovnice pomocí funkce `RovniceMnozinyBodu` programu GeoGebra pro konkrétní hodnoty parametrů r, a je zaznamenán na Obr. 5. Užití této křivky k trisekci úhlu, popsané Vaňausem, je přímým důsledkem uvedené definice. Ukážeme si to pomocí dvou nákresů na Obr. 6. Obrázek vlevo nám poskytuje celkový pohled, korespondující s Obr. 5, kterým jsme předmětnou definici ilustrovali. Ten vpravo potom přináší detailní popis prvků, které Vaňaus použil k důkazu svého tvrzení. Metoda trisekce „jeho“ křivkou je založena na skutečnosti, že úhel $\angle HOM$ je třetinou úhlu $\angle HOA$. Důkaz plyne z Obr. 6, vpravo. Ze skutečnosti, že velikost vnějšího úhlu trojúhelníku je rovna součtu jeho protilehlých vnitřních úhlů, je totiž zřejmé, že $\alpha + 2x = \alpha + y$, tj. $y = 2x$. Protože úhel u je roven součtu $x + y$, je zřejmé, že $x = \frac{1}{3}u$.

4 Závěr

Je velmi pravděpodobné, že představená metoda trisekce úhlu užitím šikmé strofoidy je jedinečným Vaňausovým poznatkem. Z pohledu dnešní geometrie se ale nejedná o žádný průlomový objev. Jinak tomu ale může být z hlediska výuky matematiky. Takovéto časem zaváté poznatky, spojené s výraznými osobnostmi z historie matematiky a založené na znalostech elementární matematiky, mohou, vhodně uchopeny, například pomocí matematického software, přinést do výuky novou aplikaci školní matematiky, spojenou se zajímavým příběhem a mnohdy také s novými „objevy". S některými historickými úlohami mohou být navíc spojeny dosud nevyřešené otázky, jako je tomu i v tomto případě. V závěru článku [6] Vaňaus uvádí, že se mu podařilo sestavit „přístroj zcela jednoduchý" s jehož pomocí lze výše popsanou trisekci realizovat. Tento přístroj, třeba jenom v podobě náčrtku, se ale nezachoval. Jak asi vypadal? Dovedli bychom sami navrhnout takový přístroj? A třeba vytisknout na 3D tiskárně? To vše nám současné digitální technologie dovolují. Stačí mít jenom nápad. Nevypadal Vaňausův přístroj třeba takto: [2]? Je však tento model opravdu „zcela jednoduchý"?

Literatura

[1] *Časopis pro pěstování mathematiky a fysiky.* JČMF, Praha, 1872-1950. Dostupné z `https://dml.cz/handle/10338.dmlcz/133460`

[2] R. Hašek: *Possible Vaňaus' trisector* GeoGebra online material. [cit. 18. 10. 2019] Dostupné z `https://www.geogebra.org/m/jdafysqv`

[3] Limacon In *Wikipedia; The Free Encyclopedia*[online] [cit. 25. 10. 2019] Dostupné z `https://en.wikipedia.org/wiki/Lima%C3%A7on`

[4] J. Lošťák: Příspěvek ku trisekci úhlu. *Časopis pro pěstování mathematiky a fysiky*, Vol. 14 (1885), No. 1. JČMF, Praha, str. 38-42. Dostupné z: `https://dml.cz/handle/10338.dmlcz/122760`

[5] H. Stachel: Strophoids, a family of cubic curves with remarkable properties. *Journal of industrial design and engineering graphics*, Volume 10, ICEGD, June 2015.

[6] J. R. Vaňaus: Trisektorie. *Časopis pro pěstování mathematiky a fysiky*, Vol. 10 (1881), No. 3. JČMF, Praha, str. 153-159. Dostupné z: `https://dml.cz/handle/10338.dmlcz/122760`

[7] J. R. Vaňaus: Úloha 36. *Časopis pro pěstování mathematiky a fysiky*, Vol. 31 (1902), No. 3. JČMF, Praha, str. 262. Dostupné z: `https://dml.cz/handle/10338.dmlcz/122611`

[8] J. R. Vaňaus: Úlohy. Řešení úloh. *Časopis pro pěstování mathematiky a fysiky*, Vol. 31 (1902), No. 5. JČMF, Praha, str. 262.
Dostupné z: `https://dml.cz/handle/10338.dmlcz/122172`

Some examples of intersection computed using Schubert calculus

Pavel Chalmovianský

Department of algebra and geometry
Mlynská dolina, 842 48 Bratislava, Slovak Republic
pavel.chalmoviansky@fmph.uniba.sk

Abstract. We recall a construction of Schubert cells and show on tractable examples how to use it for computation of intersection problems which look difficult to solve. Basic geometry and topology of Grassmannians which are intimately connected to the Schubert calculus is described.

Keywords: Schubert calculus, intersection product, Grassmannians

1 Introduction

Intersection is a basic operation in mathematics. Algebraic geometry deals with intersections on level of adding polynomial conditions over certain ring of coefficients. There is a particularly useful structure for computation the results of the intersection in theory and practically also in many applications.

Certain patterns repeat in problems of intersection. The change of coordinates, even rational equivalence of intersected varieties does not change the results. This leads to the Chow ring of a space. For intersection problems in projective space, Grassmannians play an important role.

Hermann Cäsar Hannibal Schubert (1848–1911) – a gymnasium teacher was able to compute many complicated enumerative problems with calculus which was not well founded in his days.

David Hilbert included the clarification of this concept as the 15th problem in his famous list of challenges in mathematics to be solved during the 20th century. The finally accepted version of the calculus appeared in the 70th. Many new concepts have been initiated along the way.

2 A problem of common chords of curves

Since there is not enough place for a detailed study of the whole story, we present the concepts on an example.

A chord of a curve is a line intersecting the curve in two different points. In general, the intersection multiplicity of the line with the curve is at least two.

Problem: Let C, D be two smooth curves of degree d and genus g in $P^n(\mathbb{C})$. How many common chords do they have?

We start with all secants of the curve C denoted by $\ _2(C) \subseteq \mathbb{G}(1, n)$, where $\mathbb{G}(1, n)$ represents all lines in $P^n(\mathbb{C})$ (we describe Grassmannians more precisely in the next section). Let $\mathbf{p}, \mathbf{q} \in C$, $\mathbf{p} \neq \mathbf{q}$ and $\mathbf{pq}$ be the line defined by the two points in $\ _2(C)$. Consider the mapping $\tau\colon C\times C \to \mathbb{G}(1,n)$ defined so outside the diagonal. Take an algebraic closure of the image of the τ (e.g. tangents of C are added). Clearly, the (complex) dimension of the image is 2.

Solution: Find the structural elements and their number in $\psi_2(C) \cap \ _2(D)$.

The solution structurally heavily depends on n and for $n = 3$, there is a number of common chords for curves.

3 Grassmannians

An important role is played by varieties parameterizing all linear varieties of dimension k in projective space of dimension n. It is called Grassmannian. We will work over the field of complex numbers on.

3.1 Basic properties of Grassmannians

Let $\mathbb{G}(k,n)$ denote the projective variety of all projective k-spaces in projective n-space over $\mathbb{C}$. Alternatively, one can consider as well all vector spaces $V^{k+1}(\mathbb{C})$ in $V^{n+1}(\mathbb{C})$ and denote it $G(k+1,n+1)$.

In order to obtain some structural information about Grassmannian (named after Hermann Grassmann), one picks a base $\vec{e}_0,\dots,\vec{e}_n$ in the underlying vector space. A $k+1$-dimensional subspace is given by $k+1$ linearly independent vectors, which coordinates can be written in the $(k+1)\times(n+1)$ matrix with respect to the picked base. If the first $k+1$ columns of the matrix are linearly independent, we can reduce it to

$$\begin{pmatrix} 1 & 0 & \cdots & 0 & a_{0k+1} & \cdots & a_{0n} \\ \vdots & \ddots & \dots & \vdots & \vdots & \ddots & \vdots \\ 0 & 0 & \cdots & 1 & a_{kk+1} & \cdots & a_{kn} \end{pmatrix}.$$

The coefficients a_{ij} in the matrix are free and all such matrices form an affine space with the dimension $(n-k)(k+1)$. Since any $k+1$ columns can be those linearly independent, one can cover $G(k+1,n+1)$ with maps, each of which is isomorphic to affine space with the dimension is $(n-k)(k+1)$.

3.2 Grasmannians as special exterior forms

Considering exterior algebra $\Lambda^{k+1}(V^{n+1}(\mathbb{C}))$, the elements of the Grassmannian $G(k+1,n+1)$ are all elements of the form

$$\vec{v}_0 \wedge \dots \wedge \vec{v}_k$$

in some base.

Since the exterior algebra is also a projective space of the dimension $\binom{n+1}{k+1} - 1$ and the mapping $m\colon V \to \Lambda^{k+2}(V^{n+1}(\mathbb{C}))$ given by

$$\vec{v} \mapsto \omega \wedge \vec{v}$$

has the kernel of the dimension $k+1$, and its image of the dimension at most $n-k$. Hence, the corresponding matrix of this mapping has all minors of order $n-k+1$ zero. Such relations can be used to define Grassmannian as an algebraic variety. The ideal of the variety can be generated by quadratic Plücker relations. (One knows $\mathbb{G}(1,3)$ in classical geometry as the space of all lines in $P^3(\mathbb{C})$ and the Plücker cone defined by $\omega_{01}\omega_{23} - \omega_{02}\omega_{13} + \omega_{03}\omega_{12} = 0$).

This topic is extensively studied and many facts can be found e.g. in [2].

4 Rational equivalence of algebraic varieties

Intuitively, we see that moving intersecting varieties slightly does not change the structure of the intersection. The situation is not clear in case of singular situations. The notion to be used here is rational equivalence of varieties. In algebraic geometry, it is a convenient replacement of intuitive continuity of the intersection.

Two algebraic varieties $V_0, V_\infty \subseteq P^n(\mathbb{C})$ are rationally equivalent if there is a rational mapping $\phi\colon W \to P^1(\mathbb{C})$ such that $W \subseteq P^n(\mathbb{C}) \times P^1(\mathbb{C})$, $\phi^{-1}(0) = V_0$ and $\phi^{-1}(\infty) = V_\infty$.

An example of rational equivalence of regular and singular conic section in projective lane can be computed by the mapping

$$\tilde{\phi}\colon P^1 \to P^2 \times P^1, (s,t) \mapsto xy + tz^2.$$

When $t = 0$ one gets lines, for $t \neq 0$, one gets a regular conic section.

The following theorem provides a tool of computation for intersection.

Theorem 1 (Chow ring) *The classes of all projective algebraic varieties under the relation equivalence $Rat(X)$ in $X = P^n(\mathbb{C})$ form a ring with operations of formal sum with integer coefficients (i.e. $\alpha_1 a_1 + \cdots + \alpha_k a_k$, $\alpha_i \in \mathbb{Z}$ also called degree of a_i, where a_i is a class of the rational equivalence), and intersection (i.e. $[a.b] = [a \cap b]$). Formally,*

$$A(X) = Z[X]/Rat(X) = \bigoplus_{k \in \mathbb{Z}} Z_k[X]/Rat(X).$$

One can replace projective space with a general algebraic variety X, even scheme. The computation of the Chow ring in general is not easy. We will use the case $X = \mathbb{G}(k,n)$, where the ring is known.

5 Schubert calculus

We show the way of computation with Schubert subvarieties in a particular case of lines in $P^3(\mathbb{C})$ and then give a brief sketch of the general case.

5.1 Schubert varieties in Grassmannian $\mathbb{G}(1,3)$

Consider a projective flag $V_0 \subset V_1 \subset V_2 \subset V_3$ in $P^3(\mathbb{C})$ with $\dim V_i = i$, $i = 0,1,2,3$ and the following algebraic varieties.

- All lines intersecting the fixed point V_0 denoted $\Sigma_{2,0}$.
- All lines intersecting the fixed point V_0 contained in the plane V_2 denoted $\Sigma_{2,1}$.
- All lines intersecting the fixed point V_0 contained in the line V_1 denoted $\Sigma_{2,2}$.
- All lines intersecting the fixed line V_1 denoted $\Sigma_{1,0}$.
- All lines intersecting the fixed line V_1 contained in the plane V_2 denoted $\Sigma_{1,1}$.
- All lines denoted $\Sigma_{0,0}$.

Since any complete flag can be rationally transformed to any other complete flag (just think of projective linear mapping), these varieties represent some classes in the Chow ring of $\mathbb{G}(1,3)$. For $\Sigma_{a,b}$, its class in the Chow ring is denoted by $\sigma_{a,b}$. It is not so difficult to see that the codimension of $\Sigma_{a,b}$ is $a+b$ in $\mathbb{G}(1,3)$.

5.2 Intersection table for Schubert varieties

For the sake of shorter notation $\sigma_a = \sigma_{a,0}$. The table of multiplication is as follows.

$$\begin{aligned} \sigma_1^2 &= \sigma_{1,1} + \sigma_2, \\ \sigma_1\sigma_{1,1} &= \sigma_1\sigma_2 = \sigma_{2,1}, \\ \sigma_1\sigma_{2,1} &= \sigma_{2,2}, \\ \sigma_{1,1}^2 &= \sigma_2^2 = \sigma_{2,2}, \\ \sigma_{1,1}\sigma_2 &= 0. \end{aligned}$$

Try to prove these relations by devising special situations. The complete proof requires a longer computation. It can be found e.g. in the book [1].

As a demonstration of the method, a classical problem is shown: How many lines intersect 4 lines in a generic position in $P^3(\mathbb{C})$? Taking the class σ_1 of lines intersecting a fixed line, the answer is

$$\deg(\sigma_1^4) = \deg((\sigma_{1,1} + \sigma_2)^2) = \deg(\sigma_{1,1}^2 + 2\sigma_{1,1}\sigma_2 + \sigma_2^2) = \deg(2\sigma_{2,2}) = 2.$$

A geometric approach using specialization is available. It is enough to take two pairs of intersecting lines $\ell_1 \cap \ell_2 = \mathbf{a}$, resp. $\ell_3 \cap \ell_4 = \mathbf{b}$. Each pair is spanned by a plane α_{12}, resp. α_{34}, which are not the same. Then, two lines intersection all the lines are **ab** and $\alpha_{12} \cap \alpha_{34}$.

5.3 Schubert varieties in general Grassmannian

We show the general approach on a vector space approach. Consider $G(k,n)$. Fix a complete flag $0 \subset V_1 \subset \cdots \subset V_{n-1} \subset V_n$, with $\dim V_i = i$, $i = 1, \ldots, n$. Take $\mathbf{a} = (a_1, \ldots, a_k)$ satisfying $n-k \geq a_1 \geq a_2 \cdots \geq a_k \geq 0$. Then

$$\Sigma \quad = \{W \in G(k,n)\colon \dim(V_{n-k+i-a_i} \cap W) \geq i\}$$

Similarly, we omit zeroes at the end of $\mathbf{a}$, when denoting Σ or σ . A codimension of Σ in $G(k,n)$ is $\mathbf{a} = a_1 + \cdots + a_k$.

Intuitively, the intersection of a k-plane with $V_{n-k+i-a_i}$ is a_i dimensions earlier than is the generic case. Using matrices and taking basis such that the fixed flag is $V_i = [\vec{e}_1, \ldots, \vec{e}_i]$, $i = 1, \ldots, n$, we get e.g. for $G(4,9)$ and $\Sigma_{3,2,2,1}$ a matrix

$$\begin{pmatrix} * & * & * & 0 & 0 & 0 & 0 & 0 & 0 \\ * & * & * & * & * & 0 & 0 & 0 & 0 \\ * & * & * & * & * & * & 0 & 0 & 0 \\ * & * & * & * & * & * & * & * & 0 \end{pmatrix}.$$

The space V_{5+1-3} has intersection of dimension 1, the space V_{5+2-2} has intersection of dimension 2, the space V_{5+3-2} has intersection of dimension 3, the space V_{5+4-1} has intersection of dimension 4. It is always the first index in the fixed flag with the intersection of the dimension i for all considered indices i.

5.4 General rules of multiplication of Schubert classes

Multiplication rules are more complicated in general case. For particular classes, there are explicit rules of computation.

Theorem 2 (Pieri's formula) *For any class σ and any class σ_b with b integer*

$$\sigma \quad \sigma_b = \sum_{\substack{|\mathbf{c}|=|\quad|+b \\ \forall i\, a_i \leq c_i \leq a_{i-1}}} \sigma_{\mathbf{c}}.$$

Theorem 3 (Giambelli's formula) *For any Schubert class $\sigma_{\mathbf{a}}$ holds*

$$\sigma_{a_1,\ldots,a_k} = \begin{pmatrix} \sigma_{a_1} & \sigma_{a_1+1} & \cdots & \sigma_{a_1+k-1} \\ \sigma_{a_2-1} & \sigma_{a_2} & \cdots & \sigma_{a_2+k-2} \\ \vdots & \vdots & \ddots & \vdots \\ \sigma_{a_k-k+1} & \sigma_{a_k-k+2} & \cdots & \sigma_{a_k} \end{pmatrix}$$

There are methods of computation avoiding determinants, hence higher degree polynomials for big k, n.

6 Computation of the chord problem

Now, we have all necessary notions in order to compute the chord problem in $\mathbb{G}(1,3)$.

Due to codimension 2 of ${}_2(C)$ in $\mathbb{G}(1,3)$, we have the equation

$$[\psi_2(C)] = \alpha\sigma_2 + \beta\sigma_{1,1}.$$

Multiplying the equation by $\sigma_{1,1}$ and taking degree, we have

$$\beta = \deg(\sigma_{1,1}[\psi_2(C)]) = \#\{\Sigma_{1,1} \cap \Psi_2(C)\} = \binom{d}{2},$$

since a generic curve of degree d has intersection with generic plane points $\mathbf{p}_1, \dots, \mathbf{p}_d$, they form β chords.

Multiplying the equation by σ_2 and taking degree, we have

$$\alpha = \deg(\sigma_2[\psi_2(C)]) = \#\{\Sigma_2 \cap \Psi_2(C)\} = \binom{d-1}{2} - g,$$

since the number of chords through a fixed point to C can be counted as the number of nodes of the projection $\pi\colon C \to P^2(\mathbb{C})$ through the fixed point, which is by a well known formula on counting singularities α.

For twisted cubics which have genus 0,

$$\#\Psi_2(C) \cap \Psi_2(D) = \deg(\sigma_2 + 3\sigma_{1,1})^2 = 10.$$

7 Future work

We plan to study connection of the Schubert calculus with singular varieties, local multiplicity using Schubert calculus and relate the structures with the result of Schenzel and Boďa on local Bézout theorem.

Acknowledgement

This work was supported by the Slovak Research and Development Agency under the contract No. APVV-16-0053.

References

[1] David Eisenbud and Joe Harris. *3264 and all that–a second course in algebraic geometry.* Cambridge University Press, Cambridge, 2016.

[2] Demeter Krupka and David Saunders, editors. *Handbook of global analysis.* Elsevier Science B.V., Amsterdam, 2008.

Discovering Plane Curves by GeoGebra

Mária Kmeťová

Dept. of mathematics, Fac. of Natural Sciences, Constantine the Philosopher Univ. Trieda A, Hkinku 1, 949 74 Nitra, Slovak Republic
mkmetova@ukf.sk

Abstract. The paper aims to be a motivation in high-school geometry showing different constructions of plane curves as loci of points in a dynamic geometry environment.

Key words: Curves, locus of points, GeoGebra

1 Introduction

The content of geometry taught at secondary and high schools has undergone several changes over the last decades, with the result that the elements of the synthetic geometry of curves have almost disappeared from the curriculum. This also happened due to the time-consuming point by point construction of the curves in the pen and paper environment in school praxis. The possibility to use dynamic geometric programs in lessons can contribute to the return of this nice and richly motivating chapter to the curriculum. To facilitate this step it might be a good idea to challenge prospective mathematics teachers to reinvent and/or develop different types of curves. Using dynamic programs, it is enough to construct a single point of the curve and select the "trace" option to plot the points of the curve. If a curve is defined as a set of points satisfying a given property, using the "locus" button, GeoGebra easily draws the proper curve. By continuously changing position of the input data, we can then follow the whole class of curves, observing their changes due to the mutual positions of defining entities. This subject offers many opportunities for experimentation, investigation, inspiration, and motivation.

2 Locus of points

In geometry, a set of all points satisfying one or more specified conditions is called a locus of points or simply a locus. A locus consists of different positions of tracing point L satisfying a given property. This property usually is given by the relationship between moving point M and point L, where M is a point on the one-dimensional object. While M moves along the one-dimensional object, L traces the locus. Thus the locus is defined as the image of an object under an application or transformation: the function that transforms the “mover” into the “tracer”. The points on the locus depend parametrically on the points of the object where the “mover” lives [1]. This description also corresponds with how the dynamic geometric software is able to build the image points, i.e. the locus.

2.1 Defining properties of loci of points

In school geometry education, the first locus of points is defined according to the equal distances from one point (a circle), then from two points (perpendicular to the midpoint) and from two straight lines (bisectors of their angles or a midline if there are parallel). The set of points in equal distances from one point and one straight line creates a parabola. An ellipse and a hyperbola are given by constant sum and constant difference of distances from two points, respectively. We can create an ellipse and a hyperbola also as a set of all centres of circles that touch a given circle and pass through a given point. If the given point is inside the given circle, we get an ellipse, otherwise, we get a hyperbola. The expression "set of centres of all circles …" substitutes the expression "locus of points in the same distance …". Continuing in that line of curve definition, we can use various properties to define a locus of points, as distances from a point, line or curve, perpendicularity (pedal curves), tangency, or a set of specially defined intersection points.

3 Groups of curves according to defining properties

3.1 Distance

According to a given distance (alongside the mentioned), there are generated three types of curves: strophoids, conchoids, and cissoids.

A strophoid (the name is derived from the Greek word for loop) is a curve generated from given curve c and fixed points F and P (the so-called pole). For the basic type of strophoid, the so-called right strophoid, the given curve c is a straight line with pole P on it and FP is perpendicular to c. M is a moving point on c. Let L_1 and L_2 be the two points on FM whose distances from M are the same as the distance from P to M. The locus of such points L_1 and L_2 is a right strophoid (in Fig. 1 the locus of points L_1 is red, the locus of points L_2 is blue).

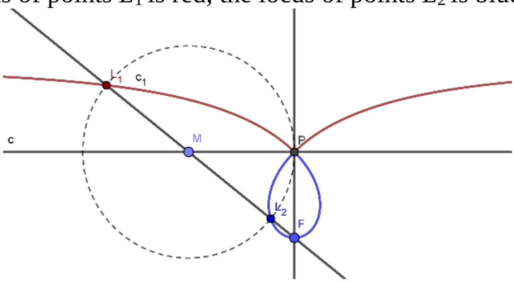

Fig. 1: Right strophoid

For a generalised strophoid then M is a moving point on arbitrary curve c and L_1 and L_2 are two points on FM whose distances from M are the same as the distance from P to M, where P and F are also arbitrary given points.

The previous construction can be modified by considering a fixed distance d of points L_1 and L_2 from moving point M instead of the distance from pole P. This gives us a curve known as a conchoid. The basic type of conchoid, where curve c is especially a straight line, was invented by the ancient Greek mathematician Nicomedes, who described it as first and also constructed the instrument for its construction [2]. In addition to the ruler and compass, it was the oldest instrument used for geometric constructions. Fig. 2 shows the strophoid and the conchoid for circle c.

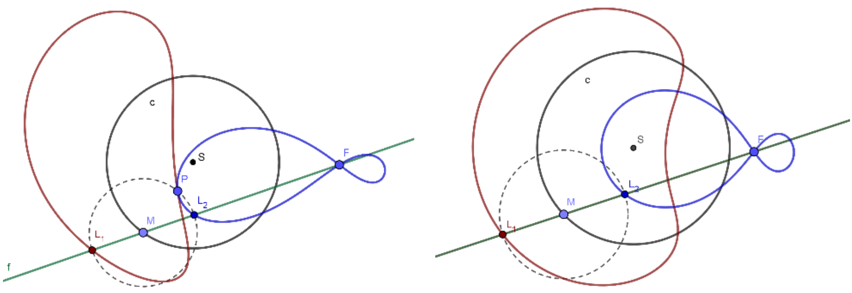

Fig. 2: Generalised strophoid and conchoid for a given circle c.

By a further variation of the preceding construction, we define a cissoid. Here, the distance d is also variable as in the strophoid construction. Generally, a cissoid is derived from two curves c_1, c_2 and a pole P. The construction is as follows. Let us give two curves c_1 and c_2 and a pole P. Let M_1 be a moving point on c_1. Draw a line passing P and M_1 and label the intersection point of this line with c_2 as M_2. Mark a point L on the line so that the distance $|PL| = |M_1M_2|$. If the line and c_2 have more than one intersection, then there are additional points (for all L_i is valid that $|PL_i|=|M_1M_i|$, $i = 2, 3, \ldots$) and the cissoid may have loops. For each distance, we get two points symmetric around the pole, so both generate the same cissoid (see the blue and the red part in Fig. 3).

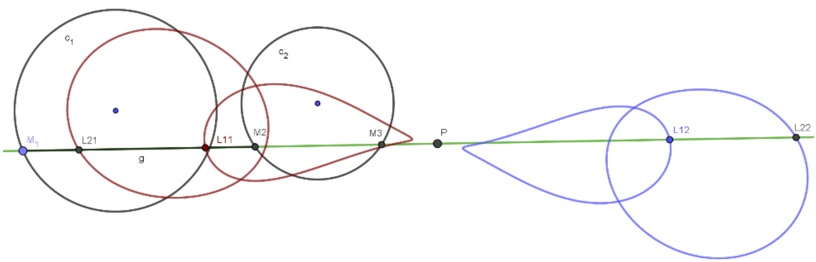

Fig. 3: Cissoid of two circles

The cissoid of an algebraic curve and a line is also an algebraic curve [3]. There are some interesting special cases. The cissoid of a circle and a line passing through the centre S of the circle with the pole P on the circle, so that PS is perpendicular to the line, is a right strophoid (compare Fig. 1 and Fig. 4).

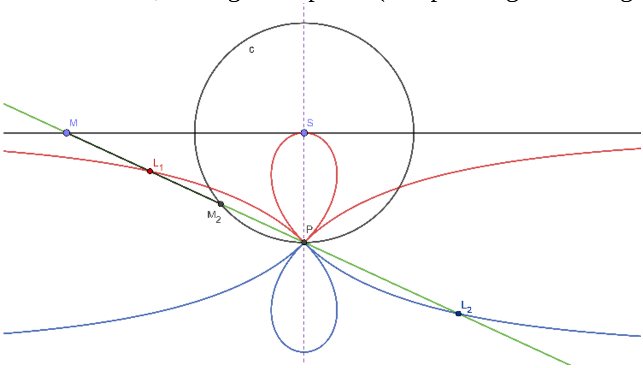

Fig. 4: Right strophoid constructed as a cissoid

The cissoid of a line and a circle with the pole in the centre of the circle is a conchoid of Nicomedes, mentioned earlier (in Fig. 5a constructed as a cissoid). The most famous cissoid is the curve invented by Diocles, cissoid of Diocles. The name cissoid (ivy-shaped) comes from the shape of the curve (Fig. 5b) which is a cissoid of a circle and a tangent line at point T of the circle so that the pole is the opposite point on the circle to T.

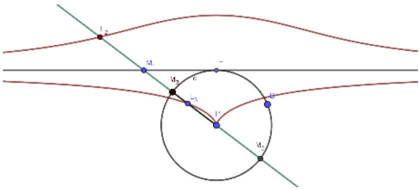

Fig. 5a: Conchoid of Nicomedes

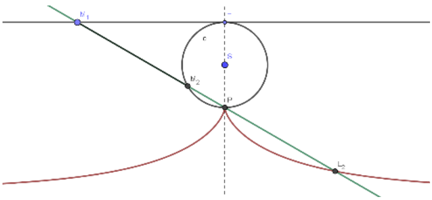

Fig. 5b: Cissoid of Diocles

3.2 Tangents and perpendiculars

In this group of curves, we come out from a curve and a point. It is formed by constructing perpendiculars through the given point to all tangent lines to a given curve. Locus of intersection points of tangents and perpendiculars to them create a so-called pedal curve. In the simplest case, we have only two points and we construct perpendiculars through the first point to all lines containing the second point. The locus of intersection points of perpendiculars is the well-known Thales circle. The pedal curve of a circle is the limacon of Pascal, the pedal curve of a hyperbola is a lemniscata (Fig. 6).

Using GeoGebra we can create a pedal curve of various curves (Fig. 7), also continuously create "a pedal of a pedal of pedal … and students might be inspired to make their own experiments" [5].

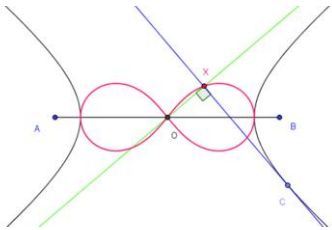

Fig. 6: Lemniscata as a pedal curve

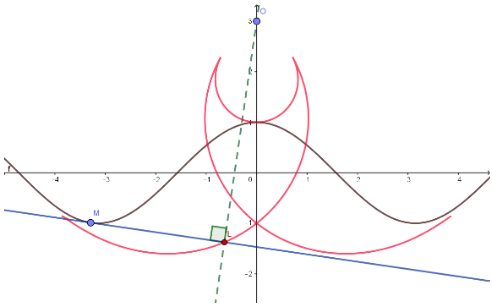

Fig. 7: Pedal curve of a cosine wave

A construction from Isaac Newton allows us to construct the cissoid of Diocles also “almost as a pedal curve” – the locus consists of the midpoints of segments *MP*, where *M* is a moving point on the given line and *P* is the pedal point (see right angle *OPM* in Fig. 8) and the length of the segment *MP* is equal to the distance from pole *O* to the given line.

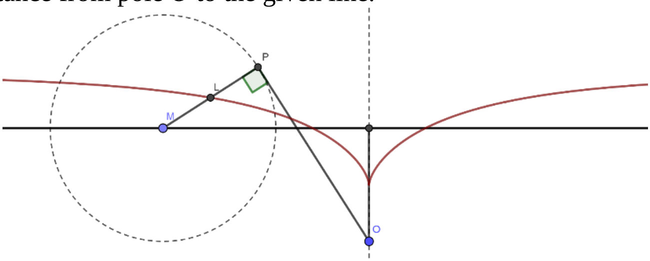

Fig. 8: Newton´s construction of cissoid of Diocles

3.3 Other defining properties

A very different definition of the cissoid of Diocles from the previous is the following. Let us construct a circle with a tangent line and a diameter parallel with the tangent (Fig. 9). Let *M* is a moving point on the circle and *M´* its symmetric point with regard to the given diameter line. Construct a parallel with the tangent through *M*. The locus of intersection points *L* of these parallel lines and lines *FM´* creates the cissoid of Diocles [6].

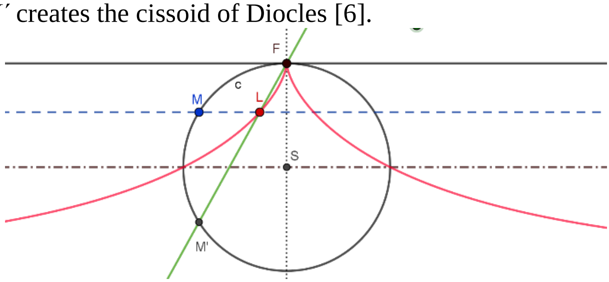

Fig. 9: Construction of the cissoids of Diocles using axial symmetry

Witch of Agnesi is constructed also from a circle and a tangent line at T. Let TF is a perpendicular diameter of c, M is the moving point on c and each secant FM intersects the tangent through T at G. Let L be the intersection of a line through M parallel to the tangent and a line through G perpendicular to the tangent (see Fig. 10). The locus of L, for all such M, is the witch of Agnesi [3].

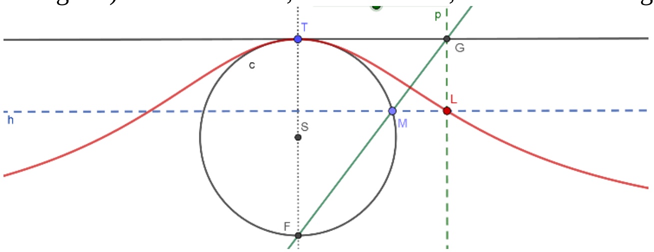

Fig. 10: Witch of Agnesi

Previous constructions illustrate the variability of possible definitions of curves given as loci of points. There are several various possibilities for inventing a new type of curve or new construction for known curves using GeoGebra.

4 Conclusion

In this paper, we have shown the construction of some planar curves based on their determining properties as loci of points using GeoGebra. We pointed out various contexts that can be used motivationally in geometry lessons at secondary schools and in the preparation of mathematics teachers.

Acknowledgments

The author has been supported by grant KEGA no. 020KU-4/2018 from Cultural and Educational Grant Agency of the Ministry of Education, Science, Research, and Sport of the Slovak Republic.

References

[1] I.M. Gómez - Chacón, J. Escribano: Geometric Locus activities in a dynamic geometry system, *Revista Lat.A de Inv. Mat. Educ.17*, 2014

[2] M. Sain, *Matematikatörténeti ABC*, Tankönyvkiadó, Budapest, 1978

[3] J.D. Lawrence: *A Catalog of Special Plane Curves*, Dover 1972

[4] M. Kmeťová: Konštrukcia kriviek ako množín bodov danej vlastnosti, *Science for education - Education for science I.*, Nitra, 2011

[5] J. Böhm: *Wonderful World of Pedal Curves*, available at http://rfdz.ph-noe.ac.at/fileadmin/Mathematik_Uploads/ACDCA/TIME2016/Boehm_Pedals_.pdf

[6] M. Kmeťová: Konštrukcia niektorých rovinných kriviek programom GeoGebra, *Veda a vzdelanie, Zborník III. m. konf. UJS*, Komárno, 2011

Tensegrity – Student Models from Basic Geometric Structures to the Bridges

Dana Kolářová, Martin Pospíšil

Dept. of load-bearing structures, Fac. of Architecture, Czech Technical University
Thákurova 9, 166 34 Prague 6, Czech Republic
kolarova@fa.cvut.cz, martin.pospisil@fa.cvut.cz

Abstract. The article describes the inclusion of tensegrity structures to the teaching program at the Faculty of Architecture, Czech Technical University in Prague. Tensegrity objects are an ideal theme that combines descriptive geometry, structural mechanics and architecture.

Key words: Tensegrity, architectural design, geometry, teaching

1 Introduction

In recent years, we can see an increased interest in tensegrity structures among architects and designers. Tensegrity are objects which integrity is ensured exclusively by axially loaded members that are in stress or in strain. In teaching of future architects, tensegrity objects are an ideal theme that combines geometry, structural mechanics and architecture. The term "Tensegrity", created by Richard Buckminster Fuller in the 1960s, is an abbreviation of the words "tensional integrity".

When looking for a definition of this term, we find a number of different interpretations; for teaching, the definition of René Motro, professor at the University of Montpellier, published in 2004, seems to be the most appropriate: „A tensegrity system is a system in a stable self-equilibrated state comprising a discontinuous set of compressed components inside a continuum of tensioned components. “ [1].

2 History

The first structure that can be described as the predecessor of tensegrity objects, was created in the 1920s by the Latvian avant-garde sculptor Karl Ioganson. He presented his tensegrity statue at an exhibition of young artists in Moscow. Its construction consisted of three rods and seven ropes.

In the 1960s, three names appeared in connection with tensegrity structures: David Georges Emmerich, Richard Buckminster Fuller and Kenneth Snelson (in alphabetical order). All three, independently of each other, patented the basic tensegrity structure in the form of three rods and nine ropes, now known as the simplex structure, in the early 1960s.

Richard Buckminster Fuller, an American architect, mathematician, author of geodesic domes, named these structures and defined them as “islands of compression within an ocean of tension”. He devoted the whole his life to tensegrity structures and he held several patents in this field, as well (star tensegrity, non-symmetrical tensegrity, tensegrity truss).

Kenneth Snelson was an American sculptor who created an incredible statue Needle Tower, where the elements under pressure don't touch each other and are held in their positions just by cables under tension. We can find it in Hirshhorn Museum & Sculpture Garden, Washington, D.C. or its second version in the Kröller Müller Museum, Otterlo, Holland. Snelson defines Tensegrity as a "continuous tension, discontinuous compression structures". Snelson and Fuller worked together in the beginning, but then they split up due to disputes over patent ownership.

At the same time, French scientist David Georges Emmerich dealt with tensegrity structures; his research seems to be independent to the work of Snelson and Fuller.

In contemporary architecture, we can find various examples of using tensegrity structures. Professor Mirko Baum, who is the closest to our school, used the tensegrity principles when designing a bridge in Jaroměř. Abroad, the most famous structure of this kind is the Kurilpa Bridge in Brisbane, Australia.

The advantage of tensegrity systems is their resistance to external influences (earthquakes, hurricanes), their easy transport, modular system and the possibility to use them as temporary structures. The disadvantage is the complex distribution of forces and a very high risk of disintegration in case of failure of a single element.

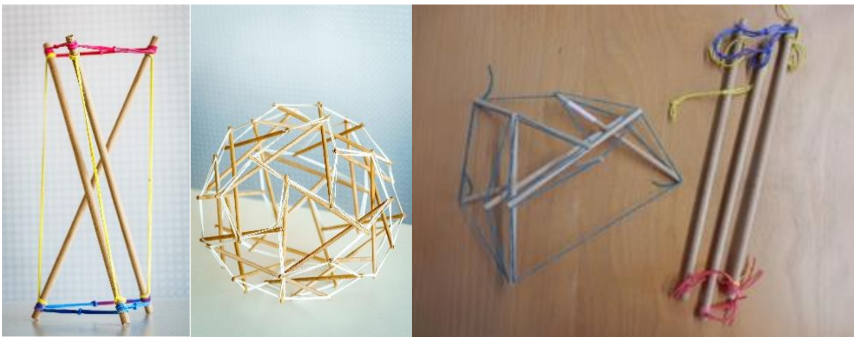

Fig. 1: Models made by students FA CTU

3 Tensegrity systems at the Faculty of Architecture, Czech Technical University in Prague

We included tensegrity systems to the summer semester of the school year 2018/19. At the beginning of the semester, there was a workshop led by a Czech-German architect Mirko Baum on the topics "World of Construction / Construction of the World"; one of the lectures was devoted just to Tensegrity. Students were acquainted with the definition of tensegrity, its use in architecture and in detail, with its implementation of the already mentioned bridge structure in Jaroměř. We followed this lecture in descriptive geometry lessons by creating models of tensegrity structures. The lecture motivated students, and although modeling was voluntary, there was a great interest in it.

The first models were designed as basic simplex models, i.e. tensegrity structures consisting of three rods and nine ropes, the basis of which is a regular triangular prism, where the solid parts form diagonals of the walls and the remaining edges of the prism are made of ropes. When creating the model, the prism sheath is first created in the plane and only when the last rope is fixed, the object is lifted into space. The same principle can be applied to quadrilateral, pentagonal and other prismas.

In the next phase we dealt with tensegrity structures, which geometric basis was formed by regular or semi-regular polyhedra, the bars are either in positions of the edges of the polyhedron or they form their body diagonals. In addition to the icosahedron, we also created a snub dodecahedron.

These models are very demanding and during their construction the whole structure collapsed many times.

Further, our effort was directed to applications of a modular tensegrity system. The basic simplex consisting of bamboo sticks and steel wires was multiplied by students who worked in three-member teams and folded into life-size triangular gates in front of the school. There are many possibilities for further applications, different possible ways of connecting modular elements bring many untested variations.

Perhaps the most beautiful model that was created in this project, was the bridge model. Manufacturing required workshop cutting out of individual parts and their careful cord connection. The model was placed on a pedestal and illuminated.

All models were exhibited at the Tensegrity models exhibition, which took place at the school building in June 2019.

After Professor Baum's lectures cycle and lessons in descriptive geometry, the third educational block deals with the tensegrity structures in the lessons of structural mechanics. Tensegrity structures are statically multiple indeterminate by their nature. This results in both structural and computational complications, because these structures can be hardly solved applying manual calculations. The geometrical bodies solved in the lessons of descriptive geometry were therefore virtually modeled in structural mechanics programs. In these programs they are now prepared for the students to simulate behavior of the tensegrity structures under different loads during the coming semester.

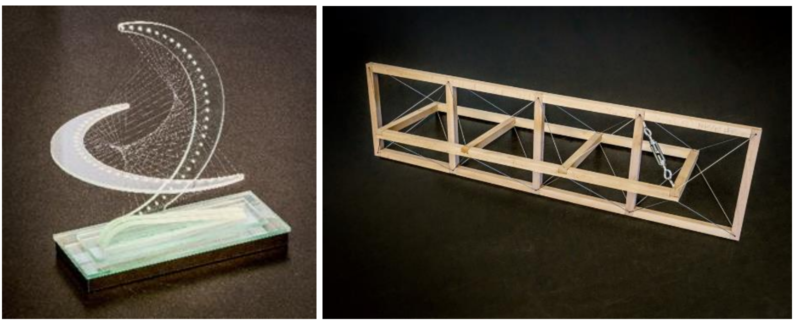

Fig. 2: Models of the bridges

4 Conclusion

The inclusion of tensegrity models to the lessons of descriptive geometry has verified a synergic effect of synchronized teaching, in which students are first motivated by lectures describing real structures, then they are given a theoretical explanation and at the end of the course they work manually on selected models. Despite its complexity, this method of teaching has met with a very favorable response both from teachers and students.

Acknowledgements

This work was supported by the Grant Agency of the Czech Technical University in Prague, grant No. SGS19/198/OHK1/3T/15.

References

[1] MOTRO, René. *Tensegrity: structural systems for the future*. Sterling, VA: Kogan Page Science, 2003. ISBN 19-039-9637-6.
[2] *Https://www.bfi.org* [online]. [cit. 2019-09-08].
[3] CSÖLLEOVÁ, Zs. The Analyses of Triangular Tensegrity Prisms' Pairs. *Procedia Engineering* [online]. 2012, 40(40), 74-78 [cit. 2019-09-08]. DOI: 10.1016/j.proeng.2012.07.058. ISSN 18777058.: https://linkinghub.elsevier.com/retrieve/pii/S1877705812024447
[4] HEARTNEY, Eleanor. *Kenneth Snelson: Art and Ideas* [online]. [cit. 2019-09-08].

Dve stratégie pre RTIN siete

Two Strategies for RTIN based Meshes

Alexej Kolcun

Institute of Geonics AS CR,
Studentská 1768, 708 00 Ostrava, Czech Republic
alexej.kolcun@ugn.cas.cz

Faculty of Science, University of Ostrava,
30. dubna 22, 710 00 Ostrava, Czech Republic
alexej.kolcun@osu.cz

Abstract. The longest-side partition of rectangular isosceles triangle is the base for Right-Triangulated Irregular Network (RTIN) meshes. In the paper the alternative approach, based on balanced QuadTree is introduced, which is more suitable for 3D extension.

Keywords: The longest-side partition, RTIN, balanced QuadTree

Kľúčové slová: Delenie trojuholníka na základe najdlhšej strany, RTIN, vyvážený kvadrantový strom

1 Úvod

Od generátorov, rozkladajúcich oblasť na elementárne prvky, požadujeme spravidla nasledujúce [3].
(a) Splnenie určitých *geometrických podmienok*, ktorým rozkladové elementy vyhovujú. Pre izotropné prostredie je najvhodnejším štvoruholníkom štvorec, resp. najvhodnejším trojuholníkom je rovnostranný trojuholník. Vzorkovacia diskretizačná chyba v tomto prípade nepreferuje žiaden smer. V praxi sú populárne Delaunayovské triangulácie, napr. [1], ktoré zo všetkých triangulácií nad množinou vrcholov P preferuje tú, ktorá maximalizuje minimálny uhol. Z hľadiska interpolácie hodnôt z vrcholov do vnútra trojuholníka je vhodnejšia stratégia minimalizácie maximálneho uhla [2].

(b) *Konformitu*, ktorá nám dovoľuje spojite interpolovať hodnoty z uzlov diskretizačnej siete na celú spojitú oblasť.

(c) *Lokálne zjemnenie*, ktoré dovoľuje iteračným spôsobom zlepšiť numerické riešenie len v podoblasti, kde je kvalita nedostačujúca.

Jedným z prístupov je metóda, zjemňujúca zadanú sieť tak, že požadovaný trojuholník rozdelí delením najdlhšej strany na polovicu [4] – kap.2. V praxi sa často používa variant, ktorý vychádza z pravouhlých rovnoramenných trojuholníkov (Right-Triangulated Irregular Network – RTIN). I my sa sústredíme na tento prípad – kap.3. Ukážeme alternatívny prístup, založený na použití vyváženého kvadrantového stromu – kap.4. Jeho výhodou je jednoduchšie zovšeobecnenie do 3D priestoru.

2 Zjemnenie triangulácie najdlhšou stranou trojuholníka

Uvažujme prvotný trojuholníkový rozklad oblasti

$$\boldsymbol{\tau} = (T_1, T_2, T_3, \ldots, T_m)$$

a usporiadaný zoznam trojuholníkov, ktoré chceme zjemniť,

$$T4R=(t_1, t_2, t_3, \ldots, t_n) \subseteq \boldsymbol{\tau}.$$

```
 1 WHILE (T4R nie je prázdny.)
 2 { Vyberme prvý trojuholník z T4R, t= ABC,
     kde a=BC je jeho najdlhšia strana.
 3   IF (a je na hranici oblasti.)
 4   { t=ABC rozdelíme na t11=ABD a t12=ADC.
 5     t11 a t12 nahradia v triangulácii τ trojuholník t.
 6     Odstránime z T4R prvý trojuholník, T4R=(t2, t3, ..., tn).
     }
 7   ELSE
 8   { tt=BCD.
 9     IF (a je najdlhšou stranou i v tt.)
10     { Dvojicu t,tt rozdelíme pomocou stredu E úsečky a
         na štyri trojuholníky ABE, AEC, DCE, DEB.
11       Tieto štyri trojuholníky nahradia v τ dvojicu t,tt.
12       Skrátime T4R, T4R=(t2, t3, ..., tn).
13       Odoberieme prvý výskyt tt z T4R (ak existuje).
       }
14     ELSE
15     { T4R=(tt, T4R). }
     }
   }
```

Algoritmus 1

Zjednodušene povedané, keď je najdlhšia strana deleného trojuholníka hraničná, delenie na dva trojuholníky je bezproblémové – Algoritmus 1, kroky 3, 4-6. Podobne, keď je vnútorná úsečka najdlhšou stranou oboch priľahlých trojuholníkov, dvojicu trojuholníkov rozdelíme na štyri (kroky 9,10-13). Konformita rozkladu sa v oboch prípadoch nenaruší.

Nekonformita v procese zjemňovania vzniká, keď najdlhšia strana deleného trojuholníka nie je najdlhšou stranou priľahlého suseda. Riešime to „odložením“ delenia pôvodného trojuholníka a analýzou suseda. V Algoritme 1 sa to prejaví zväčšovaním zjemňovaného okolia (kroky 8,9, 14-15), kde zoznam *T4R* používame ako zásobník. Toto zväčšovanie zásobníku je konečné. Vyplýva to z nasledujúceho: Označme veľkosťou trojuholníka $l(T)$ dĺžku jeho najdlhšej strany,

$$l(ABC)=\max(|AB|, |AC|, |BC|),$$

(d) Je očividné, že postupnosť vkladaných trojuholníkov do *T4R* je monotónne rastúca. Vzhľadom na konečnosť triangulácie tak do *T4R* vložíme len konečný počet trojuholníkov.

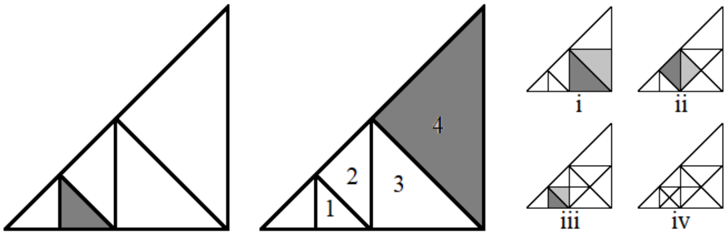

a) b) c)

Obr. 1: Demonštrácia algoritmu

Na Obr. 1a) je prvotný rozklad s označeným trojuholníkom pre zjemnenie. Postupné vkladanie ďalších trojuholníkov do *T4R* (kroky 14-15 algoritmu) ukazuje Obr. 1b). Vidíme, že analyzované okolie sa rozširuje, a v danom príklade sa zastaví až na hranici oblasti. Označený trojuholník 4 je posledný vložený (tj. na začiatku zásobníka *T4R*). Jeho zjemnením (kroky 3-6 algoritmu) máme stav z Obr. 1c)i. Tu redukujeme zásobník *T4R* na základe krokov 8-13 Algoritmu 1. Svetle šedou farbou je označený vždy doplnkový trojuholník (so spoločnou najdlhšou hranou). Postupne tak dostávame riešenia ii, iii, iv z Obr. 1c). Uvedený mechanizmus môžeme sformulovať takto:

(e) Za konečný počet delení sa fixovaná strana stáva najdlhšou stranou príslušného trojuholníka.

Vlastnosť (e) demonštruje príklad z Obr. 2. Pre konfiguráciu dvojice trojuholníkov *ABC,BDC* a požiadavke zjemniť trojuholník *ABC*, delíme trojuholník *BDC*, až kým sa strana *BC* nestane najdlhšou stranou trojuholníka, ktorý je s *ABC* susedný. V prvom prípade (Obr. 2a)) to dosiahneme jedným delením

$$BDC = BEC \cup EDC,$$

v druhom prípade delíme dvakrát:

$$BDC=BEC \cup EDC= (BFC \cup FEC) \cup EDC.$$

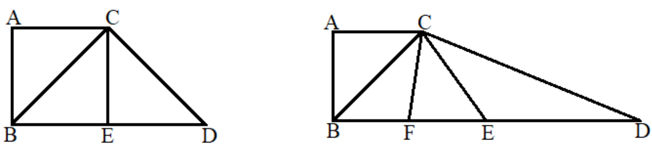

a) b)

Obr. 2: Príklad jednokrokového a dvojkrokového delenia trojuholníka *BCD*

Postup **(e)** vedie k redukcii zásobníka *T4R* (kroky 8,9, 10-13) a v konečnom dôsledku k jeho vyprázdneniu.

3 Lokálne zjemnenie nad rovnoramennými pravouhlými trojuholníkmi ($\boldsymbol{RTIN_P}$)

V prípade, keď sa obmedzíme na počiatočnú trianguláciu pozostávajúcu z rovnoramenných pravouhlých trojuholníkov (Obr. 1a)), proces **(e)** je vždy jednokrokový, čo zjednodušuje proces zjemňovania. Naviac sa v tomto prípade očividne v každom kroku generujú opäť pravouhlé rovnoramenné trojuholníky. Udržiava sa tak tvarová optimálnosť rozkladových prvkov **(a)** v celom procese zjemňovania. Tento prístup sa v literatúre označuje ako RTIN (Right-Triangle Irregular Network) a získal si obľubu napr. v kartografických aplikáciách.

Proces lokálneho zjemnenia demonštrujeme na testovacej geometrii „*štvrťkruh Q vo štvorci S, s dvojnásobnou plochou,* $p(S) = 2p(Q)$“, Obr. 3.
Lokálne zjemnenie riadime parametrami $0<h_1<h_2<1$ a ε.
Uvažujme prvotný trojuholníkový rozklad $\boldsymbol{\tau} = (T_1, T_2, T_3, ..., T_m)$.
Do zásobníka *T4R* vložíme tie trojuholníky $T \in \boldsymbol{\tau}$, pre ktoré platí:

(f) $h_1 \le \frac{p(T\cap Q)}{p(T)} \le h_2$ a zároveň $l(T) > \varepsilon$.

Automatizovaný proces generovania je nasledujúci.

```
Na základe kritéria (f) generujeme T4R.
WHILE (T4R nie je prázdny.)
{ Aplikujeme Algoritmus 1.
  Na základe kritéria (f) generujeme T4R.
}
```

Algoritmus 2

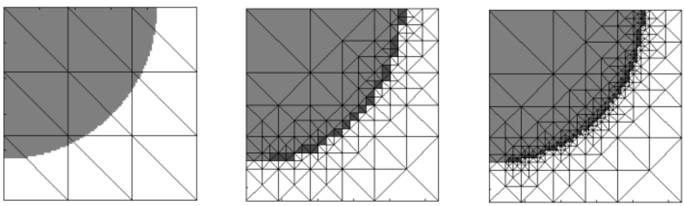

a) b) c)

Obr. 3: Lokálne zjemnenie $RTIN_P$ na testovacej geometrii

Na Obr. 3a) je testovacia geometria s prvotnou trianguláciou. Obr. 3b)-c) ukazujú nájdenú trianguláciu pre rôzne hodnoty ε. Tmavošedé sú tie trojuholníky, kde nie je splnená druhá podmienka **(f)** (tj. pri zmenšení hodnoty ε, práve tieto trojuholníky tvoria *T4R*).

Rozšíreniu tohto prístupu do trojrozmerného priestoru bráni fakt, že nevieme nájsť taký štvorsten, ktorý by pokrýval celý priestor a zároveň by sme ho vedeli rozdeliť na menej ako osem zhodných kópií, s nim tvarovo totožných.

4 Vyvážený kvadrantový strom

Kvadrantovým stromom nazývame 2D rozšírenie rekurzívneho dichotomického delenia intervalu. Výsledkom je nekonformné delenie pravouhlej oblasti na pravouholníky. Miera nekonformity η je daná rozdielom stupňov rekurzívneho delenia susedných elementov $\eta(E_1,E_2) = \sigma(E_1)\text{-}\sigma(E_2)$. Na Obr. 4a) je príklad delenia s η =3.

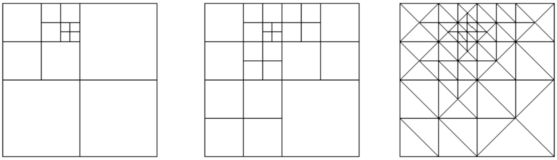

a) b) c)

Obr. 4: *RTIN*$_{\mathrm{Q}}$ na základe vyváženého kvadrantového stromu

Vyváženým kvadrantovým stromom nazveme také delenie, v ktorom je miera nekonformity pre každú dvojicu elementov $|\ \eta\ | \leq 1$ – Obr. 4b). Vyvážený strom generujeme podobne, ako v Algoritme 1, kde *E4R* je zoznam elementov, ktoré chceme zjemniť.

```
1 WHILE (E4R nie je prázdny.)
2 { Vyberme prvý element e z E4R.
3   Označme S=s1 ... sm susedné elementy elementu e.
4   FOR (si ∈ S) {IF (σ(e) > σ(si)), {E4R=( si , Q4R). refin=FALSE.} }
6   IF (refin),
7   { Zjemníme element e.
8     Odstránime e z E4R.
    }
  }
```

Algoritmus 3

Vyváženosť garantuje štvrtý krok: keď okolie požadovaného elementu má menšiu jemnosť delenia, tak delenie „odložíme“ a najprv zjemníme toto okolie.

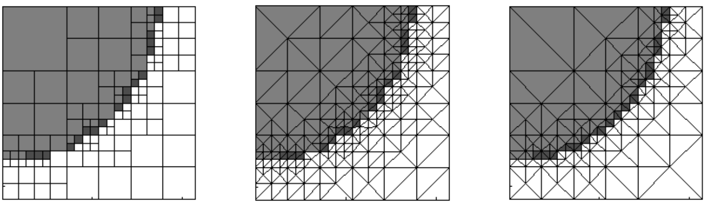

a) b) c)

Obr. 5: Lokálne zjemnenie *RTIN*$_{\mathrm{Q}}$ na testovacej geometrii.
a) vyvážený kvadrantový strom, b) výsledná triangulácia *RTIN*$_{\mathrm{Q}}$,
c) pre porovnanie *RTIN*$_{\mathrm{P}}$ z Obr. 3b).

Vyvážený kvadrantový strom vieme previesť na konformnú trianguláciu $RTIN_Q$ jednoducho – Obr. 4b):

```
IF (Element obsahuje nekonformitu.)
{ Rozdeľ element na štyri trojuholníky dvojicou diagonál.
  Trojuholníky s nekonformitou rozdeľ na dva.
}
ELSE
{ Rozdeľ element na dva trojuholníky diagonálou.}
```

Algoritmus 4

5 Záver

V príspevku sme ukázali dva spôsoby *RTIN* triangulácií: zjemňovaním trojuholníkov podľa prepony $RTIN_P$ a zjemňovaním na základe vyváženého kvadrantového stromu $RTIN_Q$. Tabuľka ukazuje počet trojuholníkov pre obe stratégie v závislosti na zvolenej hodnote ε.

ε	$n(RTIN_P)$	$n(RTIN_Q)$	n_Q/n_P
4,5	237	374	1,58
2,5	572	767	1,34
1,5	1222	1808	1,48
0,5	5682	9038	1,59

Vidíme, že lokálne zjemnenie založené na delení prepony je úspornejšie. Z druhej strany, vyvážený kvadrantový strom nám poskytuje jednoduchý spôsob, ako rozšíriť metódu do 3D. Toto dáva nástroj na efektívne automatické generovanie siete pre numerické modely, kde geometriu získame z CT snímok.

Poďakovanie

Tento článok vznikol za podpory

- GAČR projektu No. 19-11441S,
- inštitucionálnej podpory rozvoja KIP PřF Ostravskej univerzity.

Literatúra

[1] S-W. Cheng, T.K. Dey, J.R. Shewchuk: *Delaunay Mesh Generation.* CRC Press 2013.

[2] M. Křížek: *On the Maximum Angle Condition for Linear Tetrahedral Elements*, SIAM J. Numer. Anal., Vol. 29, No. 2, 1992, pp. 513-520.

[3] D. S.H. Lo: *Finite Element Mesh Generation.* CRC Press 2015.

[4] M.C. Rivara, G. Iribarren: *The 4-Triangles Longest-Side Partition of Triangles and Linear Refinement Algorithms.* Mathematics of Computation, Vol. 65, No 216, 1996, pp.1485-1502.

Constructions of G^1 continuous surfaces

Adéla Kostelecká
Faculty of Mathematics and Physics, Charles University
Sokolovská 83, 186 75, Praha 8, *Czech Republic*
adela.kostelecka@gmail.com

Abstract. We introduce an algorithm that connects two Bézier patches indistinguishtably. The algorithm modifies patches to have a common tangent plane. We use the Chiyokura Kimura method to a tensor product Bézier surfaces and Bézier triangles. We ensure this type of continuity for multiple patches by replacing the control points with rational functions. These are called the Gregory patches. Finally, we present the results of the algorithm on asymmetric icosahedron and on real geometric objects such as Standford Bunny.

Keywords: Bézier triangle, G^1 continuity, Chiyokura Kimura method.

1 Introduction

Constructions of G^1 continuous surfaces is known problem in geometric modelling. Many algorithms were developed. One of them is called Chiyokura Kimura method presented in [2]. We combine this idea with Gregory patches based on [3].

We present this method as the algorithm and we state one of theorems proved in bachelor thesis [4].

Finally, we present results of our implementation. We use mainly Bézier triangles for multiple patches.

2 Notions of geometric modelling

We introduce basic notions of geometric modelling based on [1] and we define G^1 continuity formally.

2.1 Bézier patches

We use two types of Bézier patches: tensor product Bézier patches and Bézier triangles.

Definition 1 (Tensor product Bézier patch). *Let $m, n \in \mathbb{N}_0$ and let $P_{i,j} \in \mathbb{R}^3$ for $i \in \{0, 1, \ldots, m\}$; $j \in \{0, 1, \ldots, n\}$ be called control points. We define tensor product Bézier patch by $p(u, v) = \sum_{i=0}^{n} P_i B_i^n(t) B_i^m$, $t \in [0, 1]$ where B_i^n and B_i^m are Bernstein polynomials of degrees n and m. The ordered pair (m, n) is called degree of tensor product Bézier patch.*

Definition 2 (Bernstein polynomial for triangles). *Let $n \in \mathbb{N}_0$. We define Bernstein polynomial for triangles by*

$$B^n_{i,j,k}(u, v, w) = \frac{n!}{i!j!k!} u^i v^j w^k,$$

where $i + j + k = n$; $i, j, k \geq 0$ and $u + v + w = 1$.

Definition 3 (Bézier triangle). *Let $n \in \mathbb{N}_0$ a let $P_{i,j,k} \in \mathbb{R}^3$, $i+j+k=n$ be control points. Let $B^n_{i,j,k}$ be Bernstein polynomial for triangles. We define Bézier triangle by*

$$p(u,v,w) = \sum_{\substack{i+j+k=n\\ i,j,k\geq 0}} P_{i,j,k} B^n_{i,j,k}(u,v,w),$$

where $u+v+w=1$; $u,v,w \geq 0$. We call the number n its degree.

2.2 G^1 continuity

We denote $T_x p$ a tangent space of Bézier patch p in point x. We use Γ for a Bézier curve which is a common boundary between two Bézier patches. Bézier patches are C^∞ (smooth), therefore C^1 as well.

Definition 4 (G^0 continuity). *Let p, q be Bézier patches. We say that the patches p, q are G^0 continuously connected if there exists a difeomorphism $\varphi : [0,1] \to [0,1]$ such that $\Gamma_p(v) = \Gamma_q(\varphi(v))$.*

Definition 5 (G^1 continuity). *Let p, q be Bézier patches that are G^0 continuously connected along Γ. We say that patches p, q are G^1 continuously connected along Γ if $\forall x \in \Gamma : T_x p = T_x q$.*

Our aim is to connect Bézier patches G^1 continuously. At first, we require G^1 continuity along the common boundary of two patches and then we connect G^1 continuously multiple patches.

3 Algorithm

In this section we deal with tensor product Bézier patches of degree $(3,3)$ and Bézier triangles of degree 3.

3.1 Method Chiyokura Kimura

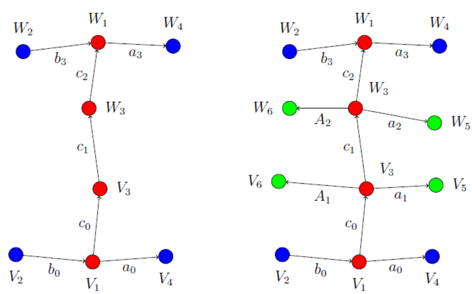

Fig. 1: Input and output of Chiyokura Kimura method

We use a notation as on figure 1. We assume that:

- Vectors a_0, b_0, c_0 are linearly dependent.
- Vectors a_3, b_3, c_2 are linearly dependent.

Red points denote control points of the common boundary of two patches. Green points are the output of the algorithm. How to compute these green points is described in [4] and there is proved that it ensures G^1 continuity along the common boundary.

Geometrically we define a tangent plane in every point of a common boundary which is a linear transition between tangent planes in corner points of the common boundary. There is an example of this method on figure 2.

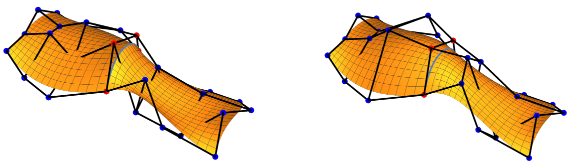

Fig. 2: Result of our implementation

Using Bézier triangle of degree 3 there is only one inner control point. So we use degree elevation for this patch (a common method described in [1]). We get the patch of degree 4 and then we use the previous method in similar way. Input is the same as previously. Black points are control points after applying degree elevation. Yellow points are the output of an algorithm for Bézier triangles. There is an example of this method on figure 4.

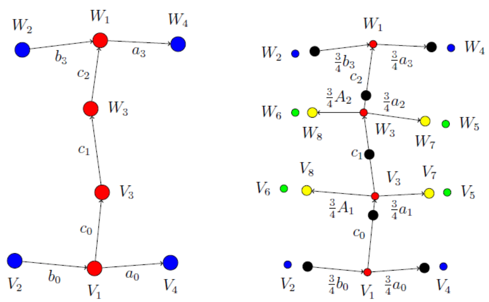

Fig. 3: Input and output of the algorithm for Bézier triangles

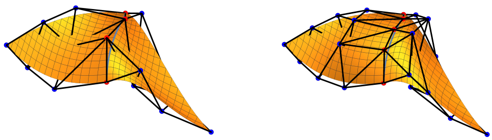

Fig. 4: Result of our implementation

3.2 Gregory patches

Gregory patches are a generalisation of Bézier patches. Instead of inner control points there are blending functions. That allows us to connect G^1 continuously multiple patches. We call this approach Gregory method.

Remark 1 (Vertex inconsistency problem)**.** *Two Bézier patches become G^1 continuously connected along a common boundary by using Chiyokura Kimura method.*

But at a point where more than two patches meet there $\frac{\partial^2 p}{\partial u \partial v} \neq \frac{\partial^2 p}{\partial v \partial u}$ in general case. It's because they are build from different constructions.

This is called vertex inconsistency problem that can be solved by using rational blending functions. These functions ensure that the second partial derivatives don't exist in control points that belong to at least two boundaries.

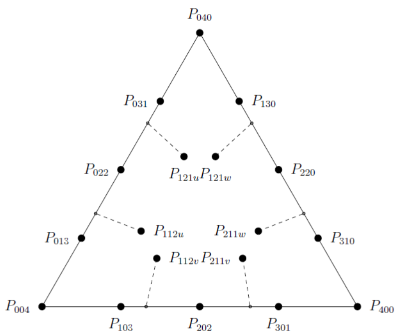

Fig. 5: Gregory triangle

Definition 6 (Gregory triangle)**.** *Let $B^n_{i,j,k}$ to be Bernstein polynomial for triangles. Let* 18 *points be given and denoted as on figure 5. We define blending functions by relationships*

$$P_{2,1,1}(u,v,w) = \frac{(1-v)wP_{2,1,1,v} + v(1-w)P_{2,1,1,w}}{(1-v)w + v(1-w)},$$
$$P_{1,2,1}(u,v,w) = \frac{(1-u)wP_{1,2,1,u} + u(1-w)P_{1,2,1,w}}{(1-u)w + u(1-w)},$$
$$P_{1,1,2}(u,v,w) = \frac{(1-u)vP_{1,1,2,u} + u(1-v)P_{1,1,2,v}}{(1-u)v + u(1-v)}.$$

We define Gregory triangle by

$$p(u,v,w) = \sum_{\substack{i+j+k=4,\\ i,j,k\geq 0}} P_{i,j,k}(u,v,w)B^n_{i,j,k}(u,v,w),$$

where $u+v+w=1$*;* $u,v,w \geq 0$*. These* 18 *points are control points of Gregory triangle.*

Lemma 1 (Blending lemma)**.** *Let* p *to be a Bézier patch of a degree* 4 *and let denote its control points as on a picture 5. Let* p_g *be a Gregory patch constructed from Bézier triangle* p *such that outer control points of* p_g *are equal to outer control points of* p *and inner control points of Gregory patch define as:* $P_{1,1,2,v}$*,* $P_{1,2,1,w}$ *are chosen arbitrarily and in addition* $P_{1,1,2,u} = P_{1,1,2}$*,* $P_{1,2,1,u} = P_{1,2,1}$ *and* $P_{2,1,1,v} = P_{2,1,1,w} = P_{2,1,1}$*.*

Then $T_xp = T_xp_g$ $\forall x \in \Gamma(v)$ *where* $\Gamma(v) = p(0,v,1-v) = p_g(0,v,1-v)$*,* $v \in [0,1]$*.*

The corollary of blending lemma is that this method can be used for G^1 continuous constructions of more complicated objects. There also exist Gregory patches for tensor product Bézier patches.

4 Examples

We show several examples of the algorithm. Algorithm was implemented in *Wolfram Mathematica* [5].

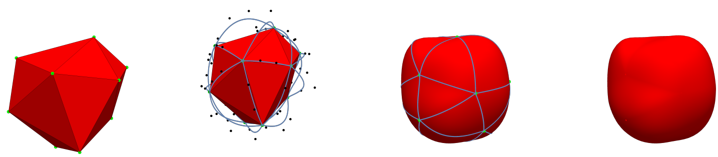

Fig. 6: Asymmetric icosahedron

For a given triangular mesh we compute every control point along a boundary by appropriately chosen intersection of three planes. After getting these points we can follow the algorithm for Gregory patches.

We applied the Gregory method for asymmetric icosahedron and geometric models as Stanford bunny and elephant.

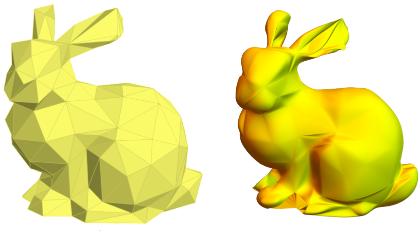

Fig. 7: Stanford bunny

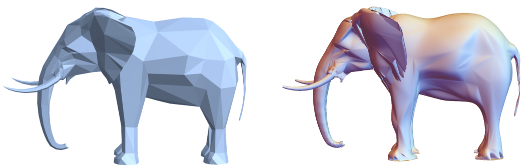

Fig. 8: Elephant

5 Conclusion

We presented theoretic base of the method Chiyokura and Kimura and we showed various examples of G^1 continuous surfaces. It would be interesting to compare efectiveness of other constructions and to study how to ensure G^1 continuity for multiside objects.

References

[1] Farin, G., Hoschek, J. a Kim, M.: *Handbook of Computer Aided Geometric Design. Elsevier Science*, Elsevier Science, 2002

[2] Chiyokura, H. a Kimura, F.: *Design of solids with free-form surfaces.* SIGGRAPH Comput. Graph., 1983

[3] Longhi, L. L.: *Interpolating patches between cubic boundaries.* 1985

[4] Adéla Kostelecká: *Metody konstrukce G^1 spojitých ploch*, Charles University, 2019, Bachelor thesis

[5] Wolfram Research Inc.: *Mathematica, Version 11.2,2017*

Compositional Geometry of the Gothic Era

Miroslav Krejčíř

Institute of Load-Bearing Structures, Faculty of Architecture,
Czech Technical University in Prague
Thákurova 9, 160 00 Prague, Czech Republic
krejcir.miroslav@gmail.com

Abstract. In the Gothic era, architectural works were designed by using geometrical frameworks based on in praxis verified measurements of a structure. The proportions of constructions, which had proved to be static and aesthetic on the implemented designs, were also applied to later designs, thus defining the actively used composition formulation. During geometric analysis, we encounter repeating rules resulting from the principle of square ("ad quadratum"), equilateral triangle ("ad triangulum") or exceptionally circle ("ad circulum").

Key words: geometry, Gothic, medieval, architecture

1 Graphical basis

The Gothic windows form a very interesting and shaped chapter of compositional geometry. Traceries, a rigid structure of stained glass fittings, are subject to a complex composition of interminable curves and bear a particularly well legible geometry.

Only a small fraction of the original Gothic structure drawings has been preserved to now. Although drawings from the reconstruction period (mainly the second half of the 19th century) appear to be a more accessible graphical basis, the question remains to what extent modern drawings rely on the original medieval building experience. However, the architects of this period approached the works with respect and intent to preserve or to highlight the architectural value of the building, only a few of them actually relied on scientifically documented historical facts about the medieval architectural composition.

Kamil Hilbert (1869–1933), one of the architects with a significant scientific overlap in history of architecture, took a substantial part in the completion of the Cathedral of St. Vitus, St. Wenceslas and St. Adalbert in Prague and one of his works, an orthogonal drawing of the great window of the Prague Cathedral's northern transept, is used as a graphical basis for this geometric analysis.

According to the number of minor inaccuracies in the basic drawing, it can be assumed that the tracery patterns were not composed through synthetic geometry procedures. However, some compositional rules may be derived from its application.

2 Procedure

The Gothic tracery is characterized by its dynamically recurring details and seemingly unfinished, harmonic curves, which fill the inside of a window opening. In order to ensure a smooth transition between the circular arches, the axes of each circling element must meet at a common point on a common tangent. Then, one of the most suitable tools for solving the composition of tangent circles is the solution of the Problem of Apollonius (Apollonius of Perga, 262 BC – 190 BC).

Since the circles consisted of many curved parts as a kit, it can be assumed that the curvature of individual arches deliberately coincided as much as possible, due to the lower cost of stonework. Rotation and translation will thus find a place in the composition design.

In the following sections, the most appropriate methods of geometrical reconstruction of a Gothic tracery will be presented.

2.1 Rotation

In order to obtain the most accurate geometrical reconstruction of the whole, it is necessary to begin the analysis from a clearly defined detail, not from the shape envelope. In the case of the discussed window tracery, it is an arrangement of six tangent circles.

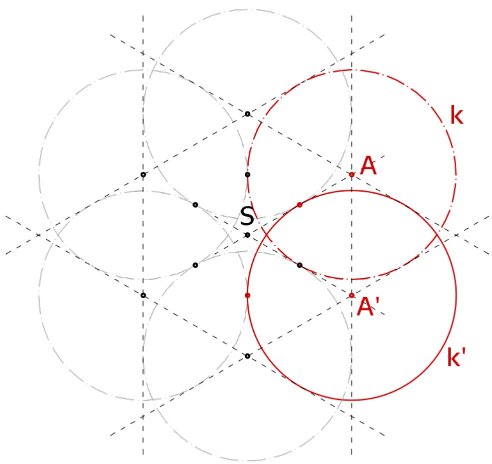

Fig. 1: Rotation of the base circle

2.2 Problem of Apollonius: the case 'LCC'

The position of the 'newly added' objects will be derived from the arrangement of the base circles. Two smaller circles of identical radius should be inscribed into the gap between the three circles forming the top of the base tracery. The contact between the two inscribed circles is defined by their common vertical tangent. The other defining objects are the two adjacent base circles. Thus a 'LCC' Problem of Apollonius (line, circle, circle) has been defined and subsequently transferred to a 'PLC' Problem of Apollonius (point, line, circle) through the application of dilatation.

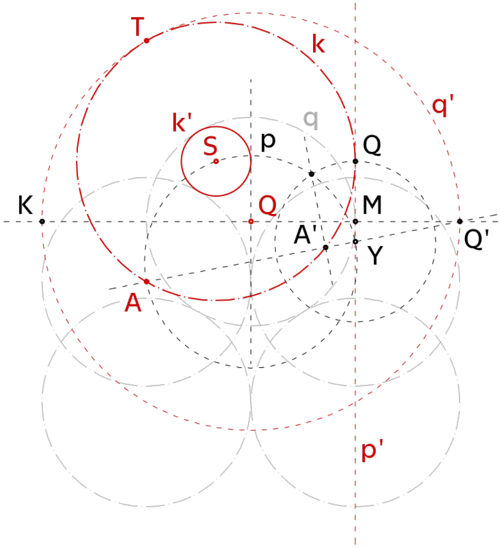

Fig. 2: Problem of Apollonius: solution of the case 'CCC'

2.3 Application of an equilateral triangle

The importance of using an equilateral triangle is closely related to the rotation tool. Through its application, not only the centre of a circle around which the other objects rotate can be found, but also a circle which creates the tracery itself can be defined.

As shown in section 2.1, the basic defining object of the central tracery is a regular hexagon. It is obvious that such a hexagon consists of just six equilateral triangles.

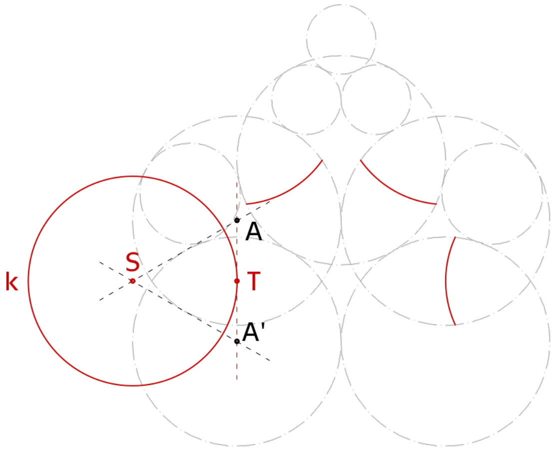

Fig. 3: Application of an equilateral triangle

2.4 Problem of Apollonius: the case ‘CCC’

According to the discussed geometry, an entirely typical situation occurs when the position of the sought circle depends on the position of three already existing circles. Therefore, a ‘CCC’ Problem of Apollonius (circle, circle, circle) has been defined and subsequently transferred to a ‘PPC’ Problem of Apollonius (point, point, circle) through the application of dilatation.

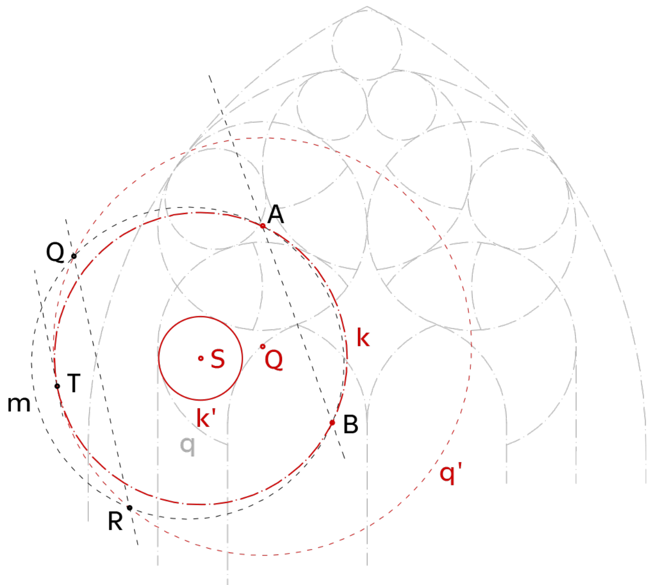

Fig. 4: Problem of Apollonius: solution of the case ‘CCC’

2.5 Translation

In the context of the mention of attempts to repeat the curvature of arches with an intent on reducing the cost of stonework, the compositional method of translating (shifting and repeating) the circled elements finds a place in the geometrical analysis.

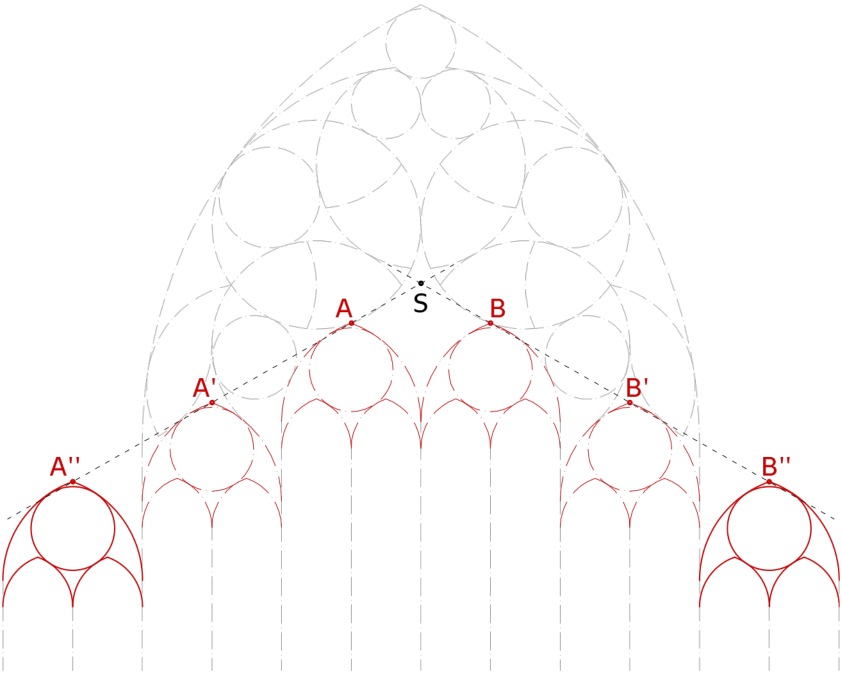

Fig. 5: Translation

3 Conclusion

The analysis of the geometry of a Gothic tracery shows that the composition of its inner elements may be governed by strict and repeating rules. In an ascending way, from a clearly shaped detail to a less legible whole, it is possible to derive the shape of individual structures.

However, it still remains a question to what extent the synthetic geometry served as a tool for a medieval design and to what extent the design was based on the previous construction experience of craftsmen and on the intuition of an architect.

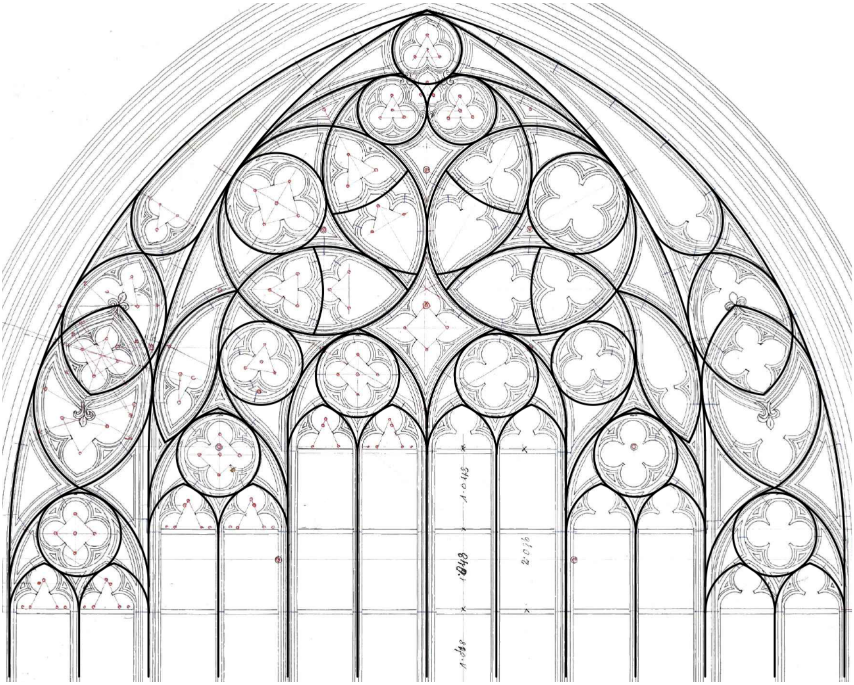

Fig. 6: Reconstructed geometry of a tracery window

Acknowledgements

The author has been supported by the Faculty of Architecture of the Czech Technical University in Prague and by the Student Grant Competition of the Czech Technical University in Prague. A financial grant supporting this article has been provided for the research project "Geometry and the Load-Bearing Structure of Historical Constructions".

References

[1] Archiv Pražského hradu. *Hilbert Kamil, Jednota pro dostavbu chrámu sv. Víta – plány. H XII 1, katedrála sv. Víta v Praze, velké okno, severní příčná loď*. Praha, 11. 8. 2019.

[2] BORK, Robert Odell. *The Geometry of Creation: Architectural Drawing and the Dynamics of Gothic Design*. Farnham: Ashgate, 2011. ISBN 978-07-5466-062-0.

[3] LIŠKA, Petr: *Apolloniova úloha*. Brno, 2007. Bakalářská práce. Přírodovědecká fakulta. Masarykova univerzita.

[4] KOSTÍLKOVÁ, Marie. *Okna Svatovítské katedrály*. Správa Pražského hradu: Praha, 1999. ISBN 80-86161-11-0.

Logické prvky v didaktickej výstavbe a praxi

Logical elements in education and practice

Soňa Kudličková, Alžbeta Mackovová, Martina Bátorová

Department of algebra and geometry
Mlynská dolina, 842 48 Bratislava, *Slovak Republic*
sona.kudlickova@fmph.uniba.sj, alzbeta.mackovova@fmph.uniba.sk,
martina.batorova@fmph.uniba.sk

Abstract. V príspevku sa sústredíme na úlohu logiky vo výučbe deskriptívnej geometrie a na techniky dokazovania tvrdení. Stručne uvádzame základné typy dôkazov s ukážkami v planimetrii a stereometrii. Upozorňujeme na metodické a technické úskalia induktívnych a deduktívnych metód dôkazov, ponúkame niekoľko náhľadov do pojmotvorného procesu v deskriptívnej geometrii a prezentujeme viacero ilustračných príkladov vhodných na priame zaradenie do vyučovacieho procesu.

Keywords: logical thinking, conceptual learning, proof techniques

Kľúčové slová: logické myslenie, pojmotvorný proces, techniky dôkazu

1 Úvod

Logika plní v didaktike úlohu pomocnej vedeckej disciplíny. Pomocou logiky možno identifikovať vo vyučovacom procese analyticko-syntetickú, induktívnu, deduktívnu a porovnávaciu metódu. Z didaktického hľadiska je uvedené rozdelenie metód len pomocné, pretože logické metódy neberú do úvahy vzájomnú súčinnosť pedagóga a študenta, čo je základným znakom a predpokladom metód vyučovacieho procesu. Logika však zasahuje do výstavby vyučovacích predmetov, rozvíjania logického myslenia, vytvárania pojmotvorného procesu a najmä do techniky dôkazov.

V našom príspevku sa sústredíme na tie poznatky z logiky, ktoré pedagóg využíva pri príprave výučby tých vyučovacích predmetov, pri ktorých je potrebné logické myslenie. Takými vyučovacími predmetmi sú matematika, geometria a v neposlednom rade aj deskriptívna geometria (DG), z ktorej vyberáme jednotlivé prezentované ukážky a ilustrácie.

2 Rozvíjanie logického myslenia

Poznatky z matematiky a DG si študenti najefektívnejšie osvojujú, ak u nich dominuje logicko-matematický alebo priestorový (vizuálny) učebný štýl [5]. Študenta s logicko-matematickým učebným štýlom zaujíma ako veci fungujú, hľadá racionálne vysvetlenie, logiku vecí a vzťahov. U študenta s priestorovým učebným štýlom prevláda schopnosť mentálne manipulovať s objektom, má vyvinutú priestorovú predstavivosť, orientáciu v priestore, zmysel pre farby, tvary a proporcie v grafickej prezentácii myšlienok.

Cieľavedomé rozvíjanie logického myslenia spolu s rozvíjaním priestorovej predstavivosti je jednou z hlavných úloh výučby DG. V tomto predmete pracujeme s pojmami, ktoré sa opierajú o predstavy, pričom niektoré pojmy a zákonitosti si osvojujeme abstrakciou prvkov reálneho sveta a ostatné pojmy a zákonitosti berieme ako logicky nevyhnutný dôsledok už známych pojmov, vzťahov a tvrdení.

Zameriame sa *geometrické pojmy*, ktoré vznikli abstrakciou reálneho sveta. Sú to vo väčšine prípadov pojmy myslené, t. j. hmotne neexistujú, existujú však ich fyzikálne modely. Práve na fyzikálnych modeloch študenti zisťujú ich spoločné vlastnosti a abstrahujú od všetkých iných vlastností. Pojmy získané abstrakciou sú *prvotné pojmy* a sú určené obsahom a rozsahom [2].

Obsah pojmu je súhrn všetkých tých znakov (vlastností, činností) príslušného pojmu (predmetu, javu, vzťahu), ktoré pojmu patria a bez ktorých by nebol tým, čím ho nazývame.

Ukážka: Obsahom pojmu hranol je teleso ohraničené hranolovou plochou a dvoma rôznymi rovnobežnými rovinami, ktoré nie sú rovnobežné s tvoriacimi priamkami hranolovej plochy. Podstavy hranola sú zhodné mnohouholníky, bočné steny sú rovnobežníky, všetky bočné hrany sú zhodné úsečky, atď'.

Rozsah pojmu je množina všetkých prvkov, ktoré majú všetky znaky patriace do obsahu pojmu.

Ukážka: Rozsahom pojmu hranol je množina všetkých hranolov, ktorých podstavy sú ľubovoľné mnohouholníky, kolmé, šikmé hranoly, hranoly zhotovené z rôzneho materiálu, ich modely, ale aj myslené hranoly, atď'.

Znaky, ktoré má každý prvok patriaci do rozsahu pojmu, sú jeho *podstatné znaky.*

Ukážka: Ihlan tvorí jeden n-uholník a n trojuholníkov, čo je jeho podstatný znak.

Znaky, ktoré nemusí mať' každý prvok z rozsahu pojmu, sú *vedľajšie znaky* prvku.

Ukážka: Ihlan má práve jeden 5-uholník a päť' trojuholníkov, alebo je kolmý či šikmý, to sú jeho vedľajšie znaky ako ihlana vôbec.

Rozsah pojmu môžeme rozdeliť' do tried, takýto proces nazývame *triedenie.* Správne triedenie má nasledujúce vlastnosti:

- *úplnosť'* – triedenie obsahuje všetky prvky množiny a každý prvok je zaradený do niektorej triedy,
- *disjunktnosť'* – pri triedení je každý prvok zaradený práve do jednej triedy.

Podkladom triedenia je *dichotomické* triedenie, pri ktorom triedime podľa jedného znaku do dvoch tried. Pri triedení používame aj *trichotomické* triedenie, je to dvakrát aplikované dichotomické triedenie.

Ukážka: Majme dve kladné číselné hodnoty d, r. Za triediaci znak vezmeme porovnávanie týchto hodnôt. Po prvom dichotomickom triedení dostaneme: $d = r$ alebo $d \neq r$. Výsledok druhého dichotomického triedenia pre $d \neq r$ je $d > r$ alebo $d < r$.

Takéto triedenie v planimetrii aplikujeme pri vzájomnej polohe priamky a kružnice, kde d označuje vzdialenosť stredu kružnice od priamky a r je polomer kružnice [3]. Následne môžeme situáciu preniesť do stereometrie k určovaniu typu kužeľosečky pri rovinnom reze rotačného kužeľa [4].

Ak triedenie spĺňa vlastnosť úplnosti, tak hovoríme o *klasifikácii* príslušného pojmu.

Ukážka: Klasifikácia vzájomnej polohy troch navzájom rôznych rovín (Obr. 1).

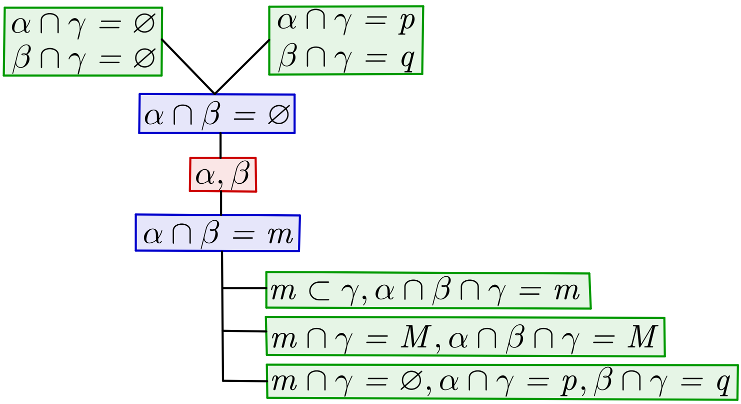

Obr. 1: Vzájomná poloha troch rovín.

3 Pojmotvorný proces – axiómy, definície, vety

Pri budovaní matematických teórií sa vychádza z axióm, definícií a viet. Axiómy predstavujú základné (prvotné) pojmy a vlastnosti budovanej teórie. Axiómy sa považujú za pravdivé a nedokazujú sa. Požadujeme, aby sústava axióm bola

- *bezosporná* – nemožno z nej vyvodiť výrok a zároveň jeho negáciu,
- *nezávislá* – nemožno vyvodiť jednu axiómu z ostatných axióm,

- *úplná* – zo sústavy axióm sa dá dokázať pravdivosť alebo nepravdivosť matematického výroku v rámci danej teórie, ktorý nie je axiómou.

Zložitejšie pojmy a postupy sú vymedzené definíciami, ktoré stanovia názov nového pojmu a určia jeho charakteristické vlastnosti, pričom sa opierajú o jednoduchšie, prípadne už známe pojmy. Ďalšie vlastnosti pojmov, zvyčajne vo forme matematickej vety, sa logicky odvodzujú zo sústavy axióm, definícií a už dokázaných tvrdení.

3.1 Axiómy v DG

Didaktická výstavba DG vychádza z Euklidových *Základov* (okolo roku 255 pred n. l.), ktoré obsahujú aj 23 definícií základných geometrických pojmov. Euklidov axiomatický systém pretrval bez zmeny až do vydania Hilbertových *Základov geometrie* v roku 1899. Hilbertova kniha je základným kameňom, na ktorom je postavená aj súčasná axiomatická výstavba geometrie.

Sústava axióm podľa Hilberta je rozdelená do piatich skupín: *axiómy incidencie* (osem axióm, ktoré opisujú reláciu vzájomnej polohy bodov, priamok, roviny); *axiómy usporiadania* (štyri axiómy vymedzujúce reláciu „ležať medzi“); *axiómy zhodnosti* (šesť axióm opisuje zhodnosť úsečiek a uhlov); *axiómy spojitosti* (dve axiómy, ktoré zabezpečujú meranie dĺžok úsečiek); *axióma rovnobežnosti* (jedna axióma, ktorá vymedzuje rovnobežnosť priamok v klasickom zmysle).

Súhrn objektov pozostávajúci zo všetkých bodov, priamok, rovín a vymenovaných vzťahov medzi nimi, ktorý vyhovuje všetkým požiadavkám Hilbertových axióm, sa nazýva *euklidovským priestorom*. Hovoríme, že euklidovský priestor je úplným systémom základných geometrických vzťahov v rovine i priestore a je pracovným priestorom aj pri didaktickej výstavbe planimetrie a stereometrie.

3.2 Definície v DG

Definícia pojmu je predpis, podľa ktorého možno o každom prvku zistiť, či ho možno zaradiť do rozsahu definovaného pojmu alebo nie. Pre DG sú charakteristické definície, ktoré:

1. vysvetľujú súhrn charakteristických znakov definovaného pojmu.
   Ukážka: Nech a, b, c sú tri nekolineárne polpriamky so spoločným začiatkom O. Zjednotenie daných polpriamok a vnútra všetkých troch konvexných uhlov určených dvojicami polpriamok ab, ac, bc sa nazýva *trojhran*.

2. opisujú konštrukciu, ktorou sa nový pojem zavádza.
   Ukážka: Nech je daná priamka o a body A, A_1, neležiace na priamke o, pričom priamka AA_1 nie je rovnobežná s priamkou o. Potom každému bodu X priradíme bod X_1 tak, že

(a) body ležiace na priamke o sú samodružné, t.j. $1 = 1_1$ (obr. 2a).

(b) ak bod $X \neq A$, zostrojíme bod X_1 tak, aby priamky $XX_1 \| AA_1$ a priamky o, AX, A_1X_1 sa pretínali v samodružnom bode $1 = 1_1$ priamky o (obr. 2b),

(c) ak $AX \| o$, tak aj $A_1X_1 \| o$ a $XX_1 \| AA_1$ (obr. 2c).

Hovoríme, že body X, X_1 si odpovedajú v *osovej afinite*, ktorej priamka o je *os* a body A, A_1 sú *určujúce body*.

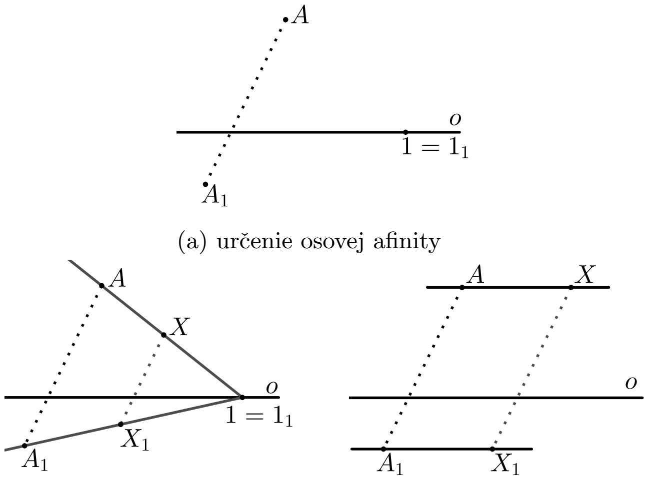

(a) určenie osovej afinity

(b) všeobecná poloha

(c) špeciálna poloha

Obr. 2: Osová afinita s osou o a určujúcou dvojicou bodov (A, A_1).

3. vymenujú všetky prvky, ktoré patria do rozsahu definovaného pojmu. **Ukážka:** Elipsa (kružnica), parabola a hyperbola sú *regulárne kužeľosečky.*

V definícii má každé slovo svoju funkciu a dôležitosť, a preto vynechanie jedného slova spôsobí, že pod definovaný pojem zahrnieme aj iné objekty alebo naopak, iba podmnožinu tých objektov, ktoré pod tento pojem majú patriť. Dôležité je, že správna formulácia definície vyjadruje nielen nevyhnutné, ale aj dostatočné podmienky [2].

V DG sa môže stať, že ten istý pojem definujeme podľa potreby rôznymi spôsobmi. Napríklad elipsu môžeme definovať pomocou jej ohnísk, (tzv. ohnisková definícia), alebo ako krivku odpovedajúcu kružnici v osovej afinite, alebo ako rovinný rez na rotačnej kužeľovej ploche a. i. Pri výučbe nie je vhodné definovať ten istý pojem rôznymi spôsobmi. Zásadou je, že za definíciu pojmu zvolíme tú formuláciu, ktorá je pre aktuálne vysvetľovanie najvhodnejšia. Ostatné „definície" sa stanú vetami, ktoré dokážeme použitím známych viet a zaradením zvolenej definície.

3.3 Vety v DG

Matematická veta je pravdivý výrok, ktorý sa dá logicky odvodiť zo sústavy axióm, definícií a už dokázaných viet. Pri odvodzovaní dôsledkov používame vety, ktoré sú vytvorené z dvoch častí: logického podmetu a logického prísudku.

Logický podmet vyjadruje, čo je alebo má byť splnené, *logický prísudok* vyjadruje, čo potom má byť splnené. V matematickej vete vytvára logický podmet *podmienku* P a logický prísudok, *záver* Z.

V matematických úvahách sú najdôležitejšie vety s dostatočnou podmienkou. Vetu, z ktorej vychádzame nazveme *pôvodná veta* a celé tvrdenie zapíšeme ako implikáciu $P \Rightarrow Z$.

Ukážka: Ak majú dve roviny spoločný bod, tak majú spoločnú priamku s týmto bodom incidentnú.

Dôležité sú aj vety, ktoré dostaneme z vety s dostatočnou podmienkou $P \Rightarrow Z$, ak zameníme podmienku so záverom. Znamená to, že z predpokladu pôvodnej vety urobíme záver a zo záveru predpoklad. Zostavíme k pôvodnej vete tzv. *obrátenú vetu*, ktorú zapisujeme $Z \Rightarrow P$.

Ukážka: Ak majú dve roviny spoločnú priamku, tak majú spoločný každý bod tejto priamky.

Významnú pozíciu v matematike k pôvodnej vete $P \Rightarrow Z$ má *obmenená veta*. Obmenenú vetu vyslovíme, ak v pôvodnej vete $P \Rightarrow Z$ nahradíme tvrdenie P negáciou tvrdenia Z a tvrdenie Z negáciou tvrdenia P, t. j. $Z' \Rightarrow P'$. Obmenená veta má vždy rovnakú pravdivostnú hodnotu ako pôvodná.

Ukážka: Ak dve roviny nemajú spoločnú priamku, tak nemajú spoločný žiadny bod.

4 Funkcia a techniky dôkazu

Podľa citátu J. A. Komenského *„Nech sa ničomu nevyučuje čistou autoritou, ale všetkému dôkazom!"* má byť dôkaz dôležitou súčasťou výučby a dôkazy je potrebné robiť. Z pohľadu logiky poznáme induktívny a deduktívny typ dôkazu [2].

4.1 Induktívny dôkaz

Prvé poznatky detí, ako aj ľudstva, sa uskutočňujú postupom od jednotlivých poznatkov k ich zovšeobecneniu, t. j. *indukciou*. Induktívny postup zaraďujeme pri vysvetľovaní vtedy, keď riešime úlohu najskôr pre niektoré špeciálne prípady, napríklad vzájomnú polohu priamky a roviny, a až následne riešime úlohu ich vzájomnej polohy vo všeobecnom prípade.

Od špeciálnych prípadov prechádzame k všeobecnejším prípadom, napríklad pri konštrukcii dĺžky úsečky v každej zobrazovacej metóde. Induktívny postup môže uľahčiť objavenie cesty, ktorá vedie k riešeniu daného problému. Dôležité je pozorovanie, overovanie, ale i používanie analógie. Postupne totiž vedú k objaveniu nových viet a vzťahov, ktoré najskôr sformujeme do *hypotézy*, tzv. domnienky, a až po dôkaze na základe logického uvažovania označíme hypotézy ako vety.

V praxi sa stretávame s úplnou a neúplnou indukciou.

Úplná indukcia je úsudok, ktorý sa zakladá na poznaní všetkých možných prípadov.

Ukážka: Regulárna kužeľosečka má s priamkou najviac dva spoločné body. Dôkaz vykonáme osobitne pre elipsu, parabolu a hyperbolu, a tak dokážeme jej platnosť o všetkých regulárnych kužeľosečkách [1], [6].

Neúplnou indukciou nazývame úsudok, ktorý sa zakladá na jednom alebo aj viacerých jednotlivých prípadoch, ale nie nevyhnutne na všetkých možných prípadoch. Ak preskúmame niekoľko prípadov a všetky vyhovujú určitému tvrdeniu a žiaden z preskúmaných prípadov mu neodporuje, prijímame tvrdenie za „pravdepodobne" správne. S neúplnou indukciou sa stretávame v prírodných vedách, kde sa prijíma ako dôkaz správnosti. Často sa prenáša aj do matematiky, kde však nemá váhu dôkazu.

Ukážka: Rovnobežným priemetom úsečky je úsečka „kratšia" než úsečka premietaná. Toto tvrdenie platí v pravouhlom premietaní, ale v šikmom premietaní to nie je vždy pravda.

Úplná matematická indukcia je induktívna metóda, v ktorej pomocou istého axiomatického tvrdenia zovšeobecňujeme platnosť tvrdení na všetky prvky, ktoré možno označiť indexmi prirodzených čísel. Riešenie dôkazovej úlohy pomocou úplnej matematickej indukcie má tri kroky:

1. odhad výsledku riešenia pomocou neúplnej indukcie,
2. odhad je správny pri určitom krajnom (najnižšom) prípade,
3. dôkaz, že ak je tvrdenie platné pre k-ty prvok, tak je platné aj pre prvok $k+1$.

Ak teda dokážeme, že nejaké tvrdenie je platné o prvku so začiatočným indexom k_0, za predpokladov, ktoré uvedieme, je tvrdenie pravdivé o každom ďalšom prvku.

Ukážka: Dokážte, že n navzájom rôznobežných priamok, z ktorých žiadne tri neprechádzajú jedným bodom rozdelia rovinu na $1 + \frac{1}{2}n(n+1)$ častí [2].

4.2 Deduktívny dôkaz

Dedukcia je úsudok, ktorým všeobecnejšie platné tvrdenia o určitej množine prvkov prenášame na jej podmnožiny. Poznatok, ktorý získame dedukciou, je na prvý pohľad skromný, ale podmnožina, ktorej znaky skúmame, môže byť podmnožinou aj inej množiny, a teda môže mať aj znaky, ktoré pôvodná množina nemala. Teda dedukciou získavame pojmy bohatšie obsahom.

Pri dedukcii pracujeme s dvomi vetami, ktoré môžeme zapísať v tvare $P \Rightarrow M, M \Rightarrow Z$. Deduktívne dokázať vetu zapísanú v tvare $P \Rightarrow Z$, znamená zostaviť postupnosť viet s dostatočnými podmienkami, ktoré možno schematicky zapísať:

$$P \Rightarrow M_1, M_1 \Rightarrow M_2, M_2 \Rightarrow M_3, ..., M_k \Rightarrow Z, \tag{1}$$

pričom jednotlivé tvrdenia M_1, M_2, atď. majú byť také, aby vety, ktoré sme zapísali v schéme (1), boli pravdivé. Schému (1) skrátene vyjadrujeme v tvare $P \Rightarrow Z$.

Ukážka: Dokážte, že ak je rovina α kolmá na rovinu β, tak je aj rovina β kolmá na rovinu α [2]. (Obr. 3)

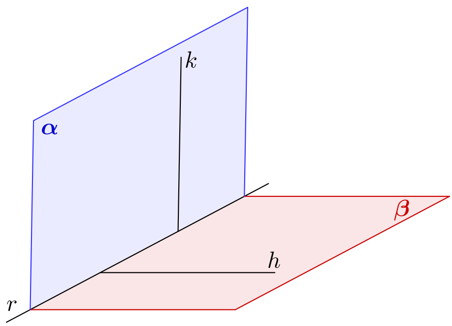

Obr. 3: Rovina α kolmá na rovinu β.

Schéma 1:

- $P \Rightarrow M_1$: Ak je rovina α kolmá na rovinu β, tak existuje priamka k roviny α kolmá na rovinu β.
- $M_1 \Rightarrow M_2$: Ak priamka k roviny α je kolmá na rovinu β, tak je priamka k roviny α kolmá na každú priamku roviny β.
- $M_2 \Rightarrow M_3$: Ak priamka k roviny α je kolmá na každú priamku roviny β, tak priamka k je kolmá na priamku h roviny β, pričom priamka h je kolmá na priamku $r = \alpha \cap \beta$.

- $M_3 \Rightarrow M_4$: Ak priamka k roviny α je kolmá na priamku h roviny β, pričom priamka h je kolmá na priamku $r = \alpha \cap \beta$, tak je aj priamka h roviny β kolmá na obe navzájom kolmé priamky k, r roviny α.
- $M_4 \Rightarrow M_5$: Ak je priamka h roviny β kolmá na navzájom kolmé priamky k, r roviny α, tak priamka h roviny β je kolmá na dve rôznobežky k, r roviny α.
- $M_5 \Rightarrow M_6$: Ak priamka h roviny β je kolmá na dve rôznobežky k, r roviny α, tak je priamka h kolmá na každú priamku roviny α.
- $M_6 \Rightarrow M_7$: Ak priamka h je kolmá na každú priamku roviny α, tak priamka h je kolmá na rovinu α.
- $M_7 \Rightarrow Z$: Ak je priamka h roviny β kolmá na rovinu α, tak je rovina β kolmá na rovinu α.

V prípade, že neopakujeme predpoklady viet a niektoré za sebou nasledujúce vety so spoločným podmetom spojíme do jednej zloženej vety, tak môžeme použiť zjednodušenú schému dôkazu:

$$P \Rightarrow M_1 \Rightarrow ... \Rightarrow M_k \Rightarrow Z. \tag{2}$$

Ukážka: Ak je rovina α kolmá na rovinu β, tak v nej leží priamka k kolmá na rovinu β. Priamka k je kolmá na priamku h roviny β, ktorá je kolmá na priesečnicu r rovín α, β. Priamka h je kolmá na obe rôznobežky roviny α a je kolmá na rovinu α. Priamka h roviny β je kolmá na rovinu α, a teda rovina β je kolmá na rovinu α.

V učebniciach aj pri výučbe DG sa používa práve zjednodušená forma dôkazu podľa schémy (2). Často sa však stáva, že študenti dôkazu podľa schémy (2) nerozumejú a je potrebné vrátiť sa k jeho úplnej forme podľa schémy (1). Príčinou neporozumenia dôkazu podľa schémy (2) môže byť, že študentom nie je jasný vzťah medzi niektorými za sebou nasledujúcimi členmi $M_k, M_{k+1}, i = 1, ..., k-1$. Najmä začiatočníkom väčšinou nebýva zrejmá funkcia podmienky P a záveru Z, prípadne úlohu hrá nepochopenie, čo sa má dokazovať a čo je dané.

5 Dôkazové techniky v DG

5.1 Priame dôkazy

Priamy dôkaz vytvárame z postupnosti pravdivých implikácií: $P \Rightarrow M_1 \Rightarrow ... \Rightarrow M_k \Rightarrow Z$, čím dokazujeme pravdivosť implikácie $P \Rightarrow Z$.

Ukážka: Dokážte, že ak je priamka kolmá na dve rôznobežky roviny, tak je kolmá na každú priamku roviny [7].

Priamy dôkaz s použitím analógie je metódou dôkazu, ktorá spočíva v tom, že vetu najskôr dokážeme o nejakom konkrétnom prípade a potom ukážeme analógiu ďalších prípadov, čím rozšírime platnosť vety aj na tieto prípady.

Priamy dôkaz na základe úplného triedenia je rozšírením priameho dôkazu o úplné triedenie. Odporúča sa pri dôkazoch tých viet, v ktorých sa robí klasifikácia a porovnávajú sa číselné hodnoty.

Ukážka: Dokážte, že priamka môže byť' nesečnicou, dotyčnicou alebo sečnicou kužeľosečky [1], [6].

5.2 Nepriame dôkazy

Nepriamy dôkaz tvoríme, ak pôvodnú vetu $P \Rightarrow Z$ dokazujeme tak, že priamo dokážeme obmenenú vetu $Z' \Rightarrow P'$. O nej vieme, že má rovnakú pravdivostnú hodnotu ako veta pôvodná.

Ukážka: Dokážte, že ak priamka p, ktorá je priesečnicou rovín σ, τ, je rovnobežná s rovinou ρ, tak sú rovnobežné priamky r, q, ktoré sú priesečnicami rovín σ, τ a roviny ρ.

Obmeny implikácií obohacujú techniky dôkazov implikácií. Nepriame dôkazy sú vhodné najmä v prípadoch, keď' sú vlastnosti objektov vyjadrené negatívne, napr. mimobežné priamky sú priamky, ktoré neležia v jednej rovine. V týchto prípadoch hovoríme, že urobíme dôkaz sporom.

V prípade *dôkazu sporom* dokazujeme k pôvodnej vete $P \Rightarrow Z$ jej negáciu, t.j. $P \wedge Z'$. Využívame fakt, že negácia výroku a pôvodný výrok majú opačnú pravdivostnú hodnotu. V priamom dôkaze negácie výroku dôjdeme k logickému sporu s predpokladom, axiómou, definíciou alebo už dokázanou vetou. Takto tvrdenie $P \wedge Z'$ bude nepravdivé, a preto musí byť' pravdivý pôvodný výrok.

Ukážka: Pôvodné tvrdenie je v tvare: Nech dve priamky a, b pretínajú priamku c pod zhodnými uhlami, potom sa priamky a, b nepretínajú. Dokazovať' budeme negáciu: Nech priamky a, b pretínajú priamku c pod zhodnými uhlami a nech majú spoločný bod.

Nepriame dôkazy patria medzi dôkazy matematických viet, ktoré sa dosť' často používajú v DG, najmä v stereometrii. Vynikajú stručnosť'ou, ale vyžadujú pochopenie a preniknutie do jeho logickej štruktúry. Nevýhodou nepriameho dôkazu v DG je náčrt obrázkov, ktorý zvyčajne kreslíme pre ilustráciu úmyselne nesprávne.

5.3 Dôkazy existencie a jednoznačnosti, konštrukčné dôkazy

V DG sa často stretávame s vetami, ktoré majú formu „existuje práve jedna" alebo „možno zostrojiť' práve jednu". K dôkazu týchto viet nevieme použiť' techniku priameho ani nepriameho dôkazu. V týchto vetách je potrebné dokázať' existenciu a jednoznačnosť' riešenia.

Dôkaz existencie používa konštrukciu vytvorenú z postupnosti krokov, pomocou ktorých sa pri použití dokázaných viet požadovaný prvok zostrojí. Zostrojený prvok, napríklad priamka či rovina, je dôkazom toho, že existuje. Túto techniku dôkazu existencie nazývame *konštrukčný dôkaz.*

Ukážka: Dokážte, že v bode roviny možno zostrojit' práve jednu priamku kolmú na túto rovinu [7], [2].

V tomto konštrukčnom dôkaze aplikujeme vetu z planimetrie: Bodom roviny možno zostrojit' práve jednu priamku kolmú na danú priamku [3].

Dôkaz jednoznačnosti použijeme vtedy, ak vo vete, ktorú máme dokázat', je aj požiadavka jednoznačnosti, čiže ak máme vylúčit' existenciu viacerých rôznych riešení. Dôkaz jednoznačnosti je priamy alebo nepriamy.

Priamy dôkaz jednoznačnosti súvisí s krokmi konštrukčného dôkazu. Ak v dôkaze aplikujeme viackrát vetu, ktorá má práve jedno riešenie, tak aj výsledok konštrukčného dôkazu má práve jedno riešenie.

Nepriamy dôkaz jednoznačnosti tiež súvisí s konštrukčným dôkazom, ale s tým rozdielom, že predpokladáme existenciu viacerých prvkov s danou vlastnost'ou a ukážeme, že to vedie k sporu s niektorým predpokladom.

Ukážka: Dôkaz jednoznačnosti kolmice na rovinu, ak bod P neleží v rovine α.

6 Záver

Uvedený text predstavuje zostručnenú kapitolu *Poznatky z logiky v didaktickej výstavbe* pripravovanej vysokoškolskej učebnice *Metodika výučby geometrie priestoru.* Táto je určená najmä študentom učitel'stva matematiky a deskriptívnej geometrie (predmet Didaktika DG), ale aj iných aprobácií s matematikou (predmet Geometria) na Univerzite Komenského. Učebnica nepredstavuje náhradu za učebné texty z DG, ale sústred'uje sa na teóriu vyučovania DG, ktorá je doplnená o históriu DG, didaktické zásady v DG, rozvíjanie priestorovej predstavivosti a moderné koncepcie vyučovacieho procesu.

Pod'akovanie

Autorky boli podporené prostriedkami z projektu KEGA 060UK-4/2018.

Literatúra

[1] Anton Dubec: *Metodika vyučovania deskriptívnej geometrie a rysovania,* SPN, Bratislava, 1961.

[2] Fratišek Hradecký, Miloslav Zedek, Jozef Šimek a kol.: *Metodika vyučovania deskriptívnej geometrie a rysovania,* Rektorát Univerzity Komenského v Bratislave, 1969.

[3] Zita Sklenáriková, Ján Čižmár: *Elementárna geometria euklidovskej roviny,* Univerzita Komenského Bratislava, 2005.

[4] Zita Sklenáriková: *Zobrazovacie metódy II.* Univerzita Komenského v Bratislave, 1976.

[5] Ivan Turek: *Didaktika,* Wolters Kluwer, Bratislava, 2014, ISBN 978-80-8168-004-5

[6] Alžbeta Mackovová: *Dynamické konštrukcie kužeľosečiek,* diplomová práca, Univerzita Komenského v Bratislave, Fakulta matematiky, fyziky a informatiky, 2018.
[7] Alois Urban: *Deskriptivní geometrie I.,* Praha, Alfa, 1982.

Voronoi diagram in hyperbolic geometry

Alžbeta Mackovová, Pavel Chalmovianský

Department of algebra and geometry
Mlynská dolina, 842 84 Bratislava, *Slovak Republic*
alzbeta.mackovova@fmph.uniba.sk, pavel.chalmoviansky@fmph.uniba.sk

Abstract. The construction and properties of Voronoi diagrams in Euclidean geometry have been studied and they are known since P. Dirichlet. In this paper, we discuss the construction and properties of the Voronoi diagram in hyperbolic geometry which are studied recently. We work with the Poincaré disk model. We focus on determining and illustrating the conditions that must be met by a Voronoi diagram for a given set of points to be non-degenerate, both in hyperbolic and Euclidean notions.

Keywords: Voronoi diagram, hyperbolic geometry, Poincaré disk model

1 Introduction

Voronoi diagrams belong to frequently studied objects of computational geometry with application in many fields of science – astronomy, crystallography, biology, robotics, computer graphics and medical diagnostics. Voronoi diagram is also a suitable mean for solving problems from several areas of everyday life. For example, urban planning for the placement of schools in cities, deployment of emergency medical centers, the problem of the nearest metro station, post office and hospital or physiological examination of nutrition of muscle tissue by capillaries. The properties of Voronoi diagram can be studied in various metric spaces – Euclidean [1], hyperbolic [4], [2], Manhattan [5] and many results are already known.

We are interested in Voronoi diagram in hyperbolic geometry, which may be represented in several isometrically equivalent models – the hyperboloid model, the hemispherical model, the Poincaré disk model, the Beltrami-Klein model and the Poincaré half-plane model. There are some results about Voronoi diagram in Poincaré half-plane model [3] and some properties and costruction of Voronoi diagram in Poincaré disk model [4] are already known.

We choose the Poincaré disk model for its geometrically attractive properties and we are focus on behavior of Voronoi diagram in this model.

2 Euclidean Voronoi diagram

Voronoi diagrams in Euclidean geometry have been already studied in sufficient width and depth. By [1] if the finite set $P = \{p_1, ..., p_n\}$ of distinct points in $\mathbb{R}^2$ is given, then we call the region

$$V(p_i) = \{x \in \mathbb{R}^2\colon \ \|x - p_i\| \leq \|x - p_j\| \text{ for } i \neq j; i, j \in I_n\}$$

the *Voronoi polygon* associated with p_i (or the Voronoi polygon of p_i), and the set given by

$$\mathcal{V} = \{V(p_1), ...V(p_n)\}$$

is called *Voronoi diagram* generated by P. We call p_i of $V(p_i)$ the *generator* of the ith Voronoi polygon and the set $P = \{p_1, ...p_n\}$ the *generator set* of the Voronoi diagram $\mathcal{V}$.

From this definition, we might see that Voronoi polygon for the generator p_i is a set of points that are not farther to the generator p_i comparing to any other generator. If we want to construct such a Voronoi diagram, we pick one generator and we construct bisector with others generators from the given set of point (usually not with all of them). Each of bisectors cut the plane in two half-planes and the intersection of these half-planes are Voronoi polygons and their union is the Voronoi diagram generated by the given set of generators.

3 The Poincaré disk model of hyperbolic geometry

The Poincaré disk model is two-dimensional space defined as

$$\mathbb{D} = \{(x, y) \in \mathbb{R}^2\colon\ x^2 + y^2 < 1\}$$

with the hyperbolic metric

$$ds^2 = \frac{4(dx^2 + dy^2)}{(1 - x^2 - y^2)^2}.$$

The boundary circle $\mathbb{S}^1 = \{(x, y) \in \mathbb{R}^2\colon\ x^2 + y^2 = 1\}$ is called *the main circle* and it does not belong to the space. The points of the main circle are called *ideal points* and they play a similar role as the points at infinity in extended Euclidean geometry.

Hyperbolic lines, or geodesics, are represented by arcs of circles that are perpendicular to the main circle. In special case, it is an open line-segment incident with the center of the disk (diameter of the main circle). For shortening we replace the adjective *hyperbolic* with *h-*.

Two h-lines may be

- *intersecting* – if the point of intersection is inside $\mathbb{D}$,
- *parallel* – if their common point is on the main circle, it is an ideal point,
- *ultraparallel* – if point of intersection is nor inside neither on the main circle.

Since we know the hyperbolic metric, we can measure the distance of two points. For the given points $x(x_1, x_2), y(y_1, y_2) \in \mathbb{D}$, and $y^* = (y_1, -y_2)$, their distance may be expressed as

$$d(x, y) = 2 \operatorname{arctanh}\left(\left|\frac{x - y}{y^* x - 1}\right|\right).$$

Then for the given line-segment with the endpoints $x(x_1, x_2)$, $y(y_1, y_2)$ a *hyperbolic bisector is the set of points* $z \in \mathbb{D}$ *for which*

$$d(x, z) = d(y, z).$$

It can be shown that hyperbolic bisector is h-line [2].

The last element we need to know is circle and then we are finally capable to define and construct Voronoi diagram in Poincaré disk model. If k is a circle in Euclidean geometry, then, if the circle k

- is inside disk $\mathbb{D}$, then it is also a *hyperbolic circle* but the Euclidean and hyperbolic centers are different,
- is tangent to the main circle at one ideal point, then it is called *horocycle* and the h-center is the ideal point,
- is intersecting the main circle in two distinct points and k is not perpendicular to the main circle, then it is called *hypercycle*.

4 Hyperbolic Voronoi diagram

The definition of Voronoi diagram in hyperbolic geometry is analogous to the definition in Eucliean geometry, but obviously we have to use the elements and relationship of hyperbolic geometry.

If the finite set $P = \{p_1, ..., p_n\} \in \mathbb{H}^2$ of distinct points is given, then we call the region given by

$$V(p_i) = \{x \in \mathbb{H}^2 \colon\ d(p_i, x) \leq d(p_j, x),\ \text{for } i \neq j;\ i, j \in I_n\}$$

the *hyperbolic Voronoi polygon* associated with p_i, and the set given by

$$\mathcal{V} = \{V(p_1), ..., V(p_n)\}$$

is the *hyperbolic Voronoi diagram* generated by P. We call p_i of $V(p_i)$ the *generator* of the i-th hyperbolic Voronoi polygon and the set P is the *generator set* of the hyperbolic Voronoi diagram $\mathcal{V}$.

We can see from the previous definition, that Voronoi h-polygon is a closed set, so it contains also the boundary which can be an h-line, an h-ray or an h-line-segment. The boundaries are called *Voronoi h-edges.* The endpoint of Voronoi h-edge is *Voronoi h-vertex* and it is mutual point for three or more Voronoi h-polygons.

It is quite obvious, that if there is a Voronoi h-vertex that is mutual for three or more Voronoi h-polygons, then the generators of these Voronoi h-polygons lie on one h-circle. The center of this circle is mutual point for h-bisectors of h-line-segments given by these generators. But depending on the type of circle in hyperbolic sense, this Voronoi h-vertex belonging to these Voronoi h-polygons does not have to exist. It occurs, if the circle is in hyperbolic sense:

- h-line, because the h-bisectors are ultraparallel (Fig. 1a),
- horocycle, because the h-center is an ideal point (it does not belong to the hyperbolic geometry) (Fig. 1b),
- hypercycle, because the center lies outside the disk $\mathbb{D}$ (Fig. 1c).

So the only satisfactory situation is, if this circle is in the hyperbolic sense a h-circle. Furthermore, as in Euclidean geometry, we call the hyperbolic Voronoi diagram *degenerate* if there exist at least one Voronoi h-vertex at which four or more Voronoi h-edges meet (Fig. 1d). Otherwise is Voronoi h-diagram *non-degenerate*.

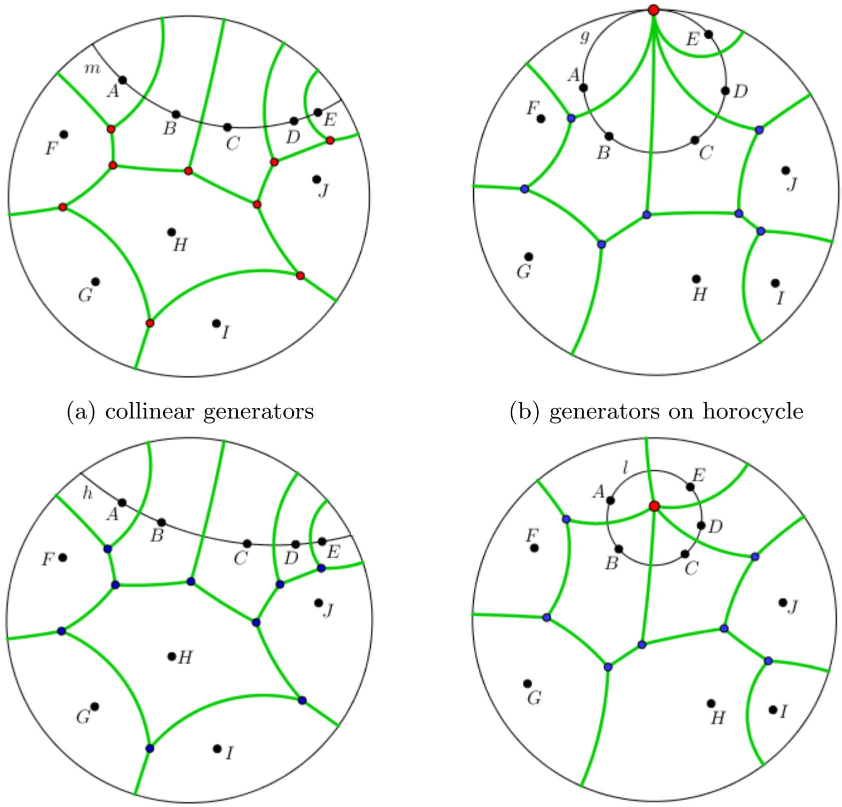

(a) collinear generators (b) generators on horocycle

(c) generators on hypercycle (d) degenerate Voronoi h-diagram

Fig. 1: Assumptions for Hyperbolic Voronoi diagram.

In order to avoid a situation when the Voronoi h-diagram is degenerate or the Voronoi h-polygon is unbounded, we assume the following conditions for the position of the generators.

Hyperbolic non-collinearity assumption (Fig. 1a)

For a given set of points $P = \{p_1, ..., p_n\} \in \mathbb{H}^2, (3 \leq n < \infty)$, there is no h-line m such that the points $p_{i_1}, ..., p_{i_k} \in P, (k \geq 3)$ lie on h-line m and all other points $P \setminus \{p_{i_1}, ...p_{i_k}\}$ are in same half-plane given by h-line m.

Horocycle assumption (Fig. 1b)

For the given set of points $P = \{p_1, ..., p_n\} \in \mathbb{H}^2, (3 \leq n < \infty)$, there is no horocycle g such that the points $p_{i_1}, ..., p_{i_k} \in P, (k \geq 3)$ lie on horocycle g and all other points $P \setminus \{p_{i_1}, ...p_{i_k}\}$ are external points of the horocycle g.

Hypercycle assumption (Fig. 1c)

For the given set of points $P = \{p_1, ..., p_n\} \in \mathbb{H}^2, (3 \leq n < \infty)$, there is no hypercycle h such that the points $p_{i_1}, ..., p_{i_k} \in P, (k \geq 3)$ lie on hypercycle h and all other points $P \setminus \{p_{i_1}, ...p_{i_k}\}$ are external points of the hypercycle h.

Hyperbolic circle assumption (Fig. 1d)

For a given set of points $P = \{p_1, ..., p_n\} \in \mathbb{H}^2, (4 \leq n < \infty)$, there is no h-circle l such that the points $p_{i_1}, ..., p_{i_k} \in P, (k \geq 4)$ lie on h-circle l and all other points $P \setminus \{p_{i_1}, ...p_{i_k}\}$ are external points of the h-circle l.

5 Conclusion

The main difference between Voronoi diagram in Euclidean and in hyperbolic geometry is, that in Euclidean geometry we need only the non-collinearity and non-circularity assumption. But as we have seen, in hyperbolic geometry, there are more cases, when the Voronoi h-polygon is unbounded.

Now when we know the behavior of Voronoi diagram in hyperbolic geometry, we would like to dynamic illustrate this situations when some generator moves along a h-line segment, a h-circle or another simple enough curve in the Poincaré disk model.

For the future, we would like to provides some statement about hyperbolic Voronoi diagrams and build the analogously theory in 3D.

Acknowledgements

This work was supported by the Slovak Research and Development Agency under the contract No. APVV-16-0053 and by Grant of Comenius University No. UK/304/2019.

References

[1] A. Okabe, B. Boots, K. Sugihara and S. Nok Chiu: *Spatial Tessellations: Concepts and Aplications od Voronoi Diagrams,* Hoboken, New Jersey, USA: John Wiley and Sons, 2010. 696 s. ISBN: 978-0-471-98635-5

[2] Z. Nilforoushan, A. Mohades: *Hyperbolic Voronoi Diagram,* In: Gavrilova M. L. et al. (eds) Computational Science and Its Applications - ICCSA 2006. ICCSA 2006. Lecture Notes in Computer Science, vol. 3984. Springer, Berlin, Heidelberg, pp. 735-742, 2006.

[3] K. Onishi and N. Takayama: *Construction of Voronoi diagram on the upper half-plane.* IEICE Transactions, vol. 79-A, no. 4, pp. 533-539, 1996.

[4] F. Nielsen and R. Nock: *Hyperbolic Voronoi diagrams made easy.* in ICCSA '10 Proceedings of the 2010 International Conference on Computational Science and Its Applications. Washington, DC, USA: IEEE Computer Society, pp. 74-80, 2010.

[5] R. Görke, A. Wolff: *Constructing the city Voronoi diagram faster* International Journal of Computational Geometry and Applications, vol. 18, no. 4, pp. 275–294, 2008.

Refinement of unorganized point sets via quadric fitting

Marcel Makovník, Pavel Chalmovianský

Department of algebra and geometry
Mlynská dolina, 842 48 Bratislava, Slovak Republic
marcel.makovnik@fmph.uniba.sk, pavel.chalmoviansky@fmph.uniba.sk

Abstract. In this paper, we propose a refinement scheme working on sets consisting of points with corresponding normal vectors. Each point of the input set and its local neighbourhood is fitted by a quadric surface. Then, a set of points is selected from the surface and included in the refined set. Particularly, we focus on the construction of such sets with respect to the uniformity of the sampling of the refined point set.

Keywords: refinement, point set, quadric fitting, sampling

1 Introduction

The problem of refinement is well studied for polygonal meshes [5]. Most of such schemes rely on the connectivity to compute the vertices of the refined mesh, i.e. the mesh with larger number of vertices and faces. The connectivity is usually provided by the suitable data structure, e.g. half-edge encoding [6].

However, only few refinement schemes do not require the connectivity [2, 4]. More precisely, the refinement is performed on an unorganized point set, i.e. the set of edges and faces is absent. This process is often referred to as point cloud refinement or meshless subdivision.

In our we work, we propose the refinement scheme with usage of quadric fitting, which takes the unorganized point set $\mathcal{P} \subset \mathcal{V} \times \mathcal{N} \subset \mathbf{A}^3(\mathbb{R}) \times \mathbf{V}^3(\mathbb{R})$ of point-normal pairs as an input. By applying the scheme we obtain the $\mathcal{P}'$ with more point-normal pairs, which also contains all elements of the set $\mathcal{P}$. This is done by assigning several new point-normal pairs for each $(P, \mathbf{n}) \in \mathcal{P}$.

2 Preprocessing

Before we start introducing new point-normal pairs, we need to assign three objects for each element of $\mathcal{P}$. Firstly, we determine the neighbourhood $\mathcal{H} \subset \mathcal{P}$ containing at least 9 elements. Then, we find the quadric surface Q, which is fitted to the neighbourhood $\mathcal{H}$. Finally, we create the modified set $\tilde{\mathcal{H}} \subseteq \mathcal{H}$, which is used in the determination of the elements of the refined set.

In order to process the set $\mathcal{P}$ efficiently, we use the octree structure for encoding.

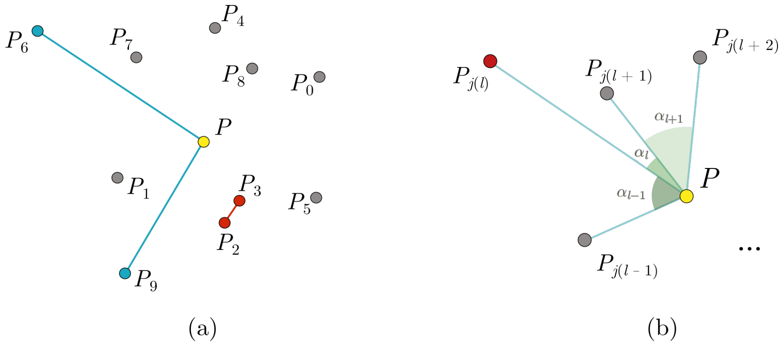

Fig. 1: (a) Points P_6 and P_9 because they are too distant from P. Also, one of the points P_2 and P_3 needs to be eliminated, since they are too close to each other. (b) The point $P_{j(l)}$ is eliminated, because the angle α_l is smaller than the minimal feasible value and its distance from the point P is larger than in the case of the point $P_{j(l+1)}$, which is also incident with the angle α_l.

2.1 Fitted quadric

Let $\mathcal{H} = \{(P_0, \mathbf{n}_0), ..., (P_k, \mathbf{n}_k)\} \subset \mathcal{P}$ be the neighbourhood assigned to the pair $(P, \mathbf{n}) \in \mathcal{P}$. All the elements of $\mathcal{H}$ lie within the sphere of the radius $r > 0$ such, that $|\mathcal{H}| \geq 9$, i.e.

$$\|P - P_i\| < r, \qquad i = 0, ..., k. \tag{1}$$

Subsequently, we approximate $\mathcal{H}$ by a quadric surface, which is given by $Q(x, y, z) = 0$ with coefficients $A, B, ..., J \in \mathbb{R}$. This is done by finding the argument of the minimum of the objective function, which is reflecting the distance of the point from the surface and deviation between the given normal and the normal of the quadric at the given point. For further details, see [1].

2.2 Points to be projected

Elements of $\mathcal{H}$ are projected onto a quadric surface and included in the refined set. However, we need to filter out those points which are too distant from P and handle those $P_i, P_j \in \mathbf{A}(\mathcal{H}), i \neq j$, which are too close to each other, as illustrated in the Fig. 1(a). The filtered set is then denoted by $\tilde{\mathcal{H}}$.

To eliminate redundant elements of $\mathcal{H}$, we orthogonally project all the points $P_0, ..., P_k \in \mathbf{A}(\mathcal{H})$ onto a plane ρ given by the normal vector $\mathbf{n}$ and passing through the point P. We denote by $P_i^{\perp}$ the projected point of the plane ρ corresponding to the point $P_i \in \mathbf{A}(\mathcal{P})$ for $i = 0, ..., k$. Then,

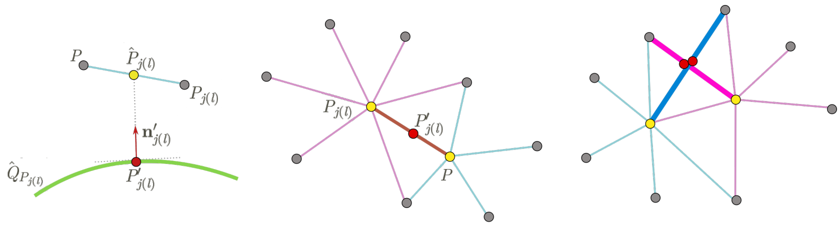

Fig. 2: (a) Projection of the point $\hat{P}_{j(l)}$ onto the quadric $\hat{Q}_{P_{j(l)}}$. (b) The point $P'_{j(l)}$ is inserted while the point P is processed, but also when the point $P_{j(l)}$ is processed. (c) The two overlapping edges (highlighted by thick lines) of two fans (teal and purple) produce two points (red) that are close to each other, but not identical.

we create a fan around P, i.e. we sort $P_0, ..., P_k$ with respect to the angle $P_0^{\perp} P P_i^{\perp}$, which results in the sequence $P_{j(0)}, ..., P_{j(k)}$.

Now we start filtering by inserting pairs $(P_{j(0)}, \mathbf{n}_{j(0)}), ..., (P_{j(k)}, \mathbf{n}_{j(k)})$ in the set $\tilde{\mathcal{H}}$. Then for each $l = 0, ..., k$, we compute the angle $\alpha_l = P_{j(l)} P P_{j(l+1)}$. Let $\varphi \in \langle 0, 2\pi)$ be the minimal feasible value of α_l within the fan. If $\alpha_l < \varphi$, we remove:

- the pair $(P_{j(l)}, \mathbf{n}_{j(l)})$, if $\|P_{j(l)} - P\| > \|P_{j(l+1)} - P\|$,
- the pair $(P_{j(l+1)}, \mathbf{n}_{j(l+1)})$ otherwise.

from the set $\tilde{\mathcal{H}}$, as can be seen in the Fig. 1(b).

3 Processing

After obtaining the set $\tilde{\mathcal{H}}$, we are allowed to project its elements onto a quadric surface. Denote by Q_P the quadric assigned to the pair $(P, \mathbf{n})$ and by $Q_{P_{j(l)}}$ the quadric assigned to the pair $(P_{j(l)}, \mathbf{n}_{j(l)}) \in \tilde{\mathcal{H}}$. Then, we project the point

$$\hat{P}_{j(l)} := \frac{1}{2} P + \frac{1}{2} P_{j(l)} \tag{2}$$

onto the quadric

$$\hat{Q}_{P_{j(l)}} := \frac{1}{2} Q_P + \frac{1}{2} Q_{P_{j(l)}} \tag{3}$$

and obtain the point $P'_{j(l)}$. The normal $\mathbf{n}'_{j(l)}$ is equal to the normal of $\hat{Q}_{P_{j(l)}}$ at the point $P'_{j(l)}$, see Fig. 2(a).

In certain cases, the point $P'_{j(l)}$ is computed twice, since it is inserted while processing both elements $(P, \mathbf{n})$ and $(P_{j(l)}, \mathbf{n}_{j(l)})$ (as can be seen in Fig. 2(b)). This may be avoided while processing the elements, i.e. while processing $(P, \mathbf{n})$, insert the pair $(P'_{j(l)}, \mathbf{n}'_{j(l)})$ into $\mathcal{P}'$ only if

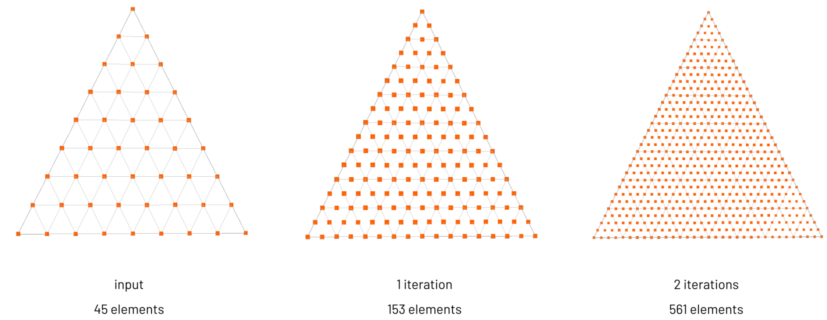

Fig. 3: The refinement on a part of a plane. (a) The input set with 45 elements. (b) The refined set after 1 iteration with 153 elements. (c) The refined set after 2 iterations with 561 elements.

- $(P, \mathbf{n})$ is not contained in the reduced neighbourhood $\tilde{\mathcal{H}}_{j(l)}$ belonging to the pair $(P_{j(l)}, \mathbf{n}_{j(l)})$,
- $(P, \mathbf{n})$ is contained in $\tilde{\mathcal{H}}_{j(l)}$, but $(P'_{j(l)}, \mathbf{n}'_{j(l)})$ was not inserted while processing the element $(P_{j(l)}, \mathbf{n}_{j(l)})$.

4 Results

The testing was performed on various unorganized sets. These sets were obtained by sampling of a part of a plane and hyperbolic paraboloid, a sphere and also Stanford bunny. For each set, we visualize the refined set after one and two iterations of refinement. We also depict the underlying mesh in the visualizations, which was used for sampling of the input sets. Note, that the information about edges is not used in our proposed method. When filtering the neighbourhood, the angle φ is set manually to the value $\varphi = {}^{2\pi}/_{9}$ in our experiments to get satisfactory results.

In the case of the regularly sampled plane, we observe, that the refinement using our method resembles the topological step of the Loop scheme [3] for polygonal meshes applied to the underlying mesh (Fig. 3).

Moreover, we applied our method on the set obtained from the unit sphere, which is actually created by the vertices and the corresponding normals of an unit icosahedron. As we see in the Fig. 4, the refinement respects the uniform sampling of the initial unorganized set with the increasing number of iterations.

The sets obtained from the hyperbolic paraboloid (Fig. 5) and Stanford bunny (Fig. 6) do not posses regular sampling. The consequence of this property is the fact, that the areas with dense sampling are also densely sampled in the refined set. Moreover, the irregular sampling contributes to locally dense sampling in the refined set in another way. When two fans

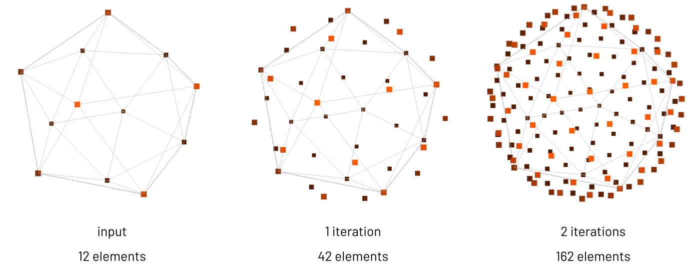

Fig. 4: The refinement on a sphere. (a) The input set with 12 elements. (b) The refined set after 1 iteration with 42 elements. (c) The refined set after 2 iterations with 162 elements.

Fig. 5: The refinement on a hyperbolic paraboloid. (a) The input set with 185 elements. (b) The refined set after 1 iteration with 686 elements. (c) The refined set after 2 iterations with 4354 elements.

overlap, the two inserted points are too close, but they are not identical, as depicted in the Fig. 2(c).

5 Conclusion

In our work we presented a refinement method operating on unorganized point sets, where the elements of the refined set are introduced by using the quadric fitting to the local neighbourhood. Our aim was to obtain a refined set which has similar sampling properties as the input set and as a main inspiration we used the Loop subdivision scheme for polygonal meshes. However, we still need to eliminate situations, which create the dense sampling artificially (i.e. the areas with the dense sampling in the refined set were not densely sampled in the input set), as stated above. Also, our aim is to estimate the minimal feasible value of the angle ρ and inspect on the geometric properties of the refined set. These are probably influenced by the weights for points and normals used in the process of

Fig. 6: The refinement on Stanford bunny. (a) The input set with 453 elements. (b) The refined set after 1 iteration with 1996 elements. (c) The refined set after 2 iterations with 9207 elements.

searching the fitted quadric and need to be explored thoroughly, since in our experiments we used constant weights in both cases and this may results in the noise in the refined set.

Acknowledgements

This work was supported by the Slovak Research and Development Agency under the contract No. APVV-16-0053.

References

[1] M. Makovník, P. Chalmovianský: *Refinement of triangle meshes using quadric fitting with algorithmic weights,* Proceedings of the Czech-Slovak Conference on Geometry and Graphics 2018. VUT Brno, Blansko, 2018.

[2] C. Moening, F. Mémoli, G. Sapiro, N. Dyn, N. Dodgson: *Meshless geometric subdivision,* Graphical Models, 69, pages 160–179. Elsevier, 2007.

[3] C. Loop: *Smooth subdivision surfaces based on triangles,* Master's thesis. Department of Mathematics, The University of Utah, 1987.

[4] G. Guennebaud, L. Barthe, M. Paulin: *Real-time point cloud refinement,* SPBG, pages 41–48, 2004.

[5] J. Peters, U. Reif: *Subdivision surfaces.* Springer, 2008.

[6] M. Botsch, L. Kobbelt, M. Pauly, P. Alliez, B. Lévy: *Polygon mesh processing.* AK Peters/CRC Press, 2010.

Grafické znázornění řešení soustav lineárních diskrétních rovnic

Graphical representation of solutions of linear discrete systems

Kristýna Mencáková, Jan Šafařík
Ústav matematiky a deskriptivní geometrie, Fakulta stavební VUT v Brně
Žižkova 17, Brno, Česká republika
mencakova.k@fce.vutbr.cz, safarik.j@fce.vutbr.cz

Abstract. This paper contains selected examples of linear discrete systems with delay and graphical representations of their solutions. A way to clearly visualise the previously published examples as figures is presented. To visualise the examples two mathematical programs Maple and GeoGebra are used.

Keywords: Linear discrete system, weakly delay, GeoGebra, Maple, LaTeX, tikzpicture.

Klíčová slova: Lineární diskrétní rovnice, slabé zpoždění, GeoGebra, Maple, LaTeX, tikzpicture.

1 Úvod

Při studiu lineárních diskrétních soustav se zpožděním a jejich následném publikování v různých článcích jsme se snažili danou problematiku vždy doplnit o příklady ukazující použití získaných poznatků. Tyto příklady jsme chtěli dopnit zajímavými a názornými obrázky. Hlavní náplní tohoto článku je několik vybraných příkladů spolu s obrázky z našich již publikovaných článků. Příklady jsou dopněny o základní pojmy k pochopení dané problematiky. U každého obrázku je dále stručně popsáno, jakým způsobem vznikl, např. pomocnými výpočty v programu Maple, zobrazením v programu GeoGebra, popřípadě dalším upravováním zdrojových dat přímo v LaTeXu.

2 Soustavy lineárních diskrétních rovnic se zpožděním

Nejprve zavedeme následující označení $\mathbb{Z}_r^s := \{r, r+1, \dots, s\}$ pro všechna $r \in \mathbb{Z}$, $s \in \mathbb{Z}$, $r \le s$. Podobně definujeme množinu $\mathbb{Z}_r^\infty$. Dále budeme používat symbol E pro jednotkovou matici.

V článku budeme pracovat jen se dvěma následujícímu speciální typy soustav lineárních diskrétních rovnic se zpožděním.

2.1 Slabě zpožděný systém lineárních diskrétních rovnic s konstantními koeficienty v $\mathbb{R}^2$

Uvažujme soustavu

$$x(k+1) = Ax(k) + Bx(k-m), \qquad k \in \mathbb{Z}_0^\infty, \tag{1}$$

kde $m \in \mathbb{N}$ je pevně dáno a nazývá se „zpoždění“, $A = \{a_{ij}\}_{i,j=1}^{2}$ a $B = \{b_{ij}\}_{i,j=1}^{2}$ jsou konstantní matice typu 2×2, $\det A \neq 0$, $B \neq \Theta$ (nulová matice řádu 2), $x\colon \mathbb{Z}_{-m}^{\infty} \to \mathbb{R}^2$.
Nechť je dána diskrétní funkce $\varphi\colon \mathbb{Z}_{-m}^{0} \to \mathbb{R}^2$ a nechť

$$x(k) = \varphi(k), \ \ k \in \mathbb{Z}_{-m}^{0}. \tag{2}$$

Pak funkci $x\colon \mathbb{Z}_{-m}^{\infty} \to \mathbb{R}^2$ nazveme řešením počáteční Cauchyovy úlohy (1), (2).

V článku [1] jsme odvodili obecné řešení slabě zpožděného systému lineárních diskrétních rovnic s konstantními koeficienty. Systém se nazývá slabě zpožděný, jestliže platí $\det\left(A + \lambda^{-m}B - \lambda E\right) = \det\left(A - \lambda E\right), \lambda \in \mathbb{C} \setminus \{0\}$, tj. charakteristické rovnice systému se zpožděním a systému bez zpoždění mají identické kořeny. Na závěr zmíněného článku byly vybrány dva příklady ilustrující výsledky prezentované v článku. První z těchto příkladů uvádíme zde.

Příklad 1. Nechť $m = 2$ a soustava (1) má tvar

$$\begin{aligned} x_1(k+1) &= -\ x_1(k) + 1.5x_2(k) + 2x_1(k-2) - \ x_2(k-2),\\ x_2(k+1) &= -3x_1(k) + 3.5x_2(k) + 4x_1(k-2) - 2x_2(k-2), \end{aligned}$$

kde

$$A = \begin{pmatrix} -1 & 1.5\\ -3 & 3.5 \end{pmatrix}, \quad B = \begin{pmatrix} 2 & -1\\ 4 & -2 \end{pmatrix}.$$

Soustavu lze zapsat ve tvaru

$$x(k+1) = Ax(k) + Bx(k-2). \tag{3}$$

Tabulka 1 ukazuje řešení dané volbou několika různých počátečních podmínek. Pro znázornění této úlohy jsme zvolili nejprve dvojrozměrný prostor (Obr. 1). Zde je zobrazeno pět vybraných počátečních podmínek $x(-2), x(-1), x(0)$ z Tabulky 1, odlišených různými barvami, a jim příslušné společné řešení $x(1), x(2), x(3), \dots$ vykreslené modrou barvou. Každý takový vektor $x(k) = (x_1(k), x_2(k))^T$ je pak v obrázku reprezentován bodem $x(k)$=$[x_1(k), x_2(k)]$. Pořadí těchto bodů odpovídající pořadí vektorů je dále naznačeno orientovanými úsečkami.

Na Obr. 2 jsou znázorněny stejné počáteční podmínky a jejich řešení z Tabulky 1 tentokrát v trojrozměrném prostoru. Zde je každý vektor $x(k) = (x_1(k), x_2(k))^T$ reprezentován bodem $x(k) = [k, x_1(k), x_2(k)]$. Obr. 1 by tedy vznikl jako bokorys, rovnoběžným promítáním ve směru

$x(-2)$	$x(-1)$	$x(0)$	$x(1), x(2), x(3), x(4), \ldots$
$(-2,5)^T$	$(4,4)^T$	$(6,-1)^T$	$(3,-4)^T, \left(\frac{3}{2},-4\right)^T, \left(\frac{3}{4},-2\right)^T, \left(\frac{3}{8},-1\right)^T, \ldots$
$(-2,4)^T$	$(4,3.5)^T$	$(6,-1)^T$	
$(-2,3)^T$	$(4,3)^T$	$(6,-1)^T$	
$(-2,2)^T$	$(4,2.5)^T$	$(6,-1)^T$	
$(-2,1)^T$	$(4,2)^T$	$(6,-1)^T$	

Tabulka 1: Počáteční podmínky soustavy (3) a jim odpovídající řešení

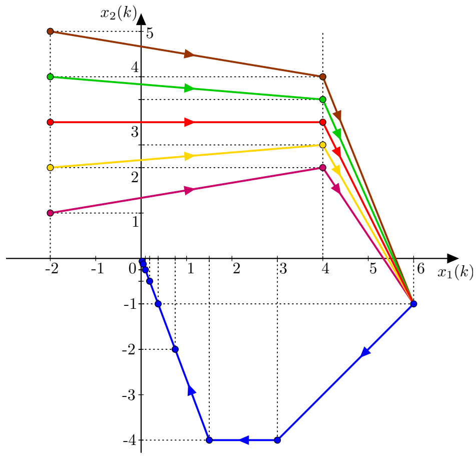

Obr. 1: Reprezentace řešení soustavy (3) v $\mathbb{R}^2$

osy k na rovinu x_1x_2. Pořadí vektorů je opět naznačeno spojením odpovídajících bodů. Pro větší přehlednost jsme nyní zvolili spojení pomocí spline křivek.

Obr. 1 i 2 vznikly přímou konstrukcí v programu GeoGebra a následným exportem PGF/TikZ kódu pro LaTeX. V programu LaTeX pak byly provedeny již jen drobné úpravy, jako posunutí některých popisků a podobně.

2.2 Lineární diskrétní soustavy řádu $(m+2)$

Uvažujme soustavu

$$\Delta^2 x(k) + B^2 x(k-m) = f(k), \quad k \in \mathbb{Z}_0^\infty, \tag{4}$$

kde $\Delta^2 x(k) := x(k+2) - 2x(k+1) + x(k)$ je druhá diference směrem dopředu, B je konstantní regulární matice typu $n \times n$, $m \in \mathbb{N}_0$, $x\colon \mathbb{Z}_{-m}^\infty \to$

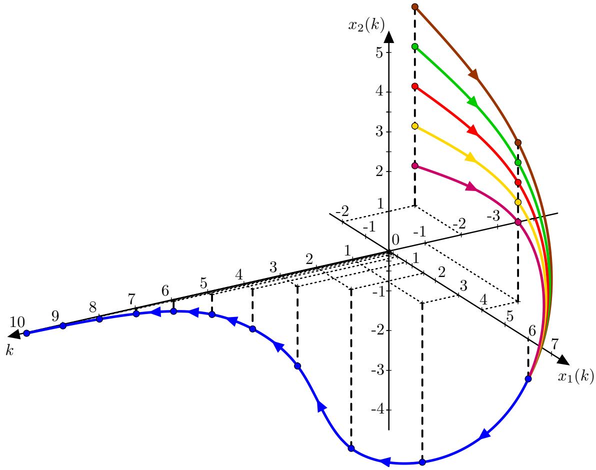

Obr. 2: Reprezentace řešení soustavy (3) v $\mathbb{R}^3$

$\mathbb{R}^n$ a $f\colon \mathbb{Z}_0^\infty \to \mathbb{R}^n$ je daná funkce.
Dále mějme dánu počáteční podmínku

$$x(k) = \varphi(k), \quad k \in \mathbb{Z}_{-m}^1. \tag{5}$$

Pak řešením počáteční Cauchyovy úlohy (4), (5) nazveme funkci $x\colon \mathbb{Z}_{-m}^\infty \to \mathbb{R}^n$.

V článku [2] jsme se zabývali vyjádřením řešení $x(k)$ úlohy (4), (5) pro předem stanovené $k = k^*$ bez nutnosti výpočtu všech předchozích hodnot řešení $x(k)$, tj. pro $k \in \mathbb{Z}_2^{k^*-1}$. Použití odvozeného vzorce jsme ukázali na následujícím příkladu.

Příklad 2. Nechť $n = 2$, $m = 3$, $k^* = 250$. Je dána soustava

$$\Delta^2 x(k) + Bx(k-3) = f(k), \tag{6}$$

s počáteční podmínkou

$$\varphi(-3) = \varphi(-2) = \varphi(-1) = \varphi(0) = (0,0)^T, \quad \varphi(1) = (0.001, 0.001)^T, \tag{7}$$

kde

$$B = \begin{pmatrix} 0.001 & -0.001 \\ 0.001 & 0 \end{pmatrix} \quad \text{a} \quad f(k) = \begin{cases} (1,1)^T & \text{pro} \quad k = 0, \\ (0,0)^T & \text{jinak.} \end{cases}$$

Na závěr příkladu jsme chtěli přiblížit chování soustavy (6) s danou počáteční podmínkou (7) pro prvních $k^* + m + 1$ hodnot jejího řešení.

Zvolili jsme znázornění v trojrozměrném prostoru, kde je opět každý vektor $x(k) = (x_1(k), x_2(k))^T$ reprezentován bodem $x(k) = [k, x_1(k), x_2(k)]$ (Obr. 3). Pro ještě lepší názornost byly do obrázku přidány půdorysy těchto bodů (vykreslené modrou barvou) a bokorysy (růžovou barvou). Pro velké množství vykreslovaných bodů je v tomto případě již nelze konstruovat jednotlivě v programu GeoGebra, jako v Příkladu 1. Tento program jsme použili pouze k narýsování souřadnicových os k, x_1, x_2 spolu s měřítky, a ty poté exportovali do PGF/TikZ kódu. Tím byla dána axonometrie, v níž jsme chtěli řešení znázorňovat. Pro zvolenou axonometrii jsme si pomocí jednotek na osách o souřadnicích (8) odvodili transformační rovnice (9).

$$X[3.55537,\ 0.26882],\quad Y[-0.394,\ 0.418],\quad Z[0,\ 6.8355] \tag{8}$$

$$g\begin{pmatrix} k \\ x_1(k) \\ x_2(k) \end{pmatrix} = \begin{pmatrix} 0.0355537 \cdot k\ -\ 3.94 \cdot x_1(k) \\ 0.0026882 \cdot k\ +\ 4.18 \cdot x_1(k)\ +\ 6.8355 \cdot x_2(k) \end{pmatrix} \tag{9}$$

Souřadnice všech požadovaných bodů, odpovídajících řešení úlohy (6), (7), i jejich půdorysů a bokorysů jsme spočítali pomocí programu Maple. Poté jsme provedli transformaci $g\colon \mathbb{R}^3 \to \mathbb{R}^2$ těchto souřadnic a nechali vypsat výsledné souřadnice jejich obrazů ve tvaru

$$zacatek(g_1(k), g_2(k)), konec\,,$$

to je například

$$zacatek(-0.1066611, -0.0080646), konec$$
$$\vdots$$

Řetězce „*zacatek*“ a „*,konec*“ jsme pak v LaTeX souboru nahradili částí příkazu pro vykreslení bodu, například

```
\fill␣[color=black]␣(-0.1066611,␣-0.0080646)␣++
(-1.5pt,0pt)--++(1.5pt,1.5pt)--++(1.5pt,-1.5pt)
    --++(-1.5pt,-1.5pt)--++(-1.5pt,1.5pt);
```

pro prostředí `tikzpicture`.

3 Závěr

V článku jsme ukázali několik možností pro tvorbu obrázků do odborných článků, ale i třeba pro tvorbu studijních materiálů. Například přímou konstrukcí obrázku v programu GeoGebra můžeme získat dynamické applety, statické obrázky v různých formátech nebo zdrojový kód pro vložení do LaTeX souboru a jeho další možnou úpravu. Program Maple zase nabízí možnosti výpočtu velkého množství dat. I když neumožňuje mnoho grafických výstupů, lze použít získaná data do zdrojového kódu pro jiné programy.

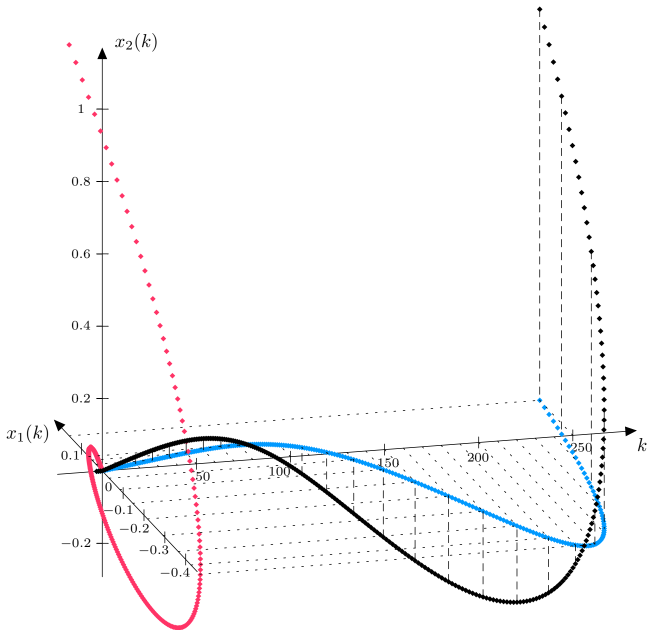

Obr. 3: Řešení Cauchyovy úlohy (6), (7)

Poděkování

Článek vznikl za podpory grantu FEKT-S-17-4225 Fakulty elektrotechniky a komunikačních technologií VUT v Brně.

Literatura

[1] J. Diblík, H. Halfarová, J. Šafařík: *Formulas for the general solution of weakly delayed planar linear discrete systems with constant coefficients and their analysis,* APPLIED MATHEMATICS AND COMPUTATION, 2019, Volume 358, No. 10, p. 363-381. ISSN: 0096-3003.

[2] J. Diblík, K. Mencáková: *Solving a higher-order linear discrete systems.* MATHEMATICS, INFORMATION TECHNOLOGIES AND APPLIED SCIENCES 2017, post-conference proceedings of extended versions of selected papers. Brno: University of Defence, 2017, p. 77-91. [Online]. [Cit. 2017-07-26]. Available at: `http://mitav.unob.cz/data/MITAV\%202017\%20Proceedings.pdf`. ISBN 978-80-7582-026-6.

$\mathbf{E}^5 \to \mathbf{E}^2$ animation of regular and other nice solids with visibility

Emil Molnár, István Prok, Jenő Szirmai

Budapest University of Technology and Economics, Institute of Mathematics, Department of Geometry

Budapest, P.O. Box: 91, H-1521, Hungary

emolnar@math.bme.hu, prok@math.bme.hu, szirmai@math.bme.hu

Abstract. In previous works (see [3], [4], [5]) the authors extended the method of central projection to higher dimensions, namely, for $\mathbf{E}^4 \to \mathbf{E}^2$ projection from a one dimensional centre figure, together with a natural visibility algorithm. All these are presented in the linear algebraic machinery of real projective sphere $\mathcal{PS}^4$ or space $\mathcal{P}^4(\mathbf{V}^5, \boldsymbol{V}_5, \mathbf{R}, \sim)$. In this presentation we further develop this method for $\mathbf{E}^5 \to \mathbf{E}^2$ animation by the exterior (Grassmann–Clifford type) algebra (with scalar product) and implement on computer with other effects of illumination, e.g. for (regular and other nice) polytopes on the base of the homepage http://www.math.bme.hu/∼ prok. The machinery is applicable for any d-dimensional projective space $\mathcal{P}^d$ and p-dimensional image.

Keywords: projective spherical space, central projection in higher dimensions, visibility algorithm, non-Euclidean geometries by projective metrics.

1 Introduction

In the Vorau Conference on Geometry, 2007 J. Katona and E. Molnár presented the problem "Visibility of the higher-dimensional central projection onto the projective sphere" appeared in *Acta Mathematica Hungarica* [3]. In that paper a general procedure was given – implemented by the first author to the central projection of the 4-cube directly (without intermediate 3-projection) into the 2-plane of the computers screen – which projects the edge framework of a d-polytope onto a p-plane from a complementary s-centre-figure ($p+s+1=d$, e.g. $p=2,\ s=1,\ d=4$). All those were embedded into the machinery of Grassmann–Clifford type algebras of $d+1$-vector- and form- spaces, describing the projective metric d-spheres, initiated by the second author. Thus, Euclidean and then other (e.g. hyperbolic, spherical and other projective metric Thurston) geometries can also uniformly be discussed [8], [10] and visualized by J. Szirmai and his (doctor) students.

In [5] we specified that procedure to the most important orthogonal (or parallel) projections of the regular 4-polytopes elaborated by I. Prok in his homepage [11] where 4-polytopes nicely move in the screen. Our initiative with visibility makes these demonstrations more attractive, and this seems to be new and timely procedure, not finished yet. Applying d-dimensional projective spherical geometry $\mathcal{PS}^d(\mathbf{V}^{d+1}, \boldsymbol{V}_{d+1}, \mathbf{R}, \sim)$, represented by the

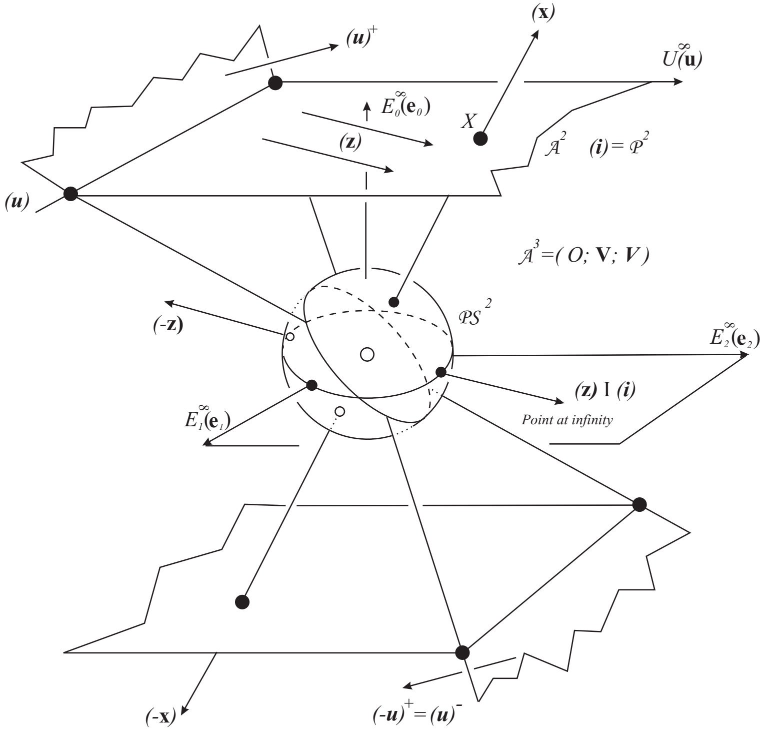

Fig. 1: The projective sphere $\mathcal{PS}^2$, the double affine plane $\mathcal{A}^2$ and the projective plane $\mathcal{P}^2$ can also be visualized by vectors of $\mathbf{V}^3$ and by forms of $\boldsymbol{V}_3$.

standard real $(d+1)$-vector space and its dual up to positive real factors as $\sim$ equivalence, the central projection from a $(d-3)$-centre to a 2-screen can be discussed in a straightforward way, but interesting visibility problems occur, first in the case of $d=4$ as a nice attractive application. So regular 4-solids can be visualized in the Euclidean space $\mathbf{E}^4$ and non-Euclidean geometries, e.g. spherical $\mathbf{S}^4$ and hyperbolic $\mathbf{H}^4$ geometry. In [5] the geodesics and geodesic spheres is also illustrated in $\mathbf{H}^2\times\mathbf{R}$ and $\widetilde{\mathbf{SL}_2\mathbf{R}}$ spaces by projective metric geometry.

In the present paper we extend the above results to the 5-dimensional space, and illustrate it with some nice pictures [11].

2 A unified vector calculus

We can describe classical planes uniformly, when we embed these planes into the projective sphere. This method suits for discussing spherical, hyperbolic, Euclidean, Minkowskian and Galilean planes. Projective and affine planes will be special cases, too [8].

Let $\mathbf{V}^3 = \mathbf{V}$ be a vector space over the real numbers $\mathbf{R}$, and $\boldsymbol{V}_3 =: \boldsymbol{V}$ is its dual space or space of its linear forms. Let $\mathbf{a}_i$ be a basis in $\mathbf{V}$. Then $\boldsymbol{b}^j$ is its dual basis in $\boldsymbol{V}$, iff $\mathbf{a}_i\boldsymbol{b}^j = \delta_i^j$ (the Kronecker symbol). We consequently denote by

$$\mathbf{x} = x^i\mathbf{a}_i = (x^0\ x^1\ x^2)\begin{pmatrix}\mathbf{a}_0\\ \mathbf{a}_1\\ \mathbf{a}_2\end{pmatrix} \in \mathbf{V} \text{ and } \boldsymbol{u} = \boldsymbol{b}^j u_j = (\boldsymbol{b}^0\ \boldsymbol{b}^1\ \boldsymbol{b}^2)\begin{pmatrix}u_0\\ u_1\\ u_2\end{pmatrix} \in \boldsymbol{V}$$

the corresponding bases and coordinates of vectors and forms, respectively, and apply Einstein-Schouten sum convention for the same upper and lower indices from 0 to 2.

Form $\boldsymbol{u} \in \boldsymbol{V}$ takes the value $\mathbf{x}\boldsymbol{u} = x^i u_i \in \mathbf{R}$ on $\mathbf{x} \in \mathbf{V}$. The vector class $\mathbf{x} \sim c\mathbf{x} \Rightarrow (\mathbf{x})$ defines a point $X = (\mathbf{x})$ in the projective sphere $\mathcal{PS}^2$ with $c > 0$ and $(\mathbf{x}) = (-\mathbf{x})$ in projective plane $\mathcal{P}^2$ with $c \in \mathbf{R}\setminus\{0\}$. In dual terms: $\boldsymbol{u} \sim \boldsymbol{u}\cdot\frac{1}{c} \Rightarrow (\boldsymbol{u})$ defines a (directed) line $u = (\boldsymbol{u})$ in $\mathcal{PS}^2$ iff $\frac{1}{c} > 0$; a line $u = (\boldsymbol{u}) = (-\boldsymbol{u})$ iff $\frac{1}{c} \in \mathbf{R}\setminus\{0\}$ for $\mathcal{P}^2$. The incidence $(\mathbf{x}) \in (\boldsymbol{u})$ means $\mathbf{x}\boldsymbol{u} = 0$. Fig. 1 shows, how an affine plane A^2 is embedded into an affine space $A^3(O;\mathbf{V},\boldsymbol{V})$, into the projective plane $\mathcal{P}^2 = A^2 \cup (\boldsymbol{i})$, furthermore, into the projective sphere $\mathcal{PS}^2$ that can be considered as a "double affine plane" extended by a "double ideal line" $(\boldsymbol{i})$ at infinity.

Let the main difference to the usual discussion be emphasized: in $\mathcal{PS}^2$ an affine line has two ideal points at infinity, one of them is distinguished, assigned by the viewing direction of the observer. Every point of the affine line is doubled in order to form a circle (see also Fig. 1). As our Fig. 2 will indicate in 4-space, visualized in the usual 3-space and in the figure plane. The observer "stands" in the vanishing hyperplane, looking ahead from $C_3(\mathbf{c}_3)$ in directions pointing to the positive halfspace where the target polytope and then behind (say for simplicity) the picture plane are placed. We can follow these analogies for the d-dimensional space $\mathcal{PS}^d$ as well.

Relative visibility of $X(\mathbf{x})$ to $X'(\mathbf{x}')$ with $(')$ coordinates can be decided by Figures 3 and by a conventional ordering prescription:

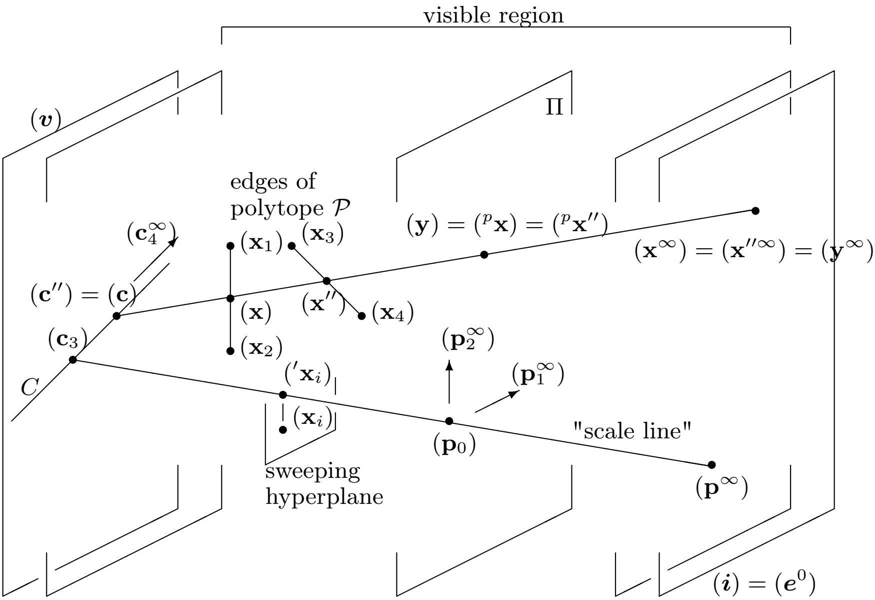

Fig. 2: Ordering vertices to vanishing hyperplane $(\boldsymbol{v})$

2.1 Higher dimensional matrix description

An affin-projective coordinate simplex represents the camera by

$$\begin{pmatrix} \mathbf{p}_0 \\ \vdots \\ \mathbf{p}_p^\infty \\ \mathbf{c}_{p+1} \\ \vdots \\ \mathbf{c}_d^\infty \end{pmatrix} \sim \begin{pmatrix} 1 & \dots & p_0^p & p_0^{p+1} & \dots & p_0^d \\ \vdots & & \vdots & \vdots & & \vdots \\ 0 & \dots & p_p^p & p_p^{p+1} & \dots & p_p^d \\ c_{p+1}^0 & \dots & c_{p+1}^p & c_{p+1}^{p+1} & \dots & c_{p+1}^d \\ \vdots & & \vdots & \vdots & & \vdots \\ 0 & \dots & c_d^p & c_d^{p+1} & \dots & c_d^d \end{pmatrix} \begin{pmatrix} \mathbf{e}_0 \\ \vdots \\ \mathbf{e}_p^\infty \\ \mathbf{e}_{p+1}^\infty \\ \vdots \\ \mathbf{e}_d^\infty \end{pmatrix} \sim:$$

$\sim:$ (Cam) $\begin{pmatrix} \mathbf{e}_0 \\ \vdots \\ \mathbf{e}_d^\infty \end{pmatrix}$. Here any point $X(\mathbf{x})$ in the visible region

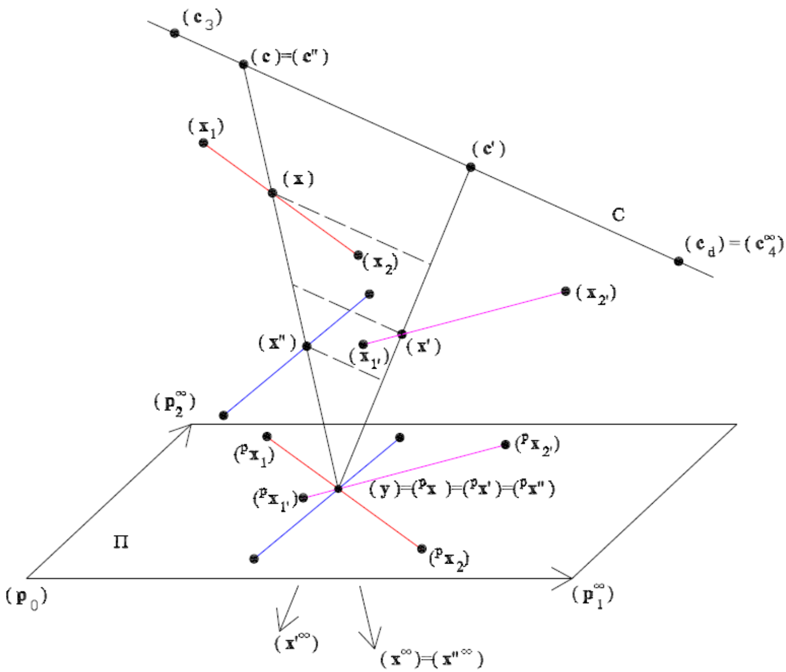

Fig. 3: Projection of segments to extended local visibility.

can be expressed as

$$\mathbf{x} \sim (1, x^1, \ldots, x^p, x^{p+1}, \ldots, x^d) \begin{pmatrix} \mathbf{e}_0 \\ \vdots \\ \mathbf{e}_d^\infty \end{pmatrix} \sim$$

$$\sim (y^0, y^1, \ldots, y^p, c^{p+1}, \ldots, c^d)(\mathrm{Cam}) \begin{pmatrix} \underline{\mathbf{e}}_0 \\ \vdots \\ \underline{\mathbf{e}}_d^\infty \end{pmatrix}, \quad \text{so that}$$

$$(1, x^1, \ldots, x^p, x^{p+1}, \ldots, x^d)(\mathrm{Cam})^{-1} \sim (y^0, y^1, \ldots, y^p, c^{p+1}, \ldots, c^d) \sim$$

$$(1, \frac{y^1}{y^0}, \ldots, \frac{y^p}{y^0}, \frac{c^{p+1}}{y^0}, \ldots, \frac{c^d}{y^0}).$$

a) *the images* $({}^p\mathbf{x}) = (\mathbf{y})$ *and* $({}^p\mathbf{x}') = (\mathbf{y}')$ *are different (both are visible);*

b) *if the images are the same, i.e.* $\mathbf{y} \sim \mathbf{y}'$*, namely* $\frac{y^1}{y^0} = \frac{y^{1'}}{y^{0'}}, \ldots, \frac{y^p}{y^0} = \frac{y^{p'}}{y^{0'}}$*, then* $\frac{c^{p+1}}{y^0} > \frac{c^{(p+1)'}}{y^{0'}}$;

c) *if the above equalities hold, then* $\frac{c^d}{y^0} < \frac{c^{d'}}{y^{0'}}$ *(the reverse inequality holds for* $d = 4 = d'$*).*

Then $X(\mathbf{x})$ is nearer the centre figure C than $X'(\mathbf{x}')$. We see here the critical points of our algorithm:

0, Premliminary triangulation of the polytope which will be projected;

1, Solution of too many linear equation systems (by Gauss-Seidel elimination);

2, Ordering the points to the centre figure C and picture plane Π (camera) by coordinates.

3 Coxeter-Schläfli diagram and matrix for 3-cube, 4-cube and regular d-polytopes

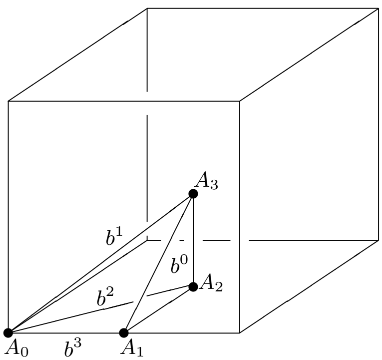

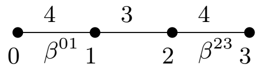

$$\begin{pmatrix} 1 & -\frac{\sqrt{2}}{2} & 0 & 0 \\ -\frac{\sqrt{2}}{2} & 1 & -\frac{1}{2} & 0 \\ 0 & -\frac{1}{2} & 1 & -\frac{\sqrt{2}}{2} \\ 0 & 0 & -\frac{\sqrt{2}}{2} & 1 \end{pmatrix} = (b^{ij})$$

Fig. 4: Cube in $\mathbb{E}^3$ and symbols for it

We illustrate the 3-cube in Fig. 4 by its characteristic simplex: vertex A_0, edge centre A_1, face centre A_2, body centre A_3, and the 4 side faces, e.g. $b^0 = (A_1 A_2 A_3)$. That means e.g.

$$\cos[\pi - (b^1 b^2)] = \cos[\pi - \frac{\pi}{3}] = -\frac{1}{2} = b^{12}$$
$$\text{in the symmetric matrix } \ (b^{ij}) \ \ (i, j = 0,\ 1,\ 2,\ 3).$$

Analogous cases are collected for the 4-cube and the regular d-polytope, respectively [4], [11].

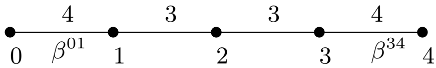

$$(b^{ij}) = \begin{pmatrix} 1 & -\frac{\sqrt{2}}{2} & 0 & 0 & 0 \\ -\frac{\sqrt{2}}{2} & 1 & -\frac{1}{2} & 0 & 0 \\ 0 & -\frac{1}{2} & 1 & -\frac{1}{2} & 0 \\ 0 & 0 & -\frac{1}{2} & 1 & -\frac{\sqrt{2}}{2} \\ 0 & 0 & 0 & -\frac{\sqrt{2}}{2} & 1 \end{pmatrix}$$

$$\{n_{01}, n_{12}, \ldots, n_{d-2,d-1}; \beta^{d-1,d}\} \Longleftrightarrow$$

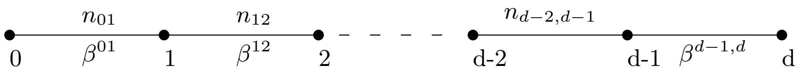

$$b^{ij} = \begin{pmatrix} 1 & -\cos\beta^{01} & 0 & \ldots & 0 & 0 \\ -\cos\beta^{01} & 1 & -\cos\beta^{12} & \ldots & 0 & 0 \\ 0 & -\cos\beta^{12} & 1 & \ldots & 0 & 0 \\ \vdots & \vdots & \vdots & \ddots & \vdots & \vdots \\ 0 & 0 & 0 & \ldots & 1 & -\cos\beta^{d-1,d} \\ 0 & 0 & 0 & \ldots & -\cos\beta^{d-1,d} & 1 \end{pmatrix}$$

where $\beta^{ij} = \frac{\pi}{n_{ij}}$ for $i, j = 0, 1, \ldots, d;\ i \neq j,\ (i,j) \neq (d-1, d);\ 1 \leq n_{ij} \in \mathbb{N}$ natural numbers.

To a regular d-polytope $\mathcal{P}$ we introduce a characteristic simplex for $\mathcal{P}$ by the following general

Definition 3.1 *We introduce an angle metric for our simplex S just by the starting bilinear form, considered as scalar product*

$$\langle \boldsymbol{b}^i, \boldsymbol{b}^j \rangle = b^{ij} = \cos(\pi - \beta^{ij}), \quad i, j = 0, 1, \ldots, d.$$

Think of $\boldsymbol{b}^i$ as the inward "normal" unit vector to the facet b^i (hyperface or $d-1$ face) and so $\boldsymbol{b}^j$ to b^j as well. $\square$

We have a well known

Theorem 3.1 *The scalar product by b^{ij} above defines a spherical, hyperbolic or Euclidean angle metric of hyperplanes for the projective sphere $\mathcal{PS}^d$ by*

$$\cos\beta^{ij} = \frac{-b^{ij}}{\sqrt{b^{ii}b^{jj}}} \quad \textit{or, in general,}$$

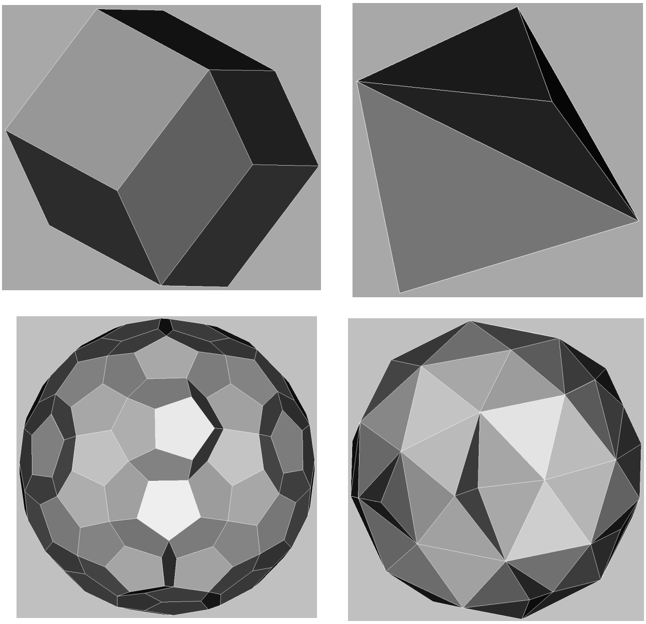

Fig. 5: a. The 4-cube with Coxeter-Schläfli symbol $(4, 3, 3)$.
b. The 4-Simplex with Coxeter-Schläfli symbol $(3, 3, 3)$.
c. The 120-cell $(5, 3, 3)$ and its dual : d. The 600-cell $(3, 3, 5)$.

$$\cos\omega = \frac{-\langle \boldsymbol{u}; \boldsymbol{v} \rangle}{\sqrt{\langle \boldsymbol{u}; \boldsymbol{u} \rangle \langle \boldsymbol{v}; \boldsymbol{v} \rangle}} = \frac{-u_i b^{ij} v_j}{\sqrt{(u_r b^{rs} u_s)(v_r b^{rs} v_s)}}$$

for generalized dihedral angle ω *of hyperplanes* $(\boldsymbol{u})$ *and* $(\boldsymbol{v})$; *according to the signature of* b^{ij}*:*

$$\langle +, +, \ldots, +; + \rangle \text{ for spherical } d\text{-space } \mathbb{S}^d,$$
$$\langle +, +, \ldots, +; - \rangle \text{ for hyperbolic } d\text{-space } \mathbb{H}^d,$$
$$\langle +, +, \ldots, +; 0 \rangle \text{ for Euclidean } d\text{-space } \mathbb{E}^d. \ \square$$

By the inverse matrix of $(b^{ij}$ in case $\mathbf{S}^d$ and $\mathbf{H}^d$, i.e. by $(b^{ij})^{-1} = a_{ij}$, we can define the distance metric of simplex $A_0 A_1 \ldots A_d$ by a coordinate presentation. $\mathbf{E}^d$ needs special discussion by the minor subdeterminant matrix (B_{ij}) of (b^{ij}). For details see [4], [10].

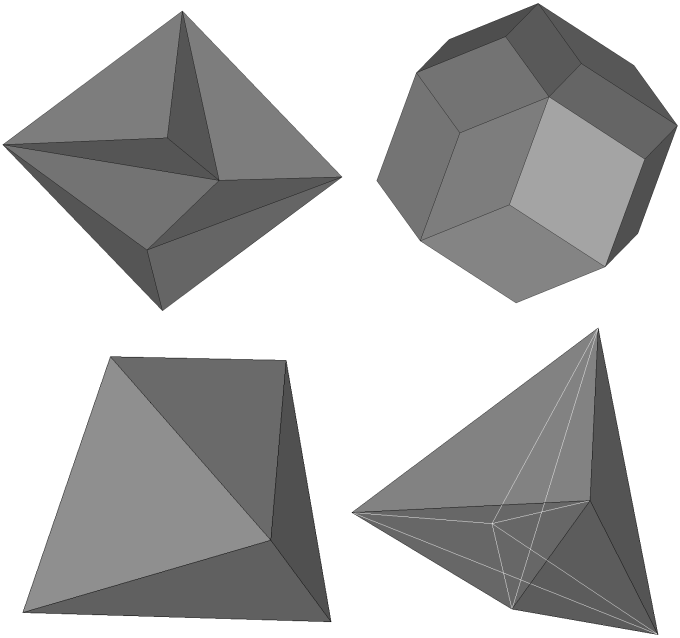

Fig. 6: a. The 5 cross-polytope with Coxeter-Schläfli symbol $(3, 3, 3, 4)$.
b. The 5-cube with Coxeter-Schläfli symbol $(4, 3, 3, 3)$. They are duals.
c. The 5-simplex $(3, 3, 3, 3)$.
d. The 5-simplex $(3, 3, 3, 3)$ with covered edges behind, it is self dual.

4 Visualization of regular solids with visibility in 4- and 5-dimensional Euclidean space

By the home page of I. Prok [11] you can wonder the $3-4-5$-dimensional Platonic solids, moving on the computer screen. Imagine light source from eyes of the observer at the infinity first, then in the centre figure in general (as our future plan). The surprising scattering effects mean that new-and-new $2-$faces come from behind, first in dark then become brighter. Not only at the border but also in middle part, since $2-$faces of $d-1$-hyperfaces also come into the play (if $d > 3$). For a while convex bodies are easier, but our algorithm can be applied to non-convex polyhedra as well (see Fig. 5-6). Our favorite is the 120-cell, where 120 pieces of 3-dimensional dodecahedra bound the 4-polytope.

References

[1] Ács, L., Fundamental D-V cells for E^4 space groups on the 2D-screen, 6^{th} ICAI, Eger, Hungary (2004), Vol. 1, 275-282.

[2] Coxeter, H.S.M., The real projective plane, 2nd Edition, Cambridge University Press, London, (1961).

[3] Katona, J. – Molnár, E., Visibility of the higher-dimensional central projection into the projective sphere, *Acta Mathematica Hungarica* **123/3**, (2009), 291-309.

[4] Katona, J. – Molnár, E. – Prok, I., Visibility of the 4-dimensional regular solids, moving on the computer screen, Proc. 13^{th} ICGG, Dresden, Germany, (2008).

[5] Katona, J. – Molnár, E. – Prok, I. – Szirmai, J., Higher-dimensional central projection into 2-plane with visibility and applications, *Kragujevac Journal of Mathematics* **Vol.35** Number 2 (2011), 249-263.

[6] Ledneczki, P. – Molnár, E., Projective geometry in engineering, *Periodica Polytechnica Ser. Mech. Eng.* Vol. **39**. No. 1., (1995), 43-60.

[7] Malkowsky E. – Veličković, V., Visualization and animation in differential geometry, Proc. Workshop Contemporary Geometry and Related Topics, Belgrade, (2002), Ed.:Bokan-Djorić-Fomenko-Rakić-Wess, Word Scientific, New Jersey-London-etc. (2004), 301-333.

[8] Molnár, E., The projective interpretation of the eight 3-dimensional homogeneous geometries, *Beiträge Alg. Geom. (Contr. Alg. Geom.)* **38**, (1997), 261-288.

[9] Molnár, E. – Prok, I. Three- and four-dimensional regular solids move in the computer 2-screen *In: Pavlekovic, M; Kolar-Begovic, Z; Kolar-Super, R (eds.) MATHEMATICS TEACHING FOR THE FUTURE Zagreb: Josip Juraj Strossmayer University of Osijek,* (2013) pp. 173-185.

[10] Molnár, E. – Szirmai, J., Symmetries in the 8 homogeneous 3-geometries, *Symmetry: Culture and Science*, Vol. **21** Numbers 1-3, (2010), 87-117.

[11] Prok, I., http://www.math.bme.hu/∼prok

[12] Weeks, J.R., Real-time animation in hyperbolic, spherical and product geometries, Non-Euclidean Geometries, János Bolyai Memorial Volume, Ed.: A. Prékopa and E. Molnár, Springer, (2006), 287-305.

Procvičování Mongeova promítání v programu GeoGebra

Practice of Monge Projection in GeoGebra

Petra Pirklová, Daniela Bímová

Dept. of Mathematics and Didactic of Mathematics, Faculty of Science, Humanities and Education, Technical university of Liberec
Studentská 1402/2, 461 17 Liberec, Czech Republic
petra.pirklova@tul.cz, daniela.bimova@tul.cz

Abstract. Monge projection, part of descriptive geometry, isn´t popular among students. There are a lot of topics for learning, on the contrary, time for learning is very short. Students very often complain for low number of exercises for practising the Monge projection. Above all most of the tasks are without solutions. But solution without construction is useless and knowledge of the construction of the solution of a problem is very important. Therefore, we created worksheets of with 133 problems concerning the Monge projection. The problems start at the basic level and end with the complex problems. Then gradual construction process (using a slider) and verbal or symbolic description of the construction were created for each problem in the dynamic 3D software GeoGebra. GeoGebra book containing solutions for all 133 problems of the worksheets was built.

Keywords: Descriptive geometry, projection, Monge projection, worksheets, practice, GeoGebra

Klíčová slova: Deskriptivní geometrie, promítání, Mongeovo promítání, pracovní listy, procvičování, GeoGebra

1 Úvod

Jedna ze základních zobrazovacích metod deskriptivní geometrie - Mongeovo promítání - je na Technické univerzitě v Liberci vyučována na fakultě strojní, fakultě architektury a fakultě přírodovědně-humanitní a pedagogické. Při studiu Mongeova promítání je velice důležité dostatečné procvičování jednotlivých úloh, jak jednoduchých tak i složitějších. Studenti si však velice často stěžují na nedostatek úloh k procvičování Mongeova promítání. Úlohy, které již v učebních textech naleznou, jsou však často bez řešení, případně pokud řešení v textu je znázorněno, pak je pro studující nepřehledné a špatně se v něm orientují, protože ve výsledném rysu jsou uvedeny všechny konstrukce najednou. Úlohy bez řešení a případně bez příslušného komentáře či popisu řešení jsou pro mnohé studenty nepoužitelné.

Proto byly vytvořeny pracovní listy s dostatkem úloh ze všech oblastí Mongeova promítání. Od úloh základních až po úlohy na sestrojování těles. Aby však pracovní listy byly pro studenty přínosné, bylo nutné vytvořit také řešení k těmto pracovním listům. Cílem také bylo, aby řešení bylo názorné a podrobné. K tomuto účelu byl s výhodou použit geometrický 3D program GeoGebra.

2 Řešení úloh v appletech

Každá úloha z pracovních listů byla dle svého zadání v těchto pracovních listech vyřešena v programu GeoGebra. Zadání je totožné jako v pracovních listech, tedy souřadnice zadaných vstupních prvků (body, přímky, roviny, atd.) jsou stejné jako v pracovních listech. Také nelze s jednotlivými určujícími prvky úlohy pohybovat. Tyto prvky jsou v appletu tzv. upevněné. Přesné zadání je samozřejmě důležité pro výsledek konstrukce, každý uživatel musí mít výsledek stejný.

Jednotlivé applety řešených úloh byly vytvářeny tak, aby byly uživatelsky přívětivé, tedy jejich ovládání je pro jednoduchost koncipováno stejně. Applety jsou rozděleny na tři části. V části první je umístěno zadání a posuvník. Při pohybování posuvníku se postupně zobrazují jednotlivé kroky konstrukce. U každého kroku se rovněž objevuje v tomto prvním okně zápis konstrukce symbolický, příp. slovní. Ve druhé části je průmět celé situace v Mongeově promítání. V části třetí, ve 3D okně, je zobrazena celá prostorová situace úlohy. Krokování konstrukce v Mongeově průmětu a ve 3D okně je provázáno. Tedy objeví-li se část konstrukce ve 2D okně, pak ta samá část konstrukce se objeví také v okně prostorovém.

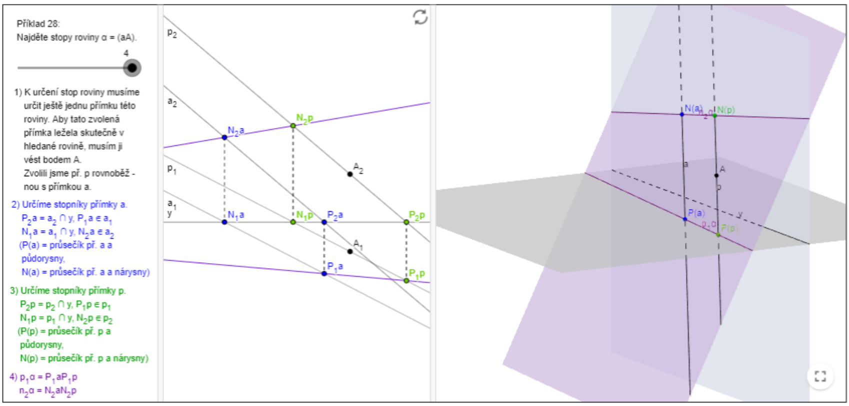

Obr. 1: Rozvržení oken v appletech

Ve 3D okně je také možné s celou prostorovou situací otáčet tak, aby se jednotlivé prvky při pohledu nepřekrývaly a také, aby bylo možné zhlédnout objekty z různých úhlů a uvědomit si jejich vzájemnou polohu.

U úloh základních je popis konstrukce podrobnější a často slovní, u úloh složitějších např. u těles je počítáno s tím, že předchozí úlohy čtenář již vyřešil a popis konstrukce je často již symbolický a stručnější.

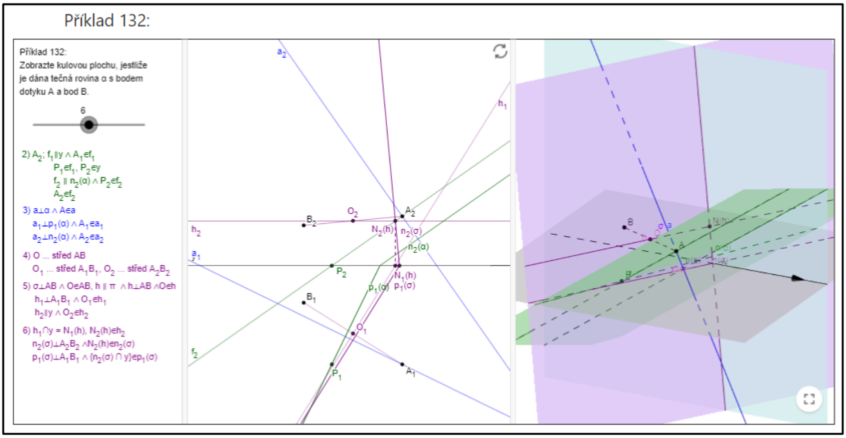

Obr. 2: Applet – sestrojení tělesa

3 GeoGebra kniha

Jednotlivé applety s řešeními úloh z pracovních listů byly vloženy do GeoGebra knihy „Mongeovo promítání“ (viz [3]) do části „04 Pracovní listy“ na stránkách geogebra.org, aby byly kdykoliv dostupné všem studentům.

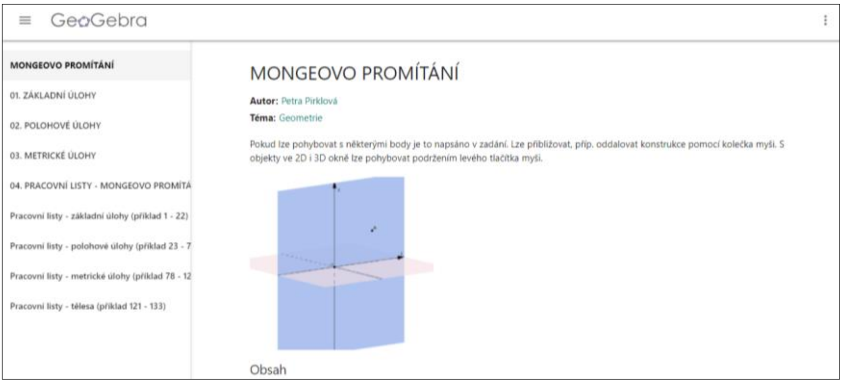

Obr. 3: GeoGebra kniha „Mongeovo promítání“

Část „Pracovní listy“ byla rozdělena do čtyř částí - základní úlohy, polohové úlohy, metrické úlohy a tělesa - podle typu vložených úloh, kvůli snadnější orientaci čtenáře mezi tématy. V úvodu GeoGebra knihy je samozřejmě také vložen pdf soubor se zadáním pracovních listů.

Práce s touto GeoGebra knihou by měla vypadat tak, že si čtenář vytiskne pracovní listy, pokusí se vyřešit danou úlohu a výsledek porovná s příslušným appletem v GeoGebra knize. Posouváním posuvníku si může zkontrolovat postup konstrukce, správnost výsledku a nastane-li nějaký problém, může s pomocí uvedeného zápisu a postupu konstrukce nalézt chybu ve svém řešení a opravit ji.

4 Závěr

Pracovní listy a hlavně jejich důkladné a podrobné řešení byly vytvořeny, aby pomohly studentům různých oborů prezenčního, ale také kombinovaného studia při studiu Mongeova promítání. S postupně ubývajícími hodinami cvičení věnovaných deskriptivní geometrii musí studenti více času trávit samostudiem. Doufáme tedy, že jim uvedená GeoGebra kniha pomůže k pochopení, procvičení a hlavně porozumění Mongeova promítání. První ohlasy na pracovní listy již nasvědčují tomu, že vytvořené applety svůj účel plní.

Poděkování

Tento článek vznikl za podpory Institucionálního plánu TUL pro rok 2019.

Literatura

[1] P. Pirklová, D. Bímová: *Metric Problems in Monge Projection in GeoGebra*, in *Proceedings of 18th Conference on Applied Mathematics (APLIMAT 2019)*, Bratislava 2019

[2] https://www.geogebra.org

[3] https://www.geogebra.org/m/dhhwyrwh

[4] URBAN, A., *Deskriptivní geometrie I*. SNTL Praha, 1967.

DIAD-tools - development of interactive and animated drawing teaching tools - the didactic materials supporting the learning of architectural-construction drawing

Monika Sroka-Bizoń

Dept. of Building Processes and Building Physics, Fac. of Civil Engineering,
Silesian Univesrsity of Technology
Akademicka 5, 44 100 Gliwice, Poland
monika.sroka-bizon@polsl.pl

Abstract. The international project under the Erasmus+ Programme “Development of Interactive and Animated Drawing Teaching Tools” - DIAD-tools No2017-1-LT01-KA202-035177 is realized by partners from Estonia, Latvia, Lithuania, Slovakia and Poland. The project implementation was started on October 1 2017 and will last until March 30, 2020. The main goal of the DIAD-tools project is to create interactive tools support the learning of technical drawing. After completing the project tools will be available on the online platform available for university’s students, college's students, school’s and universities' teachers from different countries. [3] [4] The project group from Silesian University of Technology has been elaborated didactic materials in the field of construction drawing. These materials have been divided in six parts:

1. Architectural-construction drawing - general principles,
2. Graphic designations of the building materials,
3. Dimensioning at architectural-construction drawing,
4. Scales at architectural-construction drawing,
5. Construction elements,
6. Test of architectural-construction drawing.

In the report authors will present problems in realization of the universal didactic materials in such field as construction drawing.

Key words: architectural-construction drawing

1 Introduction

At present, the Internet is one of the main places where young people, pupils, and students seek knowledge. Popular online platforms allow you to acquire knowledge in the field of mathematics, physics, drawing techniques and many other fields of science. Short instructional videos on, for example, how to use computer-aided design programs are very popular with students and pupils and provide extremely valuable scientific assistance to them. Therefore, in the author's opinion, the idea of developing didactic materials for independent study of architectural-construction drawing in the form of animated didactic tools, contained in the concept of the DIAD-tools project is extremely valuable and moving with the times. The elaboration of materials by specialists in the field of architectural-construction drawing based on European standards that are common to all countries of the project partners gives the opportunity to prepare correct teaching aids in the field of presented information. The didactic experience of authors of materials, employees of the Faculty of Civil Engineering of the Silesian University of Technology, academic teachers who have been teaching descriptive geometry and technical drawing at various faculties of the Silesian University of Technology for many years is a premise for developing correct materials also in the field of teaching methodology.

Architectural-construction drawing is a subject taught in vocational schools, technical secondary schools, and technical universities. It is an important subject for future engineers and technicians for whom architectural-construction drawing will be in their professional work the basic language of communication with other specialists working in the field of civil engineering and architecture. Beginning in the 1990s, a systematic reduction in the number of teaching hours devoted to teaching architectural-construction drawing in study plans and school programs can be observed in all project partner countries. [1] Therefore, in the process of learning and teaching, there was a need to place greater emphasis on the independent learning of the pupil and student.

2 Concept of the construction drawing materials

The main goal of the authors who developed teaching tools in the field of architectural-construction drawing was to prepare materials useful for both pupils of technical secondary schools and technical university students. The concept of developing didactic materials in the form of short animated instructions presenting the basic issues of individual thematic blocks was adopted. In three instructional parts, part 1. Architectural-construction drawing - general principles, part 3. Dimensioning at architectural-construction drawing, part 5. Construction elements, the same concept of the material layout was adopted - the axonometric drawing illustrates the spatial problem of the subject under discussion, and the rectangular projection of the building object serves to present the method of preparing the architectural drawing. A verbal commentary in the form of a description of the drawings describes the issue presented. Parts related to scales used at architectural-construction drawings and the graphics designation of building materials required the adoption of a different arrangement of materials because they are a form of an illustrated dictionary of terms. Also, the part devoted to the test in the field of architectural-construction drawing was developed in a different graphic layout because it is a compilation of thematic issues discussed in other parts of the materials. A musical background has been introduced in all parts of the teaching materials, which the user of the materials can turn off if necessary.

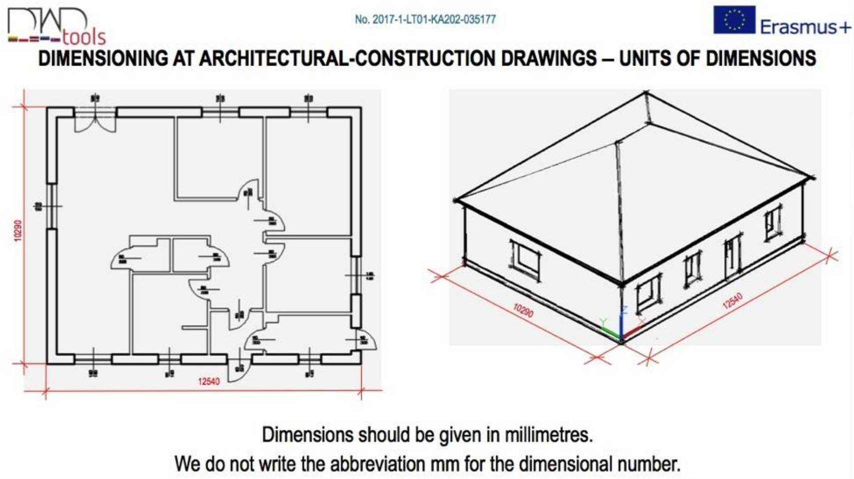

Fig. 1: The graphic layout used in three parts of teaching materials in the field of architectural-construction drawing - axonometric drawing, orthographic projection of a building object and verbal commentary discussing the presented issue.

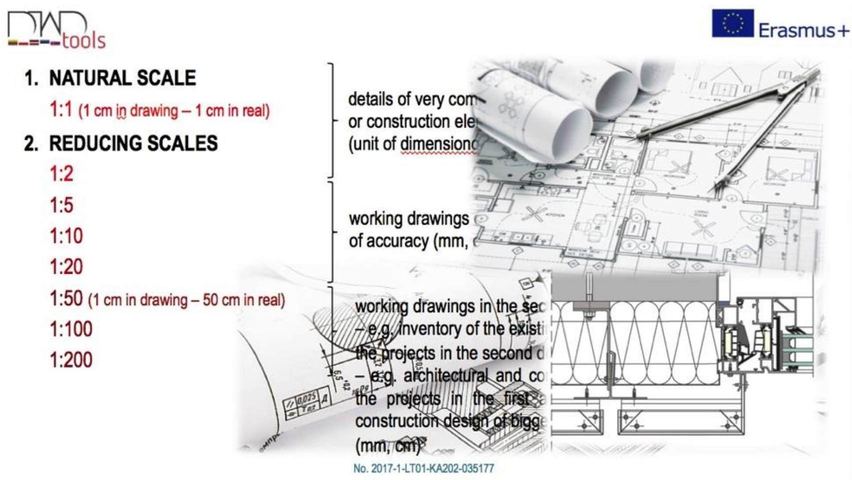

Fig. 2: The graphic layout used for dictionary parts of teaching materials in the field of architectural-construction drawing - part 3. Scales at architectural-construction drawing and part 4. Graphic designation of the building materials

2.1 Problems in realization of the universal didactic materials in such field as construction drawing

As the main substantive basis for the development of materials related to architectural and construction drawing, binding European standards from this thematic area were adopted. Adopting such a substantive basis was possible in the scope of presenting drawing lines used in architectural drawings, dimensioning methods, and ways of presenting drawing axes. In materials related to graphic designations of the building materials and drawing symbols used in architectural-construction drawings and construction elements of buildings, it was necessary to adopt as a substantive basis the developed materials of book publications from the project partner countries. This assumption resulted from the lack of applicable European standards in certain thematic areas related to architectural-construction drawing. The lack of open access to standards was a major problem related to the development of teaching materials in the field of architectural and construction drawing. In terms of the choices made in the drawing symbols used in the drawing, the authors largely had to rely on the literature on the subject - textbooks and materials available on the Internet. [2]

According to the main assumptions of the DIAD-tools project, the didactic materials developed should constitute a relatively short animated material, about 5 minutes. [4] The application of this assumption in practice, when selecting the issues presented and developing materials, required careful construction of teaching tools and selection of the issues discussed to be the most important. It was a big challenge for the authors of the materials, especially in the scope of limiting the level of detail of discussing the presented issue.

All didactic materials developed as part of the DIAD-tools project are prepared in six language versions: English, Estonian, Latvian, Lithuanian, Polish and Slovak. In the field of materials related to architectural-construction drawing, this involved the need to analyse professional vocabulary in this field used in the individual project partners' countries. An expert assessment of the didactic materials carried out in spring 2019 showed that the materials still require minor adjustments in this area.

3 Conclusion

Changes in the methods of learning and teaching in all fields of science related to the dynamic dissemination of Internet access, the constantly decreasing number of hours allocated for learning architectural-construction drawing in curricula and study plans make it necessary to develop professional teaching materials for self-study. Didactic materials in the field of architectural-construction drawing developed as part of the DIAD-tools project can constitute such materials.

Based on the evaluation of the didactic materials in the field of architectural-construction drawing carried out in spring 2018, it can be concluded that the materials were developed correctly in terms of methodology and content.

Pupils and students from all countries of the project partners assessed them directly in the formulated assessments as useful and helpful in the independent learning of drawing.

Materials were evaluated in a similar way by experts from individual project partner countries. The expert assessment was carried out in parallel with the assessment of project participants, which are pupils and students from Estonia, Latvia, Lithuania, Poland and Slovakia.

Open access to developed didactic materials and their availability in six language versions suggest that they will constitute a significant supplement to the existing didactic offer on the Internet. The advantage of the developed materials may be the fact that they have been prepared by teachers, practitioners from specific fields.

In the opinion of the author, a good solution related to the further use of materials by pupils and students would be continuous development and improvement of the developed materials, also by supplementing certain thematic areas not included in the materials developed under the project.

Acknowledgements

The author has been supported by the founds of the project No 2017-1-LT01-KA202-035177, Erasmus + Key Action 2 program.

References

[1] A. Błach, A. Kania, M. Sroka-Bizoń: *What about geometrical didactics? The results of the questionnaires*, The Journal of Polish Society for Geometry and Engineering Graphics, Vol. 22, 2011, pp.7-15

[2] M. Dobelis, P. Polinceusz, M. Sroka-Bizoń, K. Tytkowski, D. Velichova, A. Vansevicius: *Is the constructional drawing an international language for engineers?* 18th International Conference on Geometry and Graphics, ICGG 2018, Milan, Italy 3-7 August 2018, Springer-Verlag, 2019, pp.1542-1552

[3] M. Sroka-Bizoń: *DIAD-tools - development of interactive and animated drawing teaching tools*, Proceedings of the Czech-Slovak Conference on Geometry and Graphics 2018, 38th Conference on Geometry and Graphics. 27th Symposium on Computer Geometry SCG'2018, Blansko, September 10-13, 2018, Bratislava, Vydav. SCHK, 2018, pp.225-228

[4] https://liggd.lt/diad-tools/gb/training-materials - the web site of the project "Development of Interactive and Animated Drawing Teaching Tools" - DIAD-tools, No2017-1-LT01-KA202-035177

Movement of conics on quadrics

Hellmuth Stachel

Vienna University of Technology
Wiedner Hauptstr. 8-10/104, A 1040 Wien, Austria
stachel@dmg.tuwien.ac.at

Abstract. Given any regular quadric, there is a three-parameter set of cutting planes, but the size of an ellipse or hyperbola depends only on its two semiaxes. This parameter count reveals that on each quadric $\mathcal{Q}$ there exist ellipses or hyperbolas with a one-parameter set of congruent copies on $\mathcal{Q}$, which can even be moved into each other. We present parametrizations for such movements on ellipsoids and hyperboloids. There is a close connection between these movements and the theory of confocal quadrics.

Keywords: confocal quadrics, conics on quadrics

1 Introduction

There are well-known examples of conics which can be moved on quadrics. Apart from the trivial case of circles on a sphere, paraboloids are surfaces of translation, even with a continuum of translational nets of parabolas. On quadrics of revolution, each planar section can be moved.

What's about general quadrics $\mathcal{Q}$? There is a three-parameter family of cutting planes, but the size of an ellipse or hyperbola depends only on its two semiaxes. The situation for parabolas is similar: Their size depends on one single length, its parameter, while on hyperboloids and paraboloids there exists a two-parameter family of planes which intersect along parabolas.

This parameter count reveals that on each quadric $\mathcal{Q}$ there exist conics with a one-parameter family of congruent copies on $\mathcal{Q}$. Below, we focus on central quadrics and provide parametrizations for the movement of appropriate ellipses and hyperbolas $\mathcal{Q}$. It turns out that there is a close connection with the theory of confocal quadrics.

2 Moving ellipses on an ellipsoid

On any regular quadric $\mathcal{Q}$, the intersections with parallel planes are homothetic. This means, in the case ellipses or hyperbolas, that they have parallel axes and the same ratio of semiaxes $a_e : b_e$. Moreover, their centers lie on the same diameter. This is a consequence of the polarity with respect to (w.r.t., in brief) $\mathcal{Q}$.

In the case of an ellipsoid $\mathcal{E}$, we obtain the biggest ellipse of this homothetic family in the plane through the center O. On the other hand, there is a point $P \in \mathcal{E}$ with a tangent plane τ_P parallel to the cutting planes, and the axes of the conics are parallel to the principal curvature directions at P. The conics are even homothetic to the Dupin indicatrix at P. This can be confirmed, e.g., by straight forward computation using the Taylor expansion of the quadratic polynomial at P.

According to the definition of the Dupin indicatrix, the ratio of the principal curvatures κ_1, κ_2 at P is reciprocal to the ratio of the squared semiaxes of the ellipses on $\mathcal{E}$ in planes parallel to τ_P, i.e.,

$$a_e : b_e = \sqrt{\kappa_1} : \sqrt{\kappa_2}, \quad \text{if} \quad \kappa_1 > \kappa_2. \tag{1}$$

The lines of curvature on quadrics are related to confocal quadrics. Therefore, we recall the relevant properties of confocal quadrics.

2.1 Confocal central quadrics

Let $\mathcal{E}$ be a triaxial ellipsoid with semiaxes a, b, and c. The one-parameter family of quadrics being confocal with $\mathcal{E}$ is given as

$$\frac{x^2}{a^2+k} + \frac{y^2}{b^2+k} + \frac{z^2}{c^2+k} = 1, \text{ where } k \in \mathbb{R} \setminus \{-a^2, -b^2, -c^2\} \tag{2}$$

serves as parameter. In the case $a > b > c > 0$ this family includes

$$\text{for} \begin{cases} -c^2 < k < \infty & \text{triaxial ellipsoids,} \\ -b^2 < k < -c^2 & \text{one-sheeted hyperboloids,} \\ -a^2 < k < -b^2 & \text{two-sheeted hyperboloids.} \end{cases} \tag{3}$$

Confocal quadrics intersect their common planes of symmetry along confocal conics. As limits for $k \to -c^2$ and $k \to -b^2$ we obtain 'flat' quadrics, i.e., the focal ellipse and the focal hyperbola.

The confocal family sends through each point $P = (\xi, \eta, \zeta)$ outside the coordinate planes exactly one ellipsoid, one one-sheeted hyperboloid and one two-sheeted hyperboloid. The corresponding parameters k define the three *elliptic coordinates* of P. We concentrate on points P of the ellipsoid $\mathcal{E}$ with $k = 0$, and denote the parameters of the two hyperboloids $\mathcal{H}_1$ and $\mathcal{H}_2$, respectively, by k_1 and k_2. Hence,

$$\mathcal{E}: \ \frac{\xi^2}{a^2} + \frac{\eta^2}{b^2} + \frac{\zeta^2}{c^2} = 1 \tag{4}$$

and, for $i = 1, 2$ and $-a^2 < k_2 < -b^2 < k_1 < -c^2 < 0$

$$\mathcal{H}_i: \ \frac{\xi^2}{a^2+k_i} + \frac{\eta^2}{b^2+k_i} + \frac{\zeta^2}{c^2+k_i} = 1. \tag{5}$$

For given Cartesian coordinates (ξ, η, ζ) of a point $P \in \mathcal{E}$, the parameters k_1 and k_2 of the hyperboloids through P are the two roots of the quadratic equation

$$k^2 + L\,k + M = 0 \tag{6}$$

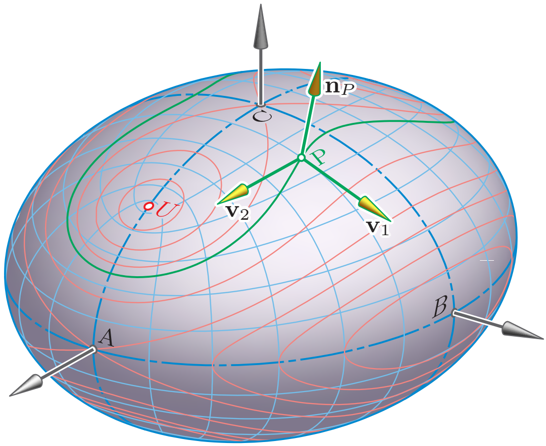

Fig. 1: Curvature lines (blue), curves of constant ratio of principal curvatures $\kappa_1 : \kappa_2$ (red), and direction vectors $\mathbf{v}_1$, $\mathbf{v}_2$ of the principal curvature tangents at P.

with coefficients

$$\begin{aligned} L &= \frac{(b^2+c^2)\xi^2}{a^2} + \frac{(c^2+a^2)\eta^2}{b^2} + \frac{(a^2+b^2)\zeta^2}{c^2}\,, \\ M &= \frac{a^2b^2c^2}{h^2}\,, \text{ where } h = \overline{O\tau_P} \text{ and } \frac{1}{h^2} = \frac{\xi^2}{a^4} + \frac{\eta^2}{b^4} + \frac{\zeta^2}{c^4}\,. \end{aligned} \tag{7}$$

If, conversely, the tripel $(0, k_1, k_2)$ of elliptic coordinates is given, then the Cartesian coordinates (ξ, η, ζ) of the corresponding points satisfy

$$\begin{gathered} \xi^2 = \frac{a^2(a^2+k_1)(a^2+k_2)}{(a^2-b^2)(a^2-c^2)}\,, \quad \eta^2 = \frac{b^2(b^2+k_1)(b^2+k_2)}{(b^2-c^2)(b^2-a^2)}\,, \\ \zeta^2 = \frac{c^2(c^2+k_1)(c^2+k_2)}{(c^2-a^2)(c^2-b^2)}\,. \end{gathered} \tag{8}$$

There exist 8 such points, symmetric w.r.t. the coordinate planes.

The differences of any two of the equations in (4) and (5) yield

$$\begin{gathered} \frac{\xi^2}{a^2(a^2+k_i)} + \frac{\eta^2}{b^2(b^2+k_i)} + \frac{\zeta^2}{c^2(c^2+k_i)} = 0,\ i = 1,2\,, \quad \text{and} \\ \frac{\xi^2}{(a^2+k_1)(a^2+k_2)} + \frac{\eta^2}{(b^2+k_1)(b^2+k_2)} + \frac{\zeta^2}{(c^2+k_1)(c^2+k_2)} = 0. \end{gathered} \tag{9}$$

This reveals, that confocal quadrics form a triply orthogonal system of surfaces. Due to a theorem of Dupin, the surfaces of a triply orthogonal system intersect each other along lines of curvature. Hence, the lines of curvature on ellipsoids and hyperboloids are of degree 4, except the principal sections in the coordinate planes (see Figure 1).

At each point P of the ellipsoid $\mathcal{E}$ the surface normal n_P to $\mathcal{E}$ at P has the direction vector

$$\mathbf{n}_P = \left(\frac{\xi}{a^2}\,,\ \frac{\eta}{b^2}\,,\ \frac{\zeta}{c^2}\right). \tag{10}$$

On the other hand, for point $P \in \mathcal{E}$ in general position, the two principal curvature tangents are the surface normals of the two hyperboloids $\mathcal{H}_1$ und $\mathcal{H}_2$ through P, therefore in direction of the vectors

$$\mathbf{v}_i := \left(\frac{\xi}{a^2+k_i}\,,\ \frac{\eta}{b^2+k_i}\,,\ \frac{\zeta}{c^2+k_i}\right). \tag{11}$$

2.2 Ellipses on ellipsoids

Now, we look for the biggest ellipse on $\mathcal{E}$ among the homothetic family in parallel planes.

Lemma 1. *The semiaxes of the ellipse in the diameter plane parallel to the tangent plane τ_P at the point $P \in \mathcal{E}$ with the elliptic coordinates $(0, k_1, k_2)$ are*

$$a_P = \sqrt{-k_2}, \quad b_P = \sqrt{-k_1}. \tag{12}$$

Proof. The diameter plane is spanned by the direction vectors $\mathbf{v}_1$ and $\mathbf{v}_2$ given in (11). We look for $\lambda \in \mathbb{R}$ with $\lambda\mathbf{v}_i \in \mathcal{E}$, hence

$$\lambda^2\left[\frac{\xi^2}{(a^2+k_i)^2a^2} + \frac{\eta^2}{(b^2+k_i)^2b^2} + \frac{\zeta^2}{(c^2+k_i)^2c^2}\right] = 1.$$

This condition does not change if we subtract from the term in square brackets the left-hand side of the first equation in (9), divided by k_i. Thus, we obtain

$$\lambda^2\left[\frac{\xi^2}{(a^2+k_i)^2a^2} - \frac{\xi^2}{k_i(a^2+k_i)a^2} + \dots\right] = 1,$$

and, finally,

$$-\frac{\lambda^2}{k_i}\left[\frac{\xi^2}{(a^2+k_i)^2} + \frac{\eta^2}{(b^2+k_i)^2} + \frac{\zeta^2}{(c^2+k_i)^2}\right] = -\frac{\lambda^2}{k_i}\,\|\mathbf{v}_i\|^2 = 1,$$

hence, $a_P = |\lambda|\,\|\mathbf{v}_2\| = \sqrt{-k_2}$ and $b_P = |\lambda|\,\|\mathbf{v}_1\| = \sqrt{-k_1}$. These equations can already be found in [1, p. 517]. □

For the movement of a given ellipse e with semiaxes (a_e, b_e), Lemma 1 implies the necessary condition

$$a_e \le a_P = \sqrt{-k_2},\ \text{where } b < \sqrt{-k_2} < a\,. \tag{13}$$

Together with (1), we conclude

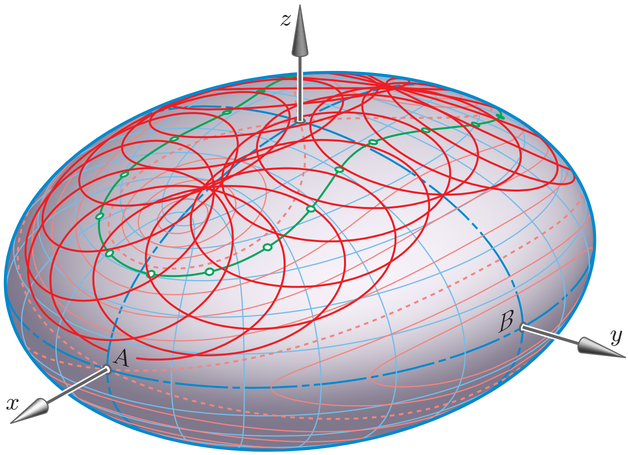

Fig. 2: Moving an ellipse on an ellipsoid.

Theorem 1. *If an ellipse e with semiaxes (a_e, b_e) is moving on a triaxial ellipsoid $\mathcal{E}$, then the points $P \in \mathcal{E}$ with tangent planes τ_P parallel to the plane of e moves on a curve with proportional elliptic coordinates $k_2 : k_1 = -a_e^2 : -b_e^2$. This curve is also the locus of points with constant ratio of principal curvatures (Figure 1).*

All ellipses in planes parallel to τ_P have their principal vertices on an ellipse with the conjugate diameters OP and the major axis of the diametral section. Let $\mathbf{p}$ denote the position vector of P and $\mathbf{m} = \mu\,\mathbf{p}$ with $0 \le \mu = \sin x < 1$ that of the center M of any ellipse in this family. Then, its major semiaxis a_e equals $a_P \cos x = a_P\sqrt{1-\mu^2}$, which results in

$$\mu^2 = 1 - \frac{a_e^2}{a_P^2} = 1 - \frac{a_e^2}{t} \ . \tag{14}$$

When, during the movement of the ellipse e, the scalar μ vanishes, then its center M coincides with the center O of $\mathcal{E}$. The corresponding point P has the elliptic coordinate $k_2 = -a_e^2$. In order to continue the motion, point P has to jump to its antipode.

We set

$$v := \frac{k_2}{k_1} = \frac{a_e^2}{b_e^2} = \text{const., where } 1 < v < \frac{a^2}{c^2}\ , \tag{15}$$

and we use the parameter $t = -k_2$ for representing the motion. Then, t is restricted by the interval

$$\max\{b^2, vc^2, a_e^2\} \le t \le \min\{a^2, vb^2\}, \tag{16}$$

and $k_1 = t/v$. From (8) follows the parametrization $\mathbf{p}(t)$ by replacing (k_1, k_2) with $(t/v,\, t)$. This implies for the trajectory of the center M of e

$$\mathbf{m}(t) = \mu(t)\,\mathbf{p}(t) \text{ with } \mu(t) = \sqrt{1 - \frac{a_e^2}{t}}\,. \tag{17}$$

Now, we can express the movement of e in matrix form, in terms of position vectors $\mathbf{x}_m$ w.r.t. the moving space (attached to e) and $\mathbf{x}_f$ w.r.t. the fixed space (attached to $\mathcal{E}$), as

$$\mathbf{x}_f = \mathbf{m}(t) + \mathbf{M}(t)\,\mathbf{x}_m, \quad \text{where } \mathbf{M}(t) = \left[\frac{\mathbf{v}_2}{\|\mathbf{v}_2\|}, \frac{\mathbf{v}_1}{\|\mathbf{v}_1\|}, \frac{\mathbf{n}_P}{\|\mathbf{n}_P\|}\right]. \tag{18}$$

The square brackets include the column vectors according to (11) and (10) in the orthogonal matrix $\mathbf{M}(t)$.

Note that this parametrization works only for point P in the octant $x, y, z > 0$. We get a closed movement after reflections in the planes of symmetry (see Figure 2). Algebraic properties of this movement are provided in [2].

3 Moving ellipses on a one-sheeted hyperboloid

Also on hyperboloids and paraboloids, the curves of intersection with parallel planes are homothetic. However, not in all cases the method, as used before for ellipsoids, can be applied since a point P either does not exist or lies at infinity. Moreover, paraboloids have no center O. Below, we analyse only the movements of ellipses on a one-sheeted hyperboloid $\mathcal{H}_1$. The case of moving parabolas is presented in [3].

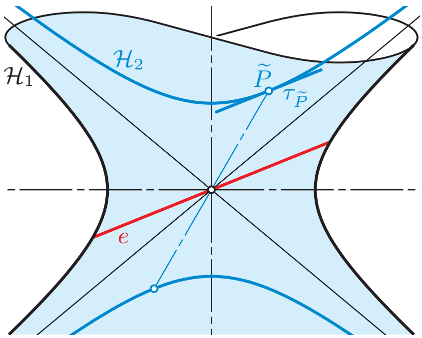

Fig. 3: For ellipses e on a one-sheeted hyperboloid $\mathcal{H}_1$, there does not exist a point $P \in \mathcal{H}_1$ with the tangent plane τ_P parallel to the plane of e.

For ellipses $e \subset \mathcal{H}_1$, there is no point $P \in \mathcal{H}_1$ with a tangent plane τ_P parallel to e. However, we find an appropriate point $\widetilde{P}$ on the 'conjugate' two-sheeted hyperboloid $\mathcal{H}_2$ (Figure 3). The hyperboloid $\mathcal{H}_2$ shares the asymptotic cone with $\mathcal{H}_1$, and, therefore, the axes of the ellipse e are parallel to the principal curvature directions of $\mathcal{H}_2$ at $\widetilde{P}$. The two hyperboloids satisfy the respective equations

$$\mathcal{H}_1\colon \frac{x^2}{a^2}+\frac{y^2}{b^2}-\frac{z^2}{c^2}=1 \quad \text{and} \quad \mathcal{H}_2\colon -\frac{x^2}{a^2}-\frac{y^2}{b^2}+\frac{z^2}{c^2}=1$$

with $a>b$. The quadrics confocal with $\mathcal{H}_2$ are given by

$$-\frac{x^2}{a^2-k}-\frac{y^2}{b^2-k}+\frac{z^2}{c^2+k}=1.$$

Again, this family sends through each point $\widetilde{P}$ outside of the planes of symmetry three mutually orthogonal quadrics, one of each type. On the two-sheeted hyperboloid $\mathcal{H}_2$ with $k=0$, we use the respective parameters k_0 and k_1 of the ellipsoid and the one-sheeted hyperboloid as the elliptic coordinates of $\widetilde{P}$ with

$$k_0>a^2 \quad \text{and} \quad a^2>k_1>b^2.$$

Then, similar to Lemma 1, the ellipse $e\in\mathcal{H}_1$ in the diameter plane parallel to $\tau_{\widetilde{P}}$ has the semiaxes

$$a_{\widetilde{P}}=\sqrt{k_0} \quad \text{and} \quad b_{\widetilde{P}}=\sqrt{k_1}.$$

This is the smallest ellipse on $\mathcal{H}_1$ in the homothetic family.

Hence, if any given ellipse with semiaxes a_e and b_e should be moved on $\mathcal{H}_1$, the corresponding point $\widetilde{P}\in\mathcal{H}_2$ has to trace a curve with proportional elliptic coordinates

$$k_0:k_1=a_{\widetilde{P}}^2:b_{\widetilde{P}}^2=a_e^2:b_e^2$$

on $\mathcal{H}_2$. Similar to (8), we can parametrize the trajectory $\widetilde{\mathbf{p}}(t)=(\xi,\eta,\zeta)$ of $\widetilde{P}$ by $t:=k_0>a^2$, where

$$v:=\frac{k_0}{k_1}=\frac{a_e^2}{b_e^2}=\text{const.},$$

hence $k_1=t/v$ with $b^2\le k_1\le a^2$.

For each $\widetilde{P}$, the principal vertices of the ellipses in planes parallel to $\tau_{\widetilde{P}}$ are placed on a hyperbola, for which one principal vertex in the diameter plane and the point $\widetilde{P}$ define conjugate diameters. If $a_e=a_{\widetilde{P}}\cosh x$, then the position vectors $\mathbf{m}$ of the center of the ellipse e and $\widetilde{\mathbf{p}}$ of the point $\widetilde{P}$ are related by $\mathbf{m}=\sinh x\,\widetilde{\mathbf{p}}$. Thus, we obtain

$$\mathbf{m}=\mu\,\widetilde{\mathbf{p}} \quad \text{with} \quad \mu^2=\frac{a_e^2}{a_{\widetilde{P}}^2}-1\,. \tag{19}$$

This yields, similar to (18), a parametrization for the movement of the ellipse e on $\mathcal{H}_1$ (Figure 4). As a consequence of (19), on the trajectory of $\widetilde{P}$ only points with $a^2_{\widetilde{P}} = k_0 \leq a^2_e$ are admitted. Therefore, the parameter $t = k_0$ runs the interval

$$\max\{a^2,\, vb^2\} \leq t \leq \min\{a^2_e,\, va^2\}.$$

In the case $a^2_e < va^2$, the same phenomenon appears as mentioned above. When the parameter t reaches a^2_e, then, for continuing the movement of the ellipse, the point $\widetilde{P}$ either has to jump to its antipode, or the scalar μ in (19) must get a negative sign.

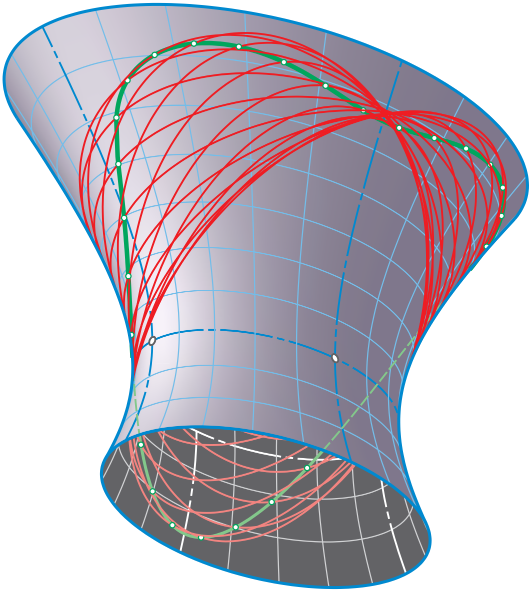

Fig. 4: Movement of an ellipse on a one-sheeted hyperboloid.

References

[1] L. Bianchi: *Vorlesungen über Differentialgeometrie,* B.G. Teubner, Leipzig, 1899.

[2] H. Brauner: *Quadriken als Bewegflächen,* Monatsh. Math. **59**, 45–63 (1955).

[3] G. Glaeser, B. Odehnal, H. Stachel: *The Universe of Quadrics,* Springer Spektrum, Heidelberg, to appear.

Removing Duplications from the List of Quadrilateral Meshes

Petra Surynková
Faculty of Mathematics and Physics, Charles University
Sokolovská 83, 186 75 Praha 8, *Czech Republic*
petra.surynkova@mff.cuni.cz

Abstract. Quadrilateral meshes are widely used in various practical applications such as computer graphics, numerical simulations, production industries and many more. We present the process of removing duplications from the list of quadrilateral meshes of a certain class. The list of quadrilateral meshes is obtained using our enumeration framework. We show the sketch of filtering the list using unique numbering.

Keywords: Quadrilateral meshes, quadrilateral, duplications, unique numbering.

1 Introduction

The range of algorithms for the construction of a quadrilateral mesh composed of quadrilaterals have been developed in the recent years and are used in many branches such as computer graphics, [5], computer-aided architectural and industrial design, [4], digital surface reconstruction from point clouds, or production industries, [9]. Although it is evident that the construction of a quadrilateral mesh is much more complicated problem then the construction of triangle meshes but in many cases quadrilateral meshes are better suited to various problems of computer graphics comparing to well-studied triangle meshes.

In our research we concentrate on quadrilateral meshes and meshing in the plane, i.e. our aim is to construct a mesh for a given planar domain. Regarding the state of the art, there exist several methods of constructing quadrilateral meshes for a given n-sided planar region which use different approaches. We summarized these methods in [10]. Let us briefly mention the most famous techniques. The paving methods are based on iteratively paving rows of elements to the interior of a region's boundary, [1]. There are also approaches which are using dual graphs of quadrilateral meshes due to its nice properties, [7]. Because the construction of a triangle mesh is well-known, some methods starts with the filling of an n-sided region with a triangle mesh and triangles are merged to quadrilaterals afterwards, [3]. There exist quadrangulations which work with the prescribed numbers of edges at the boundary, [13]. The majority of the constructing methods try to find a topology with the fewest number irregular vertices, [8].

In the present paper we introduce one step in our enumerating algorithms which remove the duplications from the output list of meshes.

2 Quadrilateral Meshes of a Certain Class and Enumerating Algorithms

We designed and analysed new algorithms for enumeration of all quadrilateral meshes of a certain class. The basic idea of enumerating algorithms is to exploit properties offered by the considering a certain class of quadrilateral meshes. To understand the terminology let us briefly summarize the main terms and define the quadrilateral meshes of a certain class. Regarding the definition of a quadrilateral mesh we refer [10] again. A quadrilateral mesh, [2, 6], is a triple (V, E, Q) where V is a set of vertices, E is a set of edges, and Q is a set of quadrilaterals. There exists an embedding of (V, E, Q) into 2D plane such that each vertex is represented as a point in the plane and each edge is represented as a curve in the plane, so that curves connect vertices and each quadrilateral is depicted in the plane as a quadrilateral. In our study we furthermore assume only quadrilateral meshes that form a connected, conforming (i.e. free from T-junctions), orientable *2D manifold with boundary*, [2], i.e. we define quadrilateral meshes for segmentation of simply connected planar domains.

For our study is also important to distinguish an internal and a boundary edge. An edge of the mesh with two incident quadrilaterals is said to be *internal*, while an edge with just one incident quadrilateral is said to be *boundary*. A vertex of a boundary edge is said to be *boundary*, otherwise it is said to be *internal*. The valence of a vertex is the number of edges incident to that vertex.

Without any further restriction the number of quadrilateral meshes would be too high. Thus we define a restricted class of quadrilateral meshes, i.e. the quadrilateral meshes satisfy the following properties:

- at least one vertex of each internal edge is internal (the Invariant),
- every vertex has valence ≤ 5, internal vertices have valences 3, 4, or 5,
- quadrangulated planar domain is simply connected.

We assume that the number of internal vertices is given as the input to our enumerating algorithms. We also distinguish the types of valences of these internal vertices. The set of defined restricted quadrilateral meshes with n_3 internal vertices of valence 3, n_4 internal vertices of valence 4, and n_5 internal vertices of valence 5 is denoted by $M_I(n_3, n_4, n_5)$.

As we have already pointed out we proposed new algorithms for enumeration of all quadrilateral meshes of a restricted class. More details will be available in [12] in our article which were submitted to CAGD journal. The algorithms enumerate all possible quadrilateral meshes with respect to the number of internal vertices with the given valences and the duplications are filtered out within a post-processing.

The process of constructing meshes is based on incremental construction starting from a trivial mesh with one internal vertex. In each step of construction the number of internal vertices of a quadrilateral mesh M is increased by one by adding new elements into a quadrilateral mesh or by additional modifying of a quadrilateral mesh using *mesh operations*. A quadrilateral mesh always satisfies the invariant and properties defined above before and after modification. The mesh operations which are used during the incremental construction of the mesh are of two types - operation *addition* and operation *gluing*. Operation of adding means to insert a new quadrilateral or quadrilaterals into the boundary of quadrilateral mesh M and operation of gluing means to glue two adjacent boundary edges in quadrilateral mesh M. Mesh operations are prescribed in [11].

3 Filtering Duplications

Our enumerating algorithms computes the list A of quadrilateral meshes which has to be filtered from the duplications. For removing meshes from the list A that are equivalent, we go through the list and filter out the duplications. For checking duplications we use a unique numbering to the quadrilaterals and boundary edges. The boundary edges are sorted in a counter-clockwise order starting at an arbitrary edge. Then all quadrilaterals of the mesh are sorted as follows. Unnumbered quadrilateral which is next to the numbered neighbor quadrilateral or has boundary edge with lowest number gets new number in each step. If more than one unnumbered quadrilateral are next to numbered quadrilateral q with the lowest number in some step of a numbering algorithm, these unnumbered quadrilaterals are sorted in counter-clockwise order starting at unnumbered quadrilateral after the lowest twisted numbered neighbor of quadrilateral q. Such an ordering is unique for a given quadrilateral mesh. For s boundary edges of quadrilateral mesh there is s different numberings. For checking whether two meshes are equivalent we number one mesh with all its numberings and the second mesh with one arbitrary numbering and compare all pairs of numberings in the first and the second mesh. This algorithm detects the topologies that are equivalent.

An example of a unique numbering of a quadrilateral mesh and possible cases of numberings of quadrilaterals is shown in Figure 1.

If we go through the list A of quadrilateral meshes with duplications, we retain the first mesh in the list A, as it is the first unique mesh. We compare the second mesh in the list A with the first unique mesh using the technique explained above. If they are equivalent, the second mesh is removed, otherwise it is retained. We continue in the same manner. We compare the next mesh in the list A with the already retained meshes one by one until we find an equivalent mesh. If we do, we stop, remove this mesh and pick up the next mesh in the list. If we look through all

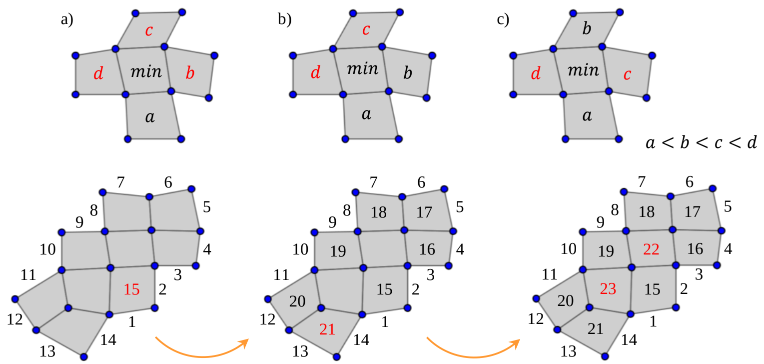

Fig. 1: Three cases (a, b, and c) of numbering of quadrilaterals in quadrilateral mesh and an example of a unique numbering of a quadrilateral mesh in three steps.

existing unique meshes without finding an equivalent, we retain this mesh in the list. After going through the entire list A it consists now of unique meshes.

4 Conclusion

The article briefly introduced the process of removing the duplications from the list of quadrilateral meshes of a certain class.

In the future work we would like to extend our enumerating methods to another types of quadrilateral meshes. We will also focus on the experimental evaluation in selecting the best mesh for a given planar region.

Acknowledgements

This work has been supported by the Fulbright Program and by the project PROGRES Q17 Teacher preparation and teaching profession in the context of science and research.

References

[1] T. Blacker, M. Stephenson: *Paving: A new approach to automated quadrilateral mesh generation,* Numerical Methods in Engineering, 32(4), 811847, 1991

[2] M. Botsch, L. Kobbelt, M. Pauly, P. Alliez, B. Lévy: *Polygon Mesh Processing,* A K Peters, Natick, 2010

[3] H. Borouchaki, P. J. Rey: *Adaptive triangular-quadrilateral mesh generation,* Numerical Methods in Engineering, 41(5), 915934, 1998

[4] F. Farin, J. Hoschek, M.-S. Kim: *Handbook of Computer Aided Geometric Design,* Elsevier Science, Amsterdam, 2002

[5] J. D. Foley, A. Dam, S. K. Feiner, J. F. Hughes: *Computer Graphics: Principle and Practice,* Addison-Wesley Publishing Company, 1995

[6] S. A. Mitchell: *A Characterization of the Quadrilateral Meshes of a Surface Which Admit a Compatible Hexahedral Mesh of the Enclosed Volume,* 13th Annual Symposium on Theoretical Aspects of Computer Science, 1996

[7] P. Murdoch, S. Benzley, T. Blacker, S. A. Mitchell: *The Spatial Twist Continuum: A Connectivity Based Method for Representing All-Hexahedral Finite Element Meshes,* Finite Elements in Analysis and Design, 28(2), 137-149, 1997

[8] A. Nasri, M. Sabin, Z. Yasseen: *Filling N-Sided Regions by Quad Meshes for Subdivision Surfaces,* Computer Graphics Forum, 28(6), 1644-1658, 2009

[9] H. Pottmann, A. Asperl, M. Hofer, A. Kilian: *Architectural Geometry,* Bentley Institute Press, Exton, 2007

[10] P. Surynková *Constructions of Quadrilateral Meshes: a Comparative Study,* South Bohemia Mathematical Letters, University of South Bohemia in esk Budjovice, Volume 24 (1), 2016

[11] P. Surynková *All Quadrilateral Meshes of Restricted Class,* Proceedings of the Czech-Slovak Conference on Geometry and Graphics, VUT Brno, Fakulta stavebn, stav matematiky a deskriptivn geometrie, 2018

[12] P. Surynková *Enumerating Quadrilateral Meshes,* CAGD journal, 2018, submitted

[13] K. Takayama, D. Panozzo, O. Sorkine-Hornung: Pattern-Based Quadrangulation for N-Sided Patches, Computer Graphics Forum, 33(5), 177184, 2014

Rational Curves of Given Direction

Zbyněk Šír

Faculty of Mathematics and Physics
Charles University, Sokolovská 83, Prague, Czech Republic
zbynek.sir@mff.cuni.cz

Abstract. We study all the rational curves tangent to a given vector field. We also analyse the degree of these curves and in particular show when occurs a degree reduction.

Keywords: Vector Field, Cross Product, Tangent Developabe Surface

1 Introduction

This paper is devoted to the construction and analysis of curves of given direction. This concept is rather trivial if we restrict ourselves to general smooth curves and use the apparatus of the classical differential geometry [5]. But the situation becomes much more complicated when the requirement of the rationality of the constructed curves is added [1].

To our knowledge this question was studied only in the special case of the curves with Pythagorean hodograph, [2, 4]. The general case was never considered.

The remainder of the paper is organized as follows. We study the general differential geometry properties of the curves tangent to a given vector field in Section 2. In Section 3 we give a general solution for the rational curves and illustrate this problem on two examples. Section 4 is devoted to the properties of polynomial fields and we show certain simplifications and degree reductions formulas. Eventually we conclude the paper.

2 Definition and preliminary observations

We will study curves and vector fields in $\mathbb{R}^3$. By a vector field we mean one parameter family of vectors depending in a smooth way on the parameter t. In order to include also the rational field we allow a zero-measure of parameter values for which the field is indefinite.

Definition 1 *We say, that the curve* $\mathbf{r}(t)$ *is tangent to the field* $\mathbf{v}(t)$ *if and only if*

$$\mathbf{v}(t) \times \mathbf{r}'(t) = \mathbf{0} \tag{1}$$

for all t*.*

It is quite obvious from the definition that there is always at least one curve tangent to a given field. Indeed we can directly integrate the input vector field.

Definition 2 *We will call the curve* $\mathbf{r}(t) = \int \mathbf{v}(t)\,\mathrm{d}t$ *the* primitive tangent curve *to the field* $\mathbf{v}(t)$.

It is also obvious that any other curve tangent to this field can be obtained in the form $\tilde{\mathbf{r}}(t) = \int l(t)\mathbf{v}(t)\,\mathrm{d}t$, where $l(t)$ is a smooth real function.

Proposition 3 *For a given field let* $\mathbf{r}(t) = \int \mathbf{v}(t)\,\mathrm{d}t$ *be its primitive tangent curve and let it has the curvature function* $\kappa(t)$ *and the torsion function* $\tau(t)$. *Let* $\tilde{\mathbf{r}}(t) = \int l(t)\mathbf{v}(t)\,\mathrm{d}t$ *be another curve tangent to the same field. Then for its curvature and torsion functions the following identities hold*

$$\tilde{\kappa}(t) = \frac{\kappa(t)}{l(t)} \qquad \textit{and} \qquad \tilde{\tau}(t) = \frac{\tau(t)}{l(t)}. \tag{2}$$

Proof: By a direct computation we obtain

$$\begin{aligned} \tilde{\mathbf{r}}'(t) &= l(t)\mathbf{r}'(t) \\ \tilde{\mathbf{r}}''(t) &= l'(t)\mathbf{r}'(t) + l(t)\mathbf{r}''(t) \\ \tilde{\mathbf{r}}'''(t) &= l''(t)\mathbf{r}'(t) + 2l'(t)\mathbf{r}''(t) + l(t)\mathbf{r}'''(t) \end{aligned}$$

which implies the following identities of the key expressions

$$\begin{aligned} \tilde{\mathbf{r}}' \times \tilde{\mathbf{r}}'' &= l^2\,\mathbf{r}' \times \mathbf{r}'' \\ \det[\,\tilde{\mathbf{r}}', \tilde{\mathbf{r}}'', \tilde{\mathbf{r}}'''\,] &= l^3 \det[\,\mathbf{r}', \mathbf{r}'', \mathbf{r}'''\,]. \end{aligned}$$

Consequently we obtain

$$\tilde{\kappa} = \frac{||\tilde{\mathbf{r}}' \times \tilde{\mathbf{r}}''||}{||\tilde{\mathbf{r}}'||^3} = \frac{\kappa}{l}, \qquad \tilde{\tau} = \frac{\det[\,\tilde{\mathbf{r}}', \tilde{\mathbf{r}}'', \tilde{\mathbf{r}}'''\,]}{||\tilde{\mathbf{r}}' \times \tilde{\mathbf{r}}''||^2} = \frac{\tau}{l}.$$

Q.E.D.

The identities obtained in the the proof provide also an information about the Frenet frame of the curves tangent to the same vector field.

Corollary 4 *All the curves tangent to the same vector field have the same binormal vector the same ratio of the curvature and torsion functions. They also have the same tangent and principal normal vectors up to the change of orientation.*

Example 5 *The following figure displays two curves which are tangent to the same vector field (not shown). They have not only the same Frenet frame but also the same rotation-minimizing frame.*

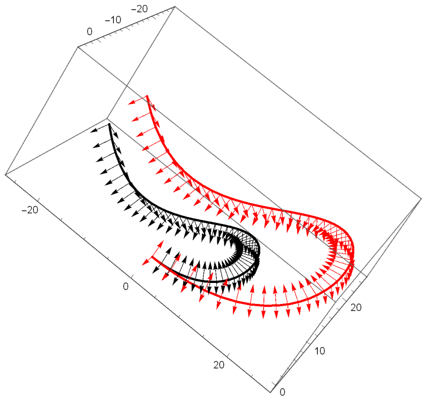

3 Rational curves

Our goal is to construct rational curves tangent to rational vector fields. Let us start this section with a simple example.

Example 6 Consider the polynomial vector field

$$\mathbf{v}(t) = \begin{pmatrix} 24t^3 - 12t^2 - 12t + 4 \\ 44t^3 - 60t^2 + 24t \\ 12t^2 - 4t^3 \end{pmatrix}$$

Set $l(t) = \frac{1+t}{3+t^2}$ and get $\tilde{\mathbf{r}}(t) = \int l(t)\mathbf{v}(t)\,\mathrm{d}t =$

$$\begin{pmatrix} t^3 + 6t^2 - 22\log\left(t^2+3\right) - 96t + \frac{292\arctan\left(\frac{t}{\sqrt{3}}\right)}{\sqrt{3}} \\ \frac{44t^3}{3} - 8t^2 + 36\log\left(t^2+3\right) - 168t + 168\sqrt{3}\arctan\left(\frac{t}{\sqrt{3}}\right) \\ -\frac{4t^3}{3} + 4t^2 - 12\log\left(t^2+3\right) + 24t - 24\sqrt{3}\arctan\left(\frac{t}{\sqrt{3}}\right) \end{pmatrix}$$

which is of course tangent to the field $\mathbf{v}(t)$.

We see that even from a rational input $\mathbf{v}(t)$ and $l(t)$ we typically obtain a non-rational curve. A different strategy therefore must be used to construct all the rational tangent curves. The geometrical essence of our approach is to construct the curve as the edge of regression of an envelope of (osculating) planes. It can be also expressed purely algebraically as shows the following proposition proved in [3].

Proposition 7 *Given a rational vector field $\mathbf{v}(t)$ all the rational tangent curves $\mathbf{r}(t)$ can be expressed in the form*

$$\mathbf{r}(t) = \frac{f(t)\,\mathbf{u}'(t)\times\mathbf{u}''(t) + f'(t)\,\mathbf{u}''(t)\times\mathbf{u}(t) + f''(t)\,\mathbf{u}(t)\times\mathbf{u}'(t)}{\det[\,\mathbf{u}(t),\mathbf{u}'(t),\mathbf{u}''(t)\,]} \qquad (3)$$

where $\mathbf{u}(t) = \mathbf{v}(t)\times\mathbf{v}'(t)$ and $f(t)$ is any rational function.

Example 8 *Given the field*

$$\mathbf{v} = \begin{pmatrix} 24t^3 - 12t^2 - 12t + 4 \\ 44t^3 - 60t^2 + 24t \\ 12t^2 - 4t^3 \end{pmatrix}$$

we compute $\mathbf{u} = \mathbf{v} \times \mathbf{v}'$ *and chose* $f = \frac{1+t}{3+t}$ *and obtain*

$$\begin{aligned} \tilde{\mathbf{r}} &= \frac{f\,(\mathbf{u}' \times \mathbf{u}'') + f'\,(\mathbf{u}'' \times \mathbf{u}) + f''\,(\mathbf{u} \times \mathbf{u}')}{\det[\,\mathbf{u}, \mathbf{u}', \mathbf{u}''\,]} = \\ &= \begin{pmatrix} \frac{144t^7+732t^6+1251t^5+189t^4-1049t^3-51t^2+213t-22}{144(t+3)^3(8t^3-3t^2-t+1)^2} \\ \frac{528t^7+2380t^6+3324t^5-1188t^4-3322t^3+2166t^2+153t-153}{288(t+3)^3(8t^3-3t^2-t+1)^2} \\ -\frac{48t^7+164t^6+24t^5-720t^4-824t^3+180t^2+27t-27}{288(t+3)^3(8t^3-3t^2-t+1)^2} \end{pmatrix}. \end{aligned}$$

4 Polynomial vector fields

We will focus on the rational and polynomial vector fields. It is obvious from the definition and equation (1) that a curve is tangent to a vector field if and only if it is tangent to its arbitrary functional multiple. We can use this fact to restrict our attention only to polynomial fields.

Lemma 9 *If a curve* $\mathbf{r}(t)$ *is tangent to a rational field* $\mathbf{v}(t)$ *then there is up to a constant multiple a unique vector field* $\tilde{\mathbf{v}}(t)$ *with relatively prime components to which the curve is tangent as well.*

Proof: Let $k(t)$ be any rational nontrivial function and define $\tilde{\mathbf{v}}(t) = k(t)\mathbf{v}(t)$. Then any curve is tangent to $\tilde{\mathbf{v}}(t)$ if and only if it is tangent to $\mathbf{v}(t)$ because

$$\tilde{\mathbf{v}}(t) \times \mathbf{r}'(t) = k(t)\mathbf{v}(t) \times \mathbf{r}'(t).$$

Now there is up to a scalar multiple precisely one rational function $k(t)$ so that $\tilde{\mathbf{v}}(t) = k(t)\mathbf{v}(t)$ is polynomial with relatively prime components. Indeed, if $k_1(t)$ denotes the polynomial least common multiple of the denominators of the components of $\mathbf{v}(t)$ then $k_1(t)\mathbf{v}(t)$ is a polynomial field. Let $k_2(t)$ be a polynomial greatest common divisor of its components. Eventually set $k(t) = k_1(t)/k_2(t)$. Q.E.D.

The previous lemma implies that we can restrict our input to the polynomial fields with relatively prime components. Let as analyze the degrees of expressions occurring in (3).

Lemma 10 *Let* $\mathbf{v}(t)$ *a polynomial vector field of degree* n *with relatively prime components. Then* $\mathbf{u}(t) = \mathbf{v}(t) \times \mathbf{v}'(t)$ *is a polynomial field of degree* $2n-2$ *and* $\det[\mathbf{v}(t), \mathbf{v}'(t), \mathbf{v}''(t)]$ *is a polynomial of degree* $3n-6$.

Proof: Writing the components of the vector field $\mathbf{v}(t)$ explicitly shows that the leading terms of the components $\mathbf{v}(t) \times \mathbf{v}'(t)$ cancel to 0 and the three leading terms of $\det[\mathbf{v}(t), \mathbf{v}'(t), \mathbf{v}''(t)]$ cancel to 0 as well. Q.E.D.

Example 11 Consider the polynomial vector field

$$\mathbf{v}(t) = \begin{pmatrix} 24t^3 - 12t^2 - 12t + 4 \\ 44t^3 - 60t^2 + 24t \\ 12t^2 - 4t^3 \end{pmatrix}$$

which is of degree $n = 3$. By a direct computation we get

$$\mathbf{u}(t) = \mathbf{v}(t) \times \mathbf{v}'(t) = \begin{pmatrix} -288t^4 - 192t^3 + 288t^2 \\ 240t^4 - 96t^3 + 192t^2 - 96t \\ 912t^4 - 2208t^3 + 1536t^2 - 480t + 96 \end{pmatrix}$$

which is of degree 4 and

$$\det[\mathbf{v}(t), \mathbf{v}'(t), \mathbf{v}''(t)] = 1152\left(16t^3 - 6t^2 - 2t + 2\right)$$

which is of degree 3.

We can obtain explicit expressions for the formulae appearing in (3) as follows.

Proposition 12 *Let $\mathbf{v}(t)$ be a vector field and $\mathbf{u}(t) = \mathbf{v}(t) \times \mathbf{v}'(t)$. Then*

$$\begin{aligned} \mathbf{u} \times \mathbf{u}' &= \det[\,\mathbf{v}, \mathbf{v}', \mathbf{v}''\,]\,\mathbf{v} \\ \mathbf{u}' \times \mathbf{u}'' &= \det[\,\mathbf{v}, \mathbf{v}'', \mathbf{v}'''\,]\,\mathbf{v} + \det[\,\mathbf{v}, \mathbf{v}', \mathbf{v}''\,]\,\mathbf{v}'' \\ \mathbf{u} \times \mathbf{u}'' &= \det[\,\mathbf{v}, \mathbf{v}', \mathbf{v}'''\,]\,\mathbf{v} + \det[\,\mathbf{v}, \mathbf{v}', \mathbf{v}''\,]\,\mathbf{v}' \\ \det[\,\mathbf{u}, \mathbf{u}', \mathbf{u}''\,] &= (\det[\,\mathbf{v}, \mathbf{v}', \mathbf{v}''\,])^2. \end{aligned}$$

Proof: By a direct differentiation we obtain

$$\mathbf{u} = \mathbf{v} \times \mathbf{v}', \quad \mathbf{u}' = \mathbf{v} \times \mathbf{v}'', \quad \mathbf{u}'' = \mathbf{v}' \times \mathbf{v}'' + \mathbf{v} \times \mathbf{v}'''$$

and the proof can be concluded using the standard vector identity

$$(\mathbf{a} \times \mathbf{b}) \times (\mathbf{c} \times \mathbf{d}) = [\,\mathbf{a} \cdot (\mathbf{b} \times \mathbf{d})\,]\,\mathbf{c} - [\,\mathbf{a} \cdot (\mathbf{b} \times \mathbf{c})\,]\,\mathbf{d}.$$

Q.E.D.

This Proposition explains the special form of the denominator of the tangent curve in Example 5. It might also help to understand possible simplifications of the formula (3) for special choices of $f(t)$.

5 Conclusion

We presented several results for curves tangent to polynomial vector fields. We have seen that the Frenet frame and the ratio between the curvature and torsion are essentially determined by the field. We have also presented the general formula for rational tangent curves and proved several results about the degrees of expressions occurring in this formula. We hope that these results will lead to the full understanding of possible cancellation of the denominator in this formula.

Acknowledgements

This research was supported by the grant 17–01171S of the Czech Science Foundation.

References

[1] M. Bartoň, B. Jüttler, W. Wang, Construction of rational curves with rational rotation–minimizing frames via Möbius transformations, Mathematical Methods for Curves and Surfaces 2008, Springer, Berlin, pp.1–25. Lecture Notes in Computer Science, vol. 5862 (2010).

[2] R. T. Farouki, *Pythagorean–Hodograph Curves: Algebra and Geometry Inseparable*, Springer, Berlin (2008).

[3] R. T. Farouki and Z. Šír, Rational Pythagorean-hodograph space curves, Computer Aided Geometric Design, 28, 75-88 (2011).

[4] R. T. Farouki and Z. Šír, Mapping rational rotation-minimizing frames from polynomial curves on to rational curves, Computer Aided Geometric Design, submitted.

[5] E. Kreyszig, *Differential Geometry*, University of Toronto Press (1959).

GeoGebra – prepojenie digitálneho a materiálneho sveta

GeoGebra - connecting the digital and the physical world

Renáta Vágová

Department of Mathematics, Faculty of Natural Sciences,
Constantine the Philosopher University in Nitra
Tr. A. Hlinku 1, 949 74 Nitra, Slovak Republic
renata.vagova@ukf.sk

Abstract. Využívanie technológií sa v posledných desaťročiach vyvíjalo veľmi rýchlo a v súčasnosti ponúkajú nové príležitosti pre výučbu matematiky. Najmä integrácia dynamických geometrických softvérov s 3D tlačou nám ponúka možnosť transformovať digitálne reprezentácie trojrozmerných objektov do ich materiálnej fyzickej podoby. V tomto príspevku uvedieme stručný prehľad a ukážku nami navrhovaných pracovných listov pre žiakov v rámci tematického celku Rez kocky. Naším cieľom je vytvoriť materiály a navrhnúť také vyučovanie, ktoré vzájomne spája digitálne (virtuálne) a fyzické (reálne) zdroje vyučovania a učenia sa priestorovej geometrie.

Keywords: GeoGebra software, 3D printing, visualisation, solid geometry

Kľúčové slová: GeoGebra software, 3D tlačené objekty, vizualizácia, priestorová geometria

1 Introduction

Understanding three–dimensional objects from their two-dimensional representations can be challenging. It means, not all students can easily transform plane representations (such as drawings, pictures or paper-and-pencil projections) of geometry solids into the correct mental representations (visual images). External representations of 3D objects in physical, digital and paper-and-pencil environment, along with mental images, processes and abilities form a model of visualisation [1]. These elements complement and influence each other and altogether play an important role mainly in teaching and learning geometry. In this paper, we present a brief summary and an example of the designed worksheets for 11th-grade students, based on the combined use of physical (3D printed) and digital (dynamic) resources for 'Cube Cross Section' lessons. In addition, we intend to share how teachers can print 3D objects using GeoGebra software to transform digital (virtual) solid representations into their physical (palpable) form. As stated by [2], 'images and objects can influence the way we think about mathematics,' and help us to understand its results. Following the mentioned, the main aim of the research project is to integrate the same external representation of 3D objects in all three working environments (paper-and-pencil, physical and digital) to support the development of students' spatial abilities and creation of their visual images.

2 Designed worksheets

The designed material 'Cube Cross Section' consists of five paper worksheets (later W1-W5) complemented by 3D printing and interactive GeoGebra applets. The PDF files and GeoGebra applets are available to students in a private Workgroup on the GeoGebra platform. To facilitate the worksheet orientation and sequencing of the tasks, the same layout was followed in the design.

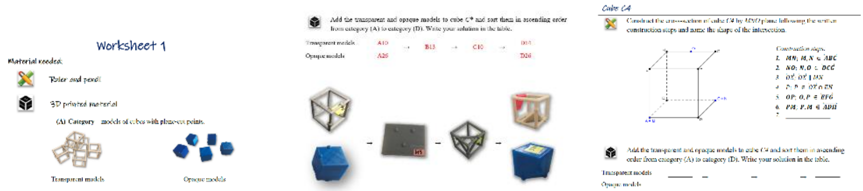

a. b. c.

Fig. 1: Layout of the worksheets

At the beginning of the worksheets, there is a list of students' working environments (see Fig. 1.a). Each environment has its own symbol and, in addition, the physical environment is complemented by pictures of specific 3D printing needed in that particular worksheet. Then, there is one exemplary solved (see Fig. 1.b) and six unresolved (see Fig. 1.c) tasks for students.

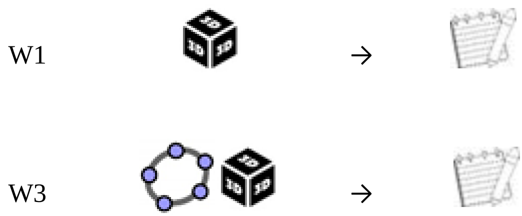

Fig. 2: Solution process in the designed worksheets

The essential difference among W1-W5 is a varying combination and sequence of the three working environments (see Fig. 2). For example, in W3, students initially work with GeoGebra applet and manipulate 3D printing. Afterwards, they make paper-and-pencil constructions.

To underline, students' paper-and-pencil constructions are required for every task in all worksheets. While manipulation with 3D printing and GeoGebra applets is not in all of them. The goal is to move **from** *3D physical representations* in a *3D physical environment* **to** *2D paper-and-pencil* *representations* in a *2D paper-and-pencil environment* **through** *2D digital (dynamic) representations* in a *3D digital environment* (see Fig. 3).

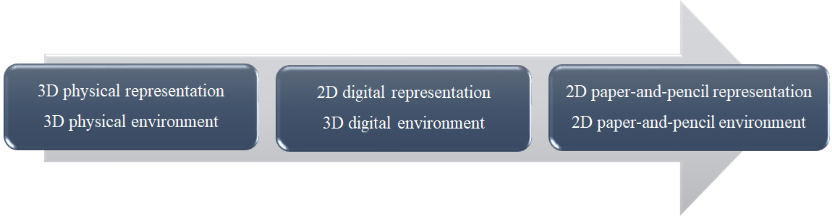

Fig. 3: Linking representations and environments among worksheets

As mentioned above, the structure of all worksheets is the same, but the combination of all three environments and linking between them is different in W1-W5. The next paragraph is focused on the detailed description of Worksheet 1.

2.1 Worksheet 1

Text Physical and paper-and-pencil environment (see Fig. 2) are those of the three mentioned in which student solve tasks *Cube C1 - C6* from W1. The 3D printing is generally divided into 5 groups and all categories are handled in W1 (see Fig. 4):

A. **Category** – transparent ("edge") and opaque cube models with intersection plane points. The models are named $A10 - A16$ and $A20 - A26$.[1]
B. **Category –** opaque models of intersecting plane. The models are named $B10 - B16$.
C. **Category** – transparent cube models of constructions of cross section of cube. The models are named $C10 - C16$.
D. **Category** – transparent and opaque cube models of cross sections of a cube. The models are named $D10 - D16$ and $D20 - D26$.

Fig. 4: 3D printing used in W1

[1] The letter A represents the category. The number 1 (2) represents the transparent (opaque) cube model. Numbers 1-6 were randomly added to the 3D printing, regardless of the task number.

As the combination and sequence of the environments indicate, each task *C1-C6* consists of two parts. W1's task solving process is as follows:

1. Students add 3D printing from categories A-D to cubes *C1-C6* and write their solution in a table (see Fig. 4 and Fig. 5).

Add the transparent and opaque models to cube C^* and sort them in ascending order from category (A) to category (D). Write your solution in the table.

Transparent models	A10	→	B13	→	C10	→	D14
Opaque models	A26						D26

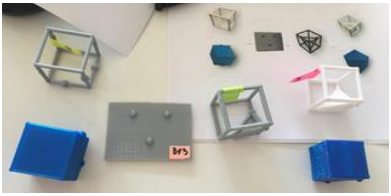

Fig. 5: Solution process in physical environment

2. Students make paper-and-pencil constructions of the cross section of a cube by following the written construction steps and name the shape of the intersection (see Fig. 6). The 3D printing is looked at, used and manipulated at the same time.

Cube C (Exemplary solution)*

Construct the cross-section of cube C^* by MNO plane following the written construction steps and name the shape of the intersection.

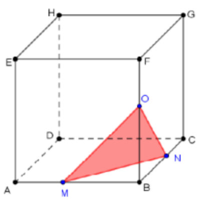

Construction steps:

1. $MN; M, N \in \overleftrightarrow{ABC}$
2. $NO; N, O \in \overleftrightarrow{BCG}$
3. $OM; O, M \in \overleftrightarrow{ABF}$
4. *Triangle MNO*

Fig. 6: Solution process in paper-and-pencil environment

As a final point, the non-inclusion of GeoGebra applet is intentional in W1. The goal is to enhance the opportunity to make connections between the physical and the paper-and-pencil environment for students. Moreover, to let them see the same external representation (geometric construction of the cube cross-section) in two different environments from different perspectives and in different situations.

Following the mentioned, there are two extra parts in W1:

1. **Bonus task** - students take 3D opaque models of category D and construct the given and missing part of cubes *C1-C6* (see Fig. 7).

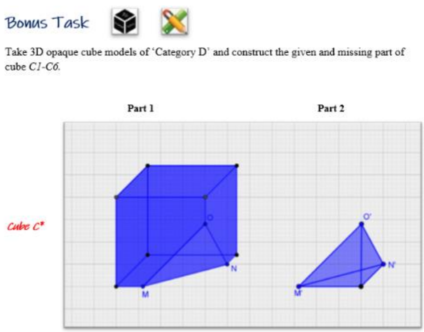

Fig. 7: Bonus task in W1

2. **GeoGebra applets**
   a. Visualisation of the cube cross section - the applet can be used at the end of W1 to make conclusions about different types of cube sections (see Fig. 8.a). Moreover, it can be used as a transition from the first to the second worksheet. Students can rotate the plane and make their own cross sections of a cube.
   b. Two parts of a cube - the applet can be used to explain not all cube dissections are the cross sections of a cube (see Fig. 8.b). Students can rotate both parts of a cube and the aim is to find its correct missing part.

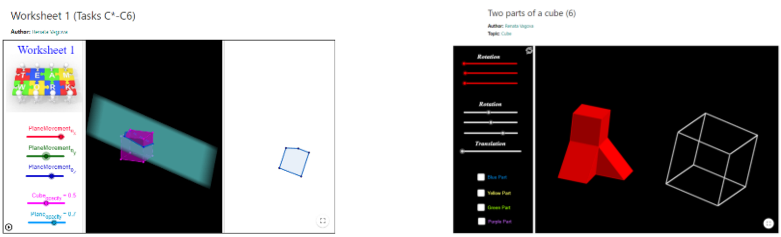

a. b.

Fig. 8: Bonus GeoGebra applets

In addition, the last section represents how teachers can print 3D objects using GeoGebra software to transform digital (virtual) solid representations into their physical (palpable) form.

3 3D printing with GeoGebra software

The GeoGebra platform provides a detailed ‘Tutorial for 3D Printing with GeoGebra’ available at https://www.geogebra.org/m/dc4gewrn or use the QR code in Fig. 9.a.

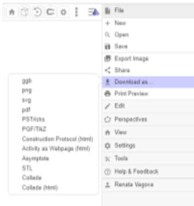

a. b. c.

Fig. 9: 3D printing with GeoGebra

To summarize the 3D printing process, the main steps are listed below:

1. **step** - find or make your own 3D objects in free online GeoGebra Apps.
2. **step** - export this file to STL format: Main Menu → Download as → STL and finally EXPORT your file (see Fig. 9. b).
3. **step** - set the object properties (see Fig. 9. c).

Although there are challenges in 3D printing, as you would expect, there is no reason to give it up. All you need is practice. Just explore and have fun.

4 Conclusion

This paper presented a brief summary and an example of designed worksheets based on the combined use of physical (3D printed) and digital (dynamic) material for solid geometry lessons. The aim was to present an integration the same external representation of 3D objects into the three working environments. In addition, the 3D printing process with GeoGebra software was introduced.

Acknowledgements

The author has been supported by project UGA-VII/18/2019.

References

[1] A. Gutiérrez: *Visualization in 3-dimensional geometry: In search of a framework*, Proceedings of the 20th PME International Conference, Vol. 1, 1996, pp. 3-19

[2] O. Knill, E. Slavkovsky: *Illustrating Mathematics 3D Printers*, ArXiv, org, 2013.

Educational videos – products of DIAD-Tools project

Daniela Velichová

Dept. of Maths and Physics, Fac. of Mech. Eng., Slovak University of Technology in Bratislava
Nám. slobody 17, 812 31 Bratislava, Slovak Republic
daniela.velichova@stuba.sk

Abstract. Paper is aimed to present information about on-line educational materials developed in the Erazmus+ project DIAD-Tools to support teaching of subjects such as Technical Drawing, Descriptive Geometry, or Constructive Geometry at secondary and tertiary level in engineering educational programmes.

Key words: technical drawing, educational video, interactive learning material

1 Introduction

Descriptive geometry was a compulsory subject proudly called „the queen of all technical disciplines“, and not so long ago it was also one of the important subjects at the secondary schools. Nowadays, hardly any of the secondary school graduates heard the name of this discipline, and few of them have experienced subject related to technical drawing at the professionally oriented secondary schools, perhaps with an exception of those oriented at civil and mechanical engineering domains. However, every professionally reliable engineer should be aware of space relations, as constructor of space objects and designer of the space arrangement itself. Lack of spatial abilities and understanding leads to many problems also in a lot of other domains, not only those related to technical disciplines.

Erazmus+ project DIAD-tools is an international project joining powers of secondary and tertiary school teachers to improve the situation in technical skills of graduates at both types of schools, technical secondary schools and technical universities, see [1]. Five European countries participate in this project - Estonia, Latvia and Lithuania, Poland and Slovakia. Partner organisations vary from secondary vocational schools to technical colleges and universities. The main goal of the project is to develop sample examples of instructional materials, interactive and dynamic, which could be used as introduction to teaching, learning and training subjects related to Descriptive geometry and Technical drawing. The idea is to establish an open learning platform available on web with a variety of training materials. Finally, the realistic expectations went to development of about 20 dynamic videos bringing basic information on different topics from the above disciplines. All materials are provided in all 5 language mutations and in English version. They were tested and updated according to needs of customers from all participating countries. In addition to videos, interactive materials developed in GeoGebra environment are available for on-line use, providing opportunity to investigate presented information in step-by-step mode and with individual speed, [2].

2 Description of materials

Scenarios and design of all videos were carefully planned in advance and discussed with the project partners. Videos lasting about 5 minutes each were designed to contain informative text bringing short factual pieces of knowledge, possibly enriched by dynamic figures interpreting presented facts in more illustrative way. Practical examples were invited suitable for the chosen domains and level of foreseen target group of students.

Each partner was responsible for one separately chosen group of related topics. The distribution of work was decided to cover the following 4 main domains and topics:

1. Execution of drawings, geometric drawing
    - Scales
    - Lines on engineering drawings
    - Dimensioning
    - Geometric relationships
    - Polygons
2. Basics of projection drawings, views and sectional views, solids
    - Projections
    - Variations of prism
    - Sectioning
    - Reconstruction
    - Solids
3. Joints of parts, working drawings of parts
    - Threads and threads representation in drawings
    - Threaded fastenings
    - Separable and permanent joints
    - Assembly drawing
    - Detailing assembly drawing
4. Construction drawings
    - Architectural and construction drawings general principles
    - Graphic designations of the building materials
    - Dimensioning in architectural-construction drawings
    - Scales at architectural-construction drawings
    - Construction

Additionally developed materials are available as tutorials on how to use some of the commands and related geometric constructions in the most used and popular CAD systems, e.g. AutoCAD or Onshape, innovative on-line design system available on any device that unites modelling tools and design data management in a secure cloud workspace, never loses data, and eliminates design gridlock.

2.1 Execution of drawings, geometric drawing

Some most important basic information on drawing practise is presented in videos form this part, developed by partner form the Vytautas Magnus University, Agricultural Academy in Kaunas, Lithuania. Normative about used lines, scales (Fig. 1) and dimensioning principles are presented in accordance to EU ISO standards.

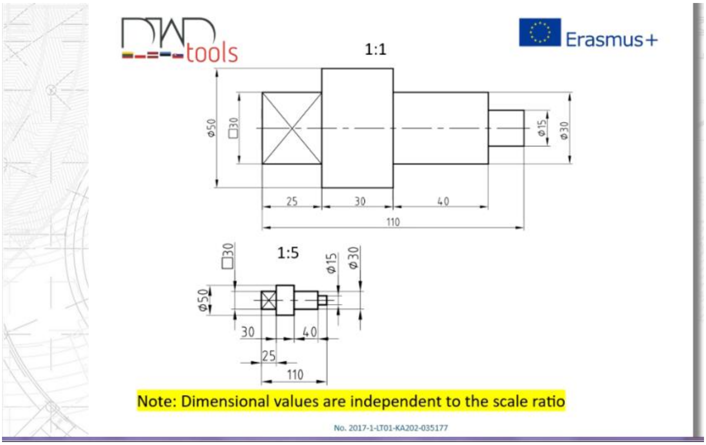

Fig. 1: Example from video Scales

Some practical examples of used geometric relations in design are presented for modelling in Onshape system, see Fig. 2.

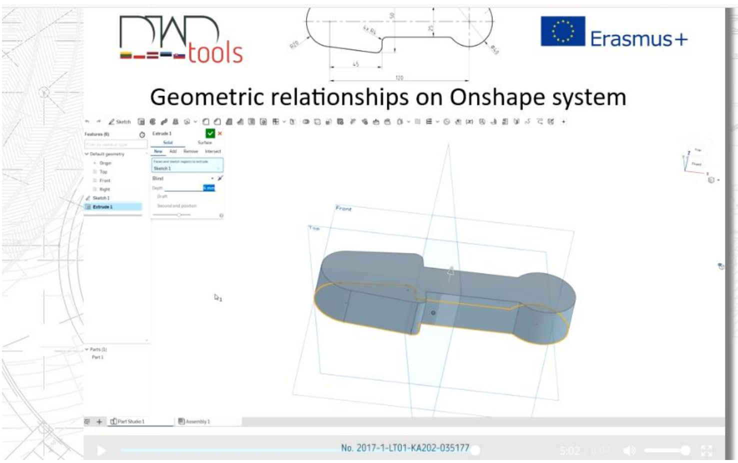

Fig. 2: Tutorial for modelling in CAD system

2.2 Basics of projection drawings, views and sections, solids

Slovak University of Technology was partner responsible for development of materials in this section. Educational videos contain information on basic projection methods mostly used in mechanical and construction engineering drawings. Animated pictures are intended to help students in understanding e.g. Monge method or Multiview projection, as well as basic principles of linear perspective, Fig. 3, or object reconstruction from related views, Fig. 4.

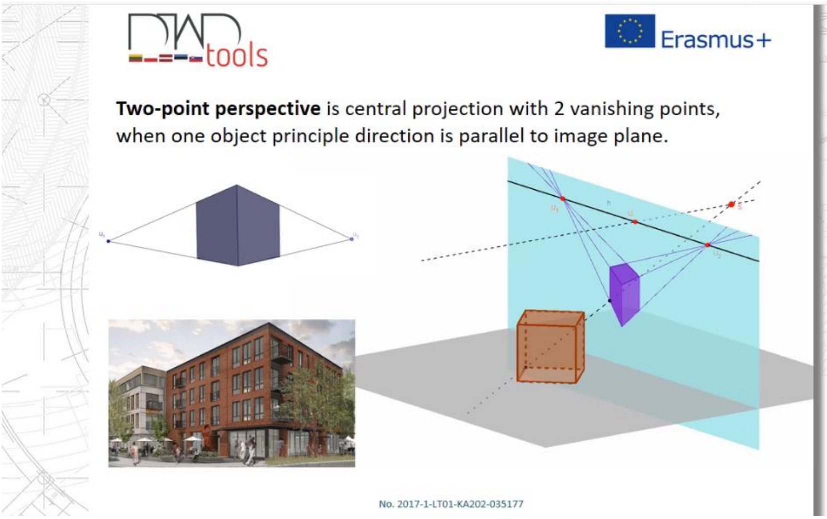

Fig. 3: Linear perspective – video Projections

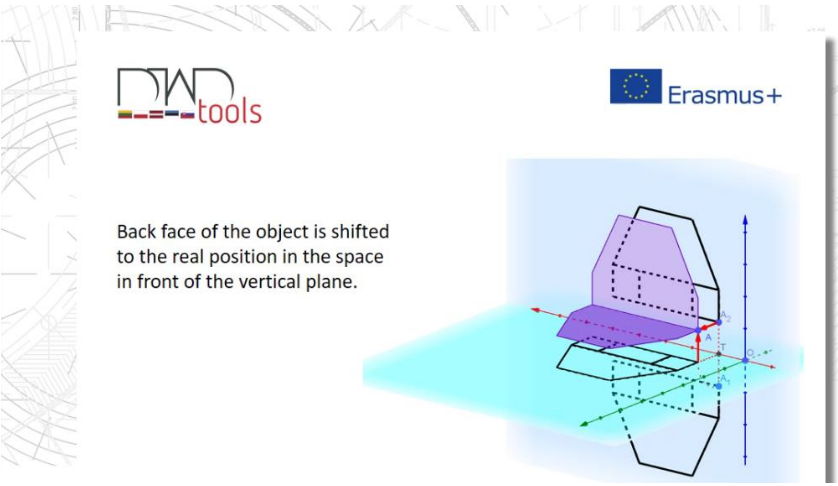

Fig. 4: Reconstruction – video Reconstruction

Material for training spatial skills and abilities of spatial imagination includes moving 3D views of prisms truncated or with some removals, accompanied by their 2 or 3 related orthographic views, see Fig. 5.

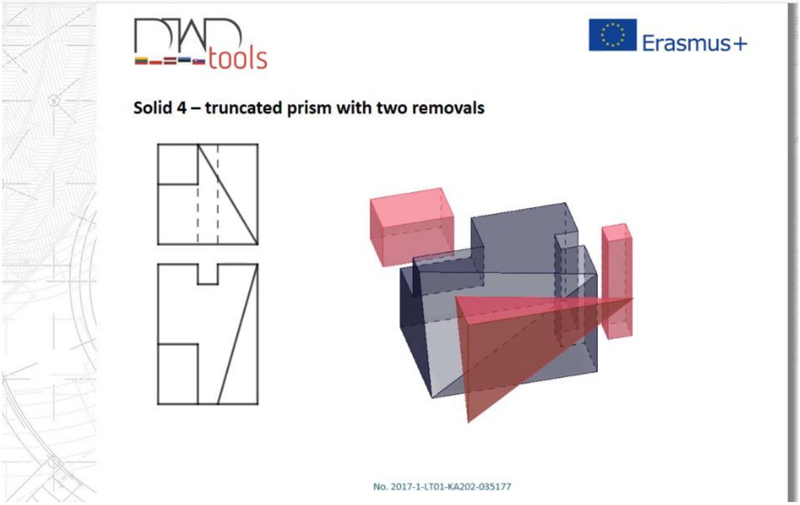

Fig. 5: Example from video Variations of prism

Examples of viewed objects, distribution of views and spatial relations between separate views can be also investigated in related Interactive materials – Monge Method, Multiview Projections EU norm, Multiview Projections - USA norm, Intersections of solid, Object Reconstruction, example see in Fig. 6.

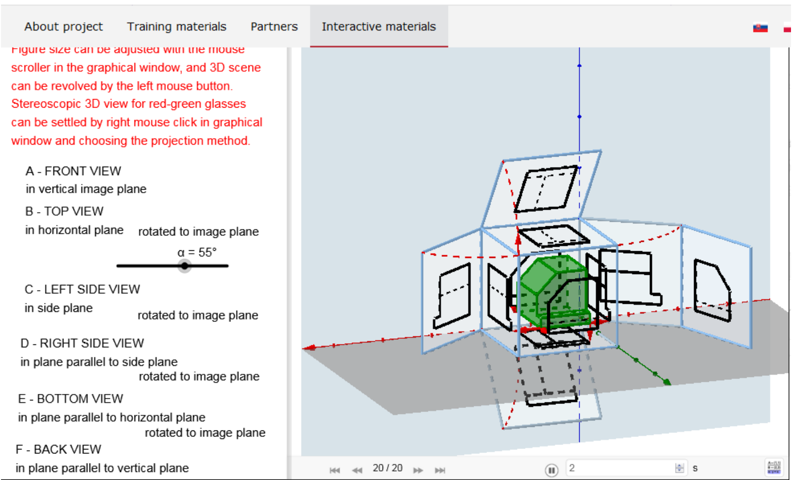

Fig. 6: Multiview Projection EU Norm

2.3 Joints of parts, working drawings of parts

Materials in this section were prepared by partner from Riga Technical University in Latvia. Educational videos bring detailed information on threads and various types of joints and their parts, and they contain many practical examples about rules for marking and presenting joints on working drawings, Fig.7. Many animations included in these materials are aimed to motivate students, raise their interest and help them to understand the topic better, Fig. 8.

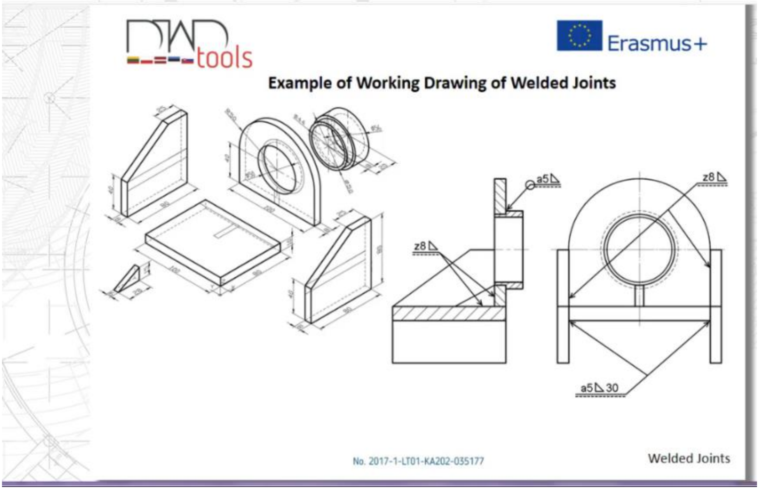

Fig. 7: Example from video Separable and permanent joints

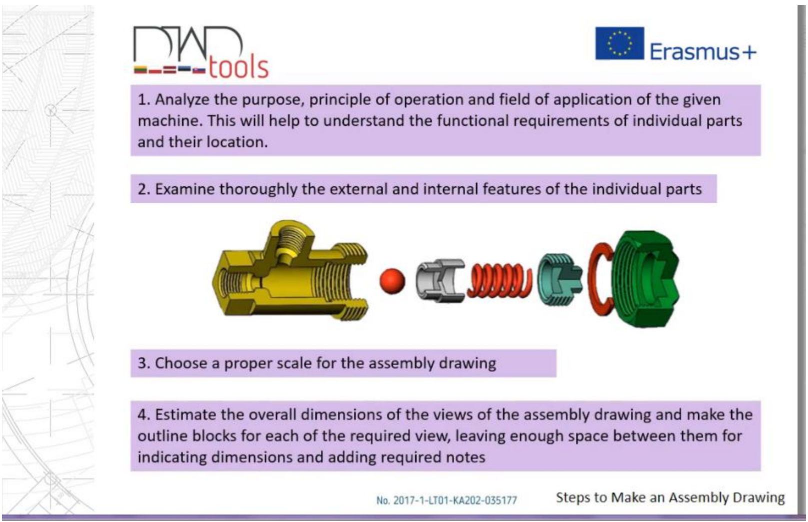

Fig. 8: Steps to make an Assembly Drawing

2.4 Construction drawings

Partner from Silesian University of Technology in Gliwice, Poland, was responsible for development of materials in this group, aimed mostly to students of construction engineering and architecture. Many interesting motivation figures are included in videos, supplemented by practical examples of general principles in architectural and construction drawings, Fig. 9, special markings and dimensioning rules and construction elements, see Fig. 10.

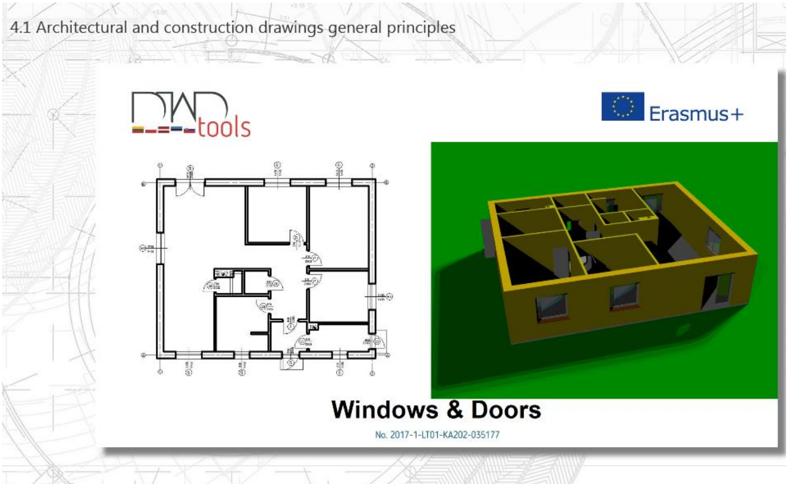

Fig. 9: Example from video on general principles

Fig. 10: Detail from construction element

3 Conclusions

In this paper we focused on presentation of instructional materials developed in the Erazmus+ European project in 6 language mutations and accessible free at the platform developed by project partners available at the project page address. Materials are suitable for subjects related to Descriptive geometry and Technical drawing at a range of schools, from vocational secondary schools to the technical universities. Design and contents of presented videos and applets was influenced by various constraints, while differences in the basic curricula of the above mentioned subjects in partner countries was one of the most limiting, see [3]. Materials were designed to be as short as possible, but to bring important pieces of information for general understanding of principles and rules for production and reading of technical documentation.

DIAD-tools materials are available free at the webpage of The Lithuanian Society for Engineering Graphics and Geometry [3]. Project partners' consortium responsible for development of educational materials and their testing consisted of the following institutions:

P1. Vilnius Builders Training Centre, Lithuania

P2. Slovak University of Technology in Bratislava, Slovakia

P3. Ida-Virumaa Vocational Education Centre, Sillamäe, Estonia

P4. Vytautas Magnus University. Agriculture Academy, Kaunas, Lithuania

P5. The Lithuanian Society for Engineering Graphics and Geometry, Kaunas, Lithuania

P6. Riga Technical University, Latvia

P7. Panevėžys University of Applied Sciences, Panevėžys, Lithuania

P8. Silesian University of Technology, Gliwice, Poland

Acknowledgements

The author has been supported by the Grant Agency Erazmus+, Strategic partnership programme, project No. 2017-1-LT01-KA202-035177, DIAD-Tools: Development of Interactive and Animated Drawing Teaching Tools.

References

[1] Project DIAD-Tools webpage, www.liggd.lt/diad-tools

[2] GeoGebra webpage, www.geogebra.org

[3] Sroka-Bizoń M., Tytkowski K., Vansevicius A., Velichová D., Dobelis M., Do Engineers Use International Language? Construction Drawing as a Way of Communication Between Engineers, Journal for Geometry and Graphics, Volume 23 (2019), Number 1, Helderman Verlag, ISSN 1433-8157, pp. 115-126

GeoGebra kniha „Slovník těles"

GeoGebra book Geometric Solids Vocabulary

Šárka Voráčová

Dept. ofApplied Mathematics, Faculty of Transport. Sciences, CTU in Prague
Konviktská 20, 11000 Prague, Czech Republic
voracova@fd.cvut.cz

Abstract. The visualization that is possible with today's dynamic software enables the student to see and explore mathematical relations and concepts that were difficult to show in past prior to technology. The most analysis show that students who use technology in their learning had positive gains in learning outcomes.
In the paper, we highlighted some opportunities and examples on how GeoGebra can be used in classrooms to explore some basic concepts in spatial geometry. GeoGebra has many possibilities to help students to get an intuitive feeling and to visualize adequate math process. In this paper we present our interactive education materials collected in GeoGebra book „Solids Vocabulary". It is designed specifically for teaching spatial geometry on interactive and creative way.

Keywords: GeoGebra, Dynamic Geometry Software, Solids, Constructive education

Klíčová slova: GeoGebra, Dynamická geometrie, Konstruktivní vyučování, Tělesa,

1 Digitální vzdělávací zdroje

Studenti středních i vysokých škol v současné době běžně pracují s°internetem a používají ho k vyhledávání informací nejrůznějšího charakteru. Podle řady průzkumů u nás i v zahraničí patří k nejčastějším činnostem, které žáci realizují prostřednictvím internetu ve svém volném čase, především hraní her, sledování videa a chatování; na druhém místě je vyhledávání informací potřebných pro studium [10]. Internet a výukové webové stránky proto dnes patří k učebním pomůckám stejně jako tištěné učebnice či sbírky úloh a je zcela jisté, že jejich význam pro učení a vyučování dále poroste.

Využití počítačových programů ve školské matematice je možné dvojím způsobem. První spočívá v řešení standardně zadaných úloh použitím příkazů daného software. V danou chvíli žák ani nemusí znát postup či vzorec vedoucí k výsledku, software provede výpočet za něj; z pohledu žáka jde tedy o jakousi černou skříňku. Druhý způsob spočívá v podpoře aktivní práce žáka, povzbuzení k vytváření a ověřování hypotéz a experimentování, jež vede k hlubšímu pochopení souvislostí [8].

2 GeoGebra – software dynamické geometrie

Dynamický geometrický program tvoří geometrickou scénu v závislosti na volitelných parametrech. Geometrickými objekty na scéně může uživatel manipulovat při zachování zadaných polohových a metrických vlastností. Experimentování s dynamikou systému, pozorování vlivu parametrů na tvar geometrických objektů i tvorba a ověřování hypotéz přispívají k lepšímu porozumění matematiky na všech stupních škol.

Pozitivní vliv dynamických geometrických programů dokládá řada kvantitativních i kvalitativních výzkumů. Žáci dosahují výrazně lepších výsledků ve standardizovaném testu na porozumění geometrickým pojmům a geometrickou představivost. Žáci využívající dynamickou geometrii prokazují hlubší a trvalejší zapamatování získaných poznatků (cit. podle [11]).

Posledních deset let je celosvětově nejpoužívanějším programem školské matematiky GeoGebra. Instalace i online verze jsou zcela zdarma, nen8ro4n0 na hardware, zadávání objektů je didakticky promyšlené a nástroje pokrývají školské kurikulum od základní školy až po základy calculu.

Prostředí GeoGebry integruje více edukačních prostředí: Nákresna, Algebraická reprezentace objektu, CAS (Computer Algebra System), Tabulka, atd. Reprezentace problému v různých modelech – numerickém, algebraickém, symbolickém i grafickém napomáhá pochopení souvislostí mezi různými přístupy k matematickým objektům.

Na serveru geogebra.org je přes milion appletů sdílených uživateli. Bohužel, vyhledávání dokumentů k danému tématu je nepřehledné, kvalita a matematická správnost nejsou nijak garantovány, hodnocení je ponecháno udílením "like".

3 Výuka stereometrie užitím GeoGebry

Prostorová geometrie patří dlouhodobě ke kritickým místům matematického vzdělávání. Dle [9] se zde výrazně projevuje, že učitelé učí tak, jak byli sami učeni, jak tomu rozumí a jak úlohy sami řeší. Nedostatky ve vyučování geometrii souvisejí s nedostatky v geometrickém vzdělávání učitelů. Odrazem představ o axiomatické výstavbě geometrie je soustředění školní geometrie na rýsování a terminologii. Geometrie by však měla být od samého počátku orientována na poznávání prostoru, v němž žák žije, a na rozvíjení představivosti [6].

Málokterá oblast školské matematiky je tak vhodná pro využití GeoGebry, jako je stereometrie. Zejména pro žáky se slabší prostorovou představivostí je kolikrát jediným možným nástrojem pro nahlédnutí vzájemné polohy 3D objektů. Jistě by etapě virtuálních manipulací v počítačovém 3D prostředí měla předcházet manipulace s reálnými objekty, ale při zkoumání složitějších těles a scén již takovou možnost nemáme.

Představivost, a to nejen geometrická se obecně rozvíjí praxí. GeoGebra v krátkém čase zprostředkuje žákům náhled řady geometrických situací a rozšiřuje tak evidované modely i zkušenosti.[11].

Průzkum [4] prokázal pozitivní vliv software dynamické geometrie na konstrukci prostorových objektů a při určování objemů a povrchů. Možnost zkoumání dynamického rysu z různých úhlů pohledu přispívá k prohloubení poznávacího procesu žáků.

4 Slovník těles

Soubor hypertextových dokumentů s interaktivními applety je vytvořen jako tzv. GeoGebra kniha s názvem „Slovník těles“ [15]. Slovník je navržen jako pomůcka k výuce těles na základní škole od úvodního seznámení s typy těles a základními pojmy až po procvičování aplikací výpočtu povrchu a objemu. Každému z těles krychle, kvádr, jehlan, válec, kužel a koule je věnována jedna kapitola, společné jsou úvodní a závěrečný oddíl se vzory pro výukové listy vytvářené samotnými žáky.

Počítač by neměl sloužit jen k prezentaci obrázků a videa, sebelepší prezentace trvající déle než deset minut vede ke ztrátě pozornosti. Pokud na počítačovou animaci nenavazuje další činnost, např. práce s applety, pracovními listy či kauzální rozhovor, zůstává žákům skryta podstata věci. Proto jsou kapitoly Slovníku těles kombinací různých forem vzdělávání prostřednictvím počítače. Úvodní applet demonstrující probíranou vlastnost, je následován testovými otázkami i písemnými úkoly v pracovním listu.

Naší snahou bylo využít možnosti dynamického software, nahradit pasivní pozorování interaktivními prvky a postupně přidávat úkoly pro samostatné konstrukce žáků. Součástí výukového materiálu jsou interaktivní applety pro zobrazení těles, dokreslování sítí těles v prostředí GeoGebra a řešení testových otázek.

4.1 Povrch a objemy

Velkou pozornost jsme věnovali povrchu a objemu těles. Tato témata považujeme za dlouhodobě zanedbávaná a problematická, přitom právě zde se dá velmi dobře uplatnit objevitelský přístup.

Zatímco pro povrch těles máme v GeoGebře neocenitelného pomocníka v příkazu Sit(<Mnohostěn>, <Číslo>), podpora výuky objemu je zastoupena jen nástrojem pro jeho výpočet. Webovské stránky Objem krychle a Objem kvádru obsahují interaktivní applety s testovými otázkami pro stavby z kostiček a určení objemu.

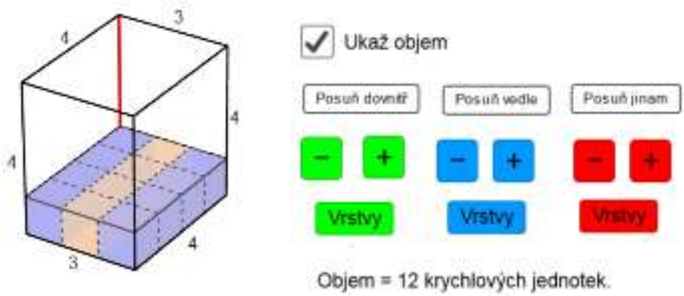

Obr. 1: Objem kvádru – přidáváním krychlových jednotek určíme objem.

Odvodit s žáky objevitelským způsobem vzorec pro objem jehlanu je komplikovanější. Ve školské praxi se často spokojíme s vyslovením vzorce bez důkazu, v lepším případě s odvoláním na Cavalieriho princip. Důvěřivější studenty by mohl přesvědčit rozklad krychle na na tři shodné čtyřboké jehlany. Podstavy jsou sousední stěny krychle, výškou je hrana na podstavu kolmá. (viz Objem jehlanu, [15]). Ovšem u kvádru je to o něco složitější. Rozklad kvádru netvoří tři shodné jehlany, jsou to jen jehlany stejného objemu. Jak ale dokázat, že dva jehlany se shodnými základnami a výškami mají stejný objem?

Vyřešení tohoto problému patří mezi významné výsledky antické geometrie. Dle Archiméda (287–212) přísluší přiřknout prvenství ve formulaci poučky Démokritovi z Abdér [14].

Dle Démokrita (460-370) se vše, co se nachází v reálném světě, skládá z malých, lidským okem neviditelných a dále již nedělitelných atomů. Jeho odvození vzorce pro jehlan muselo být velmi podobné přístupu, jenž v 17. století popsal Bonaventura Cavalieri (1598–1647). Metoda porovnávání nekonečně tenkých vrstev těles mělo velký vliv na jeho současníky i matematiky pozdějšího období. Leibniz (1646–1716) napsal, že Galilei a Cavalieri byli první, kdo začali odhalovat drahocenné metody a postupy Archiméda.

Eukleides (asi 325–260) ve 12. knize Základů dokazuje rovnost objemů jehlanů o stejných podstavách a výškám Eudoxovou exhaustační metodou. Tedy rovněž úvahami, jež daly vzniknout infinitesimálnímu počtu. O Eudoxovi z Knidu (408–355) je známo, že se stal členem Platonovy Akademie. Platon (427–347) byl nesmiřitelným odpůrcem Démokrita a zřejmě od něj vzešel podnět vyloučit z důkazů všechny úvahy o atomech.

Je důležité seznámit již na střední škole žáky s úvahami o nekonečně malých objektech, při správném vedení mohou být někteří uchváceni stejným způsobem jako současníci Newtona a Leibnize. Je dobré začít názornými problémy rovinných objektů. Eudoxovův rozklad čtyřstěnu se stěží dá označit jako názorný. Je těžké narážet na infinitezimální úvahy a nemoci se spolehnout na geometrický názor. Ve školské matematice se užívá Cavalieriho princip (viz Cavalieriho princip, [15]).

Další možností je názorný čínský důkaz, jenž je popsán v knize *Devět kapitol matematického umění*. Tato kniha pochází z přibližně stejné doby jako Eukleidovy Základy a v čínské matematice hraje i podobnou úlohu. Téměř každý čínský matematik do 20. století se na tuto knihu odkazoval [3].

Významný čínský matematik Liu Huie (20–280) popisuje rozklad trojbokého hranolu na čtyřboký (žlutý) jehlan a trojboký(červený) jehlan – viz. Obr. 2. Postupným doplňováním hranolů ukážeme, že objem žlutého jehlanu je dvakrát větší, než objem červeného jehlanu. Odtud objem jehlanu je třetinou objemu hranolu se shodnou podstavou a výškou. Animace důkazu je zpracována v materiálu Volume of Pyramid na serveru geogebra.org.

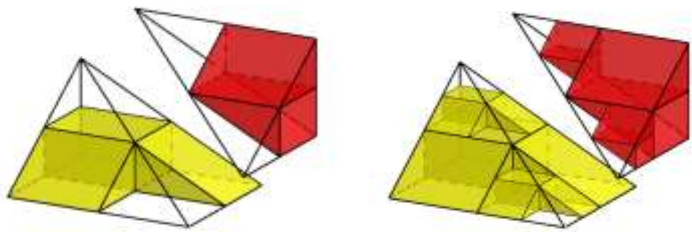

Obr. 2: Čínský důkaz objemu jehlanu – formát GCG_Caption

5 Závěr

Při osvojování matematických vědomostí s podporou moderních technologií záleží více na způsobu jejich integrace než typu použitých prostředků. Hlavním faktorem, který ovlivňuje využívání technologií ve školské matematice, se stává učitel, zejména jeho didaktické dovednosti a ICT kompetence [8].

Nespornou výhodou integrace počítače do výuky je diferenciace výuky a možnost žáků řešit úlohy svým tempem. Velký rozdíl mezi studenty je ve asi největším problémem při organizaci výuky. Je třeba mít připraveny příklady pro nadané děti, ale na druhé straně jsou i žáci, kteří nepřijmou intuitivní ovládání GeoGebry a živelné experimentování s nástroji. Doporučujeme připravit si pro takové žáky vytištěný návod nebo applet s krokovanou konstrukcí, příp. instruktážní video. Úloha učitele jako koordinátora práce dětí je nezastupitelná, práce na počítači nemůže být zcela samostatná, důležitá je zpětná reflexe a diskuse o nalezených vlastnostech a řešeních úloh. Učitel musí žáky usměrňovat a podněcovat jejich do jisté míry samostatné objevování a zkoumání daných geometrických vlastností a problémů.

Podle našeho názoru má GeoGebra potenciál pokrýt témata celé školské matematiky. Doufáme, že se podaří spojit úsilí všech nadšenců tohoto software a vytvořit jeden prostor soustředící všechny kvalitní výukové materiály, jež mohou být učitelům podporou při tvořivé integraci GeoGebry do výuky matematiky.

Literatura

[1] M. Gunzel a kol.: *Integrace elektronického prostředí pro počítačem podporovanou výuku matematiky*, Jihočeská univerzita v Českých Budějovicích, 2012

[2] M. Hejný, F. Kuřina: *Dítě, škola a matematika: Konstruktivistické přístupy k vyučování*. Praha: Portál, 2009. 232 s.

[3] J. Hudeček: Matematika v devíti kapitolách. Sbírka početních metod z doby Han skomentářem Liu Huie z doby Wei a Li Chunfenga a dalších z doby Tang. Překlad, vysvětlivky a úvod. Praha: Katedra didaktiky matematiky MFF UK, 2008. pp. 5–23

[4] K. Chino at al.: The effects of Spatial Geometry Currirulum with 3D DGS in Lower Secondary School Mathematics, *Proceedings PME* , Vol 31, part2, 2007. 137–144

[5] F. Kuřina: Geometrická představivost a vyučování stereometrii. *Matematika a fyzika ve škole*. 1987/1989, roč. 18, s. 201–212.

[6] F. Kuřina: Kritické jevy naší školské matematiky, Matematika – fyzika – informatika, Vol. 24, s. 241–251. Praha, 2015

[7] R. Plch: Využití systémů počítačové algebry ve výuce matematiky, *Univ. S. Boh. Dept. Of Mathematics Report Series*. 2005, Vol. 13,s.145–159

[8] P. Pech: Klasické nebo počítačové metody při řešení úloh v geometrii? *Univ. S. Boh. Dept. Of Mathematics Report Series*. 2005, Vol. 13,s.127–134

[9] M. Rendl, N. Vondrová a kol.: *Kritická místa matematiky na základní škole očima učitelů*. Univerzita Karlova v Praze, Praha, 2013.

[10] J. Robová: Webové aplikace ve vyučování matematiky. In Lengyelfalusy, T.; Horváth, P. (ed.). 5. žilinská didaktická konferenci s medzinárodnou účasťou. Žilina, 2008. s. 47–55.

[11] J. Robová: *Integrace informačních a komunikačních technologií jako prostředek aktivního přístupu žáků k matematice*. PeDF Univerzity Karlovy v Praze. Praha, 2012

[12] P. Sak: *Člověk a vzdělání v informační společnosti: vzdělávání a život v komputerizovaném světě*. Praha: Portál, 2007.

[13] J. Vaníček: *Počítačové kognitivní technologie ve výuce geometrie*. PedF UK, Praha, 2009.

[14] P. Vopěnka, *Nová infinitní matematika: III. Reálná čísla a jejich diskretizace*, Karolinum, Praha, 2016.

[15] Š. Voráčová: „Slovník těles“, GeoGebra kniha, soubor interaktivních materiálů, online https://www.geogebra.org/m/wfxx7zsx

Discrete connections on triangle meshes

Jana Vráblíková
Faculty of Mathematics and Physics, Charles University
Sokolovská 83, 186 75, Praha 8, *Czech Republic*
j.vrablikov@gmail.com

Abstract. In this paper we discuss constructing parallel tangent vector fields on discrete surfaces. We introduce analogies of notions from differential geometry for discrete surfaces, which we represent by triangular meshes, and we show how to use these concepts when constructing tangent vector fields that are parallel over the whole surface. At the end we describe algorithm for constructing these vector fields and show some examples.

Keywords: Discete surfaces, discrete connections, parallel transport, discrete differential geometry.

1 Introduction

Problem of constructing parallel tangent vector field on discrete surfaces was described in [1] and [2], but our aim is to build formal mathematical definitions of all used terms.

We also present algorithm for constructing such fields on given surface. The algorithm is based on algorithm introduced in [2].

This paper sums up basic thoughts of the problem. Most formal definitions as well as context from theory of smooth surfaces can be found in my bachelor thesis [3].

2 Discrete differential geometry

In this section we present theory of discrete surfaces, tangent vector fields and discrete connections. For most formal definitions see [3, Chapter 2].

2.1 Discrete surfaces

We represent discrete surfaces by triangular meshes. We describe the surface as triple $S = (V, E, F)$, where V denotes set of vertices, E set of edges and F set of faces. We need following assumptions: the set V of vertices is finite, the surface is closed and oriented.

We use following notation. Let $S = (V, E, F)$ be a discrete surface. For vertex $v \in V$ we denote F_v^* the star of the vertex. For face $f \in F_v^*$, $v \in V$, we denote θ_f angle by the vertex v.

For each vertex of a discrete surface we define its *Gaussian curvature.*

Definition 1. *Let $S = (V, E, F)$ be a discrete surface. For vertex $v \in V$ we define its* discrete Gaussian curvature *as*

$$K_v = 2\pi - \sum_{f \in F_v^*} \theta_f .$$

Our aim is to find tangent vector field that is *parallel* along every curve on a discrete surface. By discrete curve we mean a sequence of neighbouring faces. We can also desribe discrete curve as a sequence of dual edges or as a sequence of inner edges of the curve.

For curve formed by faces F_v^* for a vertex $v \in V$ de define its *discrete geodesic curvature* in face $f \in F_v^*$.

Definition 2. *For a curve formed by faces $F_v^* = (f_1, f_2, \ldots, f_n)$ for $v \in V$, we define* discrete geodesic curvature *in f_i, $i \in \{1, 2, \ldots, n\}$ as*

$$K_g(f_i) = \theta_i.$$

Now we can formulate discrete versions of theorems from classic differential geometry. Proofs for both theorems can be found in [3].

Theorem 1 (Discrete local Gauss-Bonnet theorem)**.** *Let $S = (V, E, F)$ be a discrete surface, $v \in V$, $c = F_v^* = (f_1, f_2, \ldots, f_n)$, $n \in \mathbb{N}$ be a discrete curve on S. Then*

$$K_v = 2\pi - \sum_{i=1}^{n} K_g(f_i).$$

Theorem 2 (Discrete Gauss-Bonnet theorem)**.** *Let $S = (V, E, F)$ be a discrete surface. Then*

$$\sum_{v \in V} K_v = 2\pi\chi,$$

where $\chi = |V| + |F| - |E|$ is Euler characteristic *of S.*

2.2 Discrete connections

We define *tangent plane* and *tangent space* of a discrete surface.

Definition 3. *Let $S = (V, E, F)$, $f \in F$. We define* tangent plane *of f as set of all directions of f and denote it as $T_f S$. We denote $TS = \cup_{f \in F} T_f S$.*

We are looking for a tangent vector field, which means set of vectors, one for each face of a surface. We can describe tangent vector field by so called *discrete connections.* Connections define how tangent vector changes as we move it from one face to neighbouring one along dual edge, or equivalently, across shared edge.

If two neighbouring faces f_i, f_j lie in plane, we can traslate tangent vector from f_i to f_j so that the two vectors are parallel. Otherwise, we can unfold the faces to plane, translate the vector and then fold the faces back to original configuration. Such transport of a vector is defined by *Levi-Civita connection.*

Definition 4. *Let $S = (V, E, F)$ be a discrete surface.* Discrete Levi -Civita connection *is a map $\Psi_{LC} : TS \to TS$, that to vector $\boldsymbol{u}_i \in T_{f_i}S$ assigns vector $\boldsymbol{u}_j \in T_{f_j}S$ in neighbouring face f_j so that the two vectors are parallel when we unfold the faces to plane.*

As we move vector along dual edge, we can rotate it by some angle. The angle decribes general connection as a deviation from the Levi-Civita connection.

Definition 5. *Let $S = (V, E, F)$, E' be a set of dual edges os S. We define* discrete connection *as a map $\Psi : E' \to \mathbb{R}$, that to dual edge (f_i, f_j) assigns an angle $-\alpha$, where $i, j \in \{1, 2, \ldots, |F|\}$, $i \neq j$.*

If we translate vector $\boldsymbol{u}$ from one face to another face with respect to some connection, we call the new vector *parallel transport* of the vector $\boldsymbol{u}$ and we say that the two vectors are *parallel* with respect to the connection.

As we can move vector from one face to neighbouring face, we can move it along a closed curve. We denote the map that to vector $\boldsymbol{u} \in T_fS$ assigns vector $\boldsymbol{u}' \in T_fS$ after it was translated along closed curve c as $\Pi_c^{f,f}$.

Our task is then to find tangent vector field that is parallel along every curve on the surface. However, if we move a vector along a closed curve, the vector may not end up exactly where it started. We define *discrete holonomy group* to describe this phenomena.

Definition 6. *Let $S = (V, E, F)$, $f \in F$. Set*

$$\{\Pi_c^{f,f} : T_{f_1}S \to T_{f_1}S;\ c = (f_1, \ldots, f_n), n \in \mathbb{N} \text{ closed curve on } S,\ f_1 = f\}$$

with composing forms discrete holonomy group *in f. We denote it H_f.*

We call the angle between vector in face f_i and its parallel transport to the same face a *discrete holonomy*.

Definition 7. *Let $S = (V, E, F)$, $c = (f_1, \ldots, f_n), n \in \mathbb{N}$ be a closed curve. We denote angle between vector $\boldsymbol{u} \in T_{f_1}S$ and its parallel transport along c with respect to connection Ψ back to face f_1 as $h_c(f_1)$ and we call it* discrete holonomy of curve c with respect to Ψ *in face f_1.*

For a closed curve its holonomy with respect to a connection is equal in every face, thus we can denote holonomy of a curve c as h_c.

To get parallel tangent vector field along every curve, we need to find connection for each dual edge so that discrete holonomy group of every curve on a surface is trivial in every face. We will call these connections *trivial connections*.

Thus for $S = (V, E, F)$ we want to find connections that describe tangent vector field with zero holonomy of every curve on the surface.

For curve $c = F_v^*$, $v \in V$, its holonomy with respect to Levi-Civita connection is given by the following relation

$$h_c = \sum_{f \in F_v^*} K_g(f).$$

To get zero holonomy, we need to redefine geodesic curvature in each face so that

$$\sum_{f \in F_v^*} K_g(f) \equiv 0 \qquad (mod\ 2\pi).$$

From discrete local Gauss-Bonnet theorem (1) for $v \in V$ we obtain

$$K_v = 2\pi - \sum_{f \in F_v^*} K_g(f) \equiv 0 \qquad (mod\ 2\pi),$$

thus Gaussian curvature of v must be equal to $2\pi k$, where $k \in \mathbb{Z}$ is called *index* of the vertex v.

Discrete Gauss-Bonnet theorem (2) gives us condition for the indices:

$$\sum_{v \in V} K_v = \sum_{v_i \in V} 2k_i\pi = 2\pi\chi.$$

Therefore indices of all vertices of the surface must sum up to Euler characteristic χ of the surface. In practice, we choose some vertices and prescribe their indices so that they sum up to χ and we let rest of the indices (and thus rest of Gaussian curvatures) to be zero. We will call vertices with non-zero indices *singular vertices.*

This approach provides we are able to find connections that desribe tangent vector field with zero holonomy along curves F_v^*, $\forall v \in V$. We can show that every curve on a discrete surface can be written as linear combination of curves F_v^*, $v \in V$ and generating non-contractible curves. It follows that we need to assure that there is zero holonomy along generating non-contractible curves and then we can find desired connections.

3 Algorithm

This algorithm is based on algorithm by K. Crane presented in [1].

For given surface $S = (V, E, F)$ and set of singular vertices with prescribed indices we want to find connection for each (dual) edge that describes tangent vector field parallel along every curve on the surface. We choose set of generating curves G formed by curves $F_v^*, v \in V$ and $2g$ generating non-contractible curves, where g is genus of the surface.

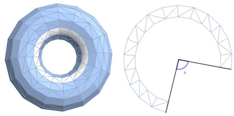

Fig. 1: holonomy of non-contractible curve

For every curve $c \in G$ we compute its holonomy h_c with respect to Levi-Civita connection. For curves $F_v^*, v \in V$ it holds $h_c = K_v$. Figure 1 indicates how to compute holonomy of a non-contractible curve.

For each curve $c \in G$ we obtain equation

$$\overrightarrow{a_c} \cdot \overrightarrow{x} = h_c,$$

where $\overrightarrow{a_c} \in \{-1, 0, 1\}^{|E|}$ describes which inner edges form curve c and $\overrightarrow{x} \in \mathbb{R}^{|E|}$ is wanted vector of connections.

Vectors $\overrightarrow{a_c}$ for each contractible curve $c \in G$ form incidency matrix for vertices and edges $\mathbf{d}_0 \in \{0, 1\}^{|V| \times |E|}$, where

$$(\mathbf{d}_0)_{i,j} = \begin{cases} \pm 1, & \text{if edge } j \text{ is incident with vertex } i, \\ 0, & \text{otherwise.} \end{cases}$$

Vectors a_c for $2g$ non-contractible curves $c \in G$ form incidency matrix $\mathbf{H} \in \{0, 1\}^{2g \times |E|}$, where

$$(\mathbf{H})_{i,j} = \begin{cases} \pm 1, & \text{if edge } j \text{ is inner edge of non-contractible curve } i, \\ 0, & \text{otherwise.} \end{cases}$$

By joining these two matrices we got matrix of system of linear equations $\mathbf{A} = \begin{pmatrix} \mathbf{d}_0 \\ \mathbf{H} \end{pmatrix}$, where $\mathbf{A} \in \{0, 1\}^{|V| + 2g \times |E|}$.

Right side of the system is formed by vector $\overrightarrow{b} \in \mathbb{R}^{|V| + 2g}$, where

$$(\overrightarrow{b})_i = \begin{cases} h_{c_i} - 2k_i\pi, & \text{if } c_i = F_{v_i}^*, \ v_i \text{ singular with index } k_i, \\ h_{c_i}, & \text{otherwise.} \end{cases}$$

Vector $\overrightarrow{x} \in \mathbb{R}^{|E|}$ of connections we are looking for is then given by system od linear equations

$$\mathbf{A}\overrightarrow{x} = \overrightarrow{b}.$$

The system does not have an unique solution, so we choose the one that is closest to the Levi-Civita connections, which is the solution with the least norm

$$\overrightarrow{x} = \underset{\overrightarrow{y}}{argmin} ||\mathbf{A}\overrightarrow{y} - b||.$$

As we have vector $\overrightarrow{x}$ of connections for each edge, we can choose tangent vector in one face of the surface and using breadth-first search translate it to neighbouring triangles rotating it by the given connection when crossing shared edge.

4 Examples

Here we show some examples of results of the algorithm. Algorithm was implemented in *Wolfram Mathematica* [4], triangle meshes were imported from *JavaView* [5].

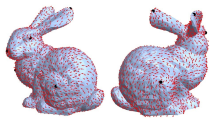

Fig. 2: Stanford bunny, front (left) and back (right)

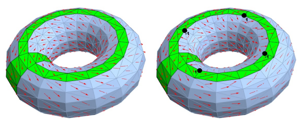

Fig. 3: discrete torus with no singular vertices (left) and various singular vertices (right), generating non-contractible curves denoted in green

5 Conclusion

We have presented some theory for consturcting parallel tangent vector fields on discrete surfaces. It would be interesting to continue studying these surfaces from the perspective of classic differential geometry as this approach can bring effective algorithms for such constructions.

References

[1] Keenan Crane: *Discrete Differential Geometry: An Applied Introduction*, Notices of the AMS, Communication, 1153-1159, 2018

[2] Keenan Crane: *Discrete connections for geometry processing* Californial institute of technology, Master thesis, 2010

[3] Jana Vráblíková: *Diskrétní konexe na trojúhelníkových sítích*, Charles University, 2019, Bachelor thesis

[4] Wolfram Research Inc.: *Mathematica, Version 11.2,2017*

[5] Conrad Polthier: *JavaView*, www.javaview.de, 2017

Simplices and Equifaced Polyhedrons

Gunter Weiss

TU Vienna, Austria, & TU Dresden, Germany
weissgunter@gmx.at

Abstract. The paper deals with some neglected views on simplices and polytopes focussing on a Euclidean place of action. It presents an elementary geometric approach of translating some classical triangle centres to tetrahedrons and simplices as well as polyhedrons and polytopes, which are equifaced with respect to congruences as well as similarities. Many properties of equifaced tetrahedrons are well-known and just repeated. New might be results on isodynamic points as well as on their stellae octangulae. The aim is to present a list of topics, which could earn recognition and to stimulate for deeper research on some of the posed open problems.

Key words: tetrahedron, simplex, equifaced polyhedron, similarfaced polyhedron

1 Introduction

The content of this paper is a roundup of a lecture given at the 5th Slovak-Czech Conference on Geometry and Graphics 2019. A more detailed presentation is reserved to other publications.

The standard point of view of a polyhedron or, in higher dimensions, a polytope is that of objects, which have vertices, line segments as edges, and domains of linear subspaces as faces, c.f. [1], [2], [4], [6], [16], [25] and, among others, also the "dictionary" [24]. Even so we follow this point of view it is worth mentioning that faces could be defined as surfaces with curvature, too, cf. [15].

Furthermore, besides the usually used Euclidean (hyper-) space as place of action, a treatment in projective or affine spaces and in non-Euclidean spaces would open up for many interesting questions. E.g., a generic triangle in the hyperbolic or elliptic plane has four circumcircles, a tetrahedron in a hyperbolic or elliptic space has eight circum-spheres. What about the configuration of their centres? What about other remarkable simplex centres? A generic tetrahedron gives rise to a Stella Octangula, does this concept make sense in a hyperbolic space, where each edge has two midpoints? In the following we refrain dealing with this this point of view and restrict ourselves to the Euclidean case.

In Chapter 2 we mention a generalised Desargues' configurations as an example of a projective geometric interpretation as images of cross polytopes.

In Chapter 3 we translate some classical triangle centres (see [12]) to tetrahedrons and simplices in Euclidean spaces. For tetrahedrons the elementary geometric treatment, combined with a 3D-graphics/calculation tool, gives rise to a broad exercise field for Maths/Geometry courses.

Chapter 4 concerns equifaced tetrahedrons and their higher dimensional counterparts in higher dimensional Euclidean spaces. Unlike *n*-simplices, equifaced tetrahedrons need not be regular. Stellae octangulae based on them allow (restricted) motions of one tetrahedron against the other.

Chapter 5 collects known results on polyhedrons, which are equifaced in the sense of having congruent faces. Simple elementary geometric principles allow to construct such polyhedrons. The question to construct a certain type of polyhedrons from a set of given congruent triangles can be answered for octahedrons, c.f. [Weiss]. Infinite polyhedrons with congruent faces occur in origami and miura ori, see e.g. [Wiltsche] and [20].

The last Chapter 6 deals with polyhedrons, which are equifaced in the sense of having similar faces. While one can construct many even closed polyhedrons with triangular faces, the author could find only one type of closed polyhedrons with similar quadrangular faces.

2 A theorem on perspective *n*-gons

In the following we present an example of special polytopes considered in projective spaces.

H. Ebisui discovered that for perspective quadrangles the intersections of corresponding sides define lines, which have a common point, (in Fig. 1a the point *H*), see [22]. This connects to the classical theorem of Desargues concerning perspective triangles, which allows an interpretation as image of a (regular) octahedron under central projection, see Fig. 1b.

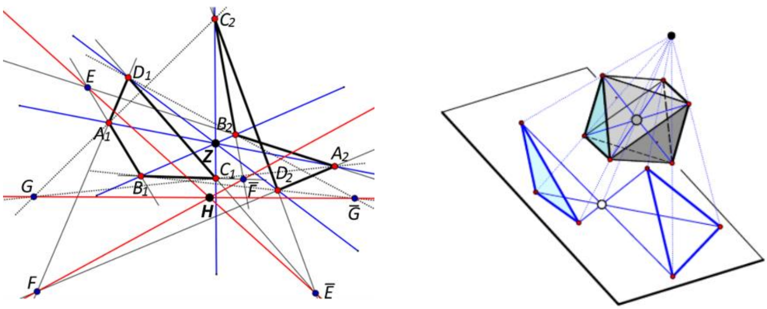

Fig. 1: a) Perspective quadrangles define perspective triangles (centre *H*), b) Perspective triangles can be interpreted as images of faces of an octahedron.

It turns out that Ebisui's discovery also can be interpreted as central projection of opposite faces of a cross polytope. For dimension 2 this principle comprises the Theorem of Fano and it can be extended to *n*-gons in any dimension, see [22]. As the analytic treatment only uses coordinates with values 0 and 1, generalisations to any commutative field with characteristic $\neq 2$ are possible, too.

3 Elementary geometry with simplices

In this chapter we translate some classical remarkable points and lines of a triangle to higher dimensions. It turns out that, in higher dimensions, there can be defined different types of such a remarkable element.

3.1 Centroids connected with simplices

Definition 1: The "d-centroid" C_d ($1 \leq d \leq n$) of an n-simplex S_n in an n-dimensional Euclidean space is the centroid of all d-faces S_d of S_n .

While the centroids C_0 and C_n coincide and are affine geometric properties of S_n, the other centroids are Euclidean properties only. E.g., for a triangle the vertex centroid C_0 coincides with the area centroid C_2, but they are, in general, different from the edge centroid C_1. Equilateral triangles are characterised by $C_0 = C_1 = C_2$. For tetrahedrons the property $C_0 = C_1 = C_2 = C_3$ characterises those having congruent face triangles. Such tetrahedrons are called "equifaced" and need not be regular. It is obvious, how to proceed in higher dimensions.

3.2 Altitude sets of simplices

Definition 2: The "d-altitude" of a simplex S_n in a Euclidean n-space is the common normal of a d-face and its opposite face; ($d < n/2$).

A triangle has only the single set of 0-altitudes, which intersect in the orthocentre O_0. A tetrahedron has four "0-altitudes", which, in general, are generators of a special hyperboloid, a so-called "trace-0-quadric", see [9]. The midpoint M_0 of this hyperboloid acts as replacement of an orthocentre O_0 and is called the 0-*Monge-point* of the tetrahedron. Furthermore, there are three "1-altitudes", the common normals of the three pairs of opposite edges of the tetrahedron. Again, these three 1-altitudes are, in general, skew and span a hyperboloid. Its midpoint M_1 then can be defined as the "1-Monge-point" of the tetrahedron, see Fig. 2 and [23].

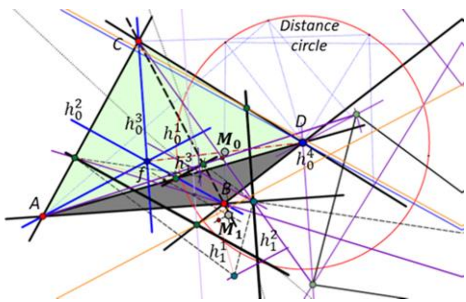

Fig. 2: Top-view of a tetrahedron with its 0- and 1-altitudes h_0^i and h_0^j as well as its Monge points M_0, M_1 (general case).

There are tetrahedrons with 0-altitudes belonging to a quadric, tetrahedrons with two pairs of intersecting ones and those having a proper orthocentre $O_0=M_0$. Another classification could concern the three 1-altitudes, which occur pairwise skew, with two intersecting ones, with one intersecting the other two in different points, and with an orthocentre O_1.

It is obvious, how to proceed in higher dimensions, but one will note differences between odd and even dimensions.

3.3 Spheres connected with simplices

Definition 3: A "d-sphere" c_d of a simplex S_n in a Euclidean n-space touches *all* subspaces spanned by d-faces S_d of S_n. The always existing 0-sphere c_d is called „circum-(hyper)-sphere, the (hyper)-spheres c_{n-1} are called "in-(hyper)-spheres". The centre Z_d of each c_d is a "remarkable point" of S_n.

A triangle has a circumcircle and 4 incircles, the centres of which form a triangle together with its orthocentre. A tetrahedron has one circumsphere and 5+3=8 inspheres, whereby 3 inspheres degenerate for equifaced triangles, see e.g. [2]. In general, there s no "edge sphere" c_1, but if there exsts one edge sphere, so four additional ones, too. For an n-simplex ($n > 3$), there exist one circum-hypersphere and n+2 in-hyperspheres, and, like for tetrahedrons, there occur additional hyperspheres, which degenerate for a regular n-simplex. In general, there are no d-spheres c_d, $1 \leq d \leq n-2$, but if there exist one, so additional ones, too. A detailed discussion of the configuration of the (hyper-) spheres' centres could be a research topic for its own.

3.4 Euler lines of simplices

Definition 4: The Euler line e_n of a simplex S_n connects the Monge point M_0 (resp. the orthocentre), the centroid $C_0 = C_n$, and the circumcentre Z_0. Thereby e_n belongs to the connection planes of vertex P_j with the Euler line e^j_{n-1} of the hyperface opposite to vertex P_j of S_n.

On the Euler line of a triangle the points O_0,C_0,Z_0 define the well-known ratio $\mathrm{R}(O_0,C_0,Z_0) = 2:1$ For an n-simplex S_n we get the ratio

$$\mathrm{R}(O_0,C_0,Z_0) = 2 : (n-1) . \tag{1}$$

In the planes $P_j \vee e^j_{n-1}$ there occur complete quadrilaterals with only rational ratios on its sides, c.f. the example S in Fig. 3. One could consider chains of such quadrilaterals, beginning with the Euler line of a 2-face and, step by step, end with the last quadrilateral containing vertex P_j.

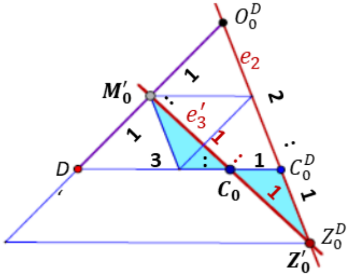

Fig. 3: Euler line e_3 of a tetrahedron *ABCD* and the complete quadrilateral in the plane *D* v e_2, (e_2 Euler line of *ABC*), with characteristic ratios.

It turns out that equifaced tetrahedrons and regular *n*-simplices are the only ones possessing no Euler line. Their Monge point, centroid and circumcentre coincide.

3.5 Isodynamic points of simplices

For a triangle, the concept "isodynamic point" is well-kown. In the classification list given by C. Kimberling they are numbered as X(15) and X(16), see [12]. These points have many interesting properties, c.f. [4], [28], and [8]. For a triangle *ABC* with sides *a*, *b*, c points *X* fulfilling

$$\mathrm{dist}(XA).a = \mathrm{dist}(XB).b = \mathrm{dist}(XC).c \tag{2}$$

are called the *isodynamic points* of *ABC*. Writing (2) as proportions we see that each of the three equations describes an Apollonius circle to one side of ABC and passing through the opposite vertex, see Fig. 4.

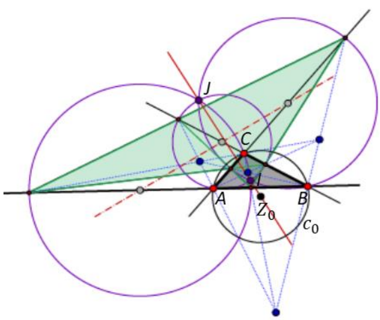

Fig. 4: A triangle with its Apollonius circles, which intersect in its isodynamic points I, J. They are also Bodenmiller points of the quadrilateral defined by the Apollonius circles.

A generalisation to higher dimensions might be possible in the following way:

Definition 6: Let S_d^i, S_d^i* be all pairs of complementary faces of a simplex $S_n = \{P_k\}$ in a Euclidean space E^n. Isodynamic points of S^n are points $\{I_d\}$ with the property

$$\mathrm{dist}(X, S_d^i).\mathrm{vol}(S_d^i*) = \mathrm{dist}(X, S_d^k).\mathrm{vol}(S_d^k*), \text{ for all } i \neq k \in \{1,..,(^n{}_d{}^{+1})\} \quad (3)$$

For general simplices and for some dimensions d the set $\{I_d\}$ solving (3) might be empty.

From Definition 6 follows for a tetrahedron $S_3 = ABCD$ with pairs (a, a'), (b, b'), (c, c') of opposite sides that there are two possibilities for sets of isodynamic points, (Fig. 5):

(a) $\mathrm{d}(X,A).\mathrm{v}(BCD) = \mathrm{d}(X,B).\mathrm{v}(CDA) = \mathrm{d}(X,C).\mathrm{v}(DAB) = \mathrm{d}(X,D).\mathrm{v}(ABC)$
with solution set $\{I_0\}$, (4a)

(b) $\mathrm{d}(X,a).a' = \mathrm{d}(X,a').a = \mathrm{d}(X,b).b' = \mathrm{d}(X,b').b = \mathrm{d}(X,c).c' = \mathrm{d}(X,c').c$
with solution set $\{I_1\}$. (4b)

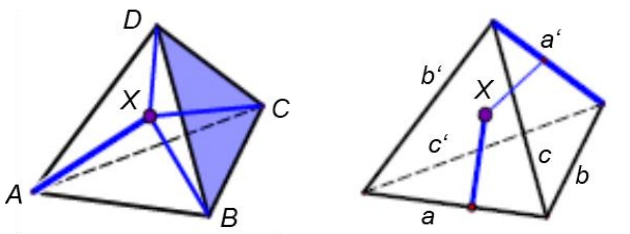

Fig. 5: Symbolic figures for the two cases of isodynamic points of a tetrahedron; left: $X = I_0$ (4a), and right $X = I_1$ (4b).

Equifaced tetrahedrons have the centroid as their (only) "vertex isodynamic point" as well as their (only) "edge isodynamic point". For general tetrahedrons one can predict the number of edge isodynamic points in case (b): The pairs of equations (4b) define a hyperboloid as a 3D-analogue of an Apollonius circle. Intersecting three such hyperboloids result in 8 isodynamic points (counted in algebraic sense).

Higher dimensional cases would need a more detailed research and remain open problems.

4 Equifaced tetrahedrons and simplices

The properties of equifaced tetrahedrons are well-known, c.f. [4], [5], [6], [7], [14], [18], and we mentioned some of them in the chapter 3. Equifaced means, that the face triangles are congruent. For the existence of such tetrahedrons it is necessary that the face triangles are acute. The edges of a generic tetrahedron are diagonals of a parallelepiped, which, in case of an equifaced tetrahedron is a prism. This is a consequence of the necessary (and sufficient) property that opposite edges have equal length. Therefore, they are also called “isosceles tetrahedrons”, c.f. [2], a term, which is neither precise nor generalisable to other polyhedrons and polytopes. (There are tetrahedrons with one isosceles pair of opposite sides, with two and with three such pairs; tetrahedrons can have three, four, five and finally six isosceles sides.) A new property might be the one concerning its isodynamic points, see the former chapter. From Fig. 6 we can read off that four incentres coincide with vertices of the circumscribed prism, while a fifth is the centre of the prism. This centre represents all the centroid, the Monge points and the circumcentre, such that there is no Euler line. Three incentres are ideal points, the corresponding inspheres degenerate.

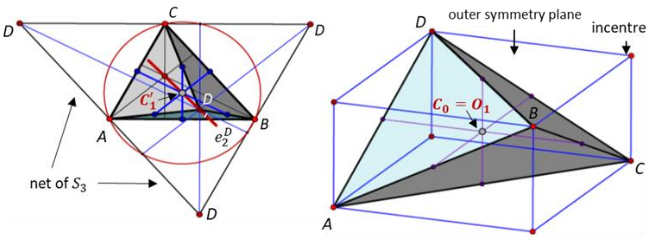

Fig. 6: Top-view and net of $S_3 = ABCD$ (left) and axonometric view (right).

It is also remarkable (and maybe a new result) that their Stella Octangula allows motions of one tetrahedron at the other, whereby originally intersecting edges keep contact. A more detailed treatment of this fact is omitted at this place.

In n-spaces ($n \geq 4$) equifaced simplices are regular. For a generic n-simplex the construction of a circumscribed parallelotope is on the lines of the parallelepiped to a tetrahedron. In Fig. 7 the principle is shown for a 4-simplex S_4. A penteract S_4 has 5 vertices, 10 edges, 10 2-faces, 5 3-faces. The resulting parallelotope has 30 vertices and 10 pairs of parallel 3-faces. For a simplex S_5 there exist two types of circumscribed parallelotopes P_5^1, P_5^2. As the 20 2-faces of S_5 occur in opposite pairs, we still receive only 10 pairs of parallel 4-faces of P_5^2 , so again one notices differences between odd and even dimensional cases.

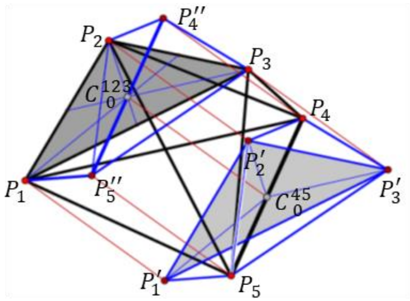

Fig. 7: Principle of the construction of parallel hyperplanes spanned by faces of a parallelotope, which is circumscribed to a simplex S_4.

5 Equifaced polyhedrons

(a) An equifaced polyhedron can be derived by intersecting the outer symmetry planes of two adjacent faces of an Archimedean or Platonic solid. This construction is also applicable to higher dimensions. Because of the regularity resp. semi-regularity of the starting polyhedron, all polyhedrons derived in such a way have an edge sphere c_1, c.f. [26].

From a regular tetrahedron one receives the circumscribed cube, from a regular icosahedron or dodecahedron one gets the rhombic triacontahedron, from a cube or octahedron the result is the rhombic dodecahedron. The latter is not the only rhombic dodecahedron; there exists one more, the Bilinski dodecahedron, see [3], [27]. It can be derived by distorting a regular octahedron and cutting off 4 of its vertices such that rhombus diagonals have golden ratio, see Fig. 8.

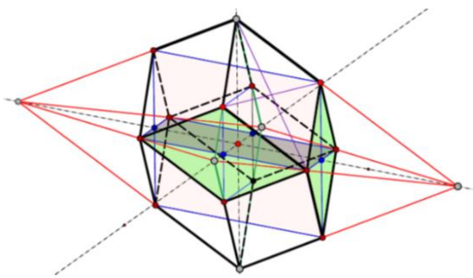

Fig. 8: Bilinski dodecahedron derived from a distorted octahedron.

(b) An equifaced polyhedron can also be derived by adding regular pyramids to the faces of a Platonic or Archimedean solid. There are two parameters to copnsider, the pyramid's height and the rotation angle of the pyramid against the face polygon. This construction can be extended to higher dimensions, construction (a) is a special case of (b).

(c) One can add regular pyramids to the regular faces of a Johnson polyhedron. There are 92 different types of such convex polyhedrons, namely double pyramids with equilateral face triangles, prisms and antiprisms without and with added pyramids, polyhedral cupolas and double-cupolas. Fig. 9 shows an example of a convex extended Johnson polyhedron. Adding similar pyramids such a polyhedron results in one, which is equifaced with respect to similarities.

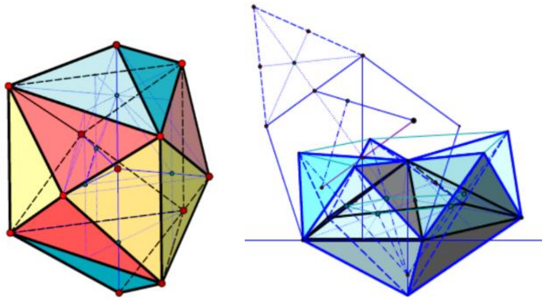

Fig. 9: An equifaced polyhedron based on a threesided Johnson prism (left) and a similar faced polyhedron (right)

(d) Dualising Archimedean solids results in the well-known Catalan solids, which are naturally equifaced. Besides triangles and rhombuses one finds deltoids and pentangles as faces. As an example the deltoidal icositetrahedron, derived from the rhomicuboctahedron, is shown in Fig. 10, together with a practical application.

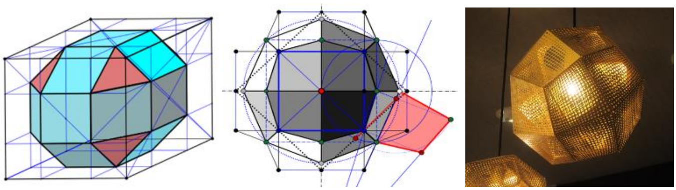

Fig. 10: The dual of a rhombicuboctahedron is a deltoidal-icositetrahedron, which received a realisation as a lampshade.

(e) Finally one can pose the question, how many different equifaced polyhedrons exist to a fixed number of faces. Given eight congruent acute triangles, one can build three types of octahedrons, which differ in their symmetry properties, c.f. [Weiss].

Cancelling the property of a polyhedron of being closed, one can construct infinite equifaced polyhedrons, too. Fig.10 (left) shows an element of such an infinite polyhedron with pentagonal congruent faces, but besides the regular dodecahedron there exist also closed ones, see Fig. 11 (middle and right), c.f. [27].

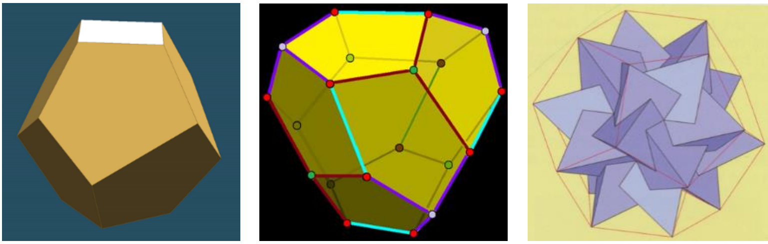

Fig. 11: Polyhedrons with congruent pentagons as faces. Left: element of an infinite column-like polyhedron, middle and right: closed examples ([27]).

6 Origami and equifaced polyhedrons

Origami and Miura-Ori with straight folding edges are polyhedrons in the classical sense, and many of them are equifaced. They occur mostly as infinite non-convex structures, and their movability makes them important for technical and architectural applications. By their nature there are many references to this topic, as e.g. [29], [21], [20], [10], [11], [17], [19]. Also Kokotsakis polyhedrons [13] having quadrangular faces are movable polyhedrons, but they are not equifaced. Among these interesting polyhedrons there are examples, which are of cupola type, besides non convex examples.

We restrict ourselves to one figure found in [21], Fig.12.

Fig. 12: Movable infinite origami polyhedrons, (from [21]).

7 Equifaced polyhedrons with respect to similarities

There exist many polyhedrons with similar triangles as faces. We mentioned one type in Fig. 8. For example, one can start with a tetrahedron or a double pyramid with isosceles triangles as faces, such that their edge lengths fulfil $a{:}b = b{:}c$, and, in a next step, insert triangles fulfilling $a{:}b = b{:}c = c{:}d$, see Fig. 13.

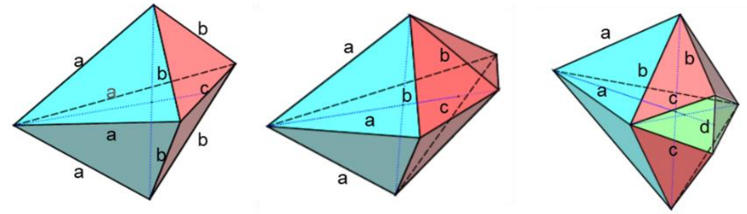

Fig. 13: Examples of polyhedrons with similar isosceles triangles as faces.

Tetrahedrons with face triangles, the sides of which are in geometric progression $a{:}b{:}c = b{:}c{:}d$ are also possible start polyhedrons. Next steps add similar tetrahedrons to its faces, see Fig. 14.

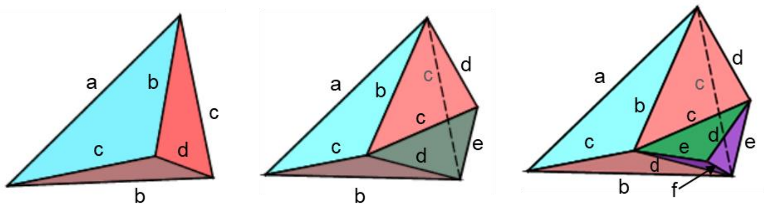

Fig. 14: Polyhedrons with similar triangles as faces, the sides of which are in geometric progression.

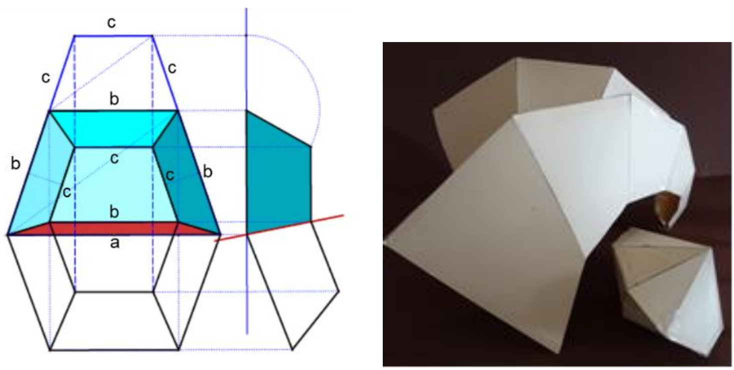

Fig. 15: A closed polyhedron with similar isosceles trapezoids as faces, (left); an infinite spiral polyhedron with quadrangular faces, (right).

Up to now only one type of closed similar-faced polyhedrons having quadrangular faces could be found. Its faces are isosceles trapezoids and to get it closed, two symmetric parts must be glued together, see Fig. 15 (left). The trapezoids have sides a:b:b:b = b:c:c:c and the lengths can be chosen such that one can generate a closed ring of a certain number of such polyhedrons. Like the cylindrical origami structures shown in Fig. 11, there are movable spiral polyhedrons, too, which have similar quadrangular faces, see Fig. 15 (right). Again, also this topic would be worthy for more attention.

8 Conclusion

We presented a collection of ideas, which follow naturally from classical triangle geometry translated to higher dimensions, and ideas resulting from an analysis of the meaning of the words “polyhedron” and “equifaced”. Obviously there occur many already well-known topics, and the paper aims to give an overview of these topics. Thereby connections to many other scientific /technical disciplines can be revealed. The treatments here remain incomplete and are meant to stimulate others for more detailed research. A more elaborated version of the elementary geometric part Chapter 3 will be submitted to “G” (Slovenský časopis pre geometriu a grafiku).

References

[1] Alsina, C., Nelson, R.B. (2015), A mathematical space odyssey: solid geometry in the 21th century. (Dolciani mathemacical expositions, no. 50), Washington: Mathematical association of America, 2015.

[2] Altshiller-Court, N., Modern Pure Solid Geometry. Macmillan, 1935

[3] Bilinski Dodecahedron (2019): https://en.wikipedia.org/wiki/Rhombic_dodecahedron#Bilinski_dodecahedron (retr. 10. 3. 2019).

[4] Bottema, O.(2008), Topics in elementary geometry (2nd ed.), Springer, p. 108, ISBN 9780387781303

[5] Bricard, R., Mémoire sur la théorie de l’octaèdre articulé. J. de Mathématiques pures et appliquées, Liouville 3:113–148 (1897).

[6] Brückner, M. (1900) Vielecke und Vielflache, Theorie und Geschichte. Verl. Teubner Leipzig, 1900. (https://archive.org/details/vieleckeund vielf 00bruoft, openlibrary_edition OL23356512M, FCRecord: MARCXML).

[7] Dirnböck, H., Das gleichflächige Tetraeder. Wissenschaftliche Nachrichten Nr. 27 (1985), p. 27-30. (edited by the Federal Ministery for Science and Art, Austria)

[8] Eves, H. W. (1995), College geometry, Jones & Bartlett Learning, pp. 69–70, ISBN 9780867204759.

[9] Havlicek, H., Weiss, G., The Altitudes of a Tetrahedron and Traceless Quadratic Forms. Am. Math. Monthly, (2002), 679-693.

[10] Heinz, A., Faltpolyeder – eine west-östliche Verbindung, IBDG 2/2012, p. 22-27.
[11] Heinz, A., F, Faltpolyeder: Papierfalten zwischen Kunst und Geometrie, Haupt, Bern 1019, ISBN 978-3-258-60198-4
[12] Kimberling, C., Encycl. of Triangle Centres – ETC, Parts 1…16 (2019) http: //faculty.evansville.edu/ck6/encyclopedia/ETC.html
[13] Kokotsakis, Antonios, Über bewegliche Polyeder. (About Movable Polyhedra), Math. Ann. 107, 627–647, 1932.
[14] Lemoine, E. (1880), Quelques théorèmes sur les tétraèdres don't les aretes sont égales deux adeux et solution de la question 1272. Nouvelle ann. de math. 39, 133-138, 1880.
[15] Pearce P. (1980): Structure in nature is a strategy for design. MIT Press, Cambridge, London 1980, ISBN 0-262-16064-1
[16] Prasolov, Viktor V., Problems in Plane and Solid Geometry. (translated and edited by Dimitry Leites): https://de.scribd.com/document/61948241/Viktor-v-Prasolov-Problems-in-plane-and-Solid-Geometry-Vol-2-Solid-Geometry-239p
[17] Röschel, O., Generalised anti-prims, Lecture at 32nd ADG-conference, Strobl, Austria 2011
[18] Rosenthal, A. (1908), Zur Theorie der gleichflächigen Polyeder. Sitzber. Akad. d. Wiss. München Bd. XXXVIII, 1908.
[19] Stachel, H., Higher order flexibility of octahedra. Period. Math. Hungar. 39:225-240 (1999).
[20] Stachel, H. (2008), Miura-Ori-Faltung, (www.geometry.at/strobl/ strobl 2008/vortrag 08/stachel/stachel08 _miura-ori-faltung.pdf).
[21] Stavric, M., Wiltsche, A.: Origami Theater, IBDG 2/2016, p. 15-19.
[22] Weiss, G., Ebisui, H., Remarks on Perspective Simplices. FME-Transactions (2017) 45, 243-250.
[23] Weiss, G., Havlicek, H., Ecken- und Kantenhöhen im Tetraeder. KoG – J. Croatian Soc. f. Constr. Geom. and Comp. Graph., Vol. 6 (2002), p.71-80.
[24] Wells, David (1991), The Penguin Dictionary of Curious and Interesting Geometry, Penguin Books, London 1991
[25] Ziegler, Günter M., Lectures on Polytopes (Graduate Texts in Mathematics. Nr.152). Springer Verlag,1995, ISBN 0-387-94365-X.
[26] Regular Polytopes: https://en.wikipedia.org/wiki/Polytope#Regular_polytopes
[27] Dodecahedron: https://en.wikipedia.org/wiki/Dodecahedron
[28] Isodynamic point: https://en.wikipedia.org/wiki/Isodynamic_point
[29] Miura-Ori: https://en.wikipedia.org/wiki/Miura_fold

1-2-3-Sphere in the 4-Space

Michal Zamboj

Department of Mathematics and Mathematical Education
Faculty of Education, Charles University
M. D. Rettigové 4, 116 39 Prague 1, Czech Republic
michal.zamboj@pedf.cuni.cz

Abstract. Recently, we have studied visualizations of the 4-space in the double orthogonal projection onto two mutually perpendicular 3-spaces. A studied object is projected onto its two conjugated images in the modeling 3-space – 3D graphics on the computer screen. In this contribution, we use this method of projection to construct spherical, circular and point intersections of a 3-sphere with a 3-space, plane, and line. The provided step-by-step constructions are created in the interactive software GeoGebra 3D.

Keywords: double orthogonal projection, multidimensional visualization, descriptive geometry, 3-sphere

1 Introduction

The set of all points at a constant non-zero distance from a given point is a circle in a plane, a sphere in a 3-space, or analogically a 3-sphere in a 4-space, or an n-sphere in an $(n+1)$-space, for $n \in \mathbb{N}_0$. Although the generalization of the definition is clear, our (three-dimensional) imagination of the whole picture fails in the fourth dimension. Instead of trying to imagine a whole 3-sphere in a given 4-space, we visualize its parts. One way to understand a four-dimensional object is to construct its sections. See the argument given by Abbott in [1], p. 71, in which a sphere attempts to persuade a 2-dimensional being into believing in the existence of three-dimensionality: *"But now prepare to receive proof positive of the truth of my assertions. You cannot indeed see more than one of my sections, or Circles, at a time; for you have no power to raise your eye out of the plane of Flatland; but you can at least see that, as I rise in Space, so my sections become smaller. See now, I will rise; and the effect upon your eye will be that my Circle will become smaller and smaller till it dwindles to a point and finally vanishes."* Now, in analogy to understanding the Sphere from Flatland as a collection of its circle sections, we may visualize a 3-sphere as a collection of classical 2-spheres. Throughout this paper, we visualize such sections of a 3-sphere with 3-spaces but also sections with planes and lines.

The visualizations are created in the double orthogonal projection of the 4-space onto two mutually perpendicular 3-spaces, which is a generalization of Monge's projection. More precisely, let us have a Euclidean 4-space with the orthogonal reference system given by axes x, y, z, and w. Each point $P(p_x, p_y, p_z, p_w)$ in the 4-space is orthogonally projected to its Ξ-image $P_3(p_x, p_y, p_z)$ in the 3-space $\Xi(x, y, z)$ and its Ω-image $P_4(p_x, p_y, p_w)$ in the 3-space $\Omega(x, y, w)$. The 3-spaces $\Xi(x, y, z)$ and $\Omega(x, y, w)$ have a common plane $\pi(x, y)$. Now, we rotate one of the 3-spaces, e.g. $\Omega(x, y, w)$ around the plane $\pi(x, y)$ onto the 3-space $\Xi(x, y, z)$ (or vice-versa), such that the axes w and z are oriented oppositely.[1] This way we have constructed a modeling 3-space in which a four-dimensional point P has two conjugated images P_3 and P_4. The modeling 3-space is either our physical 3-space or a virtual 3-space in some 3D modeling software, e.g. GeoGebra 3D, in which our constructions are carried out. Elementary constructions in the double orthogonal projection used in this paper are described in detail in [3], sections of polytopes in the consecutive article [4] and constructions of quadrics and their sections in [5]. Our constructions and methods are natural generalizations of classical constructions in Monge's projection, for example in [2].

To follow the description of our constructions, we recommend using the step-by-step constructions in the online GeoGebra Book [6], where the reader can also interactively manipulate with views and input elements of the given objects. This way the user can obtain some intuitive perception of both, a 3-sphere and the method of projection. Readers with experience in descriptive geometry may choose special views to uncover many analogies with three-dimensional cases.

2 Sections of a 3-sphere

Let us have a unit 3-sphere Σ embedded in the 4-space with the center $S[0, 0, 1, 1]$. Its orthogonal projections into 3-spaces $\Xi(x, y, z)$ and $\Omega(x, y, w)$ are 2-spheres Σ_3 and Σ_4, respectively. Both apparent contours Σ_3 and Σ_4 have the diameter equal to the diameter of Σ. We cut the 3-sphere Σ consecutively with a 3-space, plane (2-space), and line (1-space) in the following paragraphs.[2] Since we use parallel (orthogonal) projection, the resulting orthogonal images of sections will be, in general, affinely distorted: a sphere will appear as an ellipsoid and a circle will appear as an ellipse.

2.1 Spherical section of a 3-sphere with a 3-space (Figure 1)

Let us have a 3-space Γ given by its Ξ and Ω-traces ξ_3^Γ and ω_4^Γ, i.e. the intersections of Γ with the 3-spaces $\Xi(x, y, z)$ and $\Omega(x, y, w)$. In the first step, we construct the slope line perpendicular to the trace ξ_3^Γ through S_3 and find the rotated image Σ_r of the sphere Σ in the 3-space of symmetry perpendicular to $\Xi(x, y, z)$ through the slope line. Concerning the upcoming rotation of the 3-space Γ, we choose the 3-space of symmetry parallel to the intersection of Γ with the reference plane $\pi(x, y)$. Next, we

[1] For the sake of clarity we do not relabel the points in the rotated 3-space.

[2] In the presented constructions, we always assume the cutting spaces that intersect and not touch the 3-sphere.

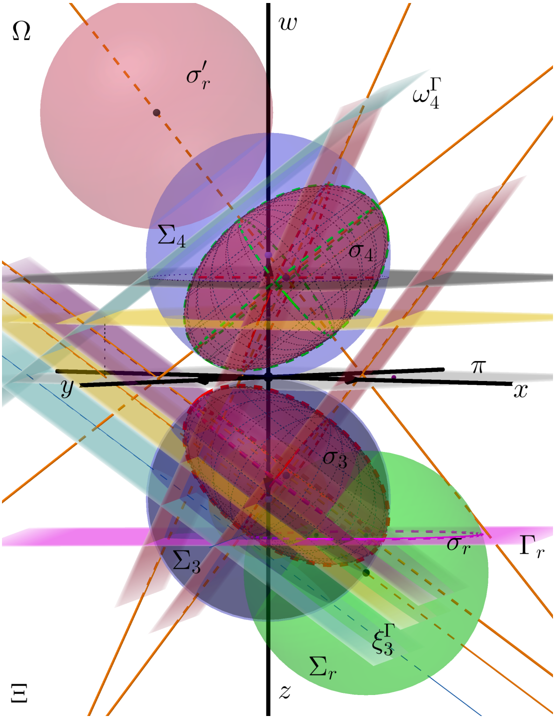

Figure 1: Spherical section σ of a 3-sphere Σ with a 3-space Γ.
Step-by-step construction:
`https://www.geogebra.org/m/a8zxntdh#material/qmfrvcew`

find the image Γ_r of Γ in the same view. The intersection of Γ_r and Σ_r is the image σ_r (circle) of the spherical section σ in the rotated view in the 3-space of symmetry of Σ. Now, we would like to reconstruct the Ξ and Ω-images of σ, which are, in general, ellipsoids σ_3 and σ_4 with a circle of the diameter equal to the diameter of σ_r in one of the principal planes. One principal plane of σ_3 is the Ξ-trace of the 3-space of symmetry used for the rotated view, and by the reverse rotation, we obtain an ellipse (and so, two semi-axes of the ellipsoid) in this principal plane. From the symmetry of the ellipse, it is apparent that the second principal plane of σ_3 is parallel to ω_3^Γ, and it cuts the ellipsoid σ_3 in the abovementioned circle of the diameter of σ_r. By finding the Ω-images of the semi-axes and applying the well-known Rytz's construction of the axis of an ellipse from two conjugated diameters, we finish the ellipsoidal orthogonal image σ_4 of the spherical section σ. Furthermore, in the figure, the true shape of the spherical section is rotated from σ_4 around the Ω-trace ω^Γ to σ'_r in the modeling 3-space.

2.2 Circular section c of a 3-sphere with a plane (Figure 2)

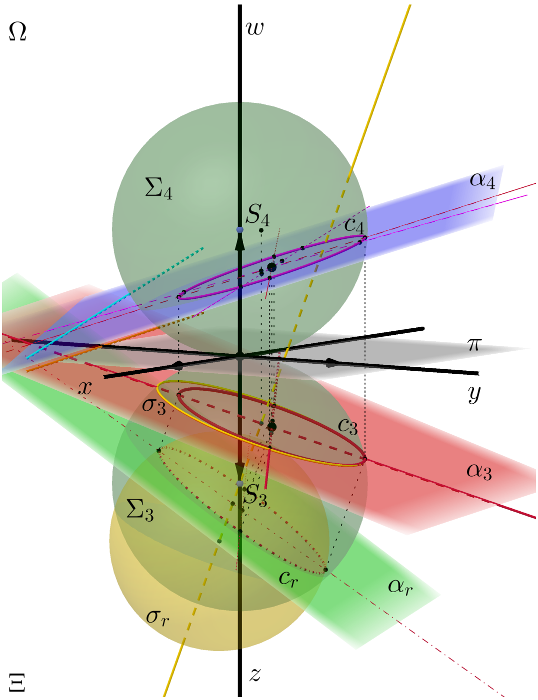

Figure 2: Circular section of a 3-sphere Σ with a plane α.
Step-by-step construction:
`https://www.geogebra.org/m/a8zxntdh#material/vgarqbmf`

Let us have a plane α given by its conjugated images α_3 and α_4. To construct the circular section c of the 3-sphere Σ, we assume the third projection is into the 3-space perpendicular to $\Xi(x, y, z)$ with the Ξ-trace being α_3. Therefore, the circular section σ_3 of α_3 and Σ_3 is the Ξ-image of a spherical section σ of Σ with the 3-space of the third view. After the rotation of the third view into the modeling 3-space, we obtain σ in its true shape as σ_r. Next, we find the rotated image α_r of the plane α. In the rotated third view, the intersection of σ_r and α_r is a circular section c_r, which is a rotated image of c. By the inverse rotation, i.e. the ellipse c_r is orthogonally projected into α_2, we construct the Ξ and Ω-images of the circular section c — ellipses c_3 and c_4.

2.3 Intersections of a 3-sphere with a line (Figure 3)

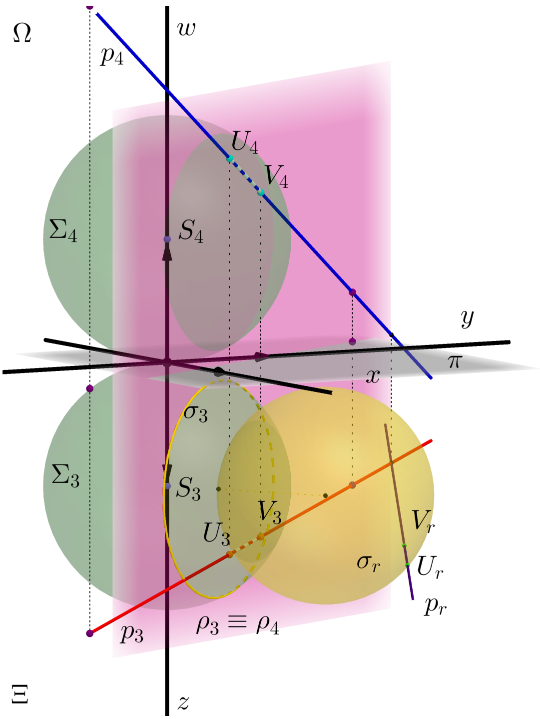

Figure 3: Intersections U and V of a 3-sphere Σ with a line p.
Step-by-step construction:
`https://www.geogebra.org/m/a8zxntdh#material/rgzvzqhg`

Let us have a line p given by its conjugated images p_3 and p_4. To construct the intersection points of the line p and the 3-sphere Σ, we again use a convenient third view rotated onto the modeling 3-space. This time, we choose the 3-space given by the plane of recall of the line p, i.e. the plane perpendicular to $\pi(x, y)$ through p_3 and p_4, and hence Ξ and Ω-traces of this 3-space of the third view become overlapping planes. The circular section σ_3 of the plane of recall with Σ_3 is an edge view of the 2-sphere σ that appears as σ_r when rotated to the modeling 3-space. With the use of the trace points of p, we find its rotated image p_r. The intersection points U_r and V_r of σ_r and p_r are rotated images of the wanted intersection points U and V. Reverting the rotation of the third view, we obtain the Ξ and Ω-images U_3, V_3 and U_4, V_4 of the intersecting points on the perpendiculars to the plane of recall of p through U_r and V_r. At last, from the four-dimensional point of view, the segment UV is inside the 3-sphere Σ, which is highlighted on its images with a dashed line in the figure.

3 Conclusion

With the use of a 3D interactive software, we have constructed sections of a 3-sphere in the four-dimensional space. These constructions are an important addition to our previous work on four-dimensional visualization using the double orthogonal projection of the 4-space onto two mutually perpendicular 3-spaces. The visualizations and interactive constructions are prepared for the use in further investigation of properties of a 3-sphere.

Acknowledgements

The author has been partially supported by the grant No. CZ.02.3.68/0.0 /0.0/16_038/0006965, Faculty of Education, Charles University.

References

[1] E. A. Abbott: *Flatland, a Romance of Many Dimensions,* Seeley & Co, London, 1884
[2] A. Urban: *Deskriptivní geometrie I.,* SNTL, Praha, 1965
[3] M. Zamboj: Double Orthogonal Projection of Four-Dimensional Objects onto Two Perpendicular Three-Dimensional Spaces, In *Nexus Network Journal*, 20 (2018), Issue 1, pp. 267-281
[4] M. Zamboj: Sections and Shadows of Four-Dimensional Objects, In *Nexus Network Journal*, 20 (2018), Issue 2, pp. 475-487
[5] M. Zamboj: Quadric Sections of Four-Dimensional Cones, In Cocchiarella (ed): *ICGG 2018 - Proceedings of the 18th International Conference on Geometry and Graphics*, Milan, Italy. Advances in Intelligent Systems and Computing, vol 809. Springer, Cham, 2018, pp. 500-513
[6] M. Zamboj: *Spherical sections of a 3-Sphere,* GeoGebra Book, 2019, online. Avalilable: `https://www.geogebra.org/m/a8zxntdh`

List of Participants

Conference

Ábrahámová	Andrea	KMDG SvF, STU v Bratislave
Bátorová	Martina	KAG FMFI, Univerzita Komenského v Bratislave
Bímová	Daniela	FPHP, Technická univerzita v Liberci
Blažek	Jiří	PF, Jihočeská univerzita v Č. Budějovicích
Bulantová	Jana	FAST, Vysoké učení technické v Brně
Čečáková	Stanislava	Fakulta architektury, ČVUT v Praze
Čmelková	Viera	Siemens Mobility, Žilina
Ferko	Andrej	FMFI, Univerzita Komenského v Bratislave
Halfarová	Hana	FAST, Vysoké učení technické v Brně
Hašek	Roman	KM PF, Jihočeská univerzita v Č. Budějovicích
Holešová	Michaela	SvF, Žilinská univerzita v Žiline
Hýrošová	Tatiana	Technická univerzita, Zvolen
Chalmoviansky	Pavel	KAG FMFI, Univerzita Komenského v Bratislave
Chodorová	Marie	KAG PF, Univerzita Palackého v Olomouci
Juklová	Lenka	KAG PF, Univerzita Palackého v Olomouci
Kmeťová	Mária	KM FPV, Univerzita Konštantína Filozofa v Nitre
Kolářová	Dana	KM Fakulta architektury, ČVUT v Praze
Kolcun	Alexej	Ústav Geoniky AV ČR, Ostrava
Kostelecká	Adéla	MFF, Univerzita Karlova, Praha
Krejčíř	Miroslav	Fakulta architektury, ČVUT v Praze
Lávička	Miroslav	KMA FAV, Západočeská univerzita v Plzni
Mackovová	Alžbeta	KAG FMFI, Univerzita Komenského v Bratislave
Magajna	Zlatan	Pedagoška fakulteta, Univerza v Ljubljani
Makovník	Marcel	KAG FMFI, Univerzita Komenského v Bratislave
Mencáková	Kristýna	FAST, Vysoké učení technické v Brně
Molnár	Emil	Budapesti Muszaki és Gazdaságtudományi Egyetem
Pech	Pavel	KM PF, Jihočeská univerzita v Č. Budějovicích
Pirklová	Petra	FPHP, Technická univerzita v Liberci
Richtáriková	Daniela	ÚMF SjF, STU v Bratislave
Sroka-Bizoń	Monika	Politechnika Śląska, Gliwice
Stachel	Hellmuth	Technische Universität Wien
Surynková	Petra	MFF, Univerzita Karlova, Praha
Szarková	Dagmar	SSGG, Bratislava
Šafařík	Jan	FAST, Vysoké učení technické v Brně
Šír	Zbyněk	MFF, Univerzita Karlova, Praha
Šrubař	Jiří	Fakulta architektury, ČVUT v Praze
Vágová	Renáta	KM FPV, Univerzita Konštantína Filozofa v Nitre
Vajsáblová	Margita	KMDG SvF, STU v Bratislave

Velich	Ilja	Bratislava
Velichová	Daniela	ÚMF SjF, STU v Bratislave
Voráčová	Šárka	Fakulta dopravní, ČVUT v Praze
Vrábliková	Jana	MFF, Univerzita Karlova, Praha
Vršek	Jan	KMA FAV, Západočeská univerzita v Plzni
Weiss	Gunter	Technische Universität Wien
Zamboj	Michal	Pedagogická fakulta, Univerzita Karlova, Praha
Zrůstová	Lucie	FAST, Vysoké učení technické v Brně

GeoGebra Workshop

Billich	Martin	PF, Katolícka univerzita Ružomberok
Čamborová	Mária	Gymnázium VPT Martin
Gergelitsová	Šárka	Gymnázium Benešov
Holéczyová	Soňa	Gymnázium, Pankúchová, Bratislava
Jirkalová	Milada	Gymnázium Ivana Kupca, Hlohovec
Konrádová	Miroslava	Evanjelická spojená škola, Martin
Lamošová	Jaroslava	Evanjelická spojená škola, Martin
Macháčová	Karin	Gymnázium Vojtecha Michálika, Sereď
Urbánková	Júlia	Gymnázium, Pankúchová, Bratislava

Proceedings of the

SLOVAK-CZECH CONFERENCE ON GEOMETRY AND GRAPHICS 2019

Editors:
Daniela Velichová, Miroslav Lávička, Dagmar Szarková

Published by

Vydavatelský servis

Republikánská 28, Plzeň

First Edition

Plzeň 2019

ISBN 978-80-86843-65-0 (online)
ISBN 978-80-86843-66-7 (CD-ROM)